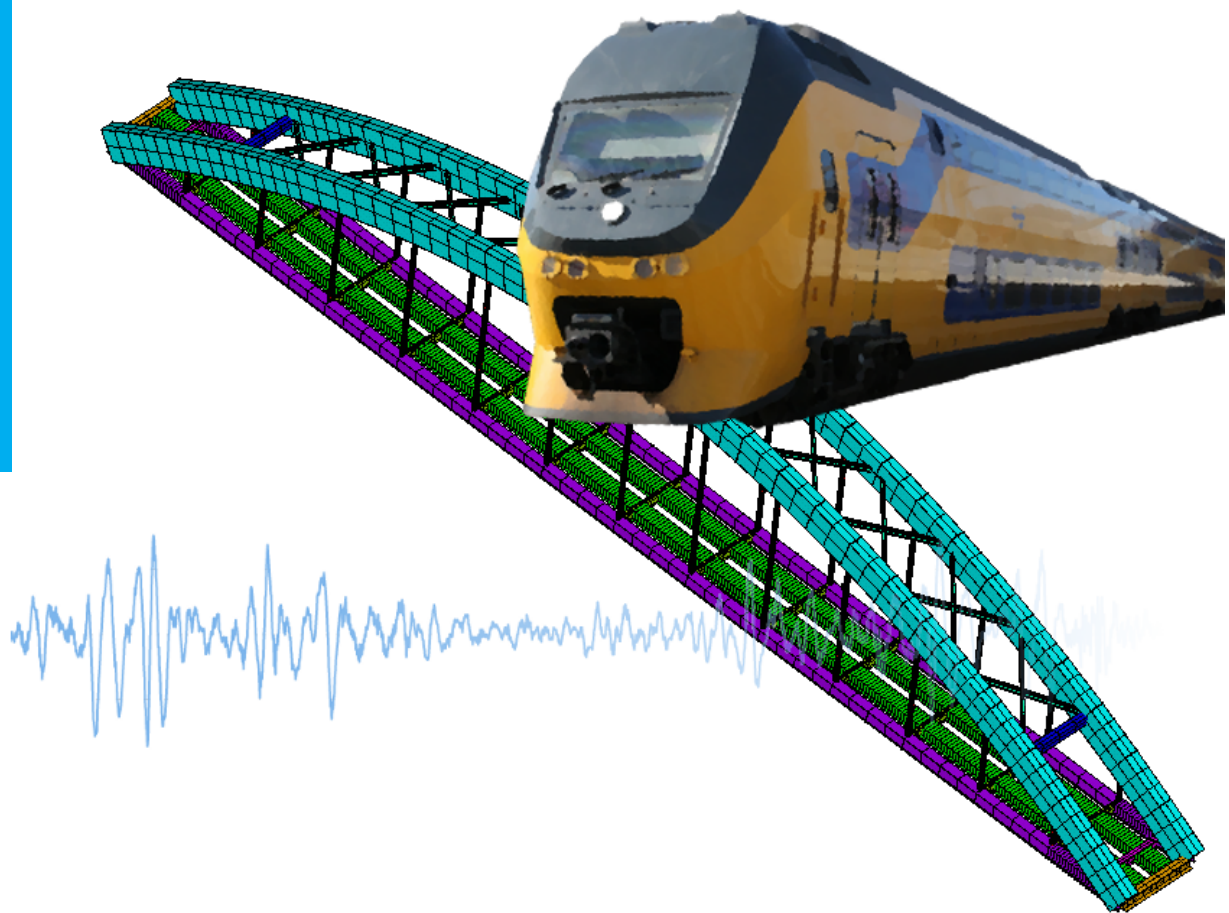


# Assessment of passenger comfort according to Eurocode in Dutch trains travelling over tied-arch railway bridges

B. Komen

Master of Science Thesis





# **Assessment of passenger comfort according to Eurocode in Dutch trains travelling over tied-arch railway bridges**

MASTER OF SCIENCE THESIS

For the degree of Master of Science in Structural Engineering at Delft  
University of Technology

B. Komen

June 15, 2016



---

# Graduation Committee

Prof. ir. F.S.K. Bijlaard (Chairman)  
Department of Structural Engineering, Steel Structures  
Faculty of Civil Engineering and Geosciences  
Delft University of Technology

Dr.ir. M.J.M.M. Steenbergen  
Department of Structural Engineering, Road and Railway Engineering  
Faculty of Civil Engineering and Geosciences  
Delft University of Technology

Dr.ir. P.C.J. Hoogenboom  
Department of Structural Engineering, Structural Mechanics  
Faculty of Civil Engineering and Geosciences  
Delft University of Technology

Ing. M. van Almen  
Section Steel and Movable Bridges  
Senior Structural Engineer at Iv-Infra B.V.

Ir. L.J.M. Houben (Secretary)  
Department of Structural Engineering, Road and Railway Engineering  
Faculty of Civil Engineering and Geosciences  
Delft University of Technology



---

# Abstract

With increasing velocities of trains, passenger comfort starts to play a larger role in the design of railway bridges. There is little experience with the Eurocode passenger comfort criterion in the Netherlands. It is relevant for the industry to have a way to fulfil this criterion, also in an early stage of railway bridge design. A sufficiently simple method to give a proper first estimation would be really useful.

According to the Eurocode, the comfort experienced by passengers in a train passing a railway bridge must be sufficient. The comfort level is expressed as a maximum vertical acceleration inside the coach. In this research, a method to compute this vertical acceleration is developed. The scope of the research is limited to steel tied-arch bridge with vertical hangers.

To find the accelerations in trains passing over bridges a numerical vehicle-bridge interaction model was developed using Ansys, a FEM program. Several bridge models and vehicle models were made using mass, spring-dashpots, bar and beam elements. Simple versions of the Ansys model were compared with analytical-numerical solutions written in Matlab and with literature. The more complex Ansys models were compared with measurements in a Dutch train travelling over a bridge. Apart from looking at the vertical accelerations also frequencies of vibrations were considered.

The used modelling technique proved to be feasible to execute with acceptable time to make and time to run. The results did compare well to analytical-numerical solutions for the simple models, but unfortunately the coach acceleration of the most complex bridge and vehicle model did not compare well with the performed measurements.

Although the results are applicable specifically for the Dutch VIRM train and steel tied-arch bridges with vertical hangers, the modelling technique can easily be generalized to other train types and other bridge types.



---

# Table of Contents

<b>Preface</b>	<b>xv</b>
<b>1 Introduction</b>	<b>1</b>
1.1 Motivation of research . . . . .	1
1.2 Aim . . . . .	2
1.3 Research questions . . . . .	2
1.4 Assumptions and limitations . . . . .	2
1.5 Structure of report . . . . .	3
1.6 Note on references . . . . .	3
<b>2 Literature review</b>	<b>5</b>
2.1 Structural standards . . . . .	5
2.1.1 Relevant Eurocodes . . . . .	5
2.1.2 Background of Eurocodes . . . . .	7
2.2 Critique on comfort criterion . . . . .	7
2.2.1 Peak acceleration . . . . .	7
2.2.2 Frequency weighting . . . . .	9
2.3 Bridge . . . . .	10
2.4 Railway track . . . . .	11
2.5 Train . . . . .	12
2.6 Structural dynamics . . . . .	13
2.6.1 Unsprung mass . . . . .	13
2.6.2 1 DOF sprung mass . . . . .	14
2.6.3 2 DOF sprung mass . . . . .	15
2.6.4 Full coach model . . . . .	16
2.7 Solution methods . . . . .	16

<b>3</b>	<b>Modelling</b>	<b>19</b>
3.1	Model choice . . . . .	19
3.1.1	Contact force model . . . . .	20
3.1.2	Direct contact model . . . . .	21
3.1.3	Choice . . . . .	22
3.2	Simple models . . . . .	23
3.2.1	Single 1 DOF sprung mass on simply supported bridge . . . . .	23
3.2.2	Multiple 1 DOF sprung masses on simply supported bridge . . . . .	23
3.3	Bridge models . . . . .	25
3.3.1	2D bridge model . . . . .	25
3.3.2	3D bridge model . . . . .	26
3.4	Vehicle models . . . . .	29
3.4.1	1 DOF schematization . . . . .	29
3.4.2	2 DOF schematization . . . . .	30
3.4.3	Full coach schematization . . . . .	31
3.5	Nodes and accuracy . . . . .	32
3.6	Parameter study . . . . .	33
3.6.1	Train velocity . . . . .	33
3.6.2	Suspension damping . . . . .	35
3.7	Model comparison . . . . .	36
3.7.1	Computation . . . . .	36
3.7.2	Acceleration . . . . .	37
<b>4</b>	<b>Measurements</b>	<b>41</b>
4.1	Why, what and how . . . . .	41
4.2	Standards . . . . .	42
4.3	Trial measurements . . . . .	42
4.4	Real measurements . . . . .	43
4.4.1	Comparison with Ansys . . . . .	46
<b>5</b>	<b>Conclusion</b>	<b>49</b>
5.1	Conclusions . . . . .	49
5.2	Response to the research questions . . . . .	51
5.3	Recommendations . . . . .	51
	<b>Appendices</b>	<b>55</b>
<b>A</b>	<b>Structural standards</b>	<b>55</b>
A.1	Eurocode 1: Actions on structures - Part 2: Traffic loads on bridges . . . . .	55
A.1.1	Results . . . . .	57
A.2	Eurocode 0 - Basis of structural design: Annex 2 . . . . .	58

A.2.1	Traffic safety . . . . .	59
A.2.2	Passenger comfort . . . . .	59
A.3	History . . . . .	60
A.3.1	Dutch codes . . . . .	60
A.3.2	International Union of Railways . . . . .	61
A.3.3	Eurocodes . . . . .	61
<b>B</b>	<b>Tied-arch bridge</b>	<b>63</b>
B.1	Types . . . . .	63
B.2	Elements . . . . .	64
B.2.1	Bearings . . . . .	64
B.2.2	Arch . . . . .	64
B.2.3	Bracing . . . . .	65
B.2.4	Hangers . . . . .	65
B.2.5	Deck . . . . .	66
B.2.6	Girder . . . . .	67
<b>C</b>	<b>VIRM train</b>	<b>69</b>
C.1	Coaches . . . . .	69
C.2	Bogies . . . . .	71
C.3	Schematization . . . . .	74
C.3.1	2 DOF schematization . . . . .	74
C.3.2	1 DOF schematization . . . . .	79
C.3.3	Full coach schematization . . . . .	80
<b>D</b>	<b>Dynamics theory</b>	<b>81</b>
D.1	Schematizing vehicle-bridge interaction . . . . .	81
D.2	Unsprung mass . . . . .	82
D.3	Single 1 DOF sprung mass . . . . .	83
D.4	Multiple 1 DOF sprung masses . . . . .	88
D.5	2 DOF sprung mass . . . . .	91
D.6	Full coach model . . . . .	93
D.7	Discretization . . . . .	94
D.8	Vibrations . . . . .	95
D.8.1	Resonance . . . . .	95
D.8.2	Track irregularities . . . . .	96
D.8.3	Wheel imperfections . . . . .	96

<b>E</b>	<b>Matlab analytical-numerical solution</b>	<b>99</b>
E.1	Single 1 DOF moving sprung mass in Matlab . . . . .	99
E.1.1	Single 1 DOF moving sprung mass script . . . . .	100
E.1.2	ODE solver script . . . . .	102
E.1.3	Verification . . . . .	102
E.2	Multiple 1 DOF moving sprung masses in Matlab . . . . .	104
E.2.1	Multiple 1 DOF moving sprung masses script . . . . .	104
E.2.2	Multiple ODE solver script . . . . .	106
E.2.3	Verification . . . . .	107
<b>F</b>	<b>Finite Element Modelling</b>	<b>109</b>
F.1	Modelling procedure . . . . .	109
F.2	Elements . . . . .	110
F.2.1	MASS21 - mass elements . . . . .	110
F.2.2	BEAM3 - beam elements . . . . .	110
F.2.3	BEAM188 - beam elements . . . . .	110
F.2.4	LINK8 - bar elements . . . . .	111
F.2.5	COMBIN14 - spring-dashpot elements . . . . .	111
F.2.6	CONTA175 - contact elements . . . . .	111
F.2.7	TARGE169 - target elements . . . . .	112
F.2.8	CONTAC48 - contact elements . . . . .	112
F.3	Analysis type . . . . .	112
F.3.1	Static analysis . . . . .	112
F.3.2	Modal analysis . . . . .	112
F.3.3	Transient analysis . . . . .	112
F.4	Time integration methods . . . . .	113
F.4.1	Direct integration method . . . . .	113
F.4.2	Mode-superposition method . . . . .	114
F.4.3	Fourier transformation method . . . . .	114
F.5	Numerical differentiation . . . . .	114
<b>G</b>	<b>Contact force model</b>	<b>115</b>
G.1	Ansys APDL code . . . . .	115
G.2	Interpretation . . . . .	117
G.2.1	Elements . . . . .	117
G.2.2	One DOF moving sprung mass . . . . .	117
G.2.3	Results . . . . .	119
<b>H</b>	<b>Bowe model</b>	<b>121</b>
H.1	Ansys APDL code . . . . .	121
H.2	Interpretation . . . . .	124
H.2.1	Elements . . . . .	124
H.2.2	Moving constraints . . . . .	124
H.3	Conclusion . . . . .	124

<b>I</b>	<b>Direct contact model</b>	<b>127</b>
I.1	Elements . . . . .	127
I.2	Stationary contact . . . . .	128
I.3	Moving contact . . . . .	129
I.4	Conclusion . . . . .	130
<b>J</b>	<b>Multiple 1 DOF sprung masses</b>	<b>133</b>
J.1	Ansys APDL code . . . . .	133
J.2	Code explanation . . . . .	137
<b>K</b>	<b>Simple model verifications</b>	<b>139</b>
K.1	Contact force model . . . . .	139
K.1.1	Ansys APDL code . . . . .	139
K.1.2	Convergence study . . . . .	142
K.2	Multiple 1 DOF sprung masses . . . . .	145
<b>L</b>	<b>Modelling results</b>	<b>149</b>
L.1	Newmark- $\beta$ versus HHT . . . . .	149
L.2	Backwards difference versus direct get . . . . .	151
L.3	Bridge models . . . . .	151
L.3.1	2D tied-arch bridge . . . . .	151
L.3.2	3D tied-arch bridge . . . . .	155
L.3.3	Comparison of bridge models . . . . .	158
L.4	Vehicle models . . . . .	161
L.4.1	1 DOF schematization . . . . .	161
L.4.2	2 DOF schematization . . . . .	168
L.4.3	Full coach schematization . . . . .	175
L.5	Model comparison . . . . .	184
L.5.1	Acceleration . . . . .	184
L.5.2	Cross-beam effect . . . . .	189
<b>M</b>	<b>2D tied-arch bridge model</b>	<b>191</b>
M.1	Railway bridge near Culemborg . . . . .	192
M.1.1	Construction elements . . . . .	192
M.1.2	Self-weight . . . . .	194
M.2	Ansys model . . . . .	194
M.2.1	Ansys APDL code . . . . .	194
M.2.2	Geometry . . . . .	198
M.2.3	Element data . . . . .	198
M.3	Verification . . . . .	200
M.3.1	Full loading . . . . .	200
M.3.2	Anti-symmetric loading . . . . .	204
M.3.3	Mode shapes . . . . .	207

<b>N</b>	<b>3D tied-arch bridge model</b>	<b>209</b>
N.1	Railway bridge near Culemborg . . . . .	209
N.1.1	Construction elements . . . . .	209
N.2	Ansys model . . . . .	212
N.2.1	Ansys APDL code . . . . .	212
N.2.2	Geometry . . . . .	224
N.2.3	Element data . . . . .	224
N.2.4	Mass modification . . . . .	228
N.3	Verification . . . . .	229
N.3.1	Self-weight . . . . .	229
N.3.2	Anti-symmetric loading . . . . .	229
N.3.3	Mode shapes . . . . .	230
<b>O</b>	<b>Acceleration measurements</b>	<b>233</b>
O.1	Bridge choice . . . . .	233
O.2	Measurement equipment . . . . .	234
O.3	Trial measurements . . . . .	235
O.4	Experimental setup . . . . .	238
O.4.1	Data to record . . . . .	238
O.4.2	Activities . . . . .	239
O.5	Real measurements . . . . .	241
O.5.1	Results . . . . .	241
O.5.2	FFT Matlab script . . . . .	245
<b>P</b>	<b>Comfort standards</b>	<b>247</b>
P.1	ISO 2631-1 . . . . .	247
P.1.1	Measurements . . . . .	247
P.1.2	Interpretation . . . . .	248
P.2	ISO 2631-4 . . . . .	250
P.2.1	Measurements . . . . .	250
P.2.2	Interpretation . . . . .	250
P.3	EN 12299 . . . . .	251
P.3.1	Comfort evaluation methods . . . . .	251
P.3.2	Measurements . . . . .	251
P.3.3	Interpretation . . . . .	253
P.4	Further reading . . . . .	254
	<b>Bibliography</b>	<b>255</b>

---

# Nomenclature

## Greek symbols

$\alpha$	load classification factor [1, sec. 6.3.2]
$\alpha$	thermal coefficient
$\beta$	stiffness multiplier in Rayleigh Damping
$\beta$	parameter in Newmark- $\beta$ method
$\gamma_{bt}, \gamma_{df}$	vertical acceleration of respectively ballast/ballastless bridge deck
$\gamma$	parameter in Newmark- $\beta$ method
$\delta(x)$	Dirac delta function
$\delta_{stat}, \delta_{dyn}$	static/dynamic deflection of bridge
$\lambda$	wavelength
$\nu$	Poisson's ratio
$\xi$	damping ratio between actual damping and critical damping
$\xi_p, \xi_s$	damping ratio primary/secondary suspension
$\rho$	density
$\sigma$	stress
$\phi_n$	shape modes of beam
$\phi$	phase
$\varphi_v$	vehicle mass rotation
$\omega_n, \omega_m$	natural frequency

## Latin symbols

$a, a_w$	acceleration, root mean square acceleration
$A$	cross sectional area
$b_v$	vertical acceleration inside the coach
$c, c_{cr}$	damping value, critical damping value
$c_v, c_p, c_s$	vehicle, primary or secondary damping value
$C$	damping matrix
$C_{Cz}$	continuous comfort in z-direction
$g$	gravitational acceleration
$D_k$	characteristic length of separation between axles

$E$	Young's Modulus
$f_0$	first natural frequency
$F$	force
$f_c$	contact force
$g$	gravitation acceleration
$h_v$	coach height
$I$	moment of inertia
$I_v$	mass moment of inertia
$k$	spring stiffness
$k_b$	beam stiffness
$k_v, k_p, k_s$	vehicle, primary or secondary spring stiffness
$K$	stiffness matrix
$L, l$	span length of bridge
$LI_h$	level of incomfort of harmonic vibration
$l_h$	centre coach to bogie distance
$m$	mass
$m_b, m_v,$ $m_{bog}, m_f,$ $m_w$	beam/bridge, vehicle, bogie, frame or wheel mass
$M$	mass matrix
$n$	mode number
$n_0, n_1, \dots, n_i$	first, second, ..., i-th natural frequency
$n_T$	first torsional frequency
$N_{MV}$	comfort index
$q$	distributed load
$R$	wheel radius
$dR$	wheel imperfection
$t, \Delta t$	time, time increment
$u$	vertical deflection
$u_b$	deflection of beam/bridge
$u_{bog}$	bogie vertical displacement
$u_f$	frame vertical displacement
$u_v$	vehicle vertical displacement
$V, v$	velocity of train
$W_b$	frequency weighting curve
$W_k$	frequency weighting curve
$w_v$	coach length
$x$	horizontal coordinate
$y$	vertical coordinate

### Abbreviations

APDL	Ansys Parametric Design Language
CEN	Comité Européen de Normalisation (European Committee for Standardization)
DB	Deutsche Bahn (German Railway company)
DOF	Degree of Freedom

EN	European Standard
ENV	European pre-Standard
ERRI	European Rail Research Institute
FEM	Finite Element Method
GPS	Global Positioning System
GUI	Graphical User Interface
ISO	International Organization for Standardization
KEYOPT	definition of settings for an Ansys element type
MU	Multiple Unit, a coupled set of train coaches
NEN	NEderlandse Norm (Dutch standard)
NS	Nederlandse Spoorwegen (Dutch railway company)
RMS	Root Mean Square
1 DOF	one degree of freedom
2 DOF	two degrees of freedom
SLS	Serviceability Limit State
SLT	Sprinter Lighttrain
SNCF	Société Nationale des Chemins de fer Français (French National Railway Company)
TGB	Technische Grondslagen voor Bouwconstructies (Technical basis for constructions)
UIC	Union Internationale des Chemins de fer (International Union of Railways)
ULS	Ultimate Limit State
VBI	Vehicle-Bridge Interaction
VDV	Vibration Dose Value, measure for acceleration
VIRM	Verlengd InterRegio Materieel (Dutch double decker train)
VOSB	Voorschriften voor het Ontwerp van Stalen Bruggen (Directions for the design of steel bridges)
VVSB	Voorschriften voor het Vervaardigen van Stalen Bruggen (Regulations for fabricating steel bridges)

## Glossary

Ansys	a commercial FEM program
Eurocode	European standard specifying structural design
Matlab	Matrix laboratory, numerical solution software
ProRail	Dutch rail infrastructure company
Stork RMO	Dutch rolling stock parts and bogie manufacturer
Thalys	type of high speed train



---

# Preface

In this document the results of my Master's thesis, carried out for the company IV-Infra B.V., are reported. This Master's thesis is part of the master track Structural Engineering.

I would like to thank my graduation committee for their guidance during the process of my graduation. I want to thank Professor Bijlaard, Dr. Steenbergen and Dr. Hoogenboom for their helpful comments and critical feedback which helped me to stay enthusiastic and constantly improve the work. I am really grateful for the daily supervision of Matthijs van Almen, who not only has a lot of in-depth knowledge but is also experienced in guiding the graduation process.

I am also very glad to have received so much help from really anybody I asked for help. I want to thank Mr. Van der Zwan (ProRail) and Professor Dollevoet for providing documents for the literature review and railway bridge data. I want to thank Mr. Bruggers for providing his Master's thesis which was of much help and inspired me to do measurements myself. With respect to the measurements I want to thank Dr. Blom for providing the app VXaccelerator which made it possible to perform these measurements. I want to thank Mr. Volgers for providing data related to bogies and explaining some railway concepts and Mr. Alta for forwarding me to Mr. Volgers in the first place. I also want to thank Mr. Kang for sending me the Ansys code mentioned in his paper. I am grateful for the answers provided by Mr. Tünnissen who is really an expert in this topic.

Furthermore I am grateful for the opportunity Mr. Koop gave me to do my graduating at IV-Infra and I am grateful for the help I received from my colleagues and the pleasant environment at IV-Infra.

Delft, University of Technology  
June 15, 2016

Benjamin Komen



"Everything should be made as simple as possible, but not simpler."

— *Albert Einstein*



---

# Chapter 1

---

## Introduction

### 1.1 Motivation of research

With increasing velocities of trains, passenger comfort starts to play a larger role in the design of railway bridges. The comfort level can be expressed as a maximum vertical acceleration inside the coach. It is useful to be able to compute the comfort level in trains, also in an early stage of railway bridge design. To compute coach accelerations, it is necessary to consider the dynamic interaction between bridges and moving trains.

When the weight of trains is relatively small compared to the weight of bridges, trains can be modelled as moving loads. [2, p. 6] To model the displacements and accelerations in the train itself, as experienced by passengers, there is a need for more complex vehicle models. One of such models considers the trains as a sprung moving mass, solved by Biggs in 1964 [3], which became possible with the availability of digital computers. Nowadays it is possible to use complex numerical models based on finite element methods, to model more complex vehicle and train models.

A lot of research is focused on the bridge response, not on the vibrations experienced by passengers of trains. Often bridges are modelled as simply supported beams, since the focus of such research is the interaction between vehicle and bridge. However, there is a significant difference between the deformation of a simply supported beam and a tied-arch bridge. In this report a measure for the effects on passengers will be investigated, by modelling train coaches by masses, springs and dashpots. The bridge model will be extended from a model for simply supported beams to a model for simply supported tied-arch bridges. Finally it will be investigated to what extent it is possible to simplify the analysis by for example comparing 3D and 2D models.

## 1.2 Aim

The aim of the research is:

To investigate the dynamic effects influencing passenger comfort caused by rail traffic actions with a velocity of up to 160 km/h on steel tied-arch railway bridges and present a simplified and validated dynamic analysis method.

## 1.3 Research questions

The aim of the research can be formulated in two questions:

1. In what ways can a dynamic vehicle-bridge interaction analysis to evaluate passenger comfort criteria prescribed in the Eurocode [4, par A2.4.4.3.3] be performed?
2. Is it possible, and if so, how can the dynamic analysis prescribed in the Eurocode [4, par A2.4.4.3.3] be simplified, not leading to unnecessary conservatism, with respect to engineering and material usage?

## 1.4 Assumptions and limitations

To narrow down the scope of the research, some assumptions are made and some limitations are set:

- Only dynamic effects caused by rail traffic actions will be analysed, these actions can cause mainly vertical but also torsional behaviour;
- Only tied-arch bridges with vertical hangers and without continuously connected sections will be analysed, not Figure 1.1b but rather Figure 1.1a;
- Only steel bridges will be studied, no concrete or composite bridges;
- Only bridges designed for train velocities up to 160 km/h will be analysed;
- The influence of the contact force between rail and wheel and similar factors, whose influence is only local (such as the Saint-Venant's local principle), will be neglected [5, page 47];
- Only trains moving at a constant velocity of motion, with no acceleration or deceleration on the bridge, will be considered. This is to prevent a dependency of the bridge deflection on the acceleration/deceleration [5, page 119];
- The scope of the research will be limited to The Netherlands. This mainly affects the real trains and bridges considered.

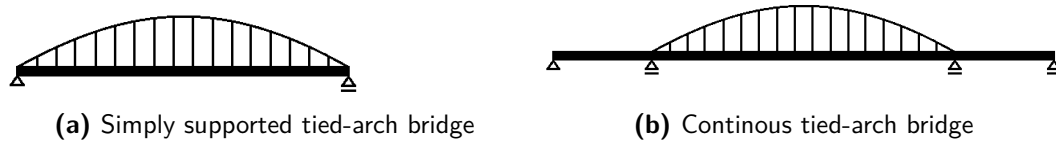


Figure 1.1: Types of tied-arch bridges

## 1.5 Structure of report

The methodology of the research can be summarized in the following way. First a literature review is performed in chapter 2, afterwards calculations and modelling are done, described in chapter 3. Finally some modelling results are compared with experimental measurements in chapter 4. The objectives are:

- Literature review
  - To investigate the background of the criteria whether a dynamic analysis is necessary or not, as prescribed in the Eurocode [1, par. 6.4.4];
  - To investigate the background of the dynamic VBI (vehicle-bridge interaction) analysis to fulfil the passenger comfort criteria prescribed in the Eurocode [4, par A2.4.4.3.3];
  - To investigate the types of dynamic VBI analysis methods used in practise, for example if they are analytical or numerical;
  - To assess what train characteristics need to be known to perform a dynamic VBI analysis for passenger comfort;
- Modelling
  - To develop a simplified analysis method to fulfil passenger comfort criteria, which can be performed at an early phase of design;
  - To evaluate the level of complexity and accuracy and validate the developed simplified analysis method;
- Experimental verification
  - To verify the developed simplified method using an existing bridge as a comparison.

## 1.6 Note on references

The references are styled in a way which might require explanation. Reference to a paragraph in a certain book is formatted as [<reference number>, <paragraph number>], for example [6, par. 2.7] would refer to paragraph 2.7 in reference number 6. All references are listed in the Bibliography, which can be found at the end of this report.



---

## Chapter 2

---

# Literature review

In section 2.1 several structural standards and their relevance to the subject are discussed. Then in section 2.2 the comfort criterion from the Eurocode [4, par A2.4.4.3] is discussed. Afterwards the physical components of the analysis are discussed, the bridge in section 2.3, the railway track in section 2.4 and the trains in section 2.5. Then section 2.6 provides some theoretical background of the structural dynamics relevant to the subject. Finally section 2.7 gives an insight into solution methods and how it can be used in this problem.

## 2.1 Structural standards

Since part of the motivation for this research is found in certain requirements from structural standards, they are examined. Reference is made to Appendix A which contains the full review.

### 2.1.1 Relevant Eurocodes

Currently, the design requirements related to the dynamics of railway bridges can be found in two different Eurocodes. Eurocode 1, part 2 [1] contains requirements related to loading and dynamic analyses, while Eurocode 0, Annex A2 [4] contains bridge performance criteria.

When designing railway bridges, it is not always necessary to perform a dynamic analysis. Section 6.4.4 of Eurocode 1, part 2 contains requirements for determining whether a static or dynamic analysis is required, elaborated in section A.1. The decision making process is graphically represented in a flow chart, see Figure A.1 in section A.1 of this report. This flow chart contains criteria such as train velocity, whether the bridge is continuous or not, length of the bridge and first natural frequency in bending and torsion. Following this flow chart results in either a dynamic analysis is required or it is not required. However, even if a dynamic analysis is required, it can still be avoided in some cases by applying a strict deflection limit ( $L/2000$  instead of  $L/800$  for a velocity of 160 km/h). [6, page 237]

A dynamic analysis can be performed looking from two different perspectives. The first perspective looks at the structural integrity of the bridge, with criteria related to **traffic safety**. Fulfilling these

criteria will prevent unsafe situations, such as trains passing the bridge causing resonance and eventually ballast instability and loss of wheel/rail contact. The other perspective is related to the perception of the passengers travelling in the train, with criteria related to **passenger comfort**. This means vibrations in the train coach must not be so excessive as to cause discomfort for the passengers. To limit the vertical acceleration of passengers in the coach, either a maximum permissible vertical deflection must be set according to Figure 2.1 for spans up to 120 meters, or a dynamic vehicle-bridge interaction (VBI) analysis must be performed.

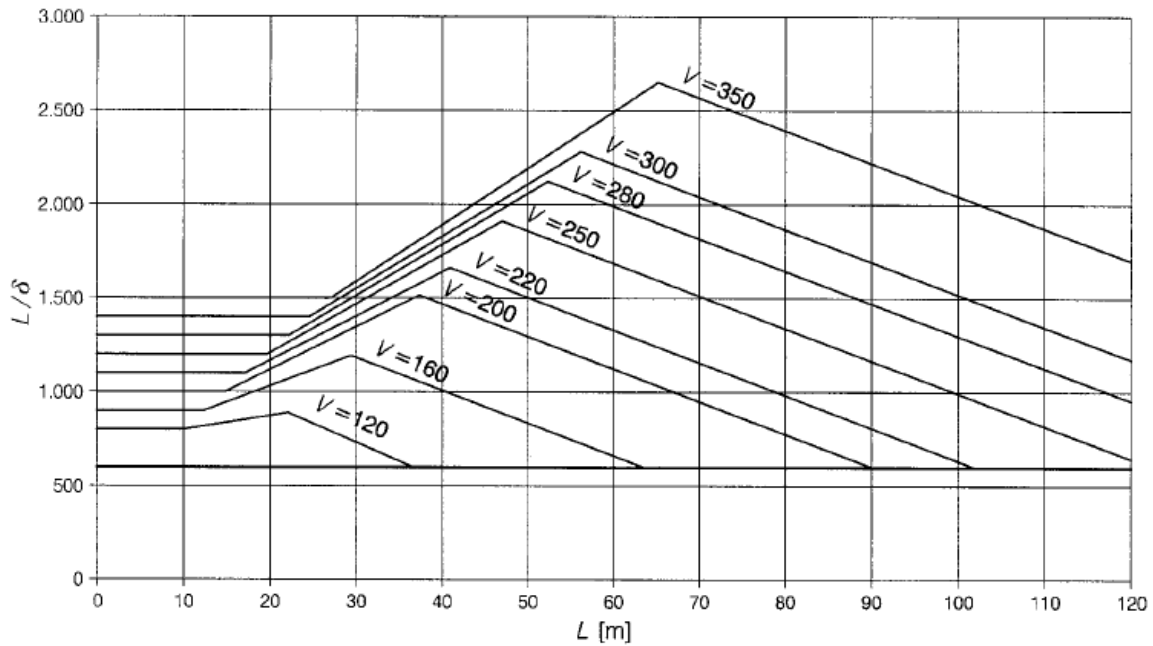


**Figure 2.1:** Maximum permissible vertical bridge deflection [4, fig. A2.3]

- $L$  = span length [m]
- $L/\delta$  = length/deflection ratio [-]
- $V$  = velocity [km/h]

Since tied-arch bridges in the Netherlands often have spans larger than 120 meters, the required dynamic VBI analysis is relevant. In such a dynamic vehicle-bridge interaction analysis, the train cannot be simply modelled as moving loads. The following requirements are given for this analysis to verify the vertical acceleration inside the coach during travel, is within limits. [4, A2.4.4.3.3]

- A series of vehicle speeds up to the maximum speed must be used;
- Characteristic loading of the real trains specified must be used;
- Dynamic mass interaction between vehicles in the real train and the structure must be used;
- The damping and stiffness characteristics of the vehicle suspension must be used;
- A sufficient number of vehicles to produce the maximum load effects in the longest span must be used;

- A sufficient number of spans in a structure with multiple spans to develop any resonance effects in the vehicle suspension must be used.

### 2.1.2 Background of Eurocodes

Prior to the Eurocodes, Dutch structural standards were used in the Netherlands, see subsection A.3.1. Although these older Dutch codes mention allowable stresses for dynamically loaded railway bridges since the *VOSB 1963*, requirements for a dynamic calculation comparable to those in the current Eurocode ([4], [1]) have not been found by the author. The dynamic calculations of railway bridges found in the Eurocodes, are not rooted in the older Dutch codes.

The international union of railways publishes leaflets with design recommendations, see subsection A.3.2. With the increasing design velocity of trains, research on railway bridge dynamics was performed and included in UIC leaflets.

With the development of the Eurocode standards (see subsection A.3.3), requirements for the dynamics of railway bridges were used from UIC leaflets. This first happened in pre-standard ENV 1991-3 [7] and afterwards in two Eurocodes: EN 1991-2 [1] and EN 1990/A2 [4].

To summarize, it can be concluded the dynamic calculation prescribed by the Eurocode ([4], [1]) is not rooted in the older Dutch codes, but is based on UIC leaflets, which are based on research done with the development of high speed trains. Old Dutch bridges designed according to the Dutch NEN standards did not have to fulfil a dynamic criterion.

## 2.2 Critique on comfort criterion

From the review of the relevant Eurocode standards in subsection A.2.2 a limit of vertical acceleration of  $b_v = 1.0 \text{ m/s}^2$  is found, to have a *very good* comfort level inside the train coach. [4, par. A2.4.4.3] However, discomfort depends on the frequency, magnitude and duration of vertical vibration. [8] The Eurocode comfort criterion is only a rough estimate for passenger comfort. There are several standards which provide better criteria to assess passenger comfort, see Appendix P.

### 2.2.1 Peak acceleration

By prescribing an absolute limit to the allowable acceleration, it is possible that one unrepresentative peak exceeds this limit, while the overall acceleration is within the limit, see Figure 2.2. Such an instantaneous peak is an artefactual extreme and is in general unrepresentative for the discomfort felt by passengers. To prevent this unnecessary conservatism, a root mean square value (RMS) of the acceleration can be used, which is a measurement for the energy level of a signal. [9, par 12.2.2] This root mean square acceleration in (m/s) can be formulated in the following manner for a continuous function [10, par. 6.1]

$$a_w = \left[ \frac{1}{T} \int_0^T a_w^2(t) dt \right]^{\frac{1}{2}} . \quad (2.1)$$

For a set of  $n$  discrete acceleration values the RMS value is defined as

$$RMS = \sqrt{\frac{\sum_{i=1}^n x_i^2}{n}}. \quad (2.2)$$

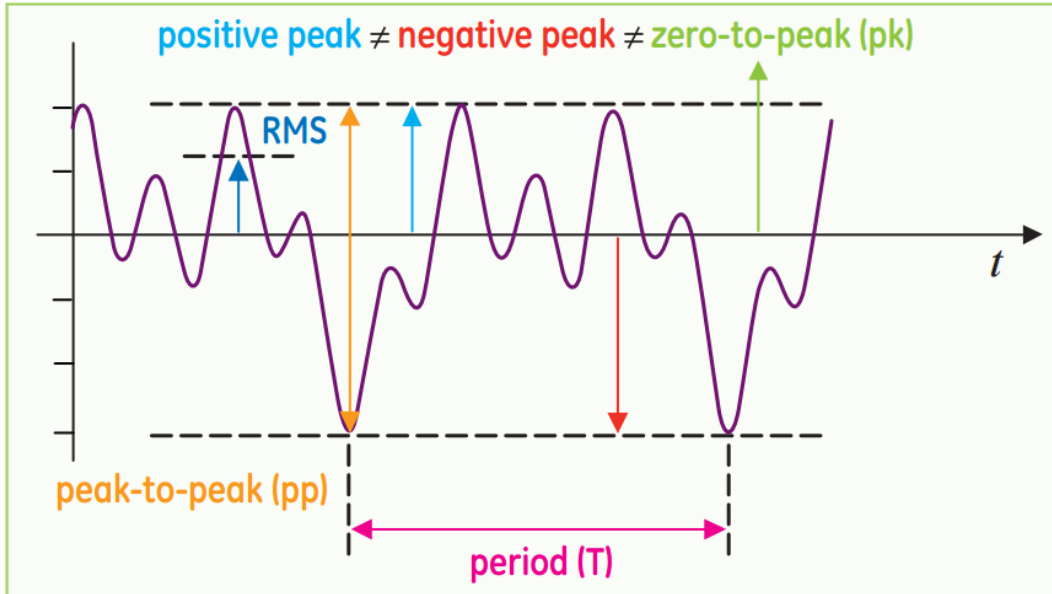


**Figure 2.2:** Peak values and RMS values of a signal [11, fig. 2]

This value is applicable if the peak values are less than nine times higher than the RMS value. [10, par. C.2.2.3] If high peak values play a dominant role, the vibration dose value (VDV) method can be used. The fourth power vibration dose value in ( $m/s^{1.75}$ ) can be formulated as [10, par. 6.3.2]

$$VDV = \left[ \int_0^T [a_w(t)]^4 dt \right]^{\frac{1}{4}}. \quad (2.3)$$

Similar to the root mean square acceleration or the vibration dose value from ISO 2631, an older criterion from the ERRI D190 exists, the level of incomfort harmonic ( $LI_h$ ) is

$$LI_h = 107.77 \sqrt[3]{\int_0^T |a(t)|^3 dt}. \quad (2.4)$$

This limit on the level of incomfort of harmonic vibration  $LI_h$  was used for the assessment of the bridge over the Hollandsch Diep. The method was used to complement the Eurocode criteria [4, par. A2.4.4.3], because the natural frequency of the bridge was close to the natural rigid car body frequencies of the trains and resonance was expected. [12, page 169]

The preferred method to use is the weighted RMS acceleration, as described by ISO 2631. This method can be used unless the crest factor (ratio between peak values and RMS value) is less than nine.

## 2.2.2 Frequency weighting

Another criticism on the Eurocode  $1 \text{ m/s}^2$  criterion [4, par. A2.4.4.3], is the absence of frequency dependency. Even if vibrations have the same acceleration, their effects on perception differ, depending on the frequency and the different axes of vibration. [13, page 5] A weighted frequency spectrum can be obtained from a frequency spectrum, which can be obtained from an acceleration time history with a Fourier transformation, as seen in Figure 2.3.

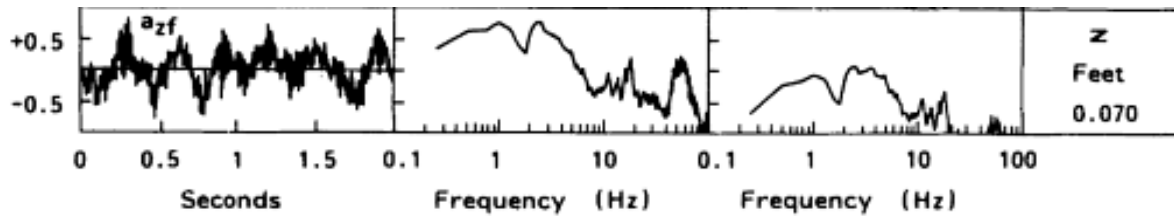


**Figure 2.3:** Acceleration time history, power spectrum and weighted power spectrum [14, fig. 12.11]

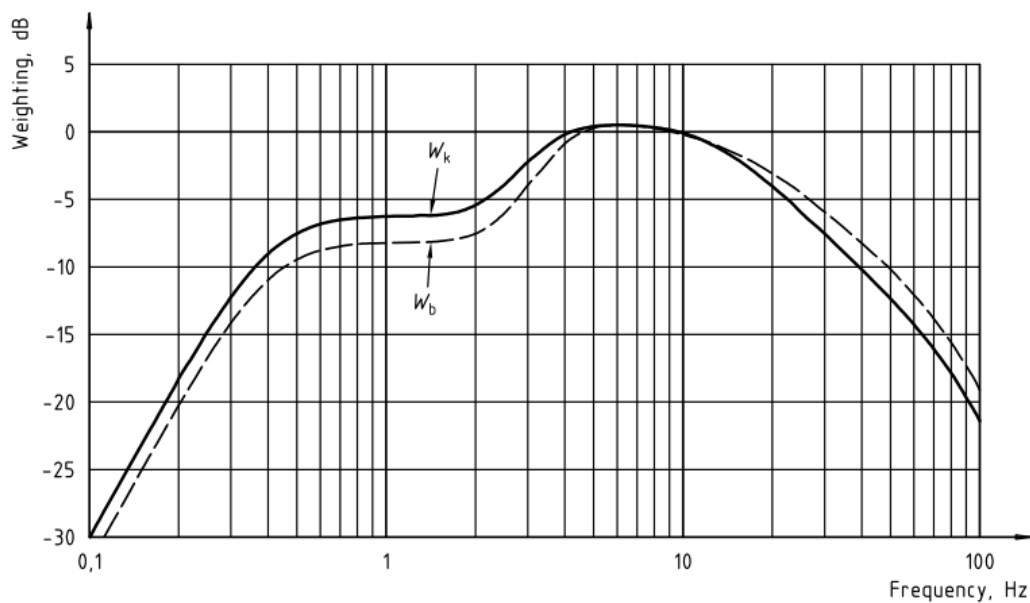


**Figure 2.4:** Frequency weighting curves for  $W_b$  and  $W_k$  [15, fig. 1]

- Frequency = number of vibrations per second [Hz]
- Weighting = intensity on logarithmic decibel scale. The zero level means no weighting, an intensity reduction of approximately 3 dB is a reduction to half the initial value. [14, p. 733 - 735]
- $W_k$  = principal frequency weighting in z direction
- $W_b$  = frequency weighting in z direction, specifically for railway vehicles

To predict what the effects of vibrations are on comfort, frequency weighting should be applied, in which case for example a frequency of 10 Hz is weighted a lot higher than a frequency of 100 Hz,

see Figure 2.4. Frequency weighting improves the comfort assessment of the measured or modelled vibrations and makes it possible to check if accelerations are perceived comfortable according to ISO 2631, see Table P.1 in the appendix of this report.

## 2.3 Bridge

Among the various types of long span railway bridges (see Table O.1), truss bridges and arch bridges are the most widely used types in the Netherlands. There are three types of arch bridges, true arch bridges, through arch bridges and tied-arch bridges, as seen in Figure 2.5.



(a) Victoria Falls Bridge, Zimbabwe [16]



(b) Bayonne Bridge, USA [17]



(c) Neville Island Bridge, USA [18]

**Figure 2.5:** Types of arch bridges: true arch (a), through arch (b) and tied-arch (c).

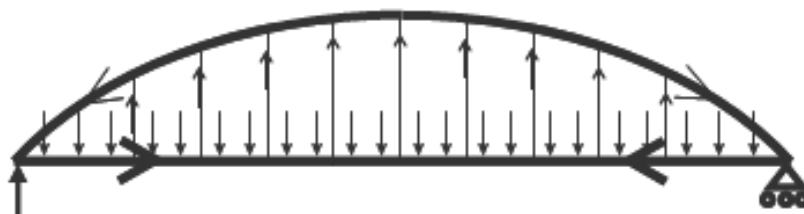


**Figure 2.6:** Tied-arch bridge loading [19]

In this report the focus will be on tied-arch bridges, where the horizontal thrusts are balanced

by a tensile tie, see Figure 2.6. Therefore the bearings are mainly loaded by vertical loads due to bridge self-weight and trains, although horizontal loads still occur due to e.g. braking of the train. Often two arches are made which are laterally connected by braces, to prevent out-of-plane buckling and withstand wind loads. The arch is connected to the main girders through hangers. In this report tied-arch bridges with vertical hangers will be analysed, but they also exist with other hanger configurations such as diagonal hangers. Depending on the stiffness distribution between stiffening girder and arch, the tied-arch bridge can be further classified, as can be seen in Figure 2.7.

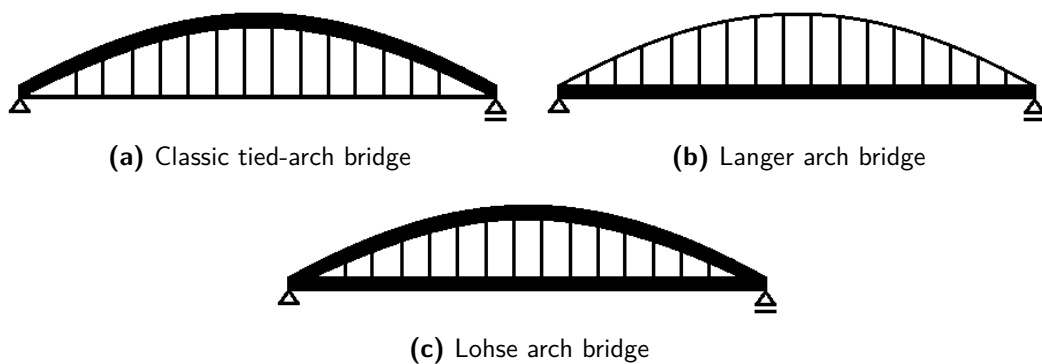


**Figure 2.7:** Various tied-arch bridge types based on [20, fig. 10.46]

More information can be found in Appendix B.

## 2.4 Railway track

The railway track is situated between the bridge and the vehicle. For the classic ballast track this includes the rails, fasteners, sleepers, ballast and subgrade, see Figure 2.8a. For ballastless track, the rails are directly fastened to a concrete slab or the bridge deck, which replaces the ballast.

Depending on the goal of the analysis, the railway track can be schematized at various levels of complexity, some of which can be seen in Figure 2.8b. This figure shows three models:

- (a) Most simple is a beam on an elastic foundation with continuous distributed stiffness and damping;
- (b) For higher frequencies (100 Hz to 1000 Hz) a double beam can be used; [21, page 116]
- (c) Discrete support which model the sleepers, can simulate the sleeper effect, which is similar to the cross-beam effect (see subsection B.2.5).

To take high frequency vibrations into account, the rail/wheel contact should be modelled with a Hertzian spring. When considering low frequency vibrations on the other hand, simpler models can be used and the track stiffness can be neglected. [21, page 113] In this report the latter is applicable. The frequency range relevant for comfort is 0.5 Hz to 80 Hz, therefore it is sufficient to model the track as part of the bridge. [10]

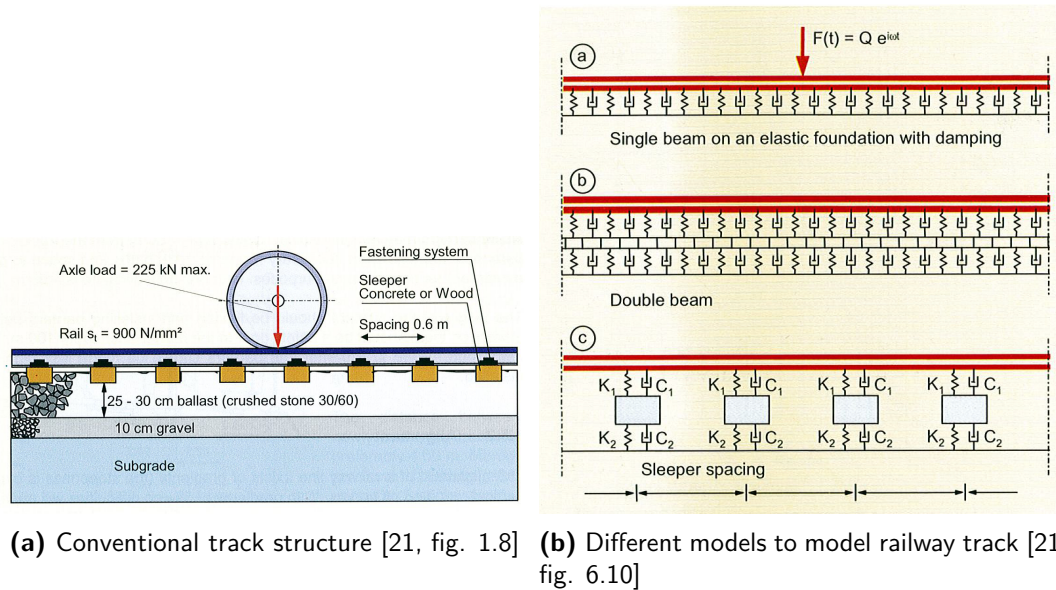


**Figure 2.8:** Track structure (a) and track modelling (b).

## 2.5 Train

Trains consist of coaches, which exist with conventional bogies, articulated bogies or single axles, see Figure 2.9.

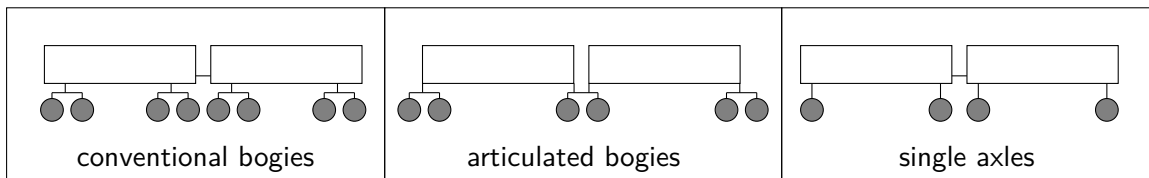


**Figure 2.9:** Three groups of coaches.

The Eurocode [1, par. 6.4.6] requires to consider real trains. In the Netherlands there are about 17 different types of passenger trains in service, see Table C.1. From these types the most used type, the VIRM train with conventional bogies is considered in this report, see Figure 2.10a.

With this train type each coach has two bogies. These bogies contain a suspension system split in a primary and secondary suspension, consisting of springs and dashpots/dampers. The VIRM double decker coaches use RMO 9000 heavy duty bogies which have coil springs and hydraulic dampers at all four wheels. In addition there are two air springs rubber sidebearer springs which act as secondary suspension. Although the exact damping and spring characteristics of bogies is usually not openly published, data has been obtained for the RMO 9000 bogie, which can be used to model the train. More information can be found in Appendix C.



(a) Dutch double decker coach (VIRM) [22]



(b) RMO 9000 motor bogie [23]

Figure 2.10: VIRM train (a) and its bogie (b).

## 2.6 Structural dynamics

An extensive review of the structural dynamics theory is outside the scope of this report. It is assumed the reader is familiar with the basic concepts of structural dynamics, reference is made to [24]. However, theory related specifically to the dynamics of railway bridges will be discussed. Several vehicle models of increasing level of complexity will be considered, as can be seen in Figure 2.11. In this section these models will only be discussed roughly, a more detailed consideration can be found in Appendix D.

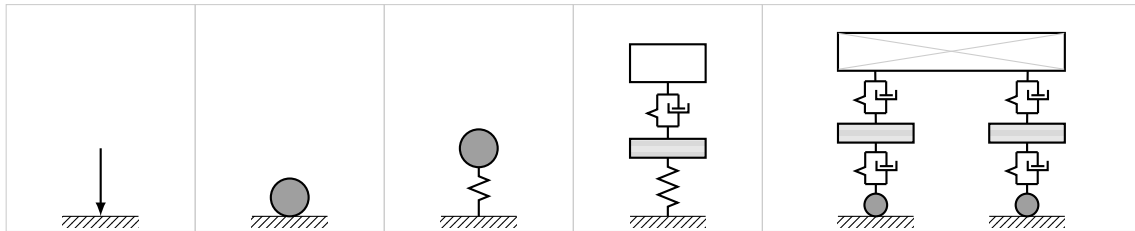


Figure 2.11: Vehicle as moving load, unsprung mass, 1 DOF sprung mass, 2 DOF sprung mass and full coach model based on [25, fig. 2.4]

### 2.6.1 Unsprung mass

When describing the train – bridge interaction two sets of equations of motions can be written, one for the bridge and the other for the vehicles. The contact forces make them coupled. [2, page 17-19] Initially the train is modelled as an unsprung mass, as can be seen in Figure 2.12.

The equation of motion related to the moving mass is

$$\underbrace{EI \frac{\partial^4 u_b(x, t)}{\partial x^4}}_{\text{beam stiffness}} + \underbrace{m_b \frac{\partial^2 u_b(x, t)}{\partial t^2}}_{\text{beam mass inertia}} = \underbrace{\delta(x - x_1)}_{\text{position}} \underbrace{[m_v g]}_{\text{mass gravity}} - \underbrace{m_v \frac{\partial^2 u_b(x_1, t)}{\partial t^2}}_{\text{mass acceleration}} \quad (2.5)$$

In this equation the horizontal position of the moving mass can be described with

$$x_1 = vt \quad (2.6)$$

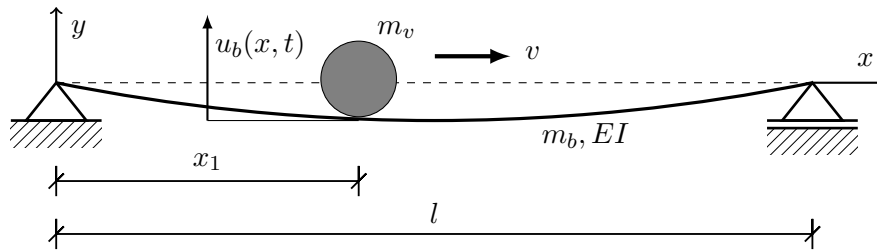


Figure 2.12: Moving unsprung mass (based on [5, fig. 3.21])

and the following parameters are used:

- $u_b(x, t)$  = deflection of beam, measured from original position [m];
- $E$  = Young's modulus of the beam [N/m<sup>2</sup>];
- $I$  = Moment of inertia of the beam in y-direction [m<sup>4</sup>];
- $m_b$  = beam mass per unit length [kg/m];
- $m_v$  = mass moving in x-direction [kg];
- $g$  = gravitational acceleration [m/s<sup>2</sup>];
- $v$  = speed of mass [m/s];
- $t$  = time [s];
- $\delta(x)$  = Dirac delta function.

A full derivation for this model can be found in section D.2.

### 2.6.2 1 DOF sprung mass

The unsprung mass, directly attached to the beam is not a good representation of a train. Therefore the more sophisticated model of a sprung mass in Figure 2.13 is analysed next, with a simple primary suspension system with one degree of freedom.

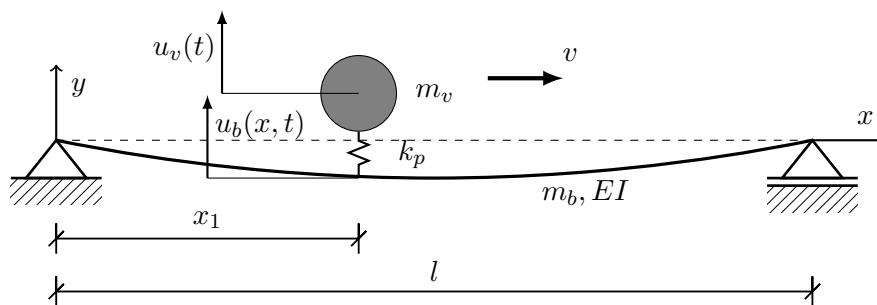


Figure 2.13: Moving sprung 1 DOF mass, based on [26, fig. 1]

The equation of motion for the beam can be expressed as

$$\underbrace{EI \frac{\partial^4 u_b(x, t)}{\partial x^4}}_{\text{beam stiffness}} + \underbrace{m_b \frac{\partial^2 u_b(x, t)}{\partial t^2}}_{\text{beam mass inertia}} = \underbrace{(-m_v g)}_{\text{mass gravity}} + \underbrace{k_p [u_v(t) - u_b(x_1, t)]}_{\text{spring force}} \underbrace{\delta(x - x_1)}_{\text{position mass}} \quad (2.7)$$

the equation of motion for the mass can be expressed as

$$\underbrace{m_v \frac{d^2 u_v(t)}{dt^2}}_{\text{mass acceleration}} + \underbrace{k_p [u_v(t) - u_b(x_1, t)]}_{\text{spring force}} = 0 \quad (2.8)$$

and the following new parameters are used:

- $u_v(t)$  = mass displacement, measured from static equilibrium position [m];
- $k_p$  = primary spring stiffness [N/m].

A full derivation of this model can be found in section D.3. In section D.4 a derivation for multiple moving 1 DOF sprung masses can be found as well.

### 2.6.3 2 DOF sprung mass

The bogies on a train actually have a more complex suspension system, consisting of a primary and secondary suspension. Therefore a more complicated model is proposed, see Figure 2.14.

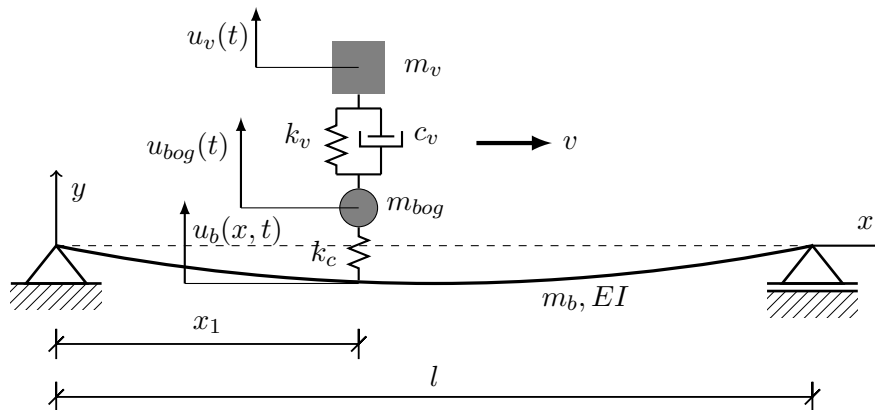


Figure 2.14: Moving sprung 2 DOF masses, based on [27, fig. 8.2]

The following new parameters are used in this figure:

- $u_{bog}(t)$  = bogie displacement, measured from static equilibrium position [m];
- $m_{bog}$  = mass of the bogie [kg];
- $k_s$  = spring stiffness secondary suspension system [N/m];
- $c_s$  = damping value secondary suspension system [Ns/m].

More on this model can be found in section D.5.

## 2.6.4 Full coach model

Finally the most complex vehicle model from Figure 2.11 is considered in this section, the full coach model. The main difference with the previous model is the addition of a rotational degree of freedom.

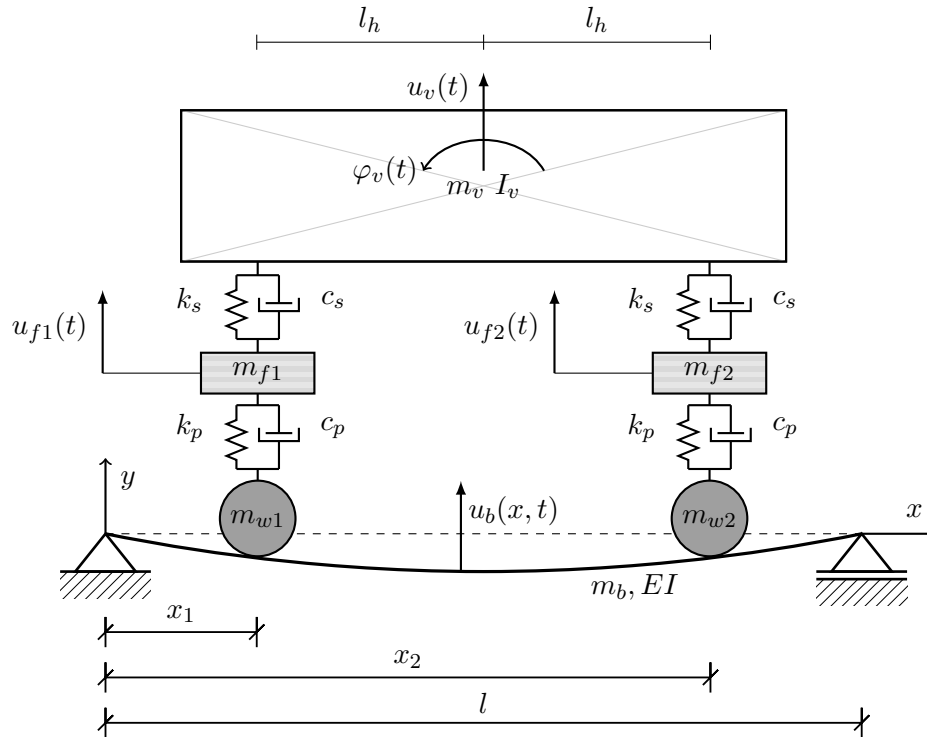


Figure 2.15: Full coach model with 4 DOF

New parameters in Figure 2.15 are:

- rotation  $\varphi_v(t)$  [rad]
- mass moment of inertia  $I_v$  [ $\text{kgm}^2$ ]
- position second bogie  $x_2$  [m]
- centre to bogie distance  $l_h$  [m]

More on this model can be found in section D.6.

## 2.7 Solution methods

An analytical solution for the equations of motion from the previous section has not been found yet. [3] Certain closed-form solutions are available, but in limited form, for example by Johansson et al. [28] The approach closest to an analytical solution is to solve the ordinary differential

equations by use of numerical solution methods, called an analytical-numerical solution method, which is worked out in Appendix E.

Since a numerical solution method is necessary either way, it is chosen to use the finite element modelling (FEM) approach, with the software package Ansys. In FEM software objects can be modelled as nodes connected by elements. Therefore the train and bridge were modelled using various elements such as masses, beams and spring-dashpots.

Various analysis types are possible in Ansys, but to model the dynamic behaviour a transient analysis should be used, where the time history of different parameters can be evaluated. The dynamic analysis can be explicit or implicit. With an explicit analysis the result in each step depends only on the quantities obtained in the preceding step and can be directly calculated. With an implicit analysis the expression for a step includes values pertaining to the same step, which means several iterations are needed each step. Because an explicit analysis has a maximum time step size and an implicit analysis does not, an implicit analysis can be done with larger and less time steps, causing the analysis to take less time to complete.

Various time integration methods are possible, such as the direct integration Newmark- $\beta$  method. In Appendix F more information about the finite element modelling can be found.



---

## Chapter 3

---

# Modelling

After having considered the relevant theory and background information in chapter 2, the process of modelling is explained in this chapter. First the choice for the Ansys model is explained in section 3.1. Afterwards the development of simple models and their verification is discussed in section 3.2. The more complex bridge models are presented in section 3.3 and the vehicle models in section 3.4. After a brief intermezzo about nodes and accuracy in section 3.5, a parameter study is presented in section 3.6. The chapter is concluded with an interpretation of the modelling results in section 3.7.

### 3.1 Model choice

When looking into literature to investigate if and how Ansys can be used to solve the dynamic train/bridge interaction, various methods are found. Two methods to model contact between train and bridge were distilled, which for convenience are labelled the:

- Contact force model;
- Direct contact model.

They will be discussed in the following subsections, as well as which model is chosen to be used.

### 3.1.1 Contact force model

In the so-called *contact force model* the interaction between the vehicle and the bridge is done by calculating a reaction force from the vehicle and moving this load along the bridge. The advantage is that a moving load is considerably simpler to implement in Ansys than a moving mass. The concept can be seen in Figure 3.1.

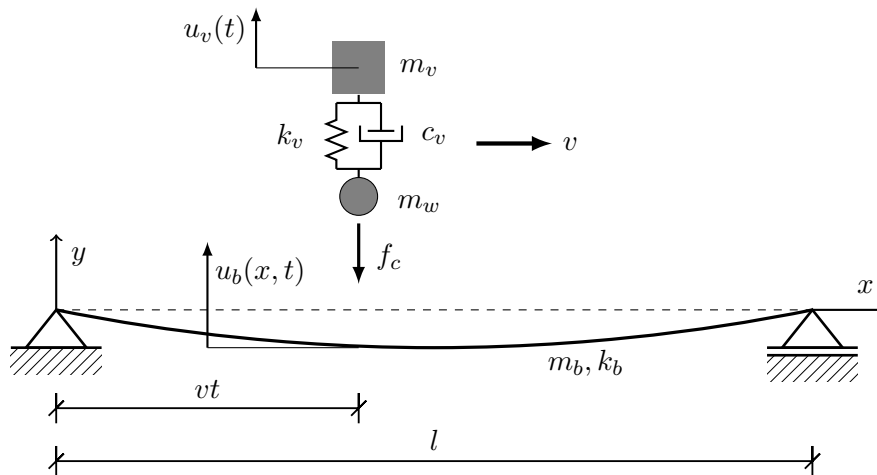
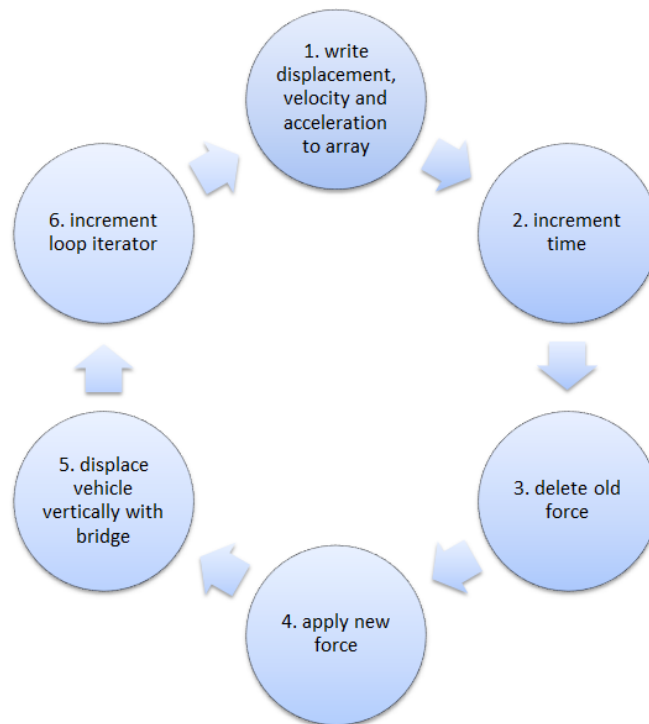


Figure 3.1: Contact force model

- $l$  = length of beam [m]
- $m_b$  = beam mass per unit length [kg/m]
- $k_b$  = beam stiffness [N/m]
- $v$  = velocity of sprung mass [m/s]
- $t$  = time [s]
- $g$  = gravitational acceleration [ $\text{m/s}^2$ ]
- $u_b(x, t)$  = deflection of beam [m]
- $u_v(t)$  = deflection of vehicle mass [m]
- $m_w$  = mass of wheel/bogie [kg]
- $m_v$  = mass of vehicle [kg]
- $k_v$  = spring stiffness vehicle [N/m]
- $c_v$  = damping value vehicle [Ns/m]
- $f_c$  = contact force [N]

Since the the bridge and the vehicles are physically decoupled and interact through contact forces, these must be manually defined in the APDL code. This is done by using a loop as can be seen in Figure 3.2. The code and a more detailed explanation how it works can be found in Appendix G.



**Figure 3.2:** Flowchart of running contact force model

### 3.1.2 Direct contact model

In the so-called *direct contact model* a different interaction system is used. The vehicles are directly put on the bridge and given a horizontal velocity. They interact with the bridge by connected contact and target elements, see Figure 3.3. This way of modelling has been used by other scholars as well, see Appendix H.

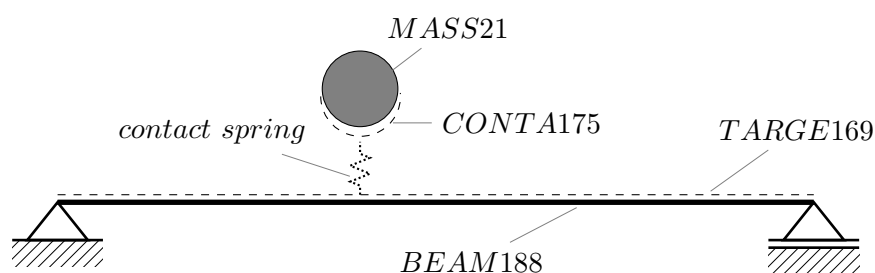


**Figure 3.3:** Direct contact model

Unfortunately the found Ansys code did not work any longer in the current version of Ansys, since certain contact elements were used which are currently deprecated. Adjustments were necessary by using modern contact and target elements, but because of the considerable amount of time needed to get this going it was chosen to not work out this way of modelling. In Appendix I further information about this model can be seen.

### 3.1.3 Choice

Eventually it was chosen to use the first model, the contact force model. The reasons to do this were mainly due to the ease of implementation in Ansys of this model, compared to the direct contact model. A smooth implementation of the direct contact model was limited due to:

- Complicated contact elements;
- Application of contact elements;
- Stiffness contact spring.

**Complicated contact elements** To implement the direct contact model in Ansys, contact elements (see subsection F.2.6) have to be used, which require quite some expertise to apply correctly. These contact elements have a lot of options which can be configured.

**Application of contact elements** Contact elements are more suitable for local contact problems and their use is computationally expensive if the target area is very large, which is the case for a bridge. Every time step the program has to determine at which positions the vehicle makes contact with the bridge, and since the whole bridge is a target area, it has to be searched every time.

**Stiffness contact spring** The contact elements make use of a contact spring to determine the amount of penetration of the contact element with the target element. Because both the steel train wheel and the steel bridge are very stiff, this contact spring is also very stiff. This causes large stiffness differences in the stiffness matrix and coefficient ratio errors.

Since the contact force model had none of these problems and could be implemented in Ansys relatively easy without compromise of accuracy, it was chosen to be used as model.

## 3.2 Simple models

After choosing the contact force model, it was first verified by comparing it to literature. However, instead of directly comparing the Ansys model to literature, an analytical-numerical solution was worked out in Matlab first, which was compared to literature in subsection E.1.3. Afterwards the Ansys model could be verified by comparing to the Matlab solution, which made it possible to vary parameters such as bridge length.

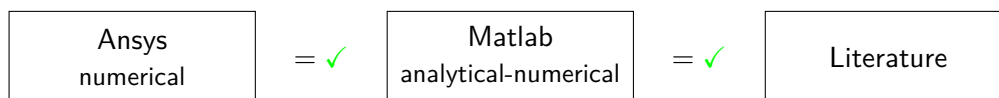


Figure 3.4: Simple model verification.

### 3.2.1 Single 1 DOF sprung mass on simply supported bridge

The first verification of the contact force model consisted of a simply supported beam with a single 1 DOF sprung mass moving over it. With a high enough node number (and thus small enough time step) this gave satisfactory results, see Figure 3.5. At a time of 0.6912 seconds a maximum difference of 3.8% is found. For the full verification the reader is referred to section K.1 in the appendices of this report.

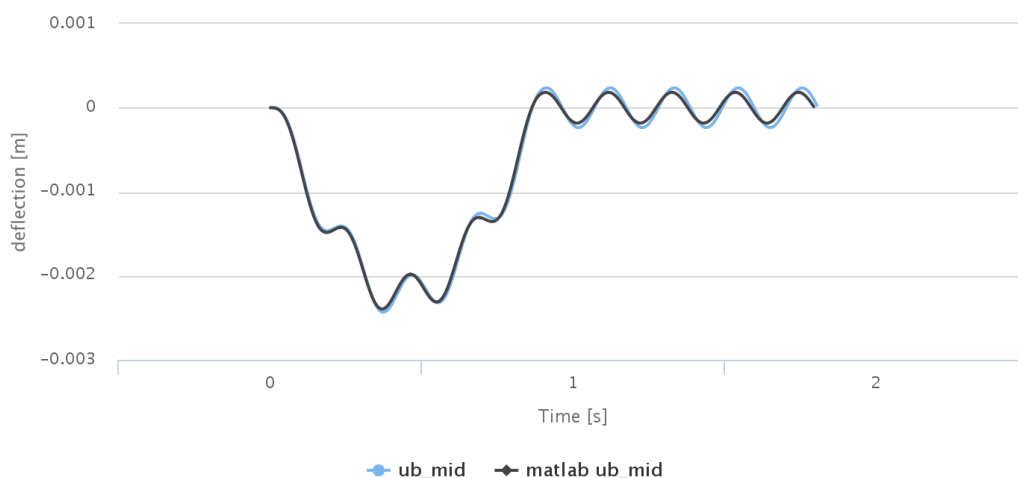


Figure 3.5: Comparison between Ansys (blue line) and analytical-numerical solution (black line). Bridge is a 25 meters long simply supported beam. A single 1 DOF sprung mass moves over it with a velocity of 100 km/h. See also [online](#), as well as the [raw ansys data](#) and [raw matlab data](#).

In Figure 3.5 it can be observed the bridge, which is undamped, continues to vibrate in its first natural frequency after the bogie has left the bridge. The frequency visible in the graph is 4.43 Hz, which is close to the first natural frequency of 4.77 Hz.

### 3.2.2 Multiple 1 DOF sprung masses on simply supported bridge

After the Ansys vehicle model of a single 1 DOF sprung mass was verified in the previous section, it was extended to a model of multiple 1 DOF sprung masses. The Ansys code and more information

about this model can be seen in Appendix J. This Ansys model was compared to the analytical-numerical Matlab solution, which can be seen in Figure 3.6. The code and more information of this Matlab model can be seen in section E.2.

The comparison between the Ansys model of two 1 DOF sprung masses and the Matlab solution can be seen in Figure 3.6. Here larger differences could be observed, but still within reasonable limits.

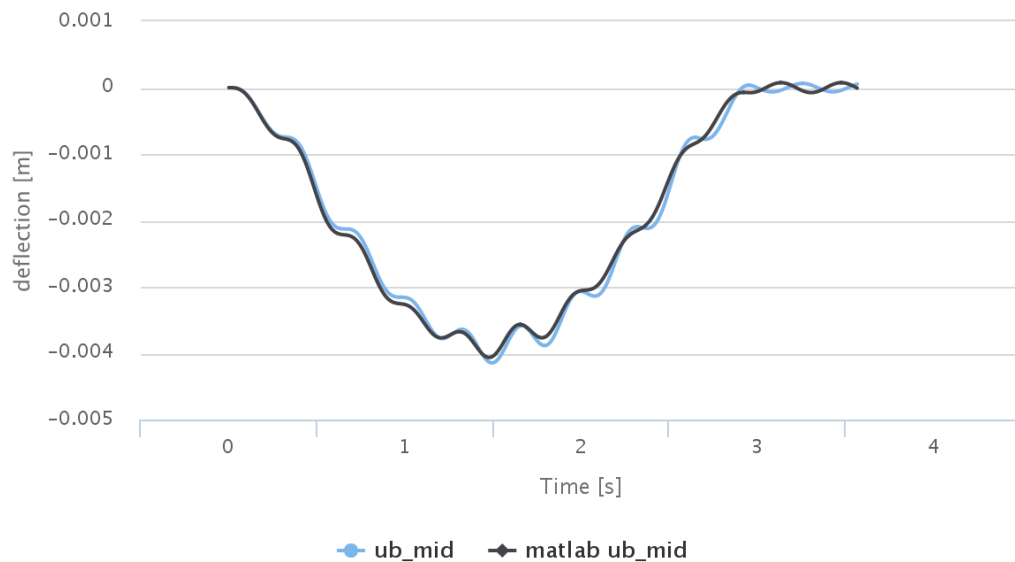


**Figure 3.6:** Midpoint bridge deflection, Ansys (blue line) compared to Matlab (black line). Bridge is a 75 meters simply supported beam. Two 1 DOF sprung masses spaced 8 meters move over it with a velocity of 100 km/h. See also [online](#), as well as the [raw ansys data](#) and [raw matlab data](#).

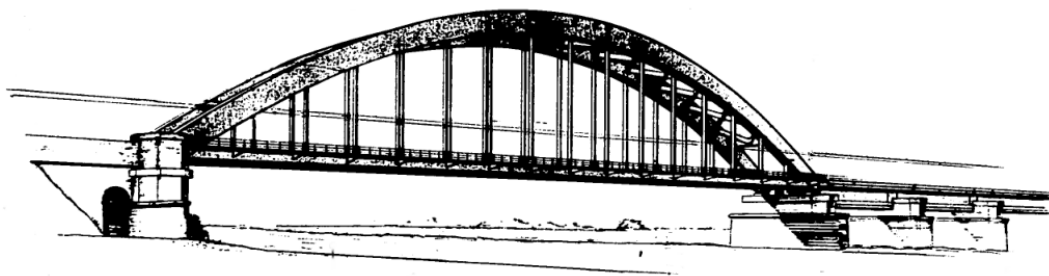
After this verification there was confidence it is possible to use any number of bogies and coaches to model the train. The train could now be modelled as twelve 1 DOF sprung masses at set distances, to represent six coaches with two bogies each. See section K.2 for a more detailed account of this verification.

### 3.3 Bridge models

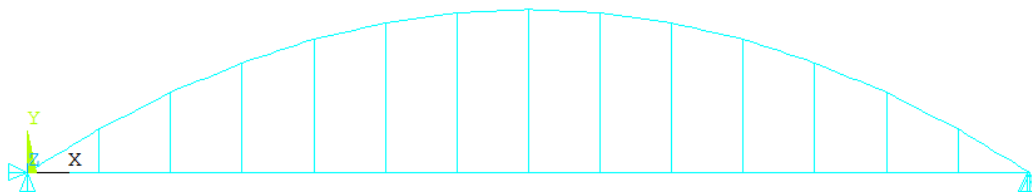
A tied-arch bridge with vertical hangers cannot be accurately modelled as a beam, the model used in the initial simple models. More complex bridge models are used, which include girders, hangers and arches. Properties of the Kuilenburgse spoorbrug, a railway bridge near Culemborg in the Netherlands are used, to be able to compare model results with measurements from reality. This steel bridge was constructed in 1981 and is 154.42 meters long. The model was initially made two-dimensionally, described in Appendix M. Afterwards a three-dimensional version was made as well, described in Appendix N.

#### 3.3.1 2D bridge model

A sketch of the Kuilenburgse spoorbrug and the two-dimensional Ansys model can be seen in Figure 3.7. The bridge is modelled as an arch, hangers and a girder, all with stiffnesses, areas and masses equivalent to the three-dimensional real situation.



(a) Sketch of Kuilenburgse spoorbrug [29, page A-3]



(b) Elements of 2D arch bridge model in Ansys

**Figure 3.7:** Drawing and model of arch bridge

To verify the accuracy of the 2D bridge model, two checks are performed. In subsection M.3.1 a distributed load is applied to the bridge girder and the resulting deflections from a static linear calculation in Ansys are compared to a simple hand calculation. The same is done with a distributed anti-symmetric load in subsection M.3.2. These verifications are meant to give a rough estimate to see if the model results are in the same order of magnitude as a hand calculation. In Appendix M the two-dimensional bridge model is further described.

Figure 3.8 shows the bridge deflection at the middle of the bridge and at one-quarter of the span length. It can be observed that the bridge deflection at one quarter of the span is larger than at midspan, a property known for tied-arch bridges with vertical hangers. Furthermore, for the bridge response it does not really matter which vehicle schematization is used for the train passing it.

The small wave-like vibrations visible in the plot correspond with the natural frequencies of the bridge. In subsection L.3.1 the results of the 2D tied-arch bridge model are further described.

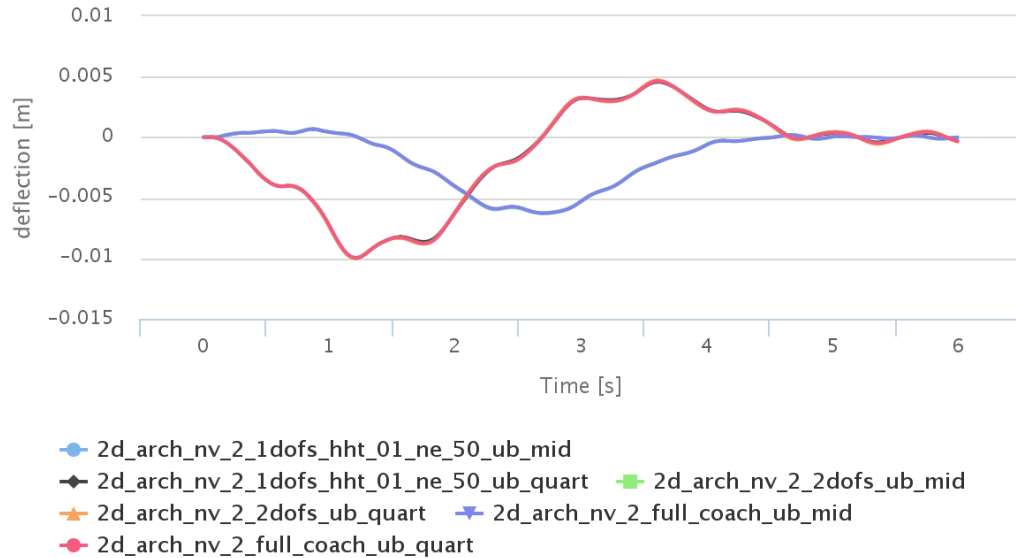


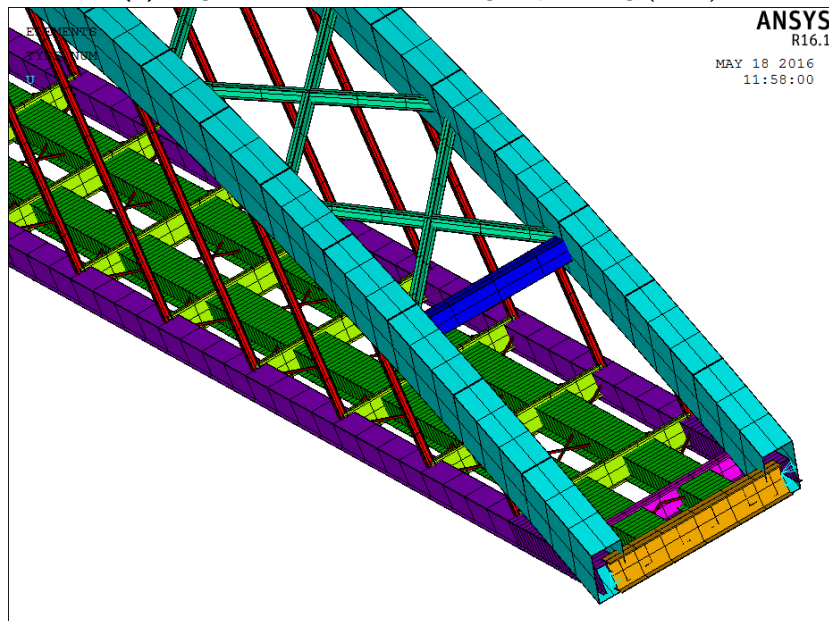
**Figure 3.8:** Comparison between 1 DOF bogie schematization, 2 DOF bogie schematization and full coach schematization. The train goes with a velocity of 125 km/h over the 2D bridge model. Blue, green and purple lines are the bridge deflection at midspan. Black, orange and pink lines are the bridge deflection at one-quarter-span. See also [online](#), as well as the [raw data 1 DOF](#), [raw data 2 DOF](#) and [raw data full coach](#).

### 3.3.2 3D bridge model

A three-dimensional model was made by expanding the two-dimensional bridge model. According to Ju and Lin the analysis of arch bridges should be three-dimensional. [30] They argue that the train loads are transmitted in a specific loading sequence through the rails, beam, girders, hangers and arches, which cannot be modelled properly in two dimensions. However, there is also another motivation for a three-dimensional model. A single train on a double track bridge causes an laterally eccentric loading, which is hard to model with a 2D model. An image is provided in Figure 3.9. In Appendix N the three-dimensional bridge model is further described.



(a) Angle view on the Kuilenburgse spoorbrug (2016)



(b) Ansys 3D bridge model

**Figure 3.9:** Photo and Ansys model of Kuilenburgse spoorbrug

Figure 3.10 shows the bridge deflection at the middle of the bridge and at one-quarter of the span length. The results for the 3D bridge model are comparable to the 2D bridge model. A full comparison can be found in subsection L.3.3.

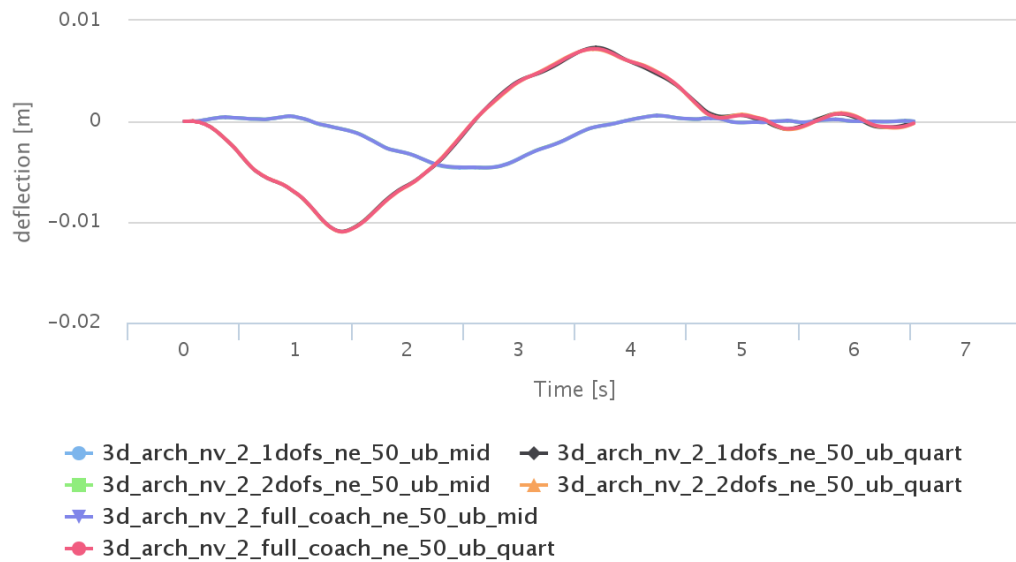


**Figure 3.10:** Comparison between 1 DOF bogie schematization, 2 DOF bogie schematization and full coach schematization. The train model goes with a velocity of 125 km/h over the 2D bridge model. Blue, green and purple lines are the bridge deflection at midspan. Black, orange and pink lines are the bridge deflection at one-quarter-span. See also [online](#), as well as the [raw data 1 DOF](#), [raw data 2 DOF](#) and [raw data full coach](#).

In subsection L.3.2 the results of the 3D tied-arch bridge model are further described.

## 3.4 Vehicle models

In section 2.6 it was already mentioned the train can be modelled at different levels of complexity. In this report is chosen to use three different vehicle models, a 1 DOF schematization, a 2 DOF schematization and a full coach schematization.

### 3.4.1 1 DOF schematization

To model the train as one DOF bogies some simplifications are made. The coach mass is split in two separate parts, it is assumed both bogies carry half the coach mass. Furthermore the primary suspension is neglected and only the secondary suspension is used, see Figure 3.11.

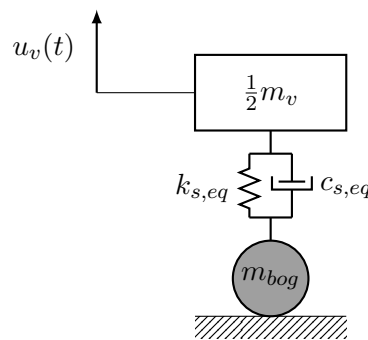


**Figure 3.11:** 1 DOF bogie schematization of RMO 9000 bogie

Figure 3.12 shows the acceleration of the vehicle above twelve 1 DOF bogies.

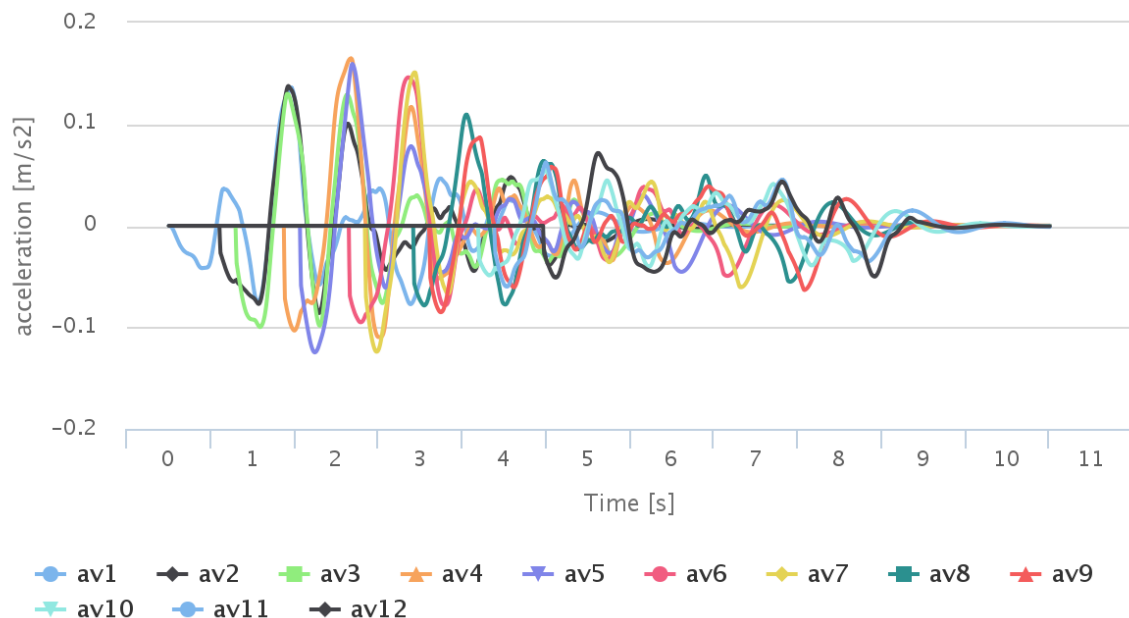


**Figure 3.12:** Vehicle acceleration above twelve bogies. The bogies go with a velocity of 125 km/h over the 2D bridge model. See also [online](#), as well as the [raw data](#).

In subsection L.4.1 the results of the 1 DOF vehicle model are further described.

### 3.4.2 2 DOF schematization

Modelling trains as one DOF bogies is still a crude model of trains, since the primary and secondary suspension in the bogies both play an important and distinct role in damping vibrations of different frequencies. Therefore the train is also modelled more realistically, using bogies with separate primary and secondary suspension, as seen in Figure 3.13. Furthermore, distinction can be made between motor and trailer bogies, which have different properties.

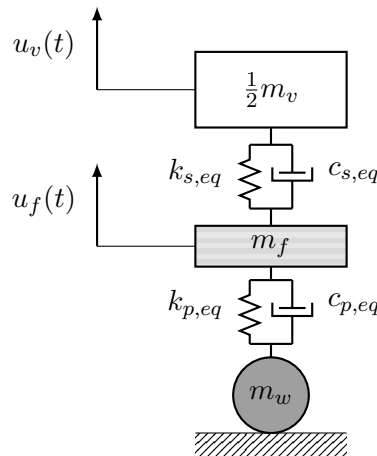


**Figure 3.13:** Simplified RMO 9000 bogie model to 2 DOF bogie.

Figure 3.14 shows the acceleration of the vehicle above twelve 2 DOF bogies.

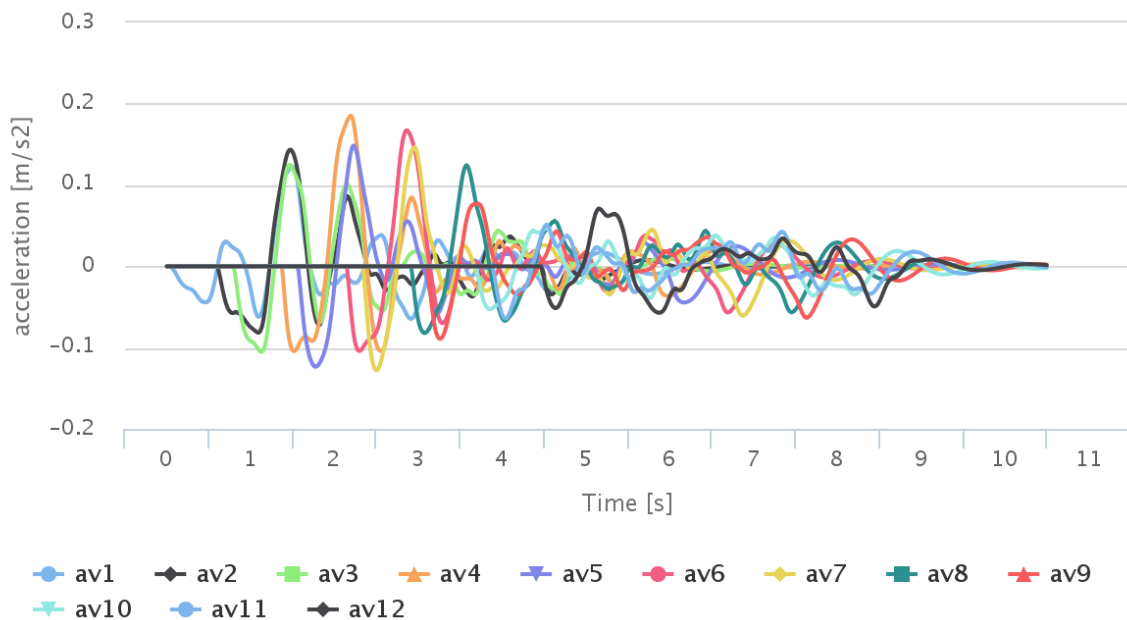


**Figure 3.14:** Vehicle acceleration above the twelve bogies. The bogies go with a velocity of 125 km/h over the 2D bridge model. See also [online](#), as well as the [raw data](#).

In subsection L.4.2 the results of the 2 DOF vehicle model are further described.

### 3.4.3 Full coach schematization

An even more refined model is the full coach schematization, as seen in Figure 3.15 and further explained in Appendix C. Modelling a full coach by connecting two bogies adds another degree of freedom (rotation of coach) in addition to vertical displacement. The front and rear part of a coach are now connected, causing an interlocking effect, where these parts are influenced by one another. [2, p. 262]

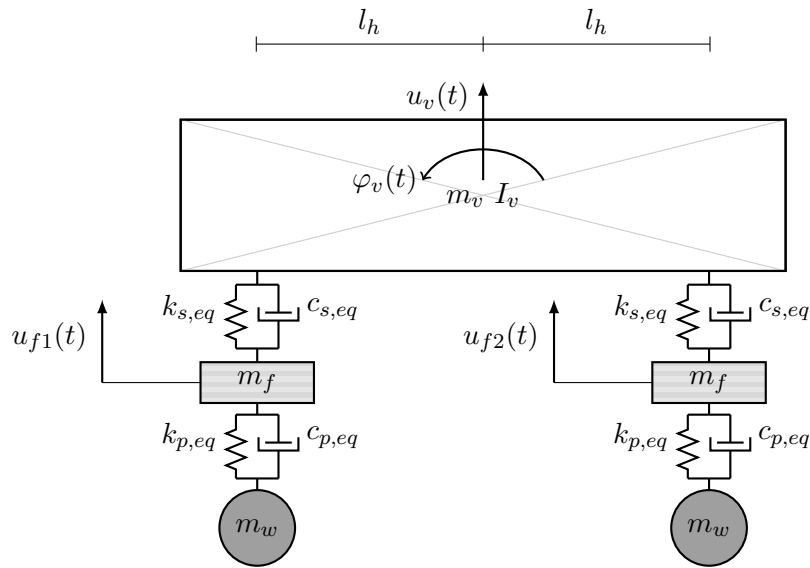


Figure 3.15: VIRM coach model with 4 DOF.

Figure 3.16 shows the acceleration of six coaches.

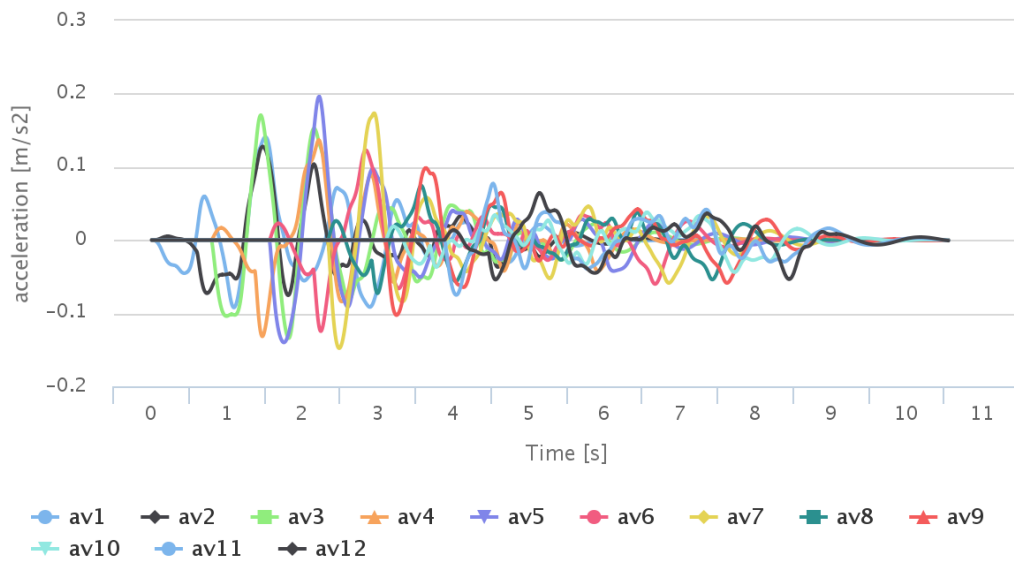
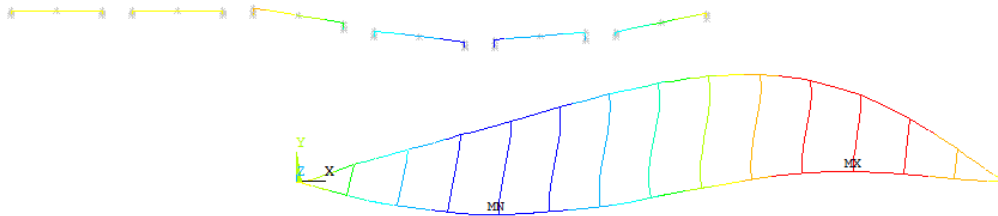


Figure 3.16: Vehicle acceleration of six coaches. The coaches go with a velocity of 125 km/h over the 2D bridge model. See also [online](#), as well as the [raw data](#).

Figure 3.17 shows the full coach model travelling over the 2D bridge model. The train model is at 60% of the bridge length, some coaches are completely on the bridge and deflect accordingly. The fourth coach is halfway on the bridge and only its front bogie is deflected, but its rear bogie is already influenced by the bridge.



**Figure 3.17:** Full coach vehicle model travelling over 2D arch bridge model, with displacements visible.

In subsection L.4.3 the results of the full coach vehicle model are further described.

### 3.5 Nodes and accuracy

In the verification of the models it was observed the simply supported beam could be accurately modelled with relatively few beam elements, which would mean only a few nodes with element are needed. However, the moving load can only be positioned at a node, not between them. Since the load moves at every time step, the number of nodes is directly related to time step length. For an accurate result a small time step is favourable, i.e. when the time step length decreases, the accuracy of the results increases.

Unfortunately this causes a conflict of interest. With the increasing number of nodes and the therefore decreasing time step and smaller discretization error, the number of elements in the stiffness matrix increases. With an increasing size of the stiffness matrix, the number of operations to accomplish row reduction increases. With these computations the arithmetic error increases. The machine accuracy of numbers often starts with 16 significant digits, but this number decreases due to round-off errors in fractions. The used time step length will therefore always be a trade-off between having the smallest discretization error and the smallest arithmetic error.

## 3.6 Parameter study

With the completion of the bridge and vehicle models, it is of interest to investigate which parameters largely influence the modelling results. Two parameters were investigated, the train velocity and the suspension damping.

### 3.6.1 Train velocity

The train velocity is a parameter which has influence on the maximum accelerations and thus on the passenger comfort. In this study the train velocity is varied from 50 km/h to 300 km/h and all other parameters are kept the same. The 2D bridge model is used as bridge model and the 2 DOF bogie schematization is used as vehicle model. This results in Figure 3.18. On the horizontal axis the vehicle velocity is shown, on the vertical axis the maximum acceleration (irrespective of the time it occurs during the ride) of the vehicle above the last bogie. Both parameters seem directly proportional, albeit some velocities which cause sudden peaks in acceleration.

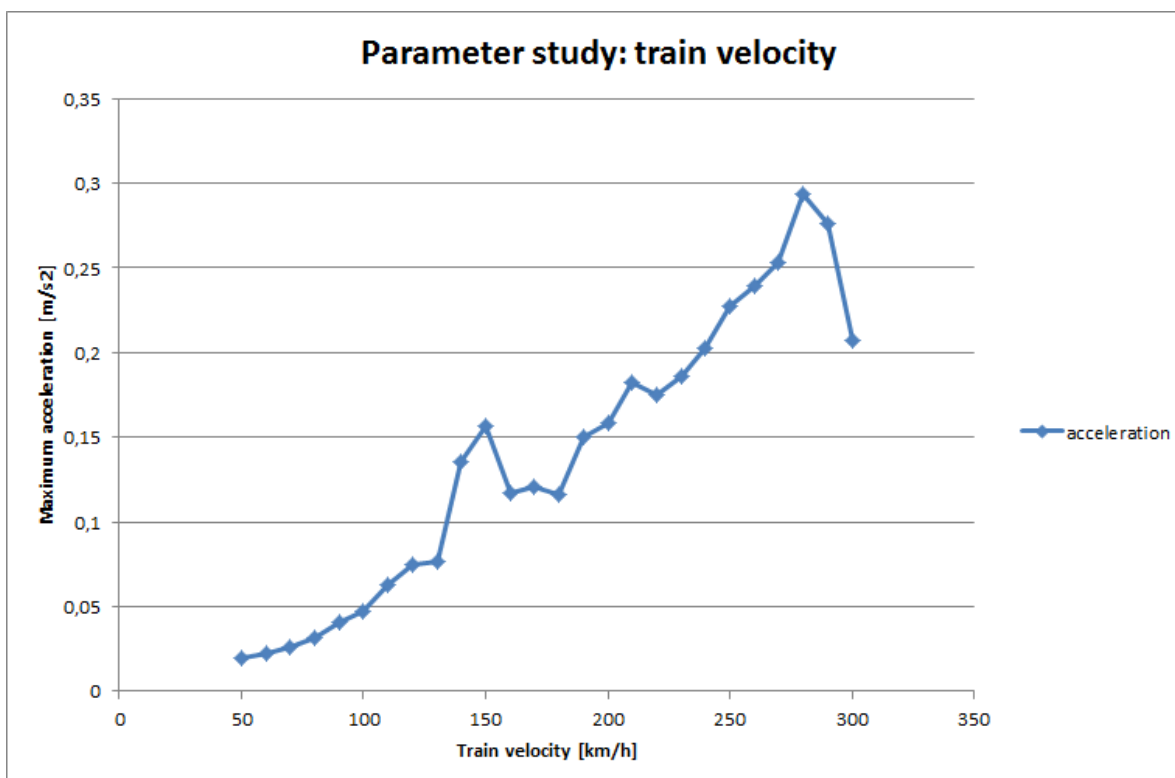
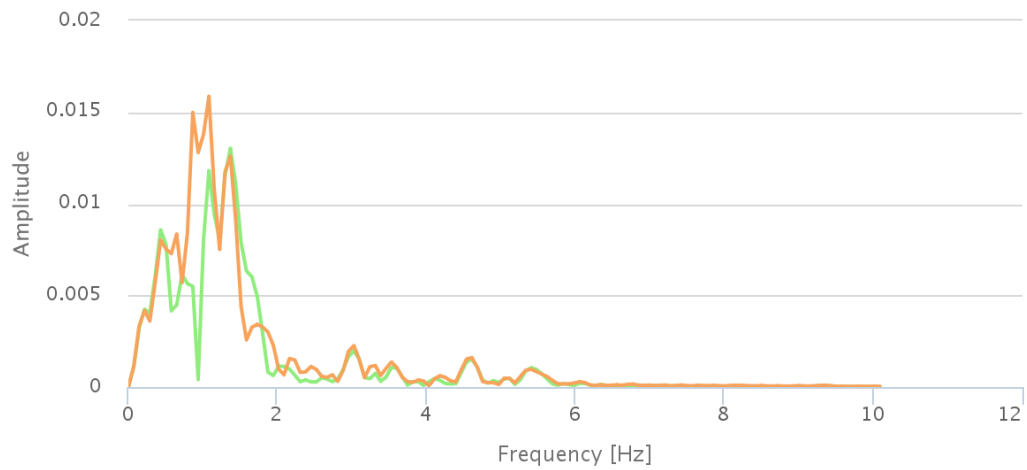


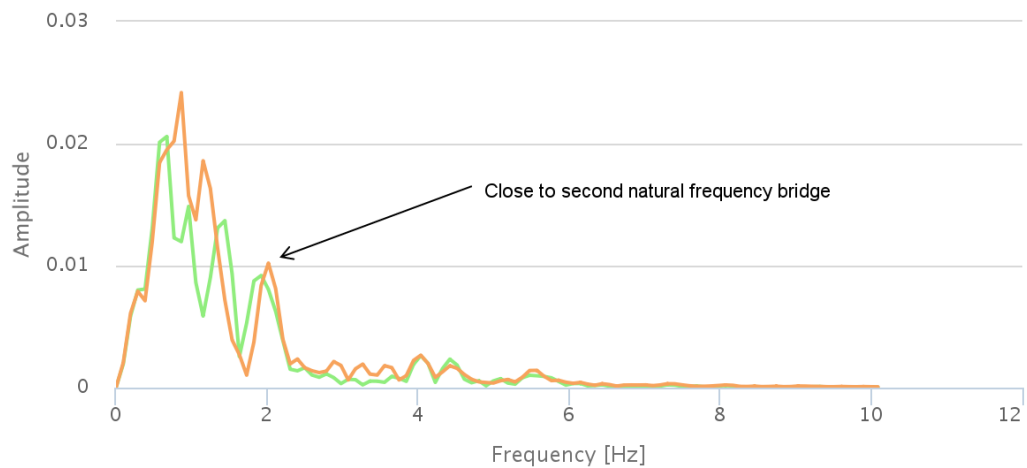
**Figure 3.18:** Parameter study of maximum acceleration of vehicle above the 12th bogie in the 2 DOF vehicle schematization, 2D arch bridge model, with increasing train velocity. See the separate graphs also [online](#).

The peaks in the acceleration can be explained in the following manner. In Figure 3.19 the Fourier transforms of the acceleration plots of a train velocity of 120 km/h (where there is no peak in Figure 3.18) and a train velocity of 160 km/h (where there is a peak) are compared. From this comparison it can be seen there is a peak in frequency in the second plot, close to the second natural frequency of the bridge, 1.91 Hz (see also subsection M.3.3). So if the vibration frequency

of the train gets close to a natural frequency of the bridge, there is an increase in acceleration of the train, caused by resonance.



(a) Frequency plot with train velocity 120 km/h



(b) Frequency plot with train velocity 160 km/h

**Figure 3.19:** Comparison between frequency plots with train velocity of 120 km/h and 160 km/h. Vehicles using 2 DOF bogie schematization travel over the 2D bridge model. See also online [here](#) and [here](#), as well as the raw data [here](#) and [here](#).

### 3.6.2 Suspension damping

The damping due to the suspension system in the bogies is also a parameters which influences the quantity of acceleration and by this the passenger comfort. Certain damping values can effectively damp out hindering frequencies and prevent resonance from occurring. The input data for the used bogies in section C.2 is a damping ratio for both the primary and secondary suspension of up to 25%. In this parameter study this damping ratio is varied from 0% to 25% with increments of 5%. Furthermore, three separate cases are considered:

- Vary primary suspension, but not secondary;
- Vary secondary suspension, but not primary;
- Vary both primary and secondary suspension at the same rate.

The results from these three cases are plotted in Figure 3.20. It can be observed that especially the secondary suspension damping has a significant influence on the accelerations.

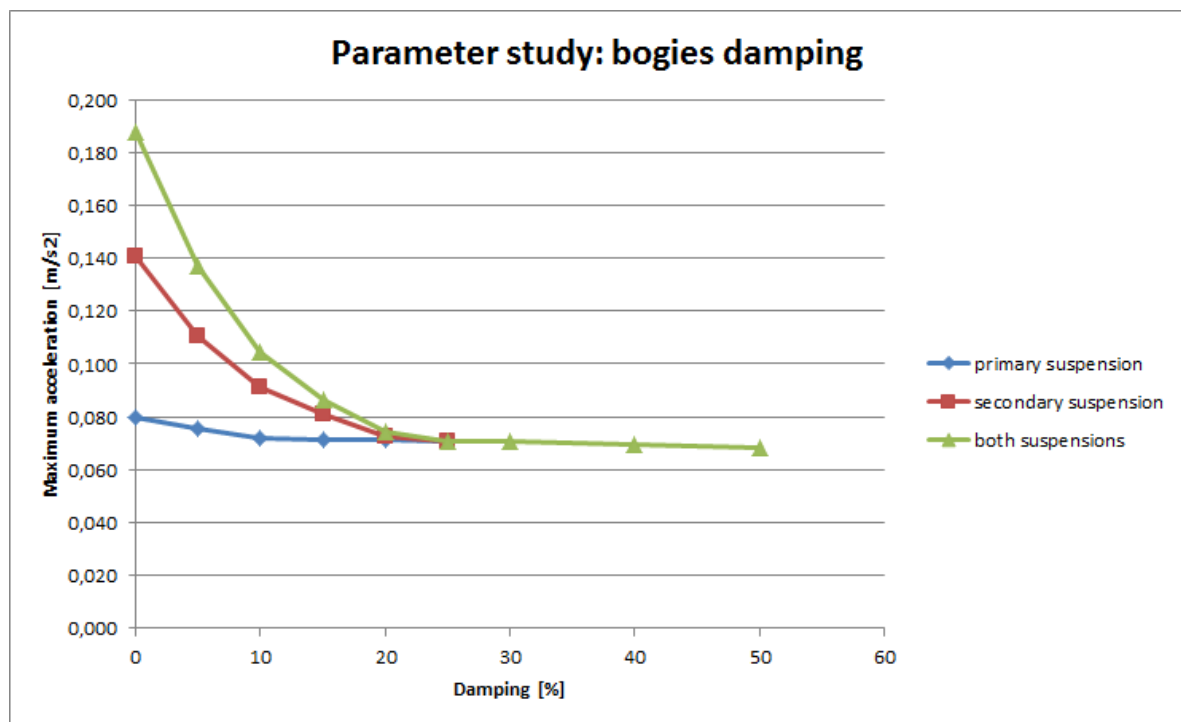


**Figure 3.20:** Parameter study of maximum acceleration of vehicle above the 12th bogie in 2 DOF vehicle schematization, 2D arch bridge model, with increasing suspension damping. See the separate graphs also [online](#).

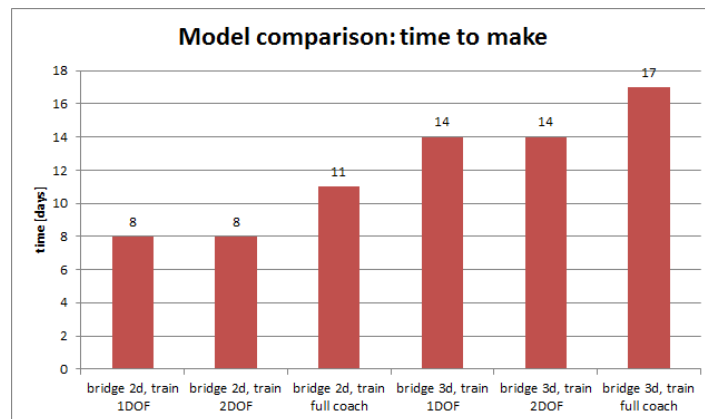
## 3.7 Model comparison

There exist two bridge models and three vehicle models, which can be combined in six combinations. See also section L.5.

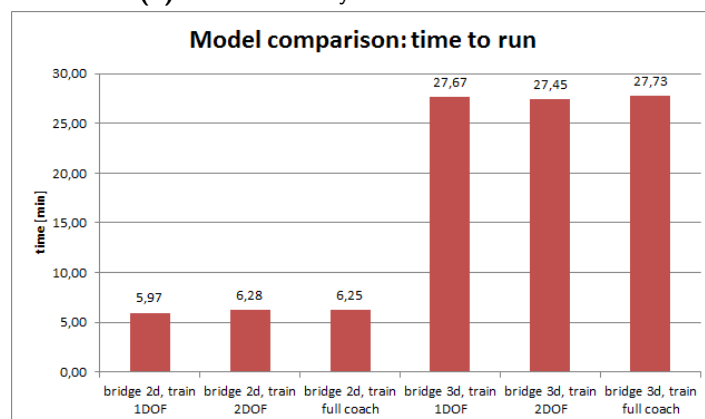
### 3.7.1 Computation

In Figure 3.21a a comparison among the six combinations of models can be seen, showing the time to make the models. These times are a rough estimate how much days it took to write the code for these models and all consist of a summation of time to write the bridge model and the time to write the vehicle model.

In Figure 3.21b a comparison among the six combinations of models can be seen, showing the time to run the models. These times are measured using 12 bogies or 6 coaches and 50 element between hangers, using Ansys 15.0 on a computer with an Intel i3-2310M CPU with 2.10 GHz, 8 GB RAM and a 256 GB SSD. One can observe the difference in time to run among the vehicle models is not significant, but the difference between the two bridge models is.



(a) Amount of days to make the models



(b) Amount of minutes to run the models

**Figure 3.21:** Comparison of models showing the amount of days to make (a) and the amount of minutes to run (b) the models.

### 3.7.2 Acceleration

To compare the accelerations of the different vehicle models, the relevant positions at which point their DOFs can be compared are labelled in Figure 3.22.

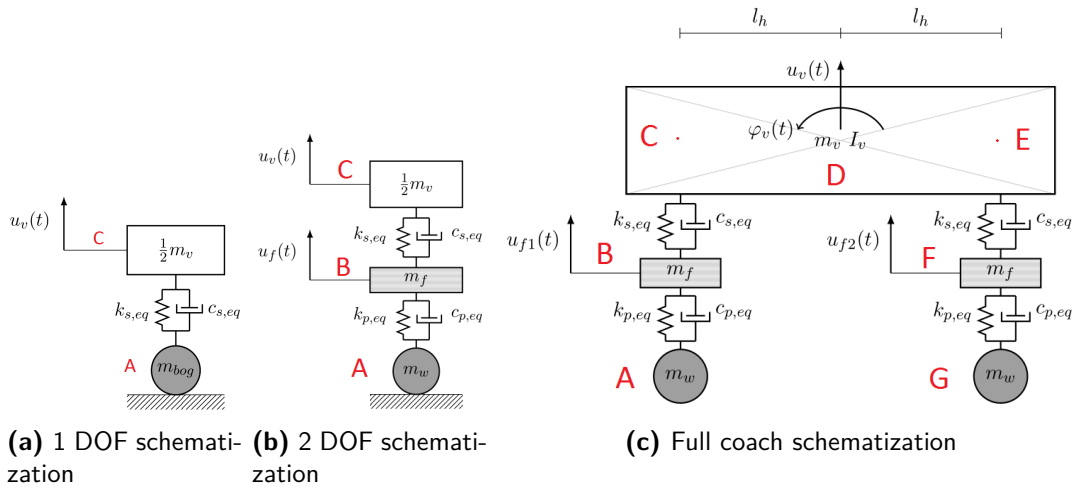


**Figure 3.22:** Various vehicle models

- Location A and G: vertical displacement ( $u_b$ ), velocity ( $v_b$ ) or acceleration ( $a_b$ ) of wheel mass or bridge at wheel position.
- Location B and F: vertical displacement ( $u_f$ ), velocity ( $v_f$ ) or acceleration ( $a_f$ ) of frame mass.
- Location C and E: vertical displacement ( $u_v$ ), velocity ( $v_v$ ) or acceleration ( $a_v$ ) of vehicle above bogie. For the full coach schematization it can be calculated as:  $u_v = u_m \pm u_r \cdot l_h$ .
- Location D: vertical displacement ( $u_m$ ), velocity ( $v_m$ ) or acceleration ( $a_m$ ) of full coach mass.
- Location D: rotation ( $u_r$ ), rotational velocity ( $v_r$ ) or rotational acceleration ( $a_r$ ) of full coach mass.

The comparison of the acceleration in the coach above the bogies is shown in Figure 3.23. This corresponds to the DOF  $a_v$  (acceleration vehicle), position C in Figure 3.22. The accelerations according to the 1 DOF and 2 DOF schematization are about 20 - 25 % lower than the full coach schematization. The results are comparable to Yang. [2, fig. 8.13]

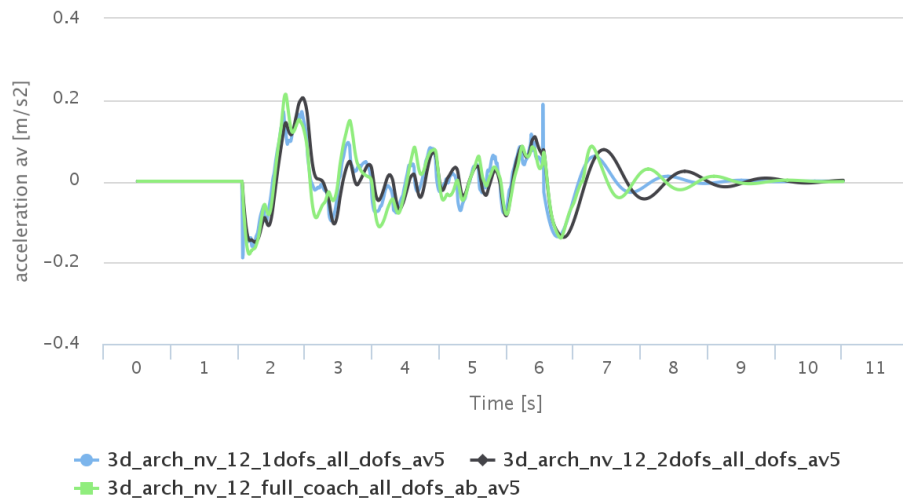


**Figure 3.23:** Comparison of 1 DOF bogie schematization, 2 DOF bogie schematization and full coach schematization travelling with a velocity of 125 km/h over the 3D bridge model. The acceleration of the vehicle mass at the position of the fifth bogie is shown. See also [online](#), as well as the [raw data 1 DOF](#), [raw data 2 DOF](#) and [raw data full coach](#).

In Figure 3.24 the frequency responses of Figure 3.23 are shown. It can be seen that the three vehicle schematizations have a very similar frequency response.

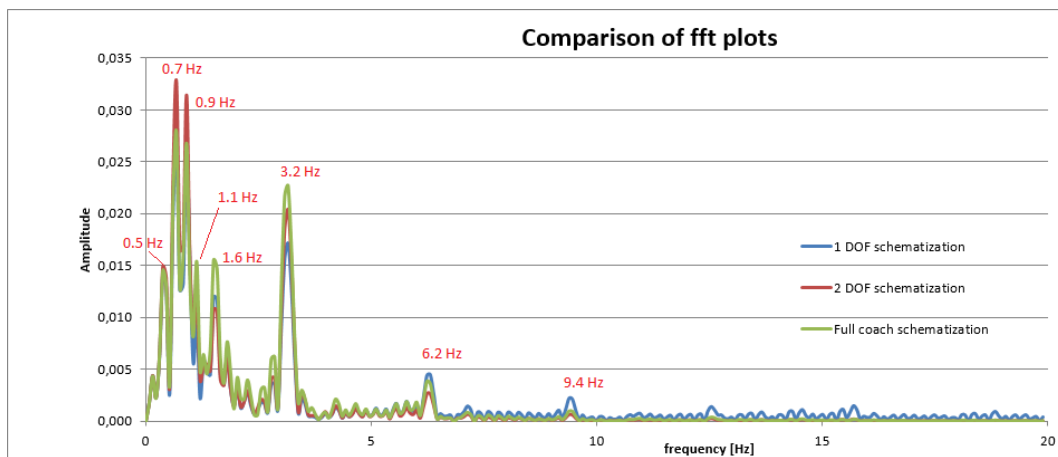


**Figure 3.24:** Comparison of vehicle model frequency responses. All are with the 3D bridge model, a train velocity of 125 km/h, taken from the sixth bogie. See also online [here \(raw data\)](#), [here \(raw data\)](#) and [here \(raw data\)](#).

The peaks at 0.9 Hz and 1.1 Hz are most likely related to the natural frequencies of the suspension system, determined in section C.3. The frequency responses at 3.2 Hz, 6.2 Hz and 9.4 Hz are related to the cross-beam effect, which is further explained in subsection L.5.2. The other peaks at 0.5 Hz, 0.7 Hz and 1.6 Hz cannot be directly related to a natural frequency of the vehicle or the bridge. However, it can be observed that they change when the train velocity changes, indicating that they are related to certain wavelengths.

In Figure 3.25 a comparison of the acceleration plots of the 2D bridge model and the 3D bridge model can be seen. The 3D bridge model features accelerations which can be 40% larger than

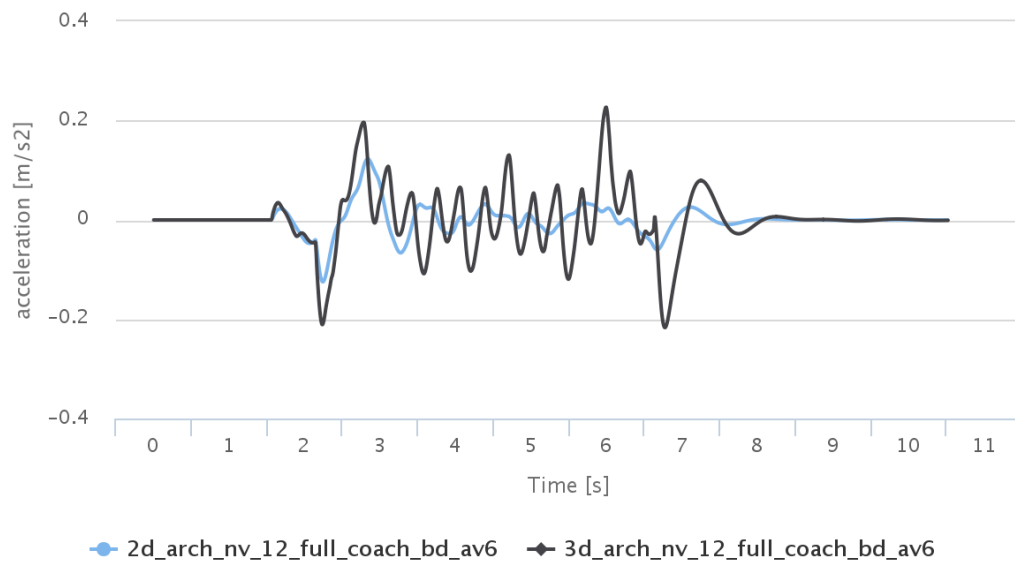


**Figure 3.25:** Comparison of 2D bridge model and 3D bridge model, both with the full coach schematization. Shown is the vehicle acceleration above the sixth bogie of the train model travelling at 125 km/h. See also [online](#), as well as the [raw data 2D](#) and [raw data 3D](#).

the 2D bridge model. This means the 2D bridge model heavily underestimated the quantity of the accelerations.

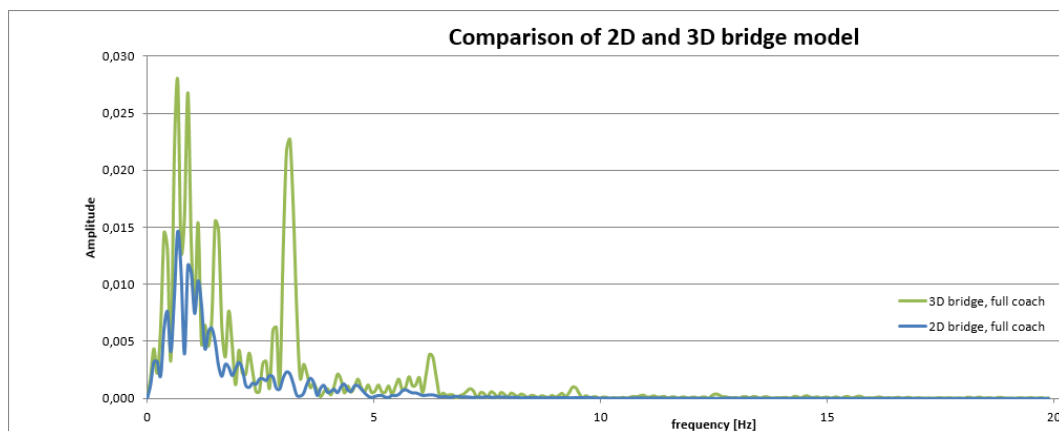


**Figure 3.26:** Comparison of frequency responses using either the 2D bridge model or the 3D bridge model. All are with the full coach schematization, a train velocity of 125 km/h, taken from the sixth bogie. See also [online here \(raw data\)](#) and [here \(raw data\)](#).

In Figure 3.26 the frequency responses of the acceleration plots from Figure 3.25 are shown. As the acceleration plots differ from each other, so do the frequency responses as well. The 2D bridge model is not so good in capturing the higher bridge frequencies related to cross-beam effect, mainly because the 2D bridge model has no transverse beams but only hangers.

In subsection L.5.1 a more elaborate comparison of all DOFs in the vehicle models is given.



---

## Chapter 4

---

# Measurements

In this chapter the measurements of accelerations in trains passing a tied-arch bridge are explained. First in section 4.1 it is explained why these measurements are necessary, what exactly is measured and how this is done. Afterwards several used standards are described in section 4.2. Then the conducted trial measurements are described in section 4.3 and the real measurements in section 4.4. For a more detailed report the reader is referred to Appendix O.

### 4.1 Why, what and how

Although the more simple numerical models of a sprung mass travelling over a simply supported beam could be verified with an analytical-numerical calculation, this was not feasible for more complex train models and the more complex tied-arch bridge models. To verify these models a comparison with real measurements seemed an appropriate approach.

For a Master's thesis written in 2002 [13], measurements in trains were done to investigate passenger comfort. Accelerations in lateral, longitudinal and vertical direction were performed using dedicated equipment. It was found 83.5 % of the discomfort is caused by vertical vibrations. [13, page 23] According to standards, if the weighted value determined in any axis is less than 25 % of the maximum value determined at the same point but in another axis, it can be excluded. [15] Roll vibrations are not so important in a railway coach, since passenger are seated above the centre of roll. [14, par. 12.3] Therefore it was chosen it would suffice to measure accelerations only in vertical direction.

According to research where several smartphones are compared to professional equipment, modern smartphone accelerometers have an inaccuracy of only 1 % to 5 %. [31] Since such a small inaccuracy seems reasonable, it was chosen to use a Samsung Galaxy Tab 2, instead of dedicated measuring equipment which would be more expensive and troublesome to get.

To process the data measured by the acceleration sensor, a smartphone application "VXaccelerator" was used. [32] With the used hardware it is able to measure accelerations in vertical direction with a sampling frequency of 63 Hertz. To measure the train velocity a smartphone with GPS is used.

## 4.2 Standards

How to perform vibrational measurements in trains is described in certain standards, more extensively examined in Appendix P. There is no single standard for measuring ride comfort in trains passing bridges, instead there are several more general standards dealing with mechanical vibration or ride comfort on railway track, not specifically on bridges.

ISO 2631-1 suggests to measure a weighted root mean square (RMS) acceleration for each translational vibration. The relevant frequency range for comfort is 0.5 Hz to 80 Hz, and the frequency-weighting curve  $W_b$  should be used for railway vehicles. If this results in values smaller than  $0.315 \text{ m/s}^2$ , the vibrations are likely to be assessed “not uncomfortable”.

ISO 2631-4 suggests to measure at the floor of railway vehicles, since seats and berths are likely to be replaced at some point in time. Measurements should be held at different locations in the coaches since vehicles cannot always be treated as a rigid body. The frequency range of motions expected to impact ride comfort significantly in the vertical direction, is 0.5 Hz to 20 Hz. As an alternative method to the RMS-based method a statistical method is suggested.

EN 12299 provides several methods to evaluate comfort, of which the Standard Method for Mean Comfort evaluation seems most appropriate for the purpose of this research. Motions with frequencies up to 40 Hz are expected to have an influence on comfort. Again it is suggested to measure at several locations in the coaches and to rigidly fix the transducer to the interface to prevent movement. It is suggested to record several metadata such as weather or vehicle loading conditions which can influence the measurements.

These standards provide good insights on the way to properly measure accelerations for comfort assessments. Because of practical limits, not all requirements from the comfort standards are followed exactly. Lack of time and manpower prevents the author from measuring at different locations in a coach. Several other suggestions from the standards are followed, such as recording metadata of measurements like weather and vehicle loading conditions.

## 4.3 Trial measurements

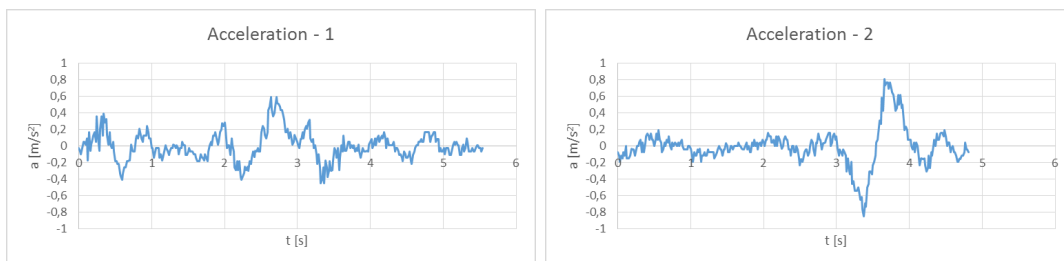
To test if the planned method of measuring accelerations works as intended, two measurements at the *Spoorbrug Twentekanaal* were done. Initially this bridge seemed a good candidate to perform the measurements on, but after closer inspection it became clear the hangers were not completely vertical but a little bit inclined, see Figure 4.1. This makes the bridge stiffer than a bridge with exactly vertical hangers, which is one of the reasons it was chosen to perform the real measurements on a different bridge.

Two measurements on the *Spoorbrug Twentekanaal* were done, the first during a ride from Zutphen to Deventer and a second one going back from Deventer to Zutphen. The measured acceleration time histories can be seen in Figure 4.2.

After the two measurements some interesting observations could be made. A very practical experience was the difficulty to determine the exact start and end times of the train being on the bridge. An improvement to the smartphone application would be GPS recording of the location, in order to derive the beginning and end of the bridge during post-processing. Furthermore it could be observed the two measurements differ in amplitude of acceleration. This can be



**Figure 4.1:** Spoorbrug Twentekanaal with hanger inclination clearly visible.



**(a)** Measurement 1, travelling from Zutphen to Deventer. **(b)** Measurement 2, travelling from Deventer to Zutphen.

**Figure 4.2:** Acceleration time histories of measurements performed in trains travelling over the Spoorbrug Twentekanaal.

explained by the fact both measurements were conducted at different measuring positions in the train. Furthermore, the direction of travel was not equal between both measurements. Lastly, the acceleration measured on the bridge were less severe than one could measure on adjacent normal track. It was expected a more severe bridge response would be noticeable in a longer bridge, with exactly vertical hangers and not slightly inclined such as is the case on the Spoorbrug Twentekanaal.

## 4.4 Real measurements

With the experience from the trial measurements, real measurements were conducted on the *Kuilenburgse spoorbrug*. For this purpose 8 trips between Station Utrecht Centraal and Station 's-Hertogenbosch were made on intercity VIRM trains. The measurements were done using a tablet with an acceleration sensor and application to process the data, which was positioned on the vestibule floor of the last coach of the train, see Figure 4.3.



**Figure 4.3:** Photo of experimental setup, location of measuring device on vestibule floor of train.

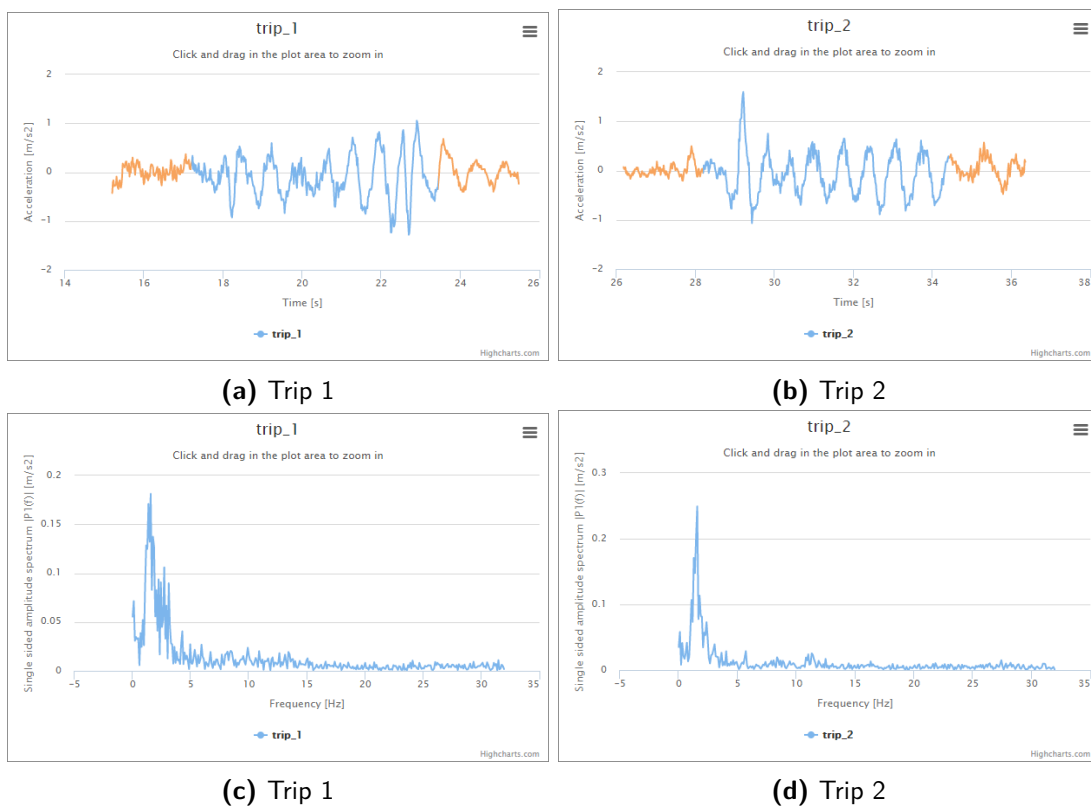
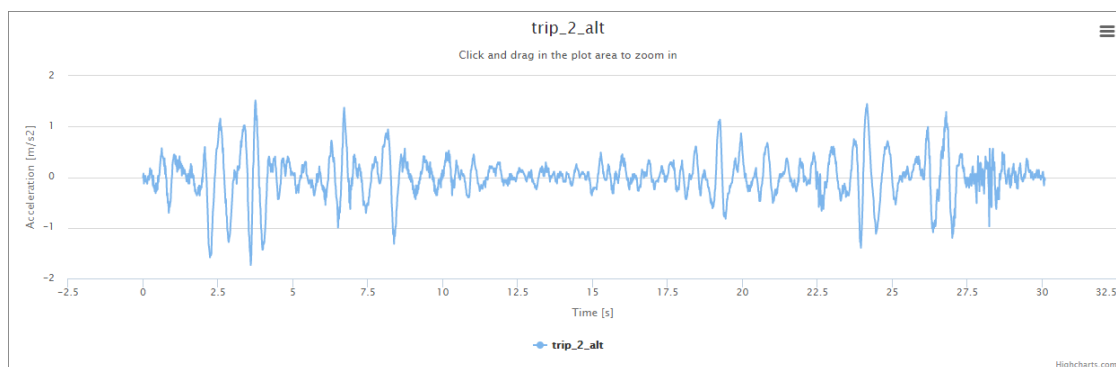


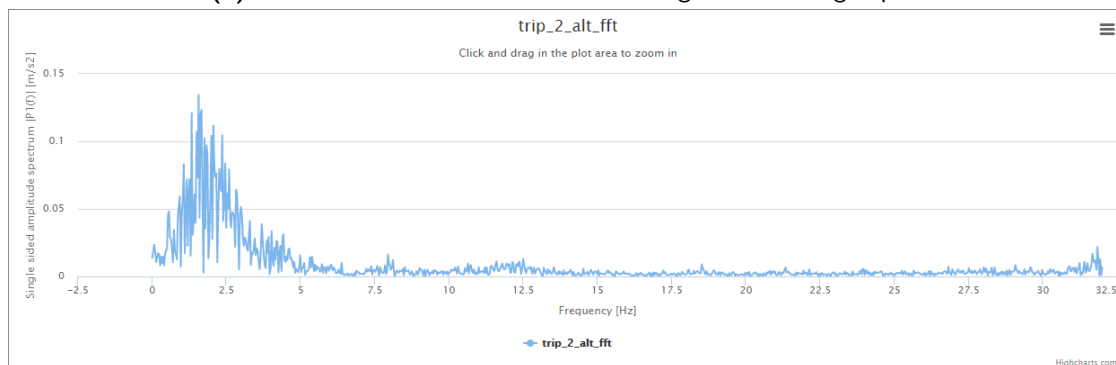
**Figure 4.4:** Selection of [acceleration](#) plots and their [fourier transforms](#) of real measurements, more in Figure O.5 and Figure O.6. The blue parts of the graphs denote the part of the acceleration measurements on the bridge, as estimated. See also the [raw data](#).

In Figure 4.4 the acceleration measurements of the first two trips can be seen. The recording was started some time before the bridge and ended some time after the bridge. It was attempted to capture the start and end moment of the bridge, which is marked blue in the graphs. Because it was difficult to determine these moments accurately an error of  $\pm 2$  seconds can be expected.

The measured accelerations are consistent, when distinguishing between the two directions of travel. In Figure 4.4 also the fourier transformation of the acceleration measurements can be seen. The dominant frequencies from the fourier transform also show consistency among all measurements. The difference in acceleration time histories between the trips from Utrecht, or the trips towards Utrecht can be explained. When approaching the tied-arch bridge from Utrecht, the train runs over approach bridges first. However, when approaching from 's-Hertogenbosch, the bridge directly starts after the regular railway track, without approach bridges. The uneven transition from settled soil to bridge is the most probable cause for the large peak at the beginning of the acceleration signal of the even numbered trips.



(a) Acceleration measurement of non-bridge track during trip 2.



(b) Fast fourier transform of the acceleration time history.

**Figure 4.5:** Acceleration plot and fast fourier transform of some non-bridge track. See also [online](#), as well as the [raw data](#).

When comparing the measurements on the bridge with those not on the bridge in Figure 4.5, several observations can be made. First of all the bridge is not more and not less comfortable than adjacent railway track. Both measurements contain peak with magnitudes as high as  $1.6 \text{ m/s}^2$ . The dominant frequency from both bridge and non-bridge measurements is approximately 1.5 Hz. This implies the frequency is not related to the bridge per se, but to the free vibrations of the coach mass.

#### 4.4.1 Comparison with Ansys

In Figure 4.6 a comparison of the measurements and Ansys model (3D arch bridge with full coach vehicle schematization) results is shown. The measurements show a big peak in the beginning, which is most likely due to the bridge-to-land transition. The measurements contain accelerations with amplitudes about five times higher than the Ansys model.

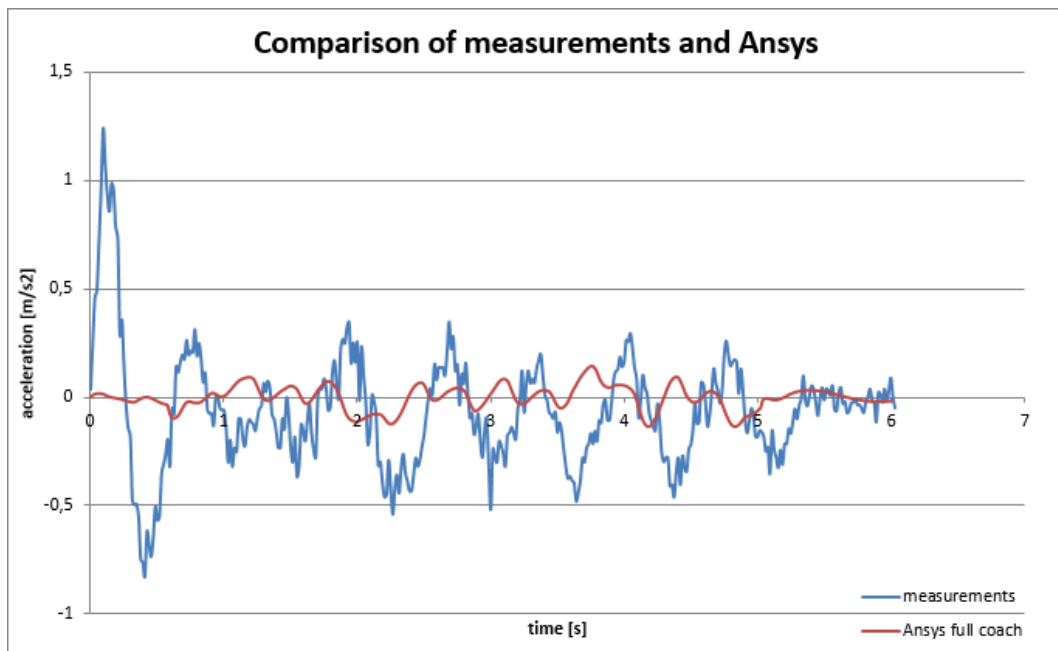


**Figure 4.6:** The blue line is an average of the even numbered measurements, the red line is the vehicle above the last bogie of the full coach vehicle model travelling over the 3D bridge model with a velocity of 125 km/h. See also online the [measurements \(raw data\)](#) and the [Ansys model \(raw data\)](#).

Furthermore, the frequencies are compared in Figure 4.7. For the measurements, the frequency plot of a trimmed down version of trip 8 is used, starting at 6.8 seconds, trimming of the big peak at the start which is believed to be related to the bridge-to-land transition. Again, the measurements show considerably higher amplitudes than the Ansys model results, also at higher frequencies. The measurements show a high peak at 0.97 Hz, which can be explained as being close to a natural frequency of the train's bogies.

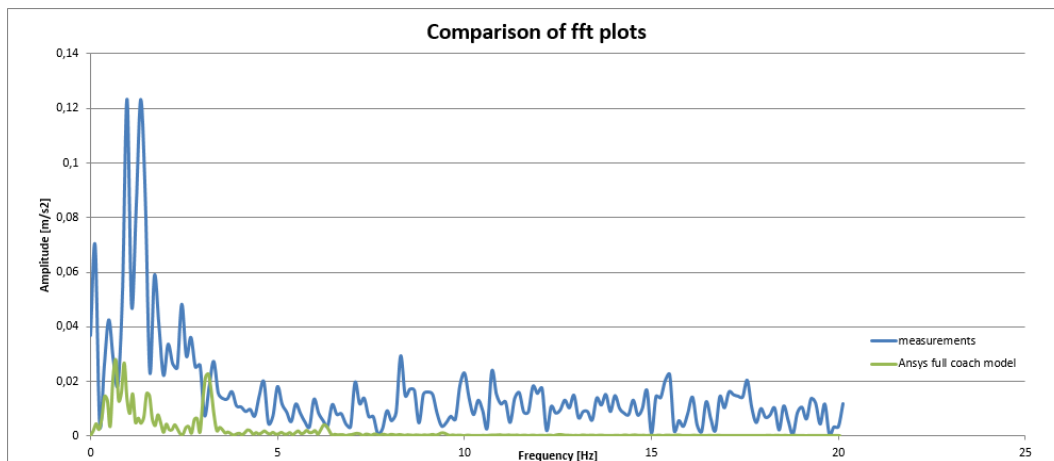


**Figure 4.7:** The blue line is the frequency response of the acceleration measurement of trip 2, the green line is the frequency response of the sixth bogie of the full coach model going over the 3D bridge model with a velocity of 125 km/h. See the measurements also [online \(raw data\)](#) and of the ansys model see also [online \(raw data\)](#).

From comparison of both the accelerations and corresponding frequencies it is clear the measurements do not correspond well with the Ansys model results.



# Conclusion

To determine the influence of Dutch trains passing over tied-arch railway bridges on passenger comfort according to Eurocode [4, par A2.4.4.3], a vehicle-bridge interaction model in the FEM software Ansys was made. Simple versions of this model were verified with an analytical-numerical method implemented in the numerical software Matlab. Afterwards two-dimensional and three-dimensional models of the Kuilenburgse spoorbrug were made, as well as three vehicle models of the Dutch VIRM train, with different levels of complexity. To obtain some real data for validation purposes, acceleration measurements were performed in a Dutch VIRM train while travelling over the Kuilenburgse spoorbrug, a tied-arch bridge in the Netherlands.

### 5.1 Conclusions

Concerning the literature review of the structural and comfort standards, the following conclusions can be drawn:

1. Dynamic calculations of railway bridges prescribed by the Eurocode ([4], [1]) are not rooted in the older Dutch codes but are based on UIC leaflets. This means older Dutch bridges are not designed according to this dynamic criterion. One could wonder if the Eurocode passenger comfort criterion [4, par A2.4.4.3] is really relevant for normal speed bridges.
2. The Eurocode  $1.0 \text{ m/s}^2$  comfort criterion [4, par A2.4.4.3] is a limited consideration of passenger comfort, since comfort not only depends on magnitude, but also on frequency and duration of the vibration. [8] Using a comfort criterion where weighted RMS accelerations are considered, would be a more accurate consideration.
3. Since the frequency range related to passenger comfort is from 0 Hz to 40 Hz, [33] the dynamic modelling should be in such a way (complexity and amount of DOFs) that it can capture these frequencies. This for example means it is sufficient to model the railway track as part of the bridge. Models with beams on elastic foundation or rail/wheel contact with a Hertzian spring are not necessary, since they are only needed to capture higher frequency vibrations. [21, page 113]

Concerning the modelling, the following conclusions can be drawn:

1. **Vehicle models** In general, the three vehicle models show comparable results and have comparable computation times. The 2 DOF bogie schematization shows less extreme peaks at the start/end of the bridge, compared to the 1 DOF bogie schematization. The full coach schematization has peaks 20 to 30 % larger than the 2 DOF schematization. The difference in frequencies among the vehicle models is small, but the accelerations of the simpler vehicle models are non-conservative. Therefore it is advised to use the full coach schematization for the train.
2. **Bridge models** The 2D and a 3D bridge models show good agreement with each other in a static comparison. The 3D bridge model shows natural frequencies which deviate 20 % from the 2D bridge model. Furthermore the 2D bridge model does not take lateral behaviour into account, which could be fixed with a lateral deflection correction factor. Because the accelerations with the 3D bridge model are up to 40 % larger than the 2D bridge model it is advised to use the 3D bridge model.
3. **Influence velocity** With an increasing train velocity, the acceleration inside the train increases as well. This increase is proportional, apart from several peaks at certain velocities. At these velocities, the vibration frequency of the train (which depends on the train velocity), collides with a natural frequency of the bridge, causing a higher acceleration amplitude due to resonance. Therefore it is wise to run the model over a range of velocities, since the maximum acceleration is not necessarily found at the maximum train velocity.
4. **Influence damping** The secondary suspension damping has a lot larger influence on the maximum acceleration than the primary suspension damping. Increasing the damping above 25 % has a negligible effect on the acceleration. The damping parameter is a parameter which has a significant influence on the results, but is generally only known to the bogie supplier. It can be used to calibrate the model results with measurements.
5. **Governing bogie** In contrast to literature [34], the last bogie does not show the governing accelerations. Depending on velocity and vehicle model, the governing bogie is a little before the middle of the train, varying between the third and sixth bogie, which is the moment the bridge is loaded by the greatest portion of the train.
6. **Model choice** The contact force model is the preferred implementation in Ansys Mechanical APDL 16.1, over the direct contact model. The drawbacks of the direct contact model are the need of complicated contact elements, which are more suitable for local contact problems and not efficient for VBI analysis. Furthermore, these contact elements work as contact springs, which are very stiff and cause large stiffness differences in the stiffness matrix.

Concerning the measurements, the following conclusions can be drawn:

1. Vertical acceleration measurements performed with a smartphone application during 8 trips show that the Kuilenburgse spoorbrug, but also the adjacent non-bridge railway track, is not so comfortable as prescribed by the Eurocode [4, par A2.4.4.3], as the limit of  $1.0 \text{ m/s}^2$  is exceeded multiple times. Especially the transition from the bridge to the adjacent tracks, result in large acceleration peaks. More attention should be paid to these transitions.

2. The acceleration measurements in a railway coach travelling over the Kuilenburgse spoorbrug and the results from an Ansys analysis are not in good agreement. This means that either the measurement results or the model results are incorrect. The Ansys model has its limitations, certain assumptions were made in the creation of the Ansys model, e.g. track irregularities were not included. Furthermore, the accuracy of the measurements is debatable, since only one measuring device was used, which was not calibrated on a shaker table.

## 5.2 Response to the research questions

The first research question is:

*In what ways can a dynamic vehicle-bridge interaction analysis to evaluate passenger comfort criteria prescribed in the Eurocode [4, par A2.4.4.3.3] be performed?*

Several methods were considered, but eventually the dynamic vehicle-bridge interaction was modelled with a “contact force model” in Ansys. Results of this modelling technique were compared to literature and an analytical-numerical method. A good comparison was found for one or more sprung mass(es) moving over a simply supported beam.

The second research question is:

*Is it possible, and if so, how can the dynamic analysis prescribed in the Eurocode [4, par A2.4.4.3.3] be simplified, not leading to unnecessary conservatism, with respect to engineering and material usage?*

During the analysis two bridge models and three vehicle models were considered and compared to each other. It was found that simplifying the bridge model by using a 2D version instead of a 3D version resulted in different natural frequencies, lower accelerations and neglecting the cross-beam effect. Therefore it is not recommended to simplify the bridge model, but use a full 3D bridge model. Furthermore it was found the vehicle models show comparable results, but the simpler vehicle models still show lower accelerations than the most complex vehicle model, indicating that in this area it is also advisable to use the full coach schematization as vehicle model.

## 5.3 Recommendations

In this section some recommendations for future research are given.

### **Realistic comfort criterion**

In the literature review it was found that the passenger comfort criterion as stated in the Eurocode [4, A2.4.4.3] is limited. It is recommended that if a comfort criterion is required, to use a comfort criterion with a frequency and time dependency, as suggested in ISO 2631. [10]

### **High frequency noise**

During the analyses high frequency noise was encountered, especially at discontinuities in graphs at the start/end of the bridge. To mitigate this phenomenon, instead of the Newmark- $\beta$  method the HHT method was used, which features numerical damping. More research is needed to investigate

what level of high frequency vibrations are realistic, i.e. to what extent this is purely a numerical error or physically existing behaviour.

**Location of measurements**

It is feasible to measure accelerations in a train moving over a bridge, but these measurements would be a lot more useful if they also contained a GPS location. This would make it easier to determine the start and end location of the bridge in the measurements. Therefore it is recommended that if acceleration measurements are performed in future research, to also record their exact location.

**Calibration of measuring device**

The used measuring device was neither calibrated on a shaker table, nor verified by comparison with another device. Such a calibration would certainly increase the reliability of the performed measurements and is recommended to do with further measurements.

**Transitions**

From the measurements it was found a large peak occurs at the transition of the bridge to the adjacent railway track. It would be interesting to investigate these bumps and ways to include them in the modelling.

# Appendices



---

# Appendix A

---

## Structural standards

In this appendix more detailed information on certain relevant Eurocodes ([4], [1]) and related structural standards is given. This appendix is referenced from section 2.1. It starts with a comprehensive look at the relevant Eurocode sections in section A.1 and section A.2. Afterwards a closer look at the history of the relevant structural standards is given in section A.3.

### A.1 Eurocode 1: Actions on structures - Part 2: Traffic loads on bridges

Section 6 of Eurocode 1, part 2 covers actions specifically for railway bridges, section 6.4 goes into more detail on dynamic effects. [1] In section 6.4.4 requirements for determining whether a static or dynamic analysis is required are given, which can be seen in Figure A.1.

The nodes in Figure A.1 contain requirements or statements which can be true or false. Assuming a maximum velocity of 160 km/h, according to section 1.4, the following requirements will be relevant.

#### 1 - Continuous bridge requirement

There is no dynamic analysis required for continuous bridges. This is the case if the three requirements from figure 6.9, note 5 [1, page 77] are fulfilled:

- The bridge meets the requirements for resistance, according to [4, A2.4.4];
- The bridge meets the deformation limits, according to [4, A2.4.4];
- The bridge meets the maximum coach body acceleration (or associated deflection limits) corresponding to a very good standard of passenger comfort, according to [4, A2.4.4.3].

#### 2 - First natural frequency limit

If the first natural frequency  $n_0$  is within the limits of [1, fig. 6.10], no dynamical analysis is required. Note that the span length on the horizontal axis of figure 6.10 goes up to 100 meters.

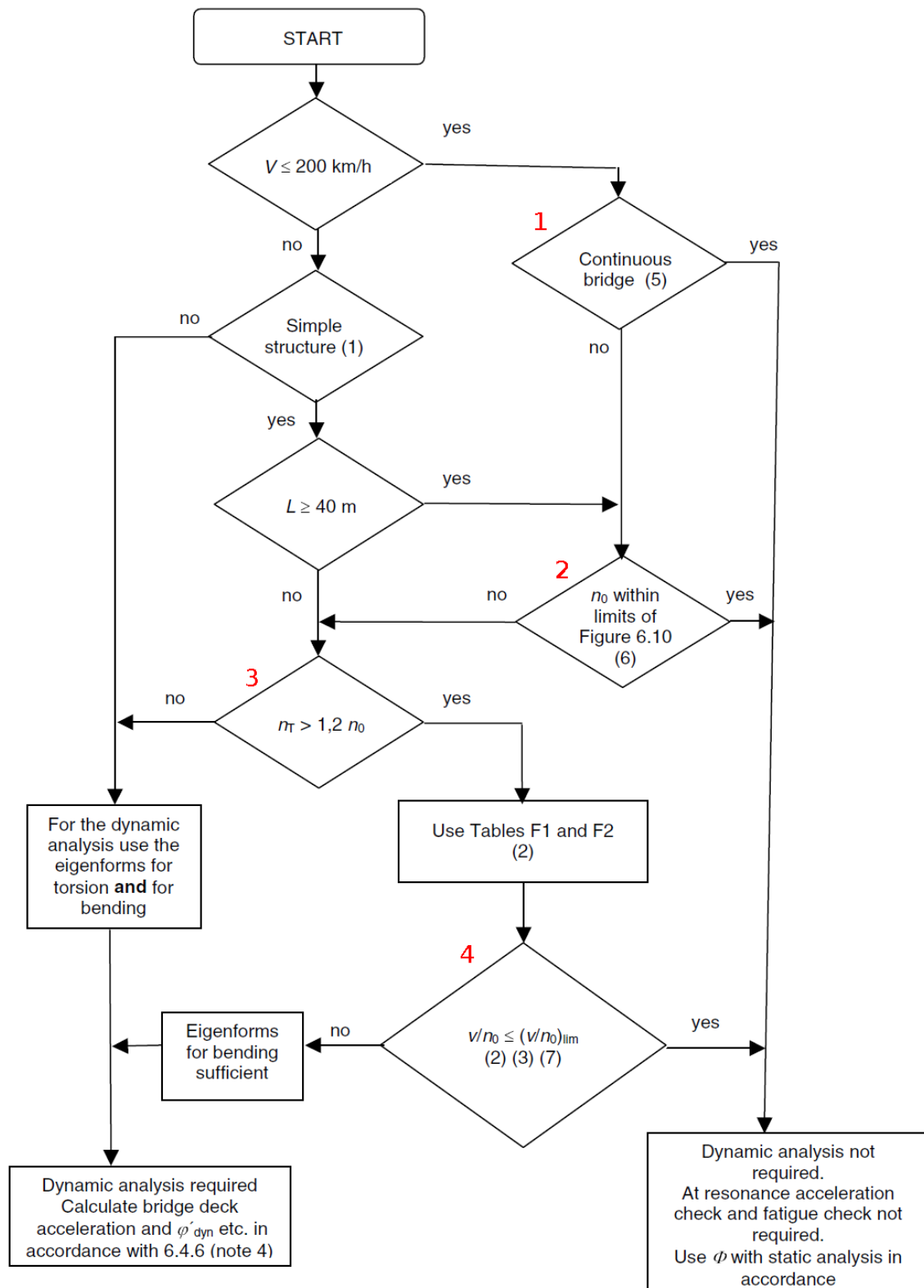


**Figure A.1:** Flow chart for determining whether a dynamic analysis is required [1, fig. 6.9]

If the first natural frequency is not within the limits or the span length is larger than 100 meters, this requirement is not met.

### 3 - First torsional frequency requirement

If the first natural frequency limit is not met, the first torsional frequency  $n_T$  must be larger than 1.2 times the first natural frequency,  $n_0$ . If this requirement is met, one must proceed with the *speed – first natural frequency ratio limit*. If this requirement is not met, a dynamical analysis is required for both torsion and bending.

### 4 - Speed – first natural frequency ratio limit

If the first torsional frequency requirement is met, the ratio between the maximum nominal speed and the first natural frequency, must be smaller than or equal to a limit set in [1, Annex F]. In this annex tabular values are given for this limit which depend on: maximum allowed acceleration (depends on ballast bed or not), span length, mass per meter and percentage of critical damping. This check only applies to simply supported structures which are high enough to distribute loads, have train types specified in Annex F(4), designed for  $\alpha \geq 1$ , carefully maintained and a first natural frequency less than the upper limit from formula 6.1. If the limit is not met or the check does not apply a dynamic analysis must be done.

The possible routes which can be taken through Figure A.1 are given in Figure A.2.

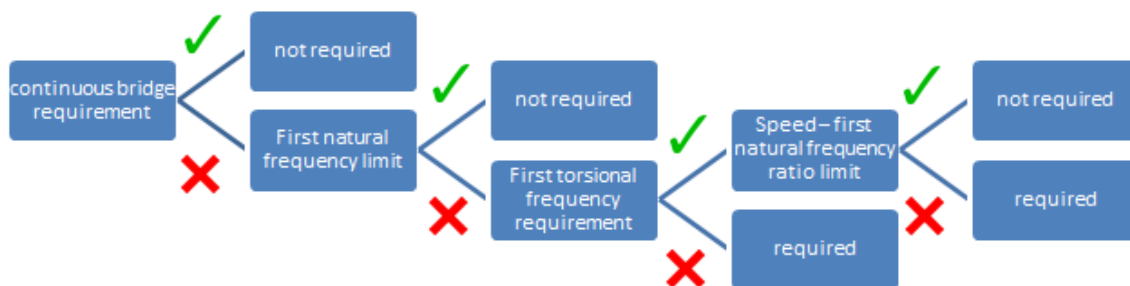


Figure A.2: Possible routes through Figure A.1

#### A.1.1 Results

From the analysis of the possible routes and destinations of Figure A.1 several results can follow.

##### Dynamic analysis is required

Proceeding through Figure A.1 can result in the fact a dynamic analysis must be done. To perform a dynamic analysis of the bridge structure, vehicle-bridge interaction can be neglected. [35, chap. 7] Therefore, a wide range of dynamic analysis programs can be used, with relatively simple load models. When a dynamic analysis is required, this has influence on the fatigue verifications. Furthermore, a quasi-static analysis is also necessary besides the dynamic analysis, the two analyses should be compared to determine which one is governing.

##### Dynamic analysis not required

Proceeding through Figure A.1 can also result in the fact a dynamic analysis is not required. This

can be the case for bridges with a span within the limits of [1, fig. 6.10], by limiting the natural frequency, the torsional frequency and abiding the limits from the tables F1 and F2 from [1, Annex F].

### Strict deflection limit

For bridges with spans outside the limits of [1, fig. 6.10], the natural frequency cannot be limited according to [1, fig. 6.10]. However, a more strict deflection limit can be set, which depends on the train velocity [6, page 237]. This strict deflection limit according to Figure A.3 can be used in the design. If this is done, a dynamic analysis is also not required.

**Table 8.12.** Permissible vertical deflections to avoid excessive track maintenance

$V < 80 \text{ km/h}$	$\delta_{\text{stat}} \leq L/800$ Note: Due to what is said above, namely that the maximum total deflection measured along any track due to rail traffic actions should not exceed $L/600$ , please note that 600 multiplied with 1.33 gives approximately 800.
$80 \leq V \leq 200 \text{ km/h}$	$\delta_{\text{stat}} \leq L/(15V - 400)$ Note: The upper limit $L/2600$ for 200 km/h is the permissible deflection which DB (Deutsche Bundesbahn – German railways) has taken following many years of designing bridges for high-speed lines in Germany, a value which gave satisfaction.
$V > 200 \text{ km/h}$	$\delta_{\text{dyn}} \leq \text{value given by the dynamic study, but } \delta_{\text{stat}} \leq L/2600$

**Figure A.3:** Permissible vertical deflections to avoid excessive track maintenance [6, table 8.12]

### Passenger comfort governing

It is also possible to avoid a dynamic analysis, by fulfilling the *continuous bridge requirement*. To do so, three requirements from [1, fig. 6.9, note 5] must be met. From these three requirements the third requirement related to passenger comfort is potentially the most laborious to meet. To meet this requirement for bridges within the limits of [4, fig. A2.3], a deflection limit can be used. However, for bridges outside the limits of [4, fig. A2.3], a complete vehicle-bridge interaction analysis must be done, to prove the coach body accelerations are within required limits.

## A.2 Eurocode 0 - Basis of structural design: Annex 2

In the aforementioned Eurocode section, multiple references are made to the Eurocode section "Verifications regarding deformations and vibrations for railway bridges". [4, A2.4.4] There are two kinds of reasons to perform these verifications. On the one hand traffic safety, excessive vibrations can lead to ballast instability and even cause derailment. On the other hand passenger comfort, excessive vibrations can cause passenger discomfort. Traditionally deformation criteria were used to cover both limits simultaneously, but this is not the case any more in the current Eurocode. [35, chap. 9] Both traffic safety and passenger comfort criteria must be considered in the Serviceability Limit State (SLS). [35] [1, table 6.10]

### A.2.1 Traffic safety

The criteria related to traffic safety can be found in the Eurocode section “Criteria for traffic safety”. [4, A2.4.4.2] These criteria are:

- A limit on vertical acceleration of the bridge deck of  $\gamma_{bt} = 3.5 \text{ m/s}^2$  (ballast) or  $\gamma_{df} = 5 \text{ m/s}^2$  (no ballast). The frequency of the acceleration must be considered to a maximum of 30 Hz,  $1.5 \cdot n_0$  or  $n_3$ .
- A limit on vertical deflection of the bridge deck of  $L/600$ , although the Dutch national annex prescribes a limit of  $L/800$ . [36, A2.4.4.2.3 (1)]
- Further criteria related to vertical deformation of the deck, twist of the deck, transverse rotation of the ends of each deck, longitudinal displacement of the end of the deck, horizontal transverse deflection, horizontal rotation of a deck and limits on the first natural frequency of lateral vibration.

All of these criteria can be met without performing an extremely complex calculation, i.e. a vehicle-bridge interaction analysis is not necessary.

### A.2.2 Passenger comfort

The criteria related to passenger comfort can be found in the Eurocode section “Limiting values for the maximum vertical deflection for passenger comfort”. [4, A2.4.4.3] The main comfort criteria is related to a maximum vertical acceleration inside the train coaches. Three different recommended levels of comfort are provided in table A2.9. To meet the third criterion from [1, fig 6.9, note 5] the level “very good” from table A2.9 must be chosen, resulting in a maximum vertical acceleration of  $b_v = 1.0 \text{ m/s}^2$ , inside the coach during travel.

To limit the vertical acceleration of passengers in the coach, either a maximum permissible vertical deflection must be set according to Figure A.4 for spans up to 120 meters, or a dynamic vehicle-bridge interaction (VBI) analysis must be performed. The requirements for a dynamic VBI analysis are: [4, A2.4.4.3.3]

- A series of vehicle speeds up to the maximum speed must be used;
- Characteristic loading of the real trains specified must be used;
- Dynamic mass interaction between vehicles in the real train and the structure must be used;
- The damping and stiffness characteristics of the vehicle suspension must be used;
- A sufficient number of vehicles to produce the maximum load effects in the longest span must be used;
- A sufficient number of spans in a structure with multiple spans to develop any resonance effects in the vehicle suspension must be used.

These requirements are quite demanding on the amount of information required. A lot of characteristic data from real trains is necessary, which can be hard and time consuming to gather, if a lot of different trains will use the bridge to be designed.

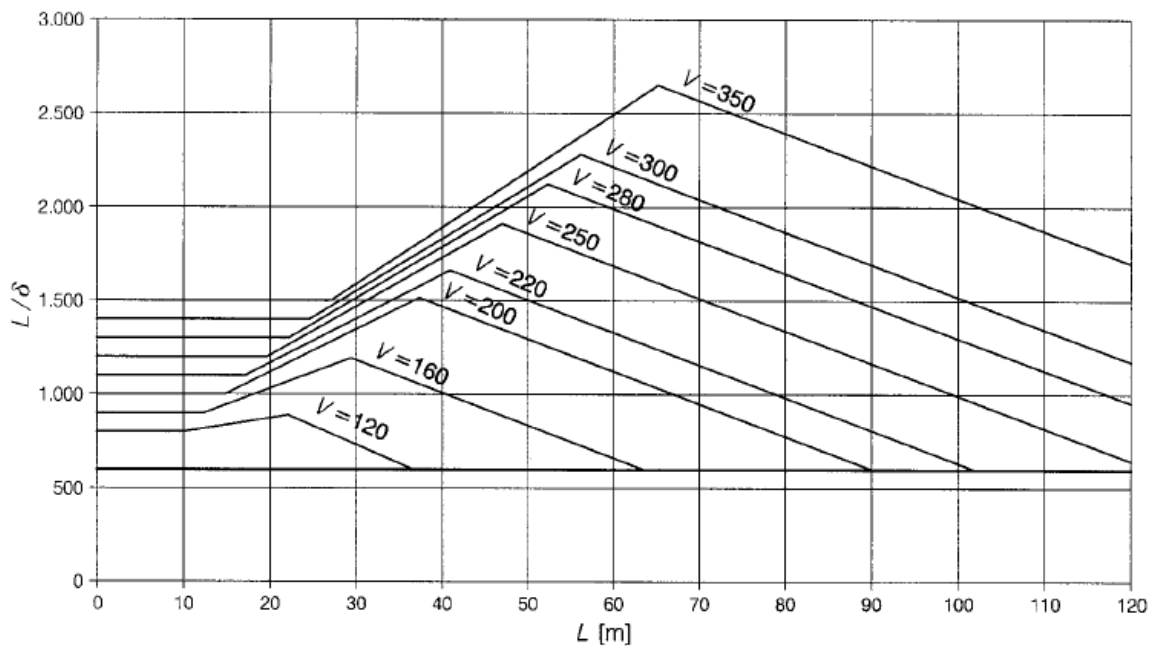


**Figure A.4:** Maximum permissible vertical deflection [4, fig. A2.3]

- $L$  = span length [m]
- $L/\delta$  = length/deflection ratio [-]
- $V$  = velocity [km/h]

## A.3 History

To understand how the requirements related to dynamics of railway bridges found their way to the current Eurocodes ([4], [1]), a look into history will be taken. First the Dutch codes will be investigated in subsection A.3.1, then in subsection A.3.2 a closer look into the regulations from the International Union of Railways will be taken and finally the development of the Eurocodes will be discussed in subsection A.3.3.

### A.3.1 Dutch codes

The Eurocodes are effective in the Netherlands since 2012. Before the introduction of the Eurocodes, all European countries had their own standards. In the Netherlands these standards were of the "NEN" series. In these NEN series, the oldest references to steel railway bridges found by the author, are the NEN 1008 from 1933 and 1938 "Directions for the designing of steel bridges".

After 1938, it was decided to split NEN 1008, which contained both the VOSB (related to design) and the VVSB (related to fabrication). The latter part can later be found in NEN 2008 "Regulations for fabricating steel bridges (VVSB 1977)". A new version of NEN 1008 was published in 1963, "Directions for the designing of steel bridges (VOSB 1963)". In this standard the allowable stress on *dynamically* loaded structures is prescribed. [37, art. 69]

The VOSB from 1963 is followed by the VOSB from 1995, named NEN 6788:1995 “The design of steel bridges - Basic requirements and simple rules (VOSB 1995)”. The requirements related to dynamics of railway bridges are not changed compared to the VOSB 1963. In 2009 the VOSB 1995 was followed by a new version, “Design rules of steel bridges (VOSB 2009)”. However, during this time the development of the Eurocodes was already at an advanced level and therefore this standard had a short lifetime and became obsolete already in 2012.

Apart from the VOSB series, the TGB series was published as well. In 2007 NEN 6706 “TGB 1990 - Traffic loads on bridges” was published, but this standard was largely based on the pre-standard ENV 1991-3. [38, page 4] With the publication of this standard it was already clear it would be replaced by the Eurocodes within a short notice. Therefore one could conclude the dynamic calculations of railway bridges found in the Eurocodes, are not really rooted in the older Dutch codes.

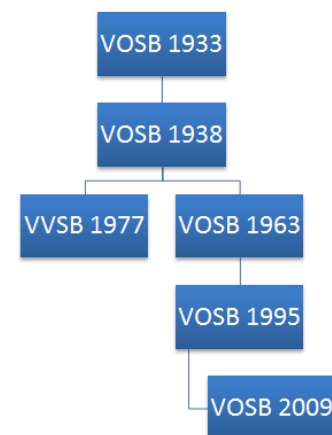


**Figure A.5:** History of Dutch codes related to railway bridges.

### A.3.2 International Union of Railways

The UIC (International Union of Railways) is an international organisation with an aim to standardize railway construction and operations around the world. [39] The UIC provides leaflets with recommendations related to railway engineering. Although the UIC leaflets have a lower legal status than national standards, they can be adapted more easily without passing through a formal and long-term legislation method. [40, page 22] The main drive behind the development of requirements related to the dynamics of railway (bridges) was the increase of train speed. Since large European railway companies such as SNCF (France) and DB (Germany) are members of the UIC, their experience with high speed railways found its way to UIC regulations. The UIC commissioned various task forces to perform research, which could be used for their regulations. One of the researches worth mentioning is ERRI (European Rail Research Institute) subcommittee D214, which performed research to dynamic calculations of railway bridges. Their findings have been included in the Eurocodes ([4], [1]), which will be further elaborated in the next section.

### A.3.3 Eurocodes

In 1974 the elaboration of the Eurocodes started [40, page 15]. In many areas the technical committees responsible for making the Eurocodes, could use various national codes from European countries and establish a consensus when there were differences. However, in the area of railway engineering the leaflets of the UIC were often used as a basis for the Eurocodes. For example, the “load model 71” (LM 71) for static railway loads was developed by the UIC in 1971 and is used in the Eurocode. Furthermore, the Eurocode was based on regulations from the UIC leaflets 700 R, 702 OR, 776-1 R, 776-2 R, 776-3 R, 778-1 R and 779-1 R. [40, page 22] Between 1992 and 1998 a first series of pre-standards was published. One of these pre-standards was ENV 1991-3:1995 “Eurocode 1. Basis of design and actions on structures. Part 3: Traffic loads on bridges”. This pre-standard required dynamic calculations of railway bridges, which was especially relevant for

high speed railway lines. The design requirements related to railway bridges which were present in pre-standard ENV 1991-3, was split over two different Eurocodes, as can be seen in Figure A.6.

To conclude, the development of high speed railway lines, caused the UIC to perform research on dynamics of railway bridges. With the introduction of the Eurocodes, this research was included in the standards, while it was not present in the old Dutch codes.

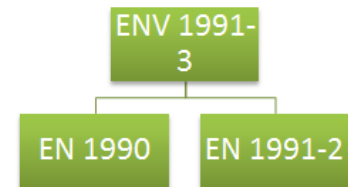


**Figure A.6:** History of Eurocodes related to railway bridges, (1995 - present).

---

# Appendix B

---

## Tied-arch bridge

One of the assumptions from section 1.4 was to limit the bridge type to steel arch bridges with vertical hangers. This appendix provides some background information about arch bridges and their elements. This appendix is referenced from section 2.3.

### B.1 Types

Arch bridges can be classified according to their element configuration in the following way: [41, page 172]

- true arch;
- through arch;
- tied-arch.

In a *true arch*, both the horizontal and vertical components of the reaction force are carried to the supports, situated at each end. This type of arch is most suited for rocky areas, since for soft soils big heavy foundations must be made to take up the horizontal thrust. An example can be seen in Figure B.1a. If the deck is not completely above or below the arch, but goes through the arch, it is called a *through arch* bridge. An example can be seen in Figure B.1b. The third and last type is the *tied-arch* bridge or bowstring bridge, where a tensile tie balances the horizontal thrusts. The supports only need to carry the vertical components of the load. An example can be seen in Figure B.1c.

They can be constructed in one place and moved to their final position afterwards, making them suitable to execute without disrupting the traffic too much. The tied-arch bridge will be the type further analysed in this report. This type is often used in the Netherlands, where the soft soil conditions are not well suited to take up the horizontal thrust which exist at true arch bridge supports. Also, the execution method where traffic hindrance is minimal, is a big advantage in the Netherlands, where a long disruption of the water channels or roads would be very inconvenient.



(a) Victoria Falls Bridge, Zimbabwe [16]



(b) Bayonne Bridge, USA [17]



(c) Neville Island Bridge, USA [18]

**Figure B.1:** Types of arch bridges: true arch (a), through arch (b) and tied-arch (c).

## B.2 Elements

A tied-arch bridge consists of various elements, they will be briefly discussed in this section. The names of some elements can be seen in Figure B.2. The bridge can be divided in a substructure and a superstructure.

### B.2.1 Bearings

The bridge is supported by bearings, which are part of the substructure. For tied-arch bridges the bearings are mainly loaded by vertical loads. Some horizontal loads apply from acceleration and deceleration of trains, but in this report a constant vehicle velocity is assumed. Assuming a simply supported static scheme and assuming the bearings can withstand enough horizontal expansion and rotation, they have little influence on the superstructure and will not be considered in detail.

### B.2.2 Arch

The arch can be shaped as (part of a) parabola or circle. This shape can also be approached by using smaller straight sections connected by an angle. The arch is mainly loaded by axial compressive stresses and to a smaller degree by bending moment stresses. [42, page 17-1] The

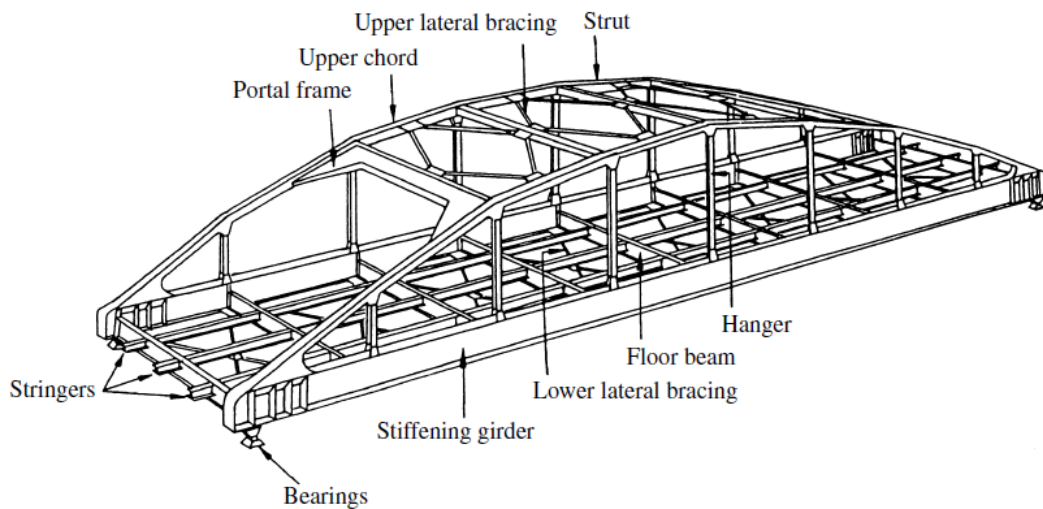


**Figure B.2:** Langer arch bridge [20, fig. 10.47]

arch can be constructed as a solid rib, which is usually a plate girder or box girder, a truss or a (circular) hollow section. Traditionally two connected arches are used, which is mainly caused by the fact a single arch is prone to out-of-plane buckling.

### B.2.3 Bracing

Arch bridges with two arches, often have lateral bracing between the arches. The bracing prevents out-of-plane buckling of the arch and takes up lateral actions such as wind loading. The bracing can be configured in multiple ways, for example straight or diagonal, see Figure B.3. Bracing can also be present in the deck, usually if it consists of beams and stringers. The lateral actions can be transmitted to the supports by rigid end portals.

### B.2.4 Hangers

Hangers or suspenders can be constructed with wire ropes, cables, rolled sections or circular hollow sections. They transfer the forces working on the edge beams to the arch. The type of hangers has influence on criteria such as static strength, fatigue strength or aerodynamics (flutter, vortex shedding). Since this report focuses on none of these criteria, the exact hanger type is not relevant. However, the hanger *configuration* is very important and can be:

- Vertical (Classic tied-arch bridge);
- Diagonal (Nielsen bridge);
- Multiple diagonals (Network arch bridge).

Traditionally vertical hangers were used. In 1926 the Swede Octavius F. Nielsen patented the diagonal hanger configuration, where hangers cross a maximum of one other hanger. This idea

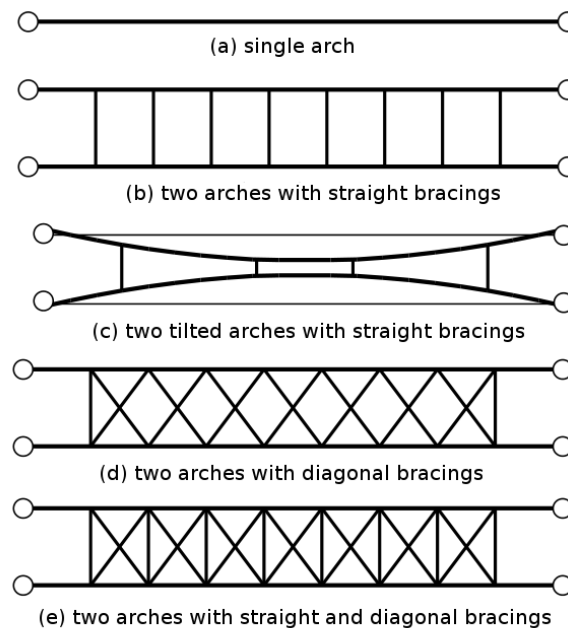


**Figure B.3:** Top view of different arch bracings, modified from [43]

was further improved at the end of the fifties, when the Norwegian Per Tveit developed the network hanger configuration, diagonal hangers crossing each other multiple times. [44]

The choice of configuration has a great influence on the stiffness of the arch bridge. When a train enters or leaves the bridge, the structure is loaded in an anti-symmetric mode. Arch bridges with vertical hangers deflect more when the load is applied at a quarter of the length and are harder to construct with enough stiffness. On the contrary, arch bridges with network hangers deflect significantly less and behave similar to a bending beam.

### B.2.5 Deck

The decks of railway bridges can be constructed as: [42, par. 23.4], [41, page 65]

- open deck; railway track and sleepers are supported by load carrying elements of superstructure, no ballast applied.
- ballast deck; railway track is supported by ballast, which is carried by the superstructure of the bridge.
- direct fixation; no sleepers are used, rails is anchored directly to superstructure.
- composite steel-concrete deck; with or without ballast.
- orthotropic steel deck; with or without ballast.

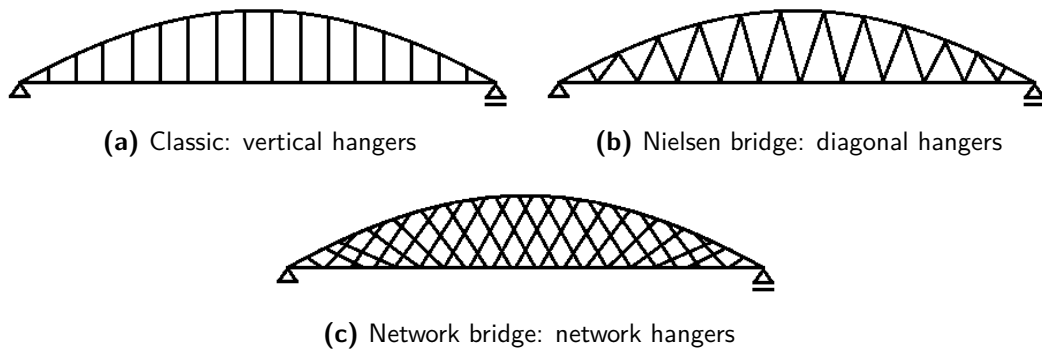


**Figure B.4:** Various tied-arch bridge hanger types based on [41, fig. 12.8]

The deck is usually supported by cross-beams (transversal beams), which transport the load to the edge beams. A cross-beam effect can occur, since cross-beams are stiffer than other parts, so the deck deflects more between the cross-beams, which causes the deck to form a wavelike shape. [5, page 38]

If the edge beams are rigidly connected to a concrete deck, the deck will also be loaded by tensile forces from the tied beam effect, besides the bending moment caused by the live load moving over the deck. If not enough longitudinal reinforcement is applied, this can cause cracks. A cross section of a possible bridge deck can be seen in Figure B.5.

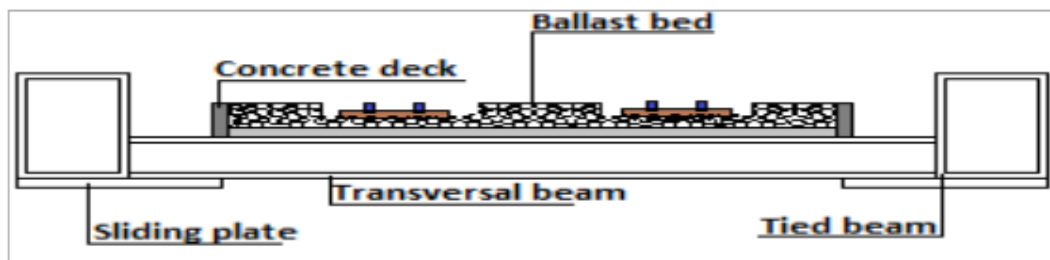


**Figure B.5:** Cross section bridge deck [45, fig. 10-4]

### B.2.6 Girder

The stiffening girders or edge beams of the bridge are located at both sides of the deck, see Figure B.2 and Figure B.5. They function as tied beams, which are loaded by tensile forces to compensate the compressive forces in the arch. They also support the bridge deck and transfer loads to the arch, through the hangers.

It is an important consideration how to distribute the stiffness of the construction between the stiffening girders and the arch. This proportion will dictate how much load each element attracts, since stiff elements attract more load. [46, page 480] In general there are three types possible:

- Classic tied-arch bridge: stiff arch and slender girder;
- Langer bridge: slender arch and stiff girder;

- Lohse bridge: both arch and girder are stiff, named after Hermann Lohse (1815–1893).

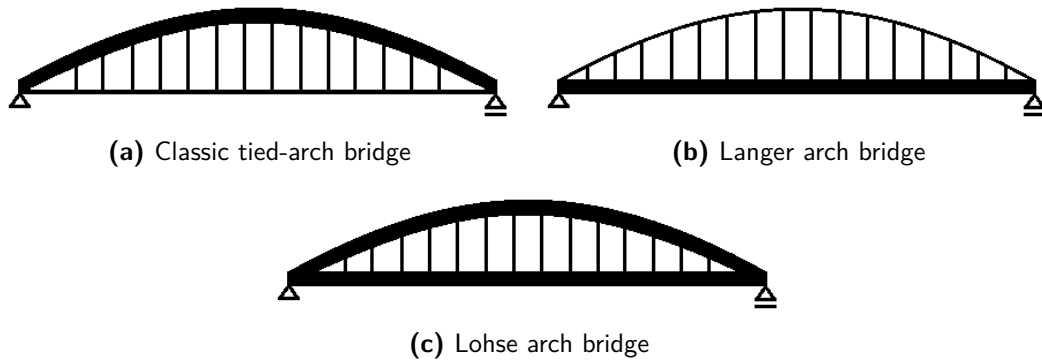


**Figure B.6:** Various tied-arch bridge types based on [20, fig. 10.46]

The classic tied-arch bridge consists of a stiff arch and a slender girder. The stiffer arch can handle bending moments in addition to axial compression. In a Langer arch bridge, it is assumed the arch rib takes only axial compression. Therefore the arch rib can be thin and the girders will be deep to resist moment, shear and axial tension. In a Lohse arch bridge on the other hand, the bending moment is carried by both the arch rib and the girder. [20, page 10-48]

---

# Appendix C

---

## VIRM train

The subject of this appendix is the *rolling stock*, the railway vehicles passing the bridge. First section C.1 discusses types of coaches encountered in Dutch trains. Afterwards section C.2 treats bogies, which are at the interface between coaches and the railway track. Lastly section C.3 describes bogie data received and an interpretation of this data. This appendix is referenced from section 2.5.

### C.1 Coaches

To understand the vibrations felt by passengers travelling in trains, the specifications of passenger coaches must be investigated. The Eurocode specifically states *real trains* must be considered in the dynamic analysis [4, A2.4.4.3.3]. To get a clear picture of which trains are used in the Netherlands, an inventory of the trains used for passenger transport is performed. The passenger coaches found by the author are listed in Table C.1. Coaches are often grouped in a coupled set called a multiple unit (MU), which can operate as a train not intended to be reconfigured. [47, 3.1.21]

According to EN15528, coaches can be grouped in three MU-groups: [47, table C.1]

- **Conventional bogie**, each coach has two bogies;
- **Articulated bogie**, coaches share a bogie;
- **Single axle**, no bogies, wheelsets directly connected to coaches.

Most of the coaches used in the Netherlands have conventional bogies, some have articulated bogies or Jacobs bogies [50, page 65]. Rolling stock with single axles has less damping and is more frequently found with freight wagons, which generally do not carry passengers. In Figure C.1 the difference between conventional bogies, articulated bogies and single axles can be seen.

From Table C.1 it can be concluded the most used type of coach in the Netherlands is the VIRM (see Figure C.2), which uses conventional bogies. Therefore this type of coach will be used in the

**Table C.1:** List of passenger coaches used in the Netherlands (November 2015).

Name	Type	Amount	Company
VIRM	double deck coach	872 <sup>a</sup>	NS
SLT	lightweight train	648 <sup>b</sup>	NS
ICM	single deck coach	581 <sup>c</sup>	NS
Stadler GTW	lightweight train	338 <sup>d</sup>	Arriva, Veolia, Breng and Connexion
ICR	single deck coach	277 <sup>e</sup>	NS
DDZ / NID	double deck coach	240 <sup>f</sup>	NS
SGM	lightweight train	240 <sup>g</sup>	NS
Thalys PBKA	high speed train	170 <sup>h</sup>	NS
ICE 3M	high speed train	136 <sup>i</sup>	NS
DM '90	diesel train	106 <sup>j</sup>	NS
Thalys PBA	high speed train	100 <sup>k</sup>	NS
DDM-1	double deck coach	66 <sup>l</sup>	NS
DD-AR	double deck coach	57 <sup>m</sup>	NS
Mat '64 / Plan V	single deck coach	48 <sup>n</sup>	NS
Talent	lightweight train	48 <sup>o</sup>	DB Regio NRW
LINT 41/H	diesel train	12 <sup>p</sup>	Syntus, Arriva and Veolia
Protos	lightweight train	10 <sup>q</sup>	Connexion

<sup>a</sup> 98 four part MUs, 80 six part MUs

<sup>b</sup> 69 four part EMUs and 62 six part MUs

<sup>c</sup> 87 three part MUs and 80 four part MUs

<sup>d</sup> 99 two and three part MUs by Arriva, 60 two and three part MUs by Veolia, 9 three part MUs by Breng and 1 three part MU by Connexion

<sup>e</sup> in three part and four part MUs

<sup>f</sup> 30 four part MUs, 20 six part MUs

<sup>g</sup> 30 two part MUs and 60 three part MUs

<sup>h</sup> 17 ten part MUs

<sup>i</sup> 17 eight part MUs

<sup>j</sup> 53 two part MUs

<sup>k</sup> 10 ten part MUs

<sup>l</sup> 11 six part MUs

<sup>m</sup> 19 three part MUs

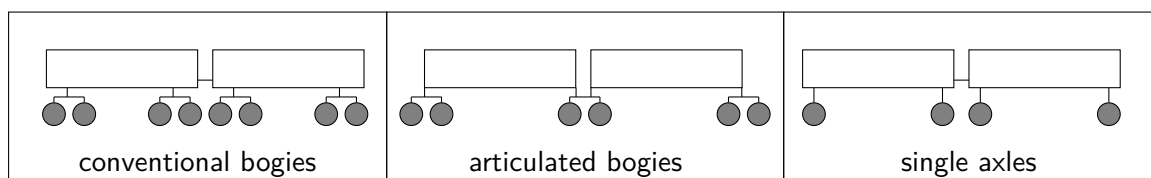
<sup>n</sup> 24 two part MUs

<sup>o</sup> 24 two part MUs

<sup>p</sup> Syntus, Arriva and Veolia all 2 two part MUs

<sup>q</sup> 5 two part MUs

Sources: [48, 49]

**Figure C.1:** Three groups of coaches

analyses of this report. VIRM trains exist as four part MUs and six part MUs. In Figure C.3 half a six part VIRM is shown with distances between bogies.



Figure C.2: Dutch double decker coach (VIRM) [22]

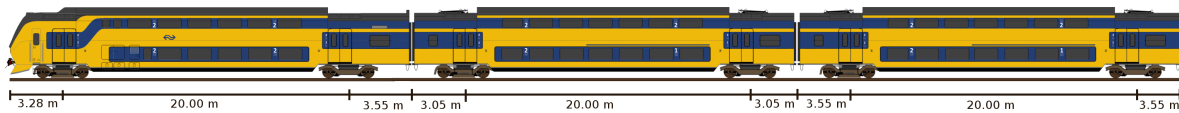


Figure C.3: Half of a VIRM with dimensions [51] [52]

## C.2 Bogies

The bogies of the coaches consist of different components: wheelsets, axleboxes, wheels, suspension, springs, dampers, constraints and bumpstops. The suspension often consists of two parts. A primary suspension transmits forces from the wheelsets to the bogie frame and the secondary suspension transmits forces from the bogie frame to the coach. [50, page 65] For the dynamic analysis the springs and dampers are most important, since they mostly influence the dynamic behaviour. Springs can be of various types, such as leaf springs, coil springs, rubber-metal springs or air springs. Dampers come in various types as well, for example friction dampers, viscous dampers, active dampers or hydraulic dampers. [50, page 47-56] The exact magnitude of spring stiffness and damping value is of great importance. In some cases the use of stiffer suspension systems will increase the frequency of the sprung mass and approach that of the bridge. This can significantly increase the vertical acceleration of the train cars in running. [2, pages 191-194]

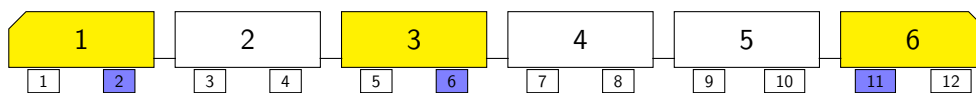


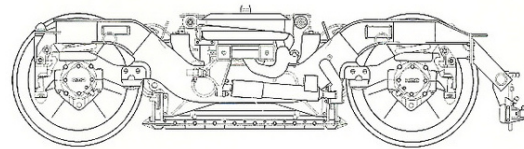
Figure C.4: Coach composition of certain 6 part VIRM trains. The first, third and sixth coach are motor coaches, the rest are trailer coaches. The second, sixth and eleventh bogies are motor bogies, the rest are trailer bogies (R. Volgers, personal communication, Mar 17, 2016 and [53]).

The VIRM trains which are chosen to be analysed have RMO 9000 heavy duty bogies manufactured by Stork RMO B.V. [23] A VIRM multiple unit consists of motor coaches and trailer coaches, as

well as motor bogies and trailer bogies. The coach composition can be seen in Figure C.4 and the two bogie types in Figure C.5. The motor bogie is longer and has electric motors, the trailer bogie is shorter and has brakes on the wheelsets. The bogie has a total of four primary springs and primary dampers between the wheels and the bogie frame. This primary suspensions consists of coil springs and hydraulic dampers. Furthermore there are two secondary springs and secondary dampers, which consist of air springs (the built up of the air ducts determines the damping) and rubber sidebearer springs. All relevant information about the bogies is listed in Table C.2.



(a) RMO 9000 motor bogie [23]



(b) RMO 9000 trailer bogie [23]

**Figure C.5:** RMO 9000 bogies.

**Table C.2:** RMO 9000 heavy duty bogie data.<sup>a</sup>

Name	Parameter	Value	Unit
<b>Coaches</b>			
Mass motor coach <sup>b</sup>	$m_{v,m}$	45 000 - 58 000	kg
Mass trailer coach <sup>b</sup>	$m_{v,t}$	37 000 - 50 000	kg
<b>Motor bogie</b>			
Mass wheelset <sup>c</sup>	$m_{w,m}$	1200	kg
Mass frame <sup>d</sup>	$m_{f,m}$	8620	kg
Mass bogie	$m_{bog,m}$	11 020	kg
Stiffness primary suspension <sup>e</sup>	$k_{p,m}$	1 250 000	N/m
Damping ratio primary suspension	$\xi_p$	$\leq 25$	%
Stiffness secondary suspension <sup>f</sup>	$k_{s,m}$	460 000	N/m
Damping ratio secondary suspension	$\xi_s$	$\leq 25$	%
<b>Trailer bogie</b>			
Mass wheelset <sup>c</sup>	$m_{w,t}$	1700	kg
Mass frame <sup>d</sup>	$m_{f,t}$	4970	kg
Mass bogie	$m_{bog,t}$	8370	kg
Stiffness primary suspension <sup>e</sup>	$k_{p,t}$	850 000	N/m
Damping ratio primary suspension	$\xi_p$	$\leq 25$	%
Stiffness secondary suspension <sup>f</sup>	$k_{s,t}$	460 000	N/m
Damping ratio secondary suspension	$\xi_s$	$\leq 25$	%

<sup>a</sup> Data received from Ricardo Rail (R. Volgers, personal communication, Nov 26, 2015 and Mar 17, 2016) and from [23].

<sup>b</sup> Range between unloaded and fully loaded mass.

<sup>c</sup> Wheelsets consist of two wheels, an axle and for the trailer bogie also brakes.

<sup>d</sup> The frame mass is the bogie mass, with two wheelset masses subtracted.

<sup>e</sup> Value for one wheel, there are four wheels per bogie.

<sup>f</sup> Value for one suspension, there are two suspensions per bogie. Value is approximate since air springs are non-linear.

### C.3 Schematization

With the data from Table C.2 a coach model can be made to use for the analysis of the dynamic behaviour. Three types of schematization are considered, of increasing level of complexity:

- Every bogie as a one DOF sprung mass;
- Every bogie as a two DOF sprung mass;
- Full coach supported by two bogies.

The three types of schematization are described in the following subsections. First the 2 DOF bogie schematization is treated, then the 1 DOF bogie schematization and lastly the full coach schematization.

#### C.3.1 2 DOF schematization

For the purpose of modelling, the complete bogie will be simplified to an equivalent system, as can be seen in Figure C.6.

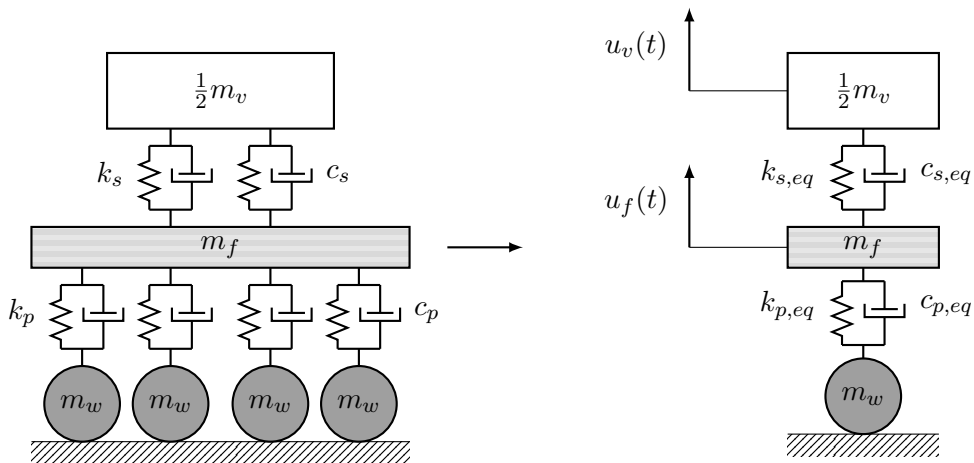


**Figure C.6:** Simplified bogie model to equivalent 2 DOF bogie

- vehicle mass  $m_v$  [kg]
- frame mass  $m_f$  [kg]
- wheel mass  $m_w$  [kg]
- primary/secondary spring stiffness  $k_p / k_s$  [N/m]
- primary/secondary damping  $c_p / c_s$  [Ns/m]
- vertical DOF vehicle mass  $u_v(t)$  [m]
- vertical DOF frame mass  $u_f(t)$  [m]

In this model the mass of the coach is assumed to be evenly distributed over the two bogies on which it rests. Therefore a bogie is loaded by half the coach mass,  $\frac{1}{2}m_v$ . The secondary suspension consists of two springs and two dampers, on both sides of the coach with the same spring stiffness  $k_s$  and damping  $c_s$ . Between the secondary and primary suspension the frame mass  $m_f$  is positioned. The frame mass is connected to the four wheels by the primary suspension. The primary suspension consists of four springs and four dampers, with the same spring stiffness  $k_p$  and damping value  $c_p$ . These parallel springs and dampers are simplified to one equivalent spring and damper. The equivalent primary and secondary spring stiffnesses for the motor and trailer bogies can be determined to be

$$k_{p,m,eq} = 4 \cdot k_{p,m} = 4 \cdot 1250000 = 5\,000\,000 \text{ N/m}, \quad (\text{C.1})$$

$$k_{p,t,eq} = 4 \cdot k_{p,t} = 4 \cdot 850000 = 3\,400\,000 \text{ N/m} \quad (\text{C.2})$$

and

$$k_{s,m,eq} = k_{s,t,eq} = 2 \cdot k_s = 2 \cdot 460000 = 920\,000 \text{ N/m}. \quad (\text{C.3})$$

To compute the damping values  $c$  for every suspension, the critical damping must be known. The critical damping can be computed with:  $c_{cr} = 2 \cdot \sqrt{k \cdot m}$  for a one DOF mass-spring-dashpot system. To calculate the critical damping for the two DOF system, it will be assumed the primary and secondary suspension are decoupled, which means if one mass moves, the other one does not move. This will result in an equivalent primary suspension of the motor bogie of

$$c_{cr,p,m} = 2 \cdot \sqrt{k_{p,m,eq} \cdot m_{f,m}} = 2 \cdot \sqrt{5000000 \cdot 8620} = 415\,210.8 \text{ Ns/m}, \quad (\text{C.4})$$

an equivalent primary suspension of the trailer bogie of

$$c_{cr,p,t} = 2 \cdot \sqrt{k_{p,t,eq} \cdot m_{f,t}} = 2 \cdot \sqrt{3400000 \cdot 4970} = 259\,984.6 \text{ Ns/m}, \quad (\text{C.5})$$

an equivalent secondary suspension of the motor bogie of

$$c_{cr,s,m} = 2 \cdot \sqrt{k_{s,m,eq} \cdot \frac{1}{2}m_{v,m}} = 2 \cdot \sqrt{920000 \cdot \frac{1}{2}58000} = 326\,680.3 \text{ Ns/m}, \quad (\text{C.6})$$

and an equivalent secondary suspension of the trailer bogie of

$$c_{cr,s,t} = 2 \cdot \sqrt{k_{s,t,eq} \cdot \frac{1}{2}m_{v,t}} = 2 \cdot \sqrt{920000 \cdot \frac{1}{2}50000} = 303\,315.0 \text{ Ns/m}. \quad (\text{C.7})$$

Knowing the critical damping values, the damping values can be computed as

$$c_{p,m,eq} = \xi_p \cdot c_{cr,p,m} = 0.25 \cdot 415210.8 = 103\,803.7 \text{ Ns/m}, \quad (\text{C.8})$$

$$c_{p,t,eq} = \xi_p \cdot c_{cr,p,t} = 0.25 \cdot 259984.6 = 64\,996.2 \text{ Ns/m}, \quad (\text{C.9})$$

$$c_{s,m,eq} = \xi_s \cdot c_{cr,s,m} = 0.25 \cdot 326680.3 = 81\,670.1 \text{ Ns/m}, \quad (\text{C.10})$$

$$c_{s,t,eq} = \xi_s \cdot c_{cr,s,t} = 0.25 \cdot 303315.0 = 75\,828.8 \text{ Ns/m}. \quad (\text{C.11})$$

This results in the following table of data which can be used as input for the analyses.

**Table C.3:** Resulting 2 DOF bogie data.<sup>a</sup>

Name	Parameter	Value	Unit
<b>Coaches</b>			
Average mass motor coach	$m_{v,m}$	51 500	kg
Average mass trailer coach	$m_{v,t}$	43 500	kg
<b>Motor bogie</b>			
Mass wheelset	$m_{w,m}$	1200	kg
Mass frame	$m_{f,m}$	8620	kg
Mass bogie	$m_{bog,m}$	11 020	kg
Equivalent stiffness primary suspension	$k_{p,m,eq}$	5 000 000	N/m
Equivalent damping primary suspension	$c_{p,m,eq}$	$\leq 103\,804$	Ns/m
Equivalent stiffness secondary suspension	$k_{s,m,eq}$	920 000	N/m
Equivalent damping secondary suspension	$c_{s,m,eq}$	$\leq 81\,670$	Ns/m
<b>Trailer bogie</b>			
Mass wheelset	$m_{w,t}$	1700	kg
Mass frame	$m_{f,t}$	4970	kg
Mass bogie	$m_{bog,t}$	8370	kg
Equivalent stiffness primary suspension	$k_{p,t,eq}$	3 400 000	N/m
Equivalent damping primary suspension	$c_{p,t,eq}$	$\leq 64\,996$	Ns/m
Equivalent stiffness secondary suspension	$k_{s,t,eq}$	920 000	N/m
Equivalent damping secondary suspension	$c_{s,t,eq}$	$\leq 75\,829$	Ns/m

<sup>a</sup> Derived from Table C.2.

The Ansys analyses using this vehicle model can be found in subsection L.4.2.

Because this system has two degrees of freedom, two natural frequencies corresponding to two modes can be found. Using the displacement method, two equations of motion can be found

$$m_1 \cdot \ddot{u}_1 + (k_1 + k_2) \cdot u_1 - k_2 \cdot u_2 = 0 \quad (\text{C.12})$$

$$m_2 \cdot \ddot{u}_2 - k_2 \cdot u_1 + k_2 \cdot u_2 = 0. \quad (\text{C.13})$$

Substituting a general solution for  $u_1$  and  $u_2$

$$u_{1,2} = \sum_{n=1}^4 U_n^{(1,2)} \cdot e^{s_n \cdot t} \quad (\text{C.14})$$

one finds

$$U_n^{(1)} \cdot (m_1 \cdot s_n^2 + k_1 + k_2) + U_n^{(2)} \cdot (-k_2) = 0 \quad (\text{C.15})$$

$$U_n^{(2)} \cdot (m_2 \cdot s_n^2 + k_2) + U_n^{(1)} \cdot (-k_2) = 0. \quad (\text{C.16})$$

To get a non-trivial solution of  $s_n$  the determinant of these two equations must be found

$$\det \begin{vmatrix} m_1 \cdot s_n^2 + k_1 + k_2 & -k_2 \\ -k_2 & m_2 \cdot s_n^2 + k_2 \end{vmatrix} = 0 \quad (\text{C.17})$$

which results in the characteristic equation

$$(m_1 \cdot s_n^2 + k_1 + k_2)(m_2 \cdot s_n^2 + k_2) - k_2^2 = 0. \quad (\text{C.18})$$

There are four imaginary solutions for  $s_n$ , which can be found using Maple's solver or WolframAlpha. By setting  $s_n = i \cdot \omega$  and expressing parts of the solution as two partial frequencies and one coupling frequency

$$\omega_a = \sqrt{\frac{k_1 + k_2}{m_1}}, \quad (\text{C.19})$$

$$\omega_b = \sqrt{\frac{k_2}{m_2}}, \quad (\text{C.20})$$

$$\omega_{ab} = \sqrt{\frac{k_2}{\sqrt{m_1 \cdot m_2}}}, \quad (\text{C.21})$$

Two natural frequencies can be found

$$\omega_1 = \frac{1}{\sqrt{2}} \cdot \sqrt{\omega_a^2 + \omega_b^2 - \sqrt{(\omega_a^2 - \omega_b^2)^2 + 4 \cdot \omega_{ab}^4}}, \quad (\text{C.22})$$

$$\omega_2 = \frac{1}{\sqrt{2}} \cdot \sqrt{\omega_a^2 + \omega_b^2 + \sqrt{(\omega_a^2 - \omega_b^2)^2 + 4 \cdot \omega_{ab}^4}}. \quad (\text{C.23})$$

The derived equations can be used to find the natural frequencies of the 2 DOF bogie schematization. The mass  $m_1$  must be substituted by the frame mass, the mass  $m_2$  by the vehicle mass. The spring stiffness  $k_1$  must be substituted by the primary spring stiffness, the spring stiffness  $k_2$  by the secondary spring stiffness. Because there are three combinations of motor and trailer bogies and coaches, six natural frequencies can be found.

#### Motor coach and motor bogie

The partial and coupling frequencies are

$$\omega_{a,mm} = \sqrt{\frac{k_{p,m,eq} + k_{s,m,eq}}{m_{f,m}}} \cdot \frac{1}{2\pi} = \sqrt{\frac{5\,000\,000 + 920\,000}{8620}} \cdot \frac{1}{2\pi} = 4.17 \text{ Hz} \quad (\text{C.24})$$

$$\omega_{b,mm} = \sqrt{\frac{k_{s,m,eq}}{\frac{1}{2}m_{v,m}}} \cdot \frac{1}{2\pi} = \sqrt{\frac{920\,000}{\frac{1}{2} \cdot 51\,500}} \cdot \frac{1}{2\pi} = 0.95 \text{ Hz} \quad (\text{C.25})$$

$$\omega_{ab,mm} = \sqrt{\frac{k_{s,m,eq}}{\sqrt{m_{f,m} \cdot \frac{1}{2} \cdot m_{v,m}}}} \cdot \frac{1}{2\pi} = \sqrt{\frac{920\,000}{\sqrt{8620 \cdot \frac{1}{2} \cdot 51\,500}}} \cdot \frac{1}{2\pi} = 1.25 \text{ Hz} \quad (\text{C.26})$$

This results in two natural frequencies of

$$\omega_{1,mm} = \frac{1}{\sqrt{2}} \cdot \sqrt{\omega_{a,mm}^2 + \omega_{b,mm}^2 - \sqrt{(\omega_{a,mm}^2 - \omega_{b,mm}^2)^2 + 4 \cdot \omega_{ab,mm}^4}} = 0.87 \text{ Hz}, \quad (\text{C.27})$$

$$\omega_{2,mm} = \frac{1}{\sqrt{2}} \cdot \sqrt{\omega_{a,mm}^2 + \omega_{b,mm}^2 + \sqrt{(\omega_{a,mm}^2 - \omega_{b,mm}^2)^2 + 4 \cdot \omega_{ab,mm}^4}} = 4.19 \text{ Hz}. \quad (\text{C.28})$$

### Motor coach and trailer bogie

The partial and coupling frequencies are

$$\omega_{a,mt} = \sqrt{\frac{k_{p,m,eq} + k_{s,m,eq}}{m_{f,m}}} \cdot \frac{1}{2\pi} = \sqrt{\frac{3\,400\,000 + 920\,000}{4970}} \cdot \frac{1}{2\pi} = 4.69 \text{ Hz} \quad (\text{C.29})$$

$$\omega_{b,mt} = \sqrt{\frac{k_{s,m,eq}}{\frac{1}{2}m_{v,m}}} \cdot \frac{1}{2\pi} = \sqrt{\frac{920\,000}{\frac{1}{2} \cdot 51\,500}} \cdot \frac{1}{2\pi} = 0.95 \text{ Hz} \quad (\text{C.30})$$

$$\omega_{ab,mt} = \sqrt{\frac{k_{s,m,eq}}{\sqrt{m_{f,m} \cdot \frac{1}{2} \cdot m_{v,m}}}} \cdot \frac{1}{2\pi} = \sqrt{\frac{920\,000}{\sqrt{4970 \cdot \frac{1}{2} \cdot 51\,500}}} \cdot \frac{1}{2\pi} = 1.44 \text{ Hz} \quad (\text{C.31})$$

This results in two natural frequencies of

$$\omega_{1,mt} = \frac{1}{\sqrt{2}} \cdot \sqrt{\omega_{a,mt}^2 + \omega_{b,mt}^2 - \sqrt{(\omega_{a,mt}^2 - \omega_{b,mt}^2)^2 + 4 \cdot \omega_{ab,mt}^4}} = 0.84 \text{ Hz}, \quad (\text{C.32})$$

$$\omega_{2,mt} = \frac{1}{\sqrt{2}} \cdot \sqrt{\omega_{a,mt}^2 + \omega_{b,mt}^2 + \sqrt{(\omega_{a,mt}^2 - \omega_{b,mt}^2)^2 + 4 \cdot \omega_{ab,mt}^4}} = 4.72 \text{ Hz}. \quad (\text{C.33})$$

### Trailer coach and trailer bogie

The partial and coupling frequencies are

$$\omega_{a,tt} = \sqrt{\frac{k_{p,t,eq} + k_{s,t,eq}}{m_{f,t}}} \cdot \frac{1}{2\pi} = \sqrt{\frac{3\,400\,000 + 920\,000}{4970}} \cdot \frac{1}{2\pi} = 4.69 \text{ Hz}. \quad (\text{C.34})$$

$$\omega_{b,tt} = \sqrt{\frac{k_{s,t,eq}}{\frac{1}{2}m_{v,t}}} \cdot \frac{1}{2\pi} = \sqrt{\frac{920\,000}{\frac{1}{2} \cdot 43\,500}} \cdot \frac{1}{2\pi} = 1.04 \text{ Hz}. \quad (\text{C.35})$$

$$\omega_{ab,tt} = \sqrt{\frac{k_{s,t,eq}}{\sqrt{m_{f,t} \cdot \frac{1}{2} \cdot m_{v,t}}}} \cdot \frac{1}{2\pi} = \sqrt{\frac{920\,000}{\sqrt{4970 \cdot \frac{1}{2} \cdot 43\,500}}} \cdot \frac{1}{2\pi} = 1.50 \text{ Hz} \quad (\text{C.36})$$

This results in two natural frequencies of

$$\omega_{1,tt} = \frac{1}{\sqrt{2}} \cdot \sqrt{\omega_{a,tt}^2 + \omega_{b,tt}^2 - \sqrt{(\omega_{a,tt}^2 - \omega_{b,tt}^2)^2 + 4 \cdot \omega_{ab,tt}^4}} = 0.91 \text{ Hz}, \quad (\text{C.37})$$

$$\omega_{2,tt} = \frac{1}{\sqrt{2}} \cdot \sqrt{\omega_{a,tt}^2 + \omega_{b,tt}^2 + \sqrt{(\omega_{a,tt}^2 - \omega_{b,tt}^2)^2 + 4 \cdot \omega_{ab,tt}^4}} = 4.72 \text{ Hz}. \quad (\text{C.38})$$

### C.3.2 1 DOF schematization

To get a one DOF schematization, the two DOF system described in the previous section must be further simplified. It is not justified to simply combine the primary and secondary suspension, since both are tuned to damp different frequency spectra. Therefore the primary suspension will be neglected and the frame mass condensed to the wheel mass. The resulting bogie can be seen in Figure C.7.

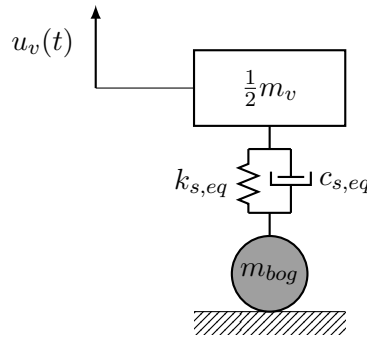


**Figure C.7:** 1 DOF bogie schematization of RMO 9000 bogie

This 1 DOF schematization uses the same parameters and values as the 2 DOF schematization, which is listed in Table C.3. The only difference is that the frame mass is not sprung by the primary suspension. The Ansys analyses using this vehicle model can be found in subsection L.4.1. The following natural frequencies can be calculated for the 1 DOF schematization. There are two cases, depending on the motor coach or trailer coach, which have different masses.

The first one is the motor coach with the motor or trailer bogie (the secondary spring stiffness is equal between the motor and trailer bogie)

$$\omega_{n,m} = \sqrt{\frac{k_{s,m,eq}}{\frac{1}{2}m_{v,m}}} \cdot \frac{1}{2\pi} = \sqrt{\frac{920\,000}{\frac{1}{2} \cdot 51\,500}} \cdot \frac{1}{2\pi} = 0.95 \text{ Hz} \quad (\text{C.39})$$

and the second one is the trailer coach with the trailer bogie

$$\omega_{n,t} = \sqrt{\frac{k_{s,t,eq}}{\frac{1}{2}m_{v,t}}} \cdot \frac{1}{2\pi} = \sqrt{\frac{920\,000}{\frac{1}{2} \cdot 43\,500}} \cdot \frac{1}{2\pi} = 1.04 \text{ Hz}. \quad (\text{C.40})$$

### C.3.3 Full coach schematization

The following more refined model will be used, as seen in Figure C.8. The coach is represented by a concentrated mass which has a vertical translational DOF and a rotational DOF related to the mass moment of inertia. The advantage of this model is that it can represent the interlocking behaviour of a coach.

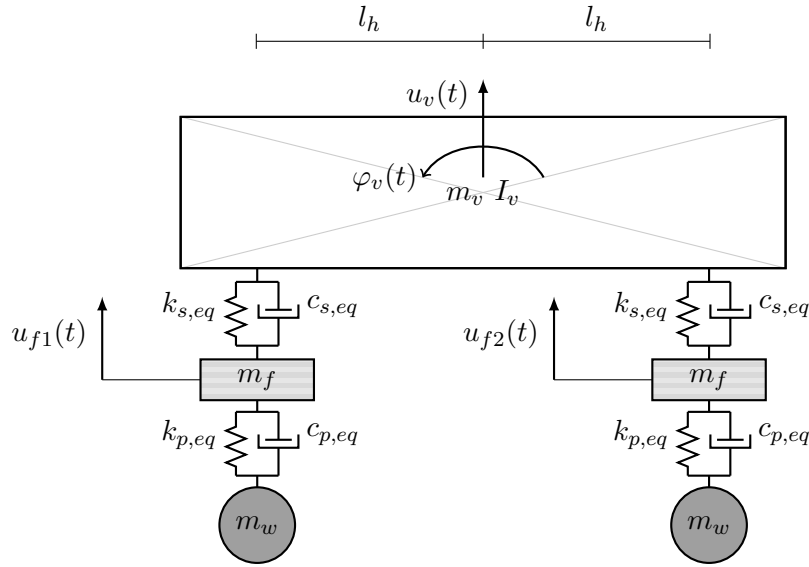


Figure C.8: VIRM coach model with 4 DOF

This vehicle model can use most the data from Table C.3, with some additional parameters.

These are:

- rotation  $\varphi_v(t)$  [rad]
- mass moment of inertia  $I_v$  [kg m<sup>2</sup>]
- coach height  $h_v$  [m]
- coach length  $w_v$  [m]

The mass moment of inertia for the motor coaches is

$$I_{v,m} = \frac{m_{v,m}}{12}(h_v^2 + w_v^2) = \frac{51500}{12}(1^2 + 26.82^2) = 3\,091\,340.7 \text{ kg m}^2, \quad (\text{C.41})$$

and for the trailer coaches it is

$$I_{v,t} = \frac{m_{v,t}}{12}(h_v^2 + w_v^2) = \frac{43500}{12}(1^2 + 26.82^2) = 2\,611\,132.5 \text{ kg m}^2. \quad (\text{C.42})$$

In these equations the real length of a coach is used, but the height is set to unity. The Ansys analyses using this vehicle model can be found in subsection L.4.3. For the full coach schematization the natural frequencies are equal to the 2 DOF schematization. For example if the full coach mass would be used, the spring stiffness must be taken twice, since this mass is supported by two springs.

---

# Appendix D

---

## Dynamics theory

This appendix gives an overview of different schematizations of vehicle-bridge interaction. In section D.1 an overview of some schematizations is given. The unsprung mass model, 1 DOF sprung mass model, multiple 1 DOF sprung masses, 2 DOF sprung masses and full coach model are discussed in section D.2, section D.3, section D.4, section D.5 and section D.6 respectively. Some information about discretization is given in section D.7 and the cause of the vibrations in section D.8. This appendix is referenced from section 2.6.

### D.1 Schematizing vehicle-bridge interaction

The dynamic interaction between trains and railway bridges consists of different components and is a coupled, non-linear dynamic problem. [2, page 1] Both trains, bridges and their interaction can be modelled with complex models taking into account all sorts of effects. When considering the bridge response, the vehicle can be schematized most simply as moving loads. This is justified if the weight of the vehicle is small compared to the bridge, which is the case with longer span bridges. However, this train model will never give any information about the vibrations felt in the train, which must be known to say something about passenger comfort. Therefore it will not be considered in this report, instead various more realistic train models will be considered, as can be seen in Figure D.1.

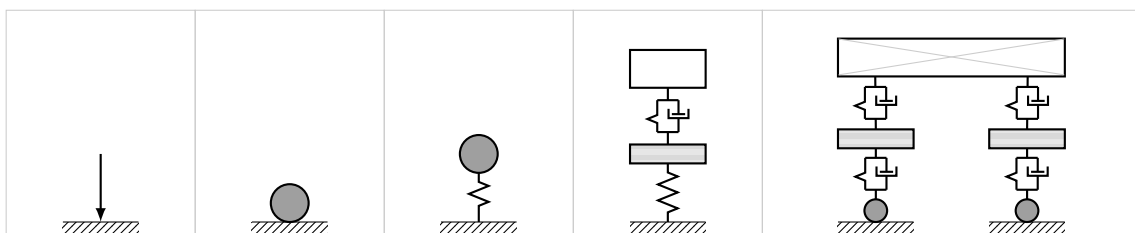


**Figure D.1:** Vehicle as moving load, unsprung mass, 1 DOF sprung mass, 2 DOF sprung mass and full coach model based on [25, fig. 2.4]

The theoretical model of a railway bridge can have continuous distributed mass or lumped mass. A continuous mass distribution is necessary if the mass of the structure cannot be neglected with respect to the mass of vehicles. [5, page 29]

## D.2 Unsprung mass

The most simple vehicle model in Figure D.1 is a moving load, which will not be considered because it cannot be used to predict passenger comfort. The next model is the unsprung mass, described by Biggs in 1964. The moving unsprung mass loads the beam with a force consisting of a gravitational part minus the inertia due to the acceleration of the mass. This model makes use of an Euler-Bernoulli beam and neglects damping of the beam. [3, par. 8.4] It is described by one equation of motion, Equation D.1, the only degree of freedom is the vertical position of the beam. [27, eq. 8.1], [3, par. 8.4]

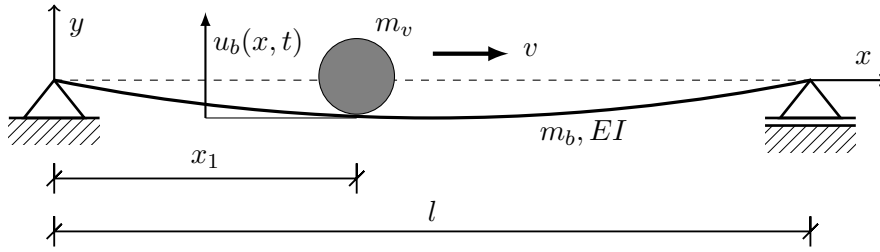


Figure D.2: Moving unsprung mass (based on [5, fig. 3.21])

$$EI \frac{\partial^4 u_b(x, t)}{\partial x^4} + m_b \frac{\partial^2 u_b(x, t)}{\partial t^2} = \delta(x - x_1) [m_v g - m_v \frac{\partial^2 u_b(x_1, t)}{\partial t^2}] \quad (D.1)$$

beam stiffness
beam mass inertia
position mass
mass gravity
mass acceleration

Where the horizontal position of the moving mass can be described with:

$$x_1 = vt \quad (D.2)$$

- $u_b(x, t)$  = deflection of beam, measured from original position [m];
- $E$  = Young's modulus of the beam [ $\text{N}/\text{m}^2$ ];
- $I$  = Moment of inertia of the beam in y-direction [ $\text{m}^4$ ];
- $m_b$  = beam mass per unit length [ $\text{kg}/\text{m}$ ];
- $m_v$  = mass moving in x-direction [kg];
- $g$  = gravitational acceleration [ $\text{m}/\text{s}^2$ ];
- $v$  = velocity of mass [ $\text{m}/\text{s}$ ];
- $t$  = time [s];
- $\delta(x)$  = Dirac delta function.

The right hand side of the equation describes the moving mass. The Dirac delta function is used to let the moving mass only act on the beam at the position it is located. Furthermore the right hand side consists of the gravitational force of the mass (mass times gravitational acceleration) and the inertia response of the beam, mass times acceleration of the beam. The latter derivative introduces complications, assuming uniform velocity it consists of: [5, formula 3.45]

$$\frac{d^2 u_b(x_1, t)}{dt^2} = \left[ c^2 \frac{\partial^2 u_b(x, t)}{\partial x^2} + 2c \frac{\partial^2 u_b(x, t)}{\partial x \partial t} + \frac{\partial^2 u_b(x, t)}{\partial t^2} \right]_{x=x_1} \quad (\text{D.3})$$

So the acceleration consist of three parts:

1. track curvature influence;
2. Coriolis acceleration;
3. influence of the acceleration of the moving load in vertical direction.

Especially the second part of this acceleration causes the differential equation to be coupled. [54] An often used simplification is to only use the dominant third term. The expression can then be simplified to Equation D.4.

$$\frac{d^2 u_b(x_1, t)}{dt^2} = \frac{\partial^2 u_b(x, t)}{\partial t^2} \Big|_{x=x_1} \quad (\text{D.4})$$

The good thing of this unsprung mass model is that the inertia of the mass is taken into account, which is not the case for the moving load model. However, the mass does not have a separate motion / degree of freedom, it moves fixed to the beam. Therefore it is necessary to consider more complicated models.

### D.3 Single 1 DOF sprung mass

In the single 1 DOF sprung mass model, a spring is put between the mass and the beam. Now the mass has its own degree of freedom and can move separate from the beam, in vertical direction. This situation can be described by a system of two coupled equations of motion. [26], [55], [56]

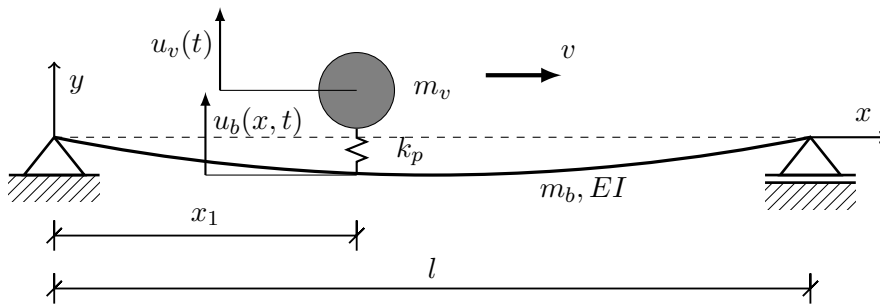


Figure D.3: Moving sprung 1 DOF mass, based on [26, fig. 1]

The equation of motion for the beam can be expressed as

$$EI \underbrace{\frac{\partial^4 u_b(x, t)}{\partial x^4}}_{\text{beam stiffness}} + m_b \underbrace{\frac{\partial^2 u_b(x, t)}{\partial t^2}}_{\text{beam mass inertia}} = ( \underbrace{-m_v g}_{\text{mass gravity}} + \underbrace{k_p [u_v(t) - u_b(x_1, t)]}_{\text{spring force}} ) \underbrace{\delta(x - x_1)}_{\text{position mass}} \quad (\text{D.5})$$

the equation of motion for the mass can be expressed as

$$\underbrace{m_v \frac{d^2 u_v(t)}{dt^2}}_{\text{mass acceleration}} + \underbrace{k_p [u_v(t) - u_b(x_1, t)]}_{\text{spring force}} = 0 \quad (\text{D.6})$$

and the following new symbols are used:

- $u_v(t)$  = mass displacement, measured from static equilibrium position [m];
- $k_p$  = primary spring stiffness [N/m].

The gravity term related to the mass appears in Equation D.5 and not in Equation D.6 because the mass displacement is measured from its static equilibrium position.

The left hand side of Equation D.5 is a partial differential equation describing the transverse vibrations of the beam. From a free vibration analysis with simply supported boundary conditions as in Equation D.7 and Equation D.8 and homogeneous initial conditions as in Equation D.9 and Equation D.10, one finds natural frequencies and modal functions as in Equation D.11 and Equation D.12 where  $n = 1, 2, 3, \dots$  as in Figure D.4.

The boundary conditions for a simply supported situation are

$$u_b(0, t) = \frac{\partial^2 u_b}{\partial x^2}(0, t) = 0 \quad (\text{D.7})$$

$$u_b(l, t) = \frac{\partial^2 u_b}{\partial x^2}(l, t) = 0. \quad (\text{D.8})$$

The homogeneous initial conditions are

$$u_b(x, 0) = 0 \quad (\text{D.9})$$

$$\frac{\partial u_b}{\partial t}(x, 0) = 0. \quad (\text{D.10})$$

The natural frequencies and eigenmodes are

$$\omega_n^2 = \frac{EI}{m_b} \left( \frac{n\pi}{l} \right)^4 \quad (\text{D.11})$$

$$\phi_n(x) = \sin \left( \frac{n\pi x}{l} \right). \quad (\text{D.12})$$

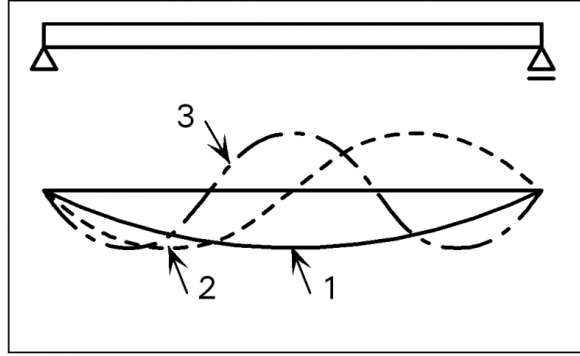


**Figure D.4:** Beam mode shapes [57]

The following help variables are defined:

$$\beta_n = \frac{n\pi}{l} \quad \beta_m = \frac{m\pi}{l}. \quad (\text{D.13})$$

With the modes of the beam known, the expansion theorem can be used to separate the differential equation into a linear combination of place dependent normal modes and a time dependent part, in Equation D.14. [25, par 2.1]

$$u_b(x, t) = \sum_{n=1}^{\infty} q_n(t) \phi_n(x) = \sum_{n=1}^{\infty} q_n(t) \sin(\beta_n x) \quad (\text{D.14})$$

Filling Equation D.14 into Equation D.5 and Equation D.6 results in

$$EI \frac{\partial^4}{\partial x^4} \left( \sum_{n=1}^{\infty} q_n(t) \sin(\beta_n x) \right) + m_b \frac{\partial^2}{\partial t^2} \left( \sum_{n=1}^{\infty} q_n(t) \sin(\beta_n x) \right) = \left( -m_v g + k_p \left[ u_v(t) - \left( \sum_{n=1}^{\infty} q_n(t) \sin(\beta_n x_1) \right) \right] \right) \delta(x - x_1), \quad (\text{D.15})$$

$$m_v \frac{d^2 u_v(t)}{dt^2} + k_p \left[ u_v(t) - \sum_{n=1}^{\infty} q_n(t) \sin(\beta_n x_1) \right] = 0. \quad (\text{D.16})$$

Working out the derivatives and some re-arranging transforms Equation D.15 into

$$EI q_n(t) \sum_{n=1}^{\infty} \sin(\beta_n x) \beta_n^4 + m_b \ddot{q}_n(t) \sum_{n=1}^{\infty} \sin(\beta_n x) = \left( -m_v g + k_p \left[ u_v(t) - \left( q_n(t) \sum_{n=1}^{\infty} \sin(\beta_n x_1) \right) \right] \right) \delta(x - x_1). \quad (\text{D.17})$$

By multiplying with an arbitrary mode  $m$  and integrating over  $x$ , Equation D.17 can be expressed

as

$$\begin{aligned} \int_0^l EIq_n(t) \sin(\beta_m x) \sum_{n=1}^{\infty} \sin(\beta_n x) \beta_n^4 dx + \int_0^l m_b \ddot{q}_n(t) \sin(\beta_m x) \sum_{n=1}^{\infty} \sin(\beta_n x) dx = \\ \int_0^l -m_v g \delta(x - x_1) \sin(\beta_m x) dx + \int_0^l k_p u_v(t) \delta(x - x_1) \sin(\beta_m x) dx + \\ \int_0^l -k_p q_n(t) \sum_{n=1}^{\infty} \sin(\beta_n x_1) \delta(x - x_1) \sin(\beta_m x) dx. \quad (\text{D.18}) \end{aligned}$$

Dividing Equation D.18 by  $\int_0^l \sin(\beta_m x) \sum_{n=1}^{\infty} \sin(\beta_n x) dx$  and putting parts of equation not depend on  $x$  in front of the integrals results in

$$\begin{aligned} EIq_n(t) \beta_n^4 + m_b \ddot{q}_n(t) = \frac{-m_v g \int_0^l \delta(x - x_1) \sin(\beta_m x) dx}{\int_0^l \sin(\beta_m x) \sum_{n=1}^{\infty} \sin(\beta_n x) dx} + \\ \frac{k_p u_v(t) \int_0^l \delta(x - x_1) \sin(\beta_m x) dx}{\int_0^l \sin(\beta_m x) \sum_{n=1}^{\infty} \sin(\beta_n x) dx} + \\ \frac{-k_p q_n(t) \sum_{n=1}^{\infty} \sin(\beta_n x_1) \int_0^l \delta(x - x_1) \sin(\beta_m x) dx}{\int_0^l \sin(\beta_m x) \sum_{n=1}^{\infty} \sin(\beta_n x) dx}. \quad (\text{D.19}) \end{aligned}$$

Note that  $\sin(\beta_n x_1)$  is not a function of  $x$ , but of  $t$ , per definition of  $x_1$  in Equation D.2. The orthogonality mode property is defined in Equation D.20. Applying this property results in the disappearance of the summation of all modes, since only one non-zero result remains when  $m$  is equal to  $n$ ,

$$\int_0^l \sin(\beta_n x) \sin(\beta_m x) dx = \int_0^l \sin\left(\frac{n\pi x}{l}\right) \sin\left(\frac{m\pi x}{l}\right) dx = \begin{cases} l/2, & m = n \\ 0, & m \neq n \end{cases} \quad (\text{D.20})$$

A fundamental property of the Dirac delta function is

$$\int_{-\infty}^{\infty} f(a \cdot x) \delta(x - b) dx = f(a \cdot b), \quad (\text{D.21})$$

but with the used integration bounds

$$\int_0^l f(a \cdot x) \delta(x - b) dx = (H(l - b) - 1 + H(b)) f(a \cdot b) = \theta(b) f(a \cdot b), \quad (\text{D.22})$$

where the Heaviside function is defined as

$$H(a) = \begin{cases} 0, & a < 0 \\ 1, & a \geq 0 \end{cases}, \quad (\text{D.23})$$

and the following help variable is introduced:

$$\theta(b) = H(l - b) - 1 + H(b). \quad (\text{D.24})$$

Changing subscript  $m$  to  $n$  when applicable, Equation D.19 can be reduced to,

$$EIq_n(t)\beta_n^4 + m_b\ddot{q}_n(t) = \frac{-m_v g \theta(x_1) \sin(\beta_n x_1)}{l/2} + \frac{k_p u_v(t) \theta(x_1) \sin(\beta_n x_1)}{l/2} + \frac{-k_p q_n(t) \sum_{n=1}^{\infty} \sin(\beta_n x_1) \theta(x_1) \sin(\beta_n x_1)}{l/2}. \quad (\text{D.25})$$

This equation can be further rewritten to

$$EIq_n(t)\beta_n^4 + m_b\ddot{q}_n(t) = \frac{-2m_v g \theta(x_1) \sin(\beta_n x_1)}{l} + \frac{2k_p \theta(x_1) \sin(\beta_n x_1)}{l} u_v(t) + \frac{-2k_p \sum_{n=1}^{\infty} \sin^2(\beta_n x_1) \theta(x_1)}{l} q_n(t). \quad (\text{D.26})$$

With the beam natural frequencies from Equation D.11 and the mass-spring system natural frequency as

$$\omega_n = \sqrt{\frac{EI}{m_b}} \beta_n^2, \quad (\text{D.27})$$

$$\omega_m = \sqrt{\frac{k_p}{m_v}} \quad (\text{note, this means } k_p = \omega_m^2 m_v), \quad (\text{D.28})$$

Equation D.26 and Equation D.16 can be expressed as two coupled ordinary differential equations

$$\omega_n^2 q_n + \ddot{q}_n = -\frac{2m_v g}{m_b l} \theta(x_1) \sin(\beta_n x_1) + \frac{2\omega_m^2 m_v}{m_b l} \theta(x_1) \sin(\beta_n x_1) \cdot u_v - \frac{2\omega_m^2 m_v}{m_b l} \theta(x_1) \sum_{n=1}^{\infty} \sin^2(\beta_n x_1) \cdot q_n, \quad (\text{D.29})$$

$$\ddot{u}_v + \omega_m^2 u_v = \omega_m^2 \sum_{n=1}^{\infty} \sin(\beta_n x_1) \cdot q_n. \quad (\text{D.30})$$

This can be represented in matrix form as well. Here only the first mode  $n = 1$  is considered, since it can be shown the influence of higher modes is not large. [2] Please note this assumption is not absolutely needed to obtain a solution, it is just a simplification useful for subsequent implementation in Matlab.

$$\begin{bmatrix} \ddot{q}_n \\ \ddot{u}_v \end{bmatrix} + \begin{bmatrix} \frac{2\omega_m^2 m_v}{m_b l} \theta(x_1) \sin^2(\frac{\pi x_1}{l}) + \omega_n^2 & -\frac{2\omega_m^2 m_v}{m_b l} \theta(x_1) \sin(\frac{\pi x_1}{l}) \\ -\omega_m^2 \sin(\frac{\pi x_1}{l}) & \omega_m^2 \end{bmatrix} \begin{bmatrix} q_n \\ u_v \end{bmatrix} = \begin{bmatrix} -\frac{2m_v g}{m_b l} \theta(x_1) \sin(\frac{\pi x_1}{l}) \\ 0 \end{bmatrix} \quad (\text{D.31})$$

These equations can be expressed as a system of first order differential equations to be solved by numerical software such as Matlab, which is presented in section E.1.

## D.4 Multiple 1 DOF sprung masses

A more realistic representation of the vehicle is a representation by multiple sprung masses, instead of just one. It is assumed the approach bridge before and after the main bridge are completely rigid. When the train bogies arrive at the main bridge they have not experienced any vertical displacement yet. The previously provided equations of motion Equation D.5 and Equation D.6 will slightly change to

$$\underbrace{EI \frac{\partial^4 u_b(x, t)}{\partial x^4}}_{\text{beam stiffness}} + \underbrace{m_b \frac{\partial^2 u_b(x, t)}{\partial t^2}}_{\text{beam mass inertia}} = \sum_{r=1}^s \left( \underbrace{-m_{v,r}g}_{\text{mass gravity}} + \underbrace{k_{p,r} [u_{v,r}(t) - u_b((x_1 - x_{0,r}), t)]}_{\text{spring force}} \right) \underbrace{\delta(x - (x_1 - x_{0,r}))}_{\text{position r-th mass}}, \quad (\text{D.32})$$

$$\sum_{r=1}^s \underbrace{m_{v,r} \frac{d^2 u_{v,r}(t)}{dt^2}}_{\text{mass acceleration}} + \underbrace{k_{p,r} [u_{v,r}(t) - u_b((x_1 - x_{0,r}), t)]}_{\text{spring force}} = 0 \quad (\text{D.33})$$

and the following new symbols are used:

- $s$  = total number of sprung masses;
- $r$  = index of sprung mass;
- $u_{v,r}$  = displacement of r-th sprung mass [m];
- $m_{v,r}$  = r-th sprung mass [kg];
- $k_{p,r}$  = r-th spring stiffness [N/m];
- $x_{0,r}$  = starting position of r-th sprung mass.

These equations of motion will be rewritten to a form suitable to solve in Matlab, but to ease the process and prevent a high number of summation signs in the derivation, only two bogies will be considered. The equations of motion for two sprung masses are

$$EI \frac{\partial^4 u_b(x, t)}{\partial x^4} + m_b \frac{\partial^2 u_b(x, t)}{\partial t^2} = (-m_{v,1}g + k_{p,1} [u_{v,1}(t) - u_b((x_1 - x_{0,1}), t)]) \delta(x - (x_1 - x_{0,1})) + (-m_{v,2}g + k_{p,2} [u_{v,2}(t) - u_b((x_1 - x_{0,2}), t)]) \delta(x - (x_1 - x_{0,2})), \quad (\text{D.34})$$

$$m_{v,1} \frac{d^2 u_{v,1}(t)}{dt^2} + k_{p,1} [u_{v,1}(t) - u_b((x_1 - x_{0,1}), t)] + m_{v,2} \frac{d^2 u_{v,2}(t)}{dt^2} + k_{p,2} [u_{v,2}(t) - u_b((x_1 - x_{0,2}), t)] = 0. \quad (\text{D.35})$$

With the same boundary conditions, initial conditions and mode shapes as the single moving sprung mass, a solution in the form of Equation D.14 is assumed, which results in

$$EIq_n(t) \sum_{n=1}^{\infty} \sin(\beta_n x) \beta_n^4 + m_b \ddot{q}_n(t) \sum_{n=1}^{\infty} \sin(\beta_n x) = \left( -m_{v,1} g + k_{p,1} \left[ u_{v,1}(t) - q_n(t) \sum_{n=1}^{\infty} \sin(\beta_n (x_1 - x_{0,1})) \right] \right) \delta(x - (x_1 - x_{0,1})) + \left( -m_{v,2} g + k_{p,2} \left[ u_{v,2}(t) - q_n(t) \sum_{n=1}^{\infty} \sin(\beta_n (x_1 - x_{0,2})) \right] \right) \delta(x - (x_1 - x_{0,2})), \quad (\text{D.36})$$

$$m_{v,1} \ddot{u}_{v,1}(t) + k_{p,1} \left[ u_{v,1}(t) - q_n(t) \sum_{n=1}^{\infty} \sin(\beta_n (x_1 - x_{0,1})) \right] + m_{v,2} \ddot{u}_{v,2}(t) + k_{p,2} \left[ u_{v,2}(t) - q_n(t) \sum_{n=1}^{\infty} \sin(\beta_n (x_1 - x_{0,2})) \right] = 0. \quad (\text{D.37})$$

Multiplying Equation D.36 with an arbitrary mode  $m$ , integrating over  $x$  and dividing by  $\int_0^l \sin(\beta_m x) \sum_{n=1}^{\infty} \sin(\beta_n x) dx$  results in

$$EIq_n(t) \beta_n^4 + m_b \ddot{q}_n(t) = \frac{-m_{v,1} g \int_0^l \delta(x - (x_1 - x_{0,1})) \sin(\beta_m x) dx}{\int_0^l \sin(\beta_m x) \sum_{n=1}^{\infty} \sin(\beta_n x) dx} + \frac{k_{p,1} u_{v,1}(t) \int_0^l \delta(x - (x_1 - x_{0,1})) \sin(\beta_m x) dx}{\int_0^l \sin(\beta_m x) \sum_{n=1}^{\infty} \sin(\beta_n x) dx} + \frac{-k_{p,1} q_n(t) \sum_{n=1}^{\infty} \sin(\beta_n (x_1 - x_{0,1})) \int_0^l \delta(x - (x_1 - x_{0,1})) \sin(\beta_m x) dx}{\int_0^l \sin(\beta_m x) \sum_{n=1}^{\infty} \sin(\beta_n x) dx} + \frac{-m_{v,2} g \int_0^l \delta(x - (x_1 - x_{0,2})) \sin(\beta_m x) dx}{\int_0^l \sin(\beta_m x) \sum_{n=1}^{\infty} \sin(\beta_n x) dx} + \frac{k_{p,2} u_{v,2}(t) \int_0^l \delta(x - (x_1 - x_{0,2})) \sin(\beta_m x) dx}{\int_0^l \sin(\beta_m x) \sum_{n=1}^{\infty} \sin(\beta_n x) dx} + \frac{-k_{p,2} q_n(t) \sum_{n=1}^{\infty} \sin(\beta_n (x_1 - x_{0,2})) \int_0^l \delta(x - (x_1 - x_{0,2})) \sin(\beta_m x) dx}{\int_0^l \sin(\beta_m x) \sum_{n=1}^{\infty} \sin(\beta_n x) dx}. \quad (\text{D.38})$$

With the solutions for the integrals as in Equation D.20, Equation D.22, Equation D.24 and changing subscript  $m$  to  $n$  when applicable, Equation D.38 can be reduced to

$$\begin{aligned}
EI\beta_n^4 q_n(t) + m_b \ddot{q}_n(t) = & \\
& \frac{-2m_{v,1} g \theta(x_1 - x_{0,1}) \sin(\beta_n(x_1 - x_{0,1}))}{l} + \\
& \frac{2k_{p,1} \theta(x_1 - x_{0,1}) \sin(\beta_n(x_1 - x_{0,1}))}{l} u_{v,1}(t) + \\
& \frac{-2k_{p,1} \sum_{n=1}^{\infty} \theta(x_1 - x_{0,1}) \sin^2(\beta_n(x_1 - x_{0,1}))}{l} q_n(t) + \\
& \frac{-2m_{v,2} g \theta(x_1 - x_{0,2}) \sin(\beta_n(x_1 - x_{0,2}))}{l} + \\
& \frac{2k_{p,2} \theta(x_1 - x_{0,2}) \sin(\beta_n(x_1 - x_{0,2}))}{l} u_{v,2}(t) + \\
& \frac{-2k_{p,2} \sum_{n=1}^{\infty} \theta(x_1 - x_{0,2}) \sin^2(\beta_n(x_1 - x_{0,2}))}{l} q_n(t). \quad (D.39)
\end{aligned}$$

With the previously defined beam natural frequencies in Equation D.11 and the sprung masses natural frequencies as

$$\omega_{m,r} = \sqrt{\frac{k_{p,r}}{m_{v,r}}} \quad (\text{note, this means } k_{p,r} = \omega_{m,r}^2 m_{v,r}), \quad (D.40)$$

considering only mode  $n = 1$ , Equation D.39 and Equation D.37 can be expressed as two coupled ordinary differential equations

$$A_1 q_n + \ddot{q}_n = -A_2 + A_3 \cdot u_{v,1} - A_4 \cdot q_n - A_5 + A_6 \cdot u_{v,2} - A_7 \cdot q_n, \quad (D.41)$$

$$\ddot{u}_{v,1} + B_1 u_{v,1} - B_2 \cdot q_n + \ddot{u}_{v,2} + C_1 u_{v,2} - C_2 \cdot q_n = 0. \quad (D.42)$$

with coefficients

$$\begin{aligned}
A_1 &= \omega_n^2 \\
A_2 &= \frac{2m_{v,1} g}{m_b l} \theta(x_1 - x_{0,1}) \sin\left(\frac{\pi(x_1 - x_{0,1})}{l}\right) \\
A_3 &= \frac{2\omega_{m,1}^2 m_{v,1}}{m_b l} \theta(x_1 - x_{0,1}) \sin\left(\frac{\pi(x_1 - x_{0,1})}{l}\right) \\
A_4 &= \frac{2\omega_{m,1}^2 m_{v,1}}{m_b l} \theta(x_1 - x_{0,1}) \sin^2\left(\frac{\pi(x_1 - x_{0,1})}{l}\right) \\
A_5 &= \frac{2m_{v,2} g}{m_b l} \theta(x_1 - x_{0,2}) \sin\left(\frac{\pi(x_1 - x_{0,2})}{l}\right) \\
A_6 &= \frac{2\omega_{m,2}^2 m_{v,2}}{m_b l} \theta(x_1 - x_{0,2}) \sin\left(\frac{\pi(x_1 - x_{0,2})}{l}\right) \\
A_7 &= \frac{2\omega_{m,2}^2 m_{v,2}}{m_b l} \theta(x_1 - x_{0,2}) \sin^2\left(\frac{\pi(x_1 - x_{0,2})}{l}\right) \\
B_1 &= \omega_{m,1}^2 \\
B_2 &= \omega_{m,1}^2 \sin\left(\frac{\pi(x_1 - x_{0,1})}{l}\right) \\
C_1 &= \omega_{m,2}^2 \\
C_2 &= \omega_{m,2}^2 \sin\left(\frac{\pi(x_1 - x_{0,2})}{l}\right)
\end{aligned} \tag{D.43}$$

This can be represented in matrix form as

$$\begin{bmatrix} \ddot{q}_n \\ \ddot{u}_{v,1} \\ \ddot{u}_{v,2} \end{bmatrix} + \begin{bmatrix} (A_1 + A_4 + A_7) & -A_3 & -A_6 \\ -B_2 & B_1 & 0 \\ -C_2 & 0 & C_1 \end{bmatrix} \begin{bmatrix} q_n \\ u_{v,1} \\ u_{v,2} \end{bmatrix} = \begin{bmatrix} -A_2 - A_5 \\ 0 \\ 0 \end{bmatrix} \tag{D.44}$$

These equations can be expressed as a system of first order differential equations to be solved by numerical software such as Matlab, which is presented in section E.2.

## D.5 2 DOF sprung mass

To even better represent the vehicle, it can be modelled by two connected sprung masses, with separate primary and secondary suspension. The model hereby presented is based on Fryba. [27, chap. 8]

The set of three simultaneous equations of motion, can be written in the following way (based on [27, eq. 8.7 - 8.10], [3, par. 8.5]).

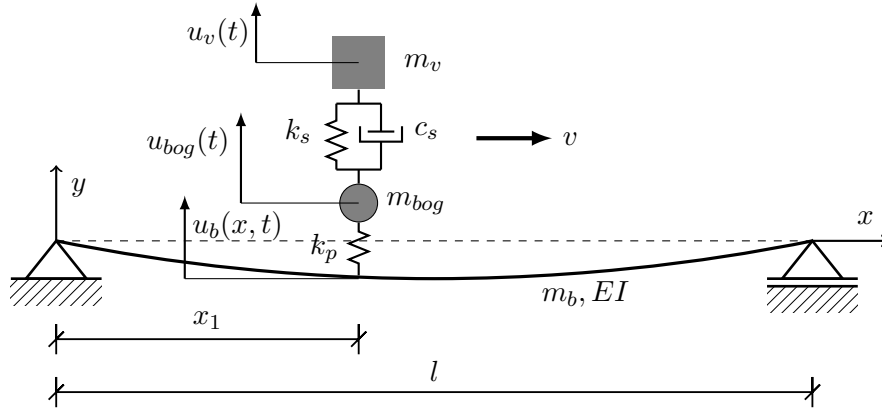


Figure D.5: Moving sprung 2 DOF masses, based on [27, fig. 8.2]

The equation of motion for the beam is

$$\underbrace{EI \frac{\partial^4 u_b(x, t)}{\partial x^4}}_{\text{beam stiffness}} + \underbrace{m_b \frac{\partial^2 u_b(x, t)}{\partial t^2}}_{\text{beam mass inertia}} = \underbrace{-(m_v + m_{bog})g}_{\text{mass gravity}} + \underbrace{k_p [u_{bog}(t) - u_b(x_1, t)]}_{\text{spring force}} \underbrace{\delta(x - x_1)}_{\text{position mass}} \quad (\text{D.45})$$

the equation of motion for the bogie mass is

$$\underbrace{m_{bog} \frac{d^2 u_{bog}(t)}{dt^2}}_{\text{mass acceleration}} - \underbrace{k_s [u_v(t) - u_{bog}(t)]}_{\text{sec. spring force}} - \underbrace{c_s \left[ \frac{d}{dt} u_v(t) - \frac{d}{dt} u_{bog}(t) \right]}_{\text{sec. damper force}} + \underbrace{k_p [u_{bog}(t) - u_b(x_1, t)]}_{\text{prim. spring force}} = 0, \quad (\text{D.46})$$

and the equation of motion for the vehicle mass is

$$\underbrace{m_v \frac{d^2 u_v(t)}{dt^2}}_{\text{mass acceleration}} + \underbrace{k_s [u_v(t) - u_{bog}(t)]}_{\text{sec. spring force}} + \underbrace{c_s \left[ \frac{d}{dt} u_v(t) - \frac{d}{dt} u_{bog}(t) \right]}_{\text{sec. damper force}} = 0. \quad (\text{D.47})$$

The following new parameters are used in these equations:

- $u_{bog}(t)$  = bogie displacement, measured from static equilibrium position [m];
- $m_{bog}$  = mass of the bogie [kg];
- $k_v$  = spring stiffness suspension system [N/m];
- $c_v$  = damping value suspension system [Ns/m].

Please note that the mass gravity term  $(m_v + m_{bog})g$  could also be moved to the bogie mass equation, which is how it is done in some literature [27, eq. 8.8]. It is chosen to put it in the beam equation of motion, to make it more clear what forces act on the beam from the moving sprung masses.

## D.6 Full coach model

Finally the most complex vehicle model from Figure D.1 is considered in this section, the full coach model. The main difference with the previous model is the addition of a rotational degree of freedom.

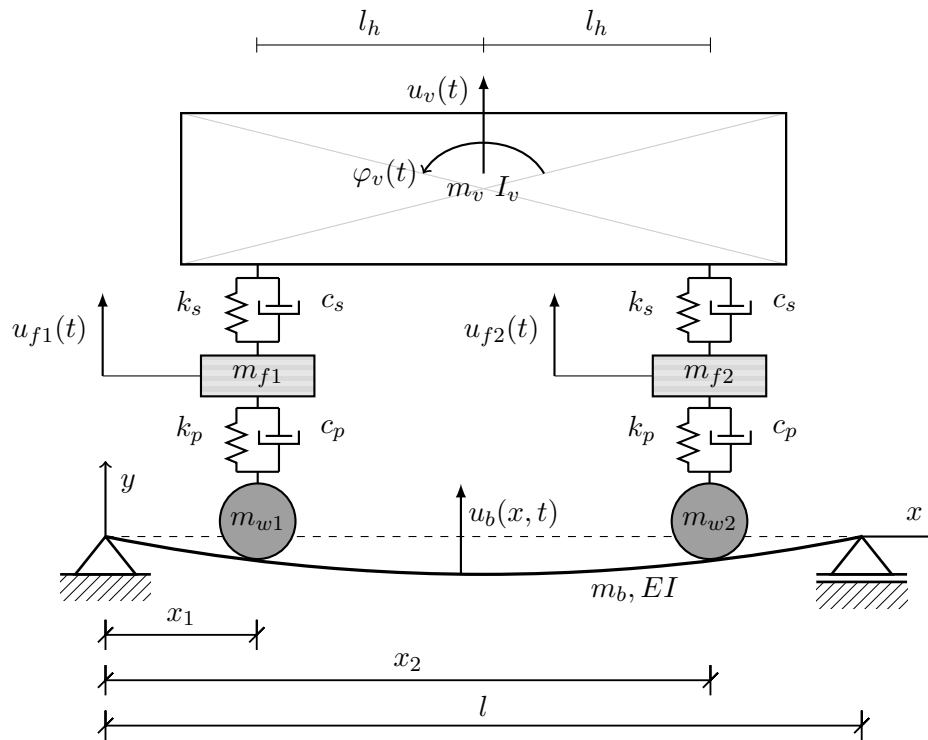


**Figure D.6:** Full coach model with 4 DOF

New parameters in Figure D.6 are:

- rotation  $\varphi_v(t)$  [rad]
- mass moment of inertia  $I_v$  [ $\text{kg m}^2$ ]
- position second bogie  $x_2$  [m]
- centre to bogie distance  $l_h$  [m]

The set of three simultaneous equations of motion, can be written in the following way by derivation using the displacement method, based on [58] and [59].

The equation of motion for the beam is

$$\begin{aligned}
 \underbrace{EI \frac{\partial^4 u_b(x, t)}{\partial x^4}}_{\text{beam stiffness}} + \underbrace{m_b \frac{\partial^2 u_b(x, t)}{\partial t^2}}_{\text{beam mass inertia}} = \sum_{i=1}^2 \left( \underbrace{\left( -\left( \frac{1}{2} m_v + m_{f_i} + m_{w_i} \right) g - m_{w_i} \frac{\partial^2 u_b(x_i, t)}{\partial t^2} \right)}_{\text{mass gravity}} \right. \\
 \left. + \underbrace{k_p [u_{f_i}(t) - u_b(x_i, t)]}_{\text{prim. spring force}} + \underbrace{c_p \left[ \frac{d}{dt} u_{f_i}(t) - \frac{d}{dt} u_b(x_i, t) \right]}_{\text{prim. damper force}} \right) \underbrace{\delta(x - x_i)}_{\text{position mass}} \quad (\text{D.48})
 \end{aligned}$$

the equation of motion for the frame masses is

$$\begin{aligned}
 \sum_{i=1}^2 \left( \underbrace{m_{f_i} \frac{d^2 u_{f_i}(t)}{dt^2}}_{\text{mass acceleration}} - \underbrace{k_s [u_v(t) \pm \varphi_v l_h - u_{f_i}(t)]}_{\text{sec. spring force}} - \underbrace{c_s \left[ \frac{d}{dt} u_v(t) \pm \frac{d}{dt} \varphi_v l_h - \frac{d}{dt} u_{f_i}(t) \right]}_{\text{sec. damper force}} \right. \\
 \left. + \underbrace{k_p [u_{f_i}(t) - u_b(x_i, t)]}_{\text{prim. spring force}} + \underbrace{c_p \left[ \frac{d}{dt} u_{f_i}(t) - \frac{d}{dt} u_b(x_i, t) \right]}_{\text{prim. damper force}} \right) = 0, \quad (\text{D.49})
 \end{aligned}$$

and the equations of motion for the vehicle mass are

$$\underbrace{m_v \frac{d^2 u_v(t)}{dt^2}}_{\text{mass acceleration}} + \sum_{i=1}^2 \left( \underbrace{-k_s [u_v(t) \pm \varphi_v l_h - u_{f_i}(t)]}_{\text{sec. spring force}} - \underbrace{c_s \left[ \frac{d}{dt} u_v(t) \pm \frac{d}{dt} \varphi_v l_h - \frac{d}{dt} u_{f_i}(t) \right]}_{\text{sec. damper force}} \right) = 0, \quad (\text{D.50})$$

$$\underbrace{I_v \frac{d^2 \varphi_v(t)}{dt^2}}_{\text{angular acceleration}} + \sum_{i=1}^2 \left( \underbrace{-k_s l_h [u_v(t) \pm \varphi_v l_h - u_{f_i}(t)]}_{\text{sec. spring force}} - \underbrace{c_s l_h \left[ \frac{d}{dt} u_v(t) \pm \frac{d}{dt} \varphi_v l_h - \frac{d}{dt} u_{f_i}(t) \right]}_{\text{sec. damper force}} \right) = 0. \quad (\text{D.51})$$

Please note that in the above equations of motion the  $\pm$  means: for  $i = 1$  there is a plus and for  $i = 2$  there is a minus. When the coach rotates this means a tension force for the first bogie and a compression force for the second bogie, or the other way around.

Although these equations of motion are more complicated than in previous sections and more degrees of freedom are taken into account, the contact forces remain fairly simple. The forces transmitted from the vehicle wheels to the bridge are not complicated by adding springs, dampers or extra masses above it.

## D.7 Discretization

The equations of motion presented in the previous sections were all descriptions of the continuous structure. When using FEM the structure will be discretised and the equation of motion turns into:

$$M\ddot{u} + C\dot{u} + Ku = f(t) \quad (\text{D.52})$$

- $M$  = mass matrix
- $C$  = damping matrix
- $K$  = stiffness matrix
- $f(t)$  = external load vector
- $u$  = vector of nodal displacements
- $\dot{u}$  = vector of nodal velocities, displacements differentiated with respect to time
- $\ddot{u}$  = vector of nodal accelerations, displacements differentiated twice with respect to time

The damping matrix is usually defined with Rayleigh damping theory, which makes it a linear multiplication of the mass and stiffness matrices.

## D.8 Vibrations

All vertical movements start with vertical displacement. This displacement can be caused by the weight of the vehicle (the mass of the vehicle which is pulled down by gravity) and forces the bridge, which is not infinitely stiff, to displace. The bridge bends down and bends up, which causes vibration.

The Eurocode provides several factors contributing to the total dynamic interaction between vehicle and bridge: inertial response, resonance effects and additional dynamic effects (due to track irregularities, wheel defects and suspension defects). [1, 6.4.1 (1)]

### D.8.1 Resonance

Resonance is a phenomenon which can occur when an excitation frequency, for example of a train, coincides with a natural frequency of another object subject to the excitation frequency, for example the bridge. When resonance occurs, the vibrations will grow linearly with time and is limited by damping.

If the wavelength of excitation is defined as  $\lambda$  in Equation D.53, resonance can occur if the length  $D_k$  coincides with a multiple of this wavelength, as in Equation D.54. [40, page 31-32]

$$\lambda = \frac{v}{f_0} \quad (\text{D.53})$$

$$\lambda = \frac{D_k}{i} \quad (\text{D.54})$$

- $f_0$  = first natural frequency of deck vibration [Hz = 1/s]
- $v$  = train velocity [m/s]
- $D_k$  = characteristic length of separation between axles [m]

- $\lambda$  = wavelength [m]
- $i$  = integer number [-]

Dynamic behaviour occurs in a fairly wide band ranging from 0.5 Hz to 2000 Hz. Short waves correspond to high frequencies and originate from rail corrugation, wheel irregularities and weld imperfections. For these frequencies the Hertzian contact spring should be taken into account. Long waves correspond to low frequencies and are caused by rail rolling defects and inertia from bogies. [21, page 113]

Higher frequency vibrations have less influence on passenger comfort, since they are easier damped out by the train suspension. It is likely passengers will feel low order frequencies to a higher extend, which also follows from the frequency weighting curve  $W_b$  in ISO 2631. [10]

### D.8.2 Track irregularities

Four types of track irregularities can be distinguished: elevation, alignment, superelevation and gauge irregularity. [5, page 120] The alignment and gauge irregularities are lateral, while the elevation and superelevation are vertical. Irregularities can be periodic, for example wheel flats, rail joints, corrugated rail surface. But the cross-beam and the sleeper effects are also periodic irregularities.

Zhang compares plane and space models. [58] In the plane model the left and right rails are considered with the same roughness, in the space model the left and right rail have separate roughness. It is concluded there is no large difference between the results of both approaches.

Irregularities can be random or stochastic [5, page 126], caused by wear, clearness, subsidence, insufficient maintenance. They are characterised by a power spectral density function. Rail joints have large dynamic effects and should not occur on bridges. [5, page 123]

For the purpose of this research it is chosen to **not** include track irregularities and assume the railway track to be relatively smooth on the bridge.

### D.8.3 Wheel imperfections

Two types of wheel imperfections can be considered, depending on the shape of deformation as can be seen in Figure D.7.

The displacement of the axle as a result of these imperfections can be calculated with: [13, par 5.2.2]

$$u_{axle} = dR \sin\left(\frac{nvt}{R + \phi}\right) \quad (D.55)$$

- $dR$  = imperfection [m]
- $t$  = time [s]
- $v$  = velocity of train [m/s]

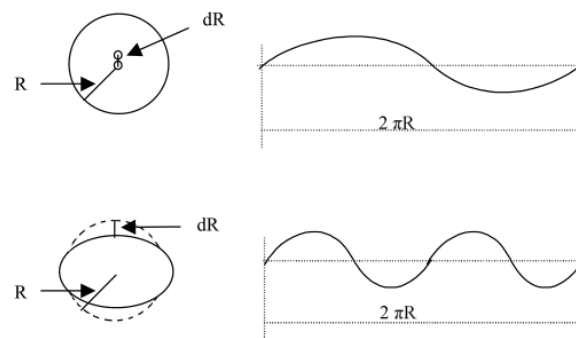


**Figure D.7:** Two wheel imperfections, above one period per rotation caused by a not centred axle, below, two periods per rotation, caused by elliptically shaped wheels. [13, fig. 40]

- $R$  = wheel radius, default of 0.46 [m]
- $\phi$  = phase [rad]
- $n$  = number of periods per rotation, 1 or 2 [-]

For the purpose of this research it is chosen to **not** include wheel imperfections and assume the train wheels are relatively smooth. For freight trains it is more common to encounter deformed wheels, but for passenger trains wheels are often in generally good conditions.



---

## Appendix E

---

# Matlab analytical-numerical solution

In this appendix the differential equations derived in Appendix D are solved numerically using Matlab. In section E.1 the most simple case of a single 1 DOF from section D.3 is solved. In section E.2 the case of multiple 1 DOFs from section D.4 is solved. This appendix is referenced from section 3.2.

### E.1 Single 1 DOF moving sprung mass in Matlab

The system of partial differential equations for a single one degree of freedom moving sprung mass solved in section D.3, must be rewritten to a system of first order ordinary differential equations, so it can be solved in Matlab. First a change of variable is performed by defining  $x_1$  through  $x_4$  as

$$\begin{aligned}x_1 &= q_n, \\x_2 &= \dot{q}_n, \\x_3 &= u_v, \\x_4 &= \dot{u}_v,\end{aligned}\tag{E.1}$$

and defining their derivatives as

$$\begin{aligned}\dot{x}_1 &= x_2, \\ \dot{x}_2 &= -\left(\frac{2\omega_m^2 m_v}{m_b l} \theta(x_1) \sin^2\left(\frac{\pi x_1}{l}\right) + \omega_n^2\right) x_1 + \left(\frac{2\omega_m^2 m_v}{m_b l} \theta(x_1) \sin\left(\frac{\pi x_1}{l}\right)\right) x_3 - \frac{2m_v g}{m_b l} \theta(x_1) \sin\left(\frac{\pi x_1}{l}\right), \\ \dot{x}_3 &= x_4, \\ \dot{x}_4 &= \left(\omega_m^2 \sin\left(\frac{\pi x_1}{l}\right)\right) x_1 - \left(\omega_m^2\right) x_3.\end{aligned}\tag{E.2}$$

This can be solved in Matlab, using the following scripts.

### E.1.1 Single 1 DOF moving sprung mass script

```

1 % Title:      SDOF moving sprung mass
2 % Date:      February 12, 2016
3 % Last modified: April 1, 2016
4 % Description: Analytical-numerical solver of one moving sprung mass
   on simply supported beam
5
6 clear all;
7 clc;
8
9 % 1. Defining variables
10 n      = 1; % number of modes
11 L      = 25; % length bridge [m]
12 g      = 9.81; % gravitational acceleration [m/s^2]
13 m_vehicle = 5750; % mass [kg]
14 k_vehicle = 1.595e6; % spring stiffnes [N/m]
15 E_b     = 2.87e9; % Youngs modulus bridge [N/m^2]
16 m_bridge = 2303; % mass bridge [kg/m]
17 h_b     = 2.77; % height beam [m]
18 w_b     = 1.63; % width beam [m]
19 I_b     = (1/12)*w_b*h_b^3; % Moment of inertia beam [m^4]
20 EI      = E_b*I_b; % stiffness bridge [Nm^2]
21 v      = 100/3.6; % velocity vehicle [m/s]
22 t0     = 0; % start time [s]
23 tf     = 2*L/v; % end time [s]
24 nsteps = 250; % amount of time steps
25 tspan  = linspace(t0,tf,nsteps); % timespan for solution [s]
26 Omega_bridge = (n^2*pi^2)/L^2*sqrt(EI/m_bridge); % frequency bridge (
   euler-bernoulli beam) [rad/s]
27 Omega_vehicle = sqrt(k_vehicle/m_vehicle); % frequency vehicle (mass-
   spring) [rad/s]
28
29 % Initial conditions
30 y_0     = [0; 0; 0; 0]; % initial conditions for the equation f1, f2,
   f3 and f4 of the solver
31
32 % 2. Solve system of ODE using ode45 runga kutta solver, pass on
   variables
33 [T,Y]   = ode45(@(t1,x) odesolver(t1,x,n,m_vehicle,v,m_bridge,L,g,
   Omega_bridge,Omega_vehicle),tspan,y_0);
34
35 % Explanation:
36 % T = output, array of time points with related solutions
37 % Y = output, array of solutions for every time point
38 % t1 = input, current time point parameter
39 % x = input, current location parameter
40 % the rest is input
41
42 % Extract parts of solution from rows of vector
43 x1     = Y(:,1); % equal to qn, time related part of bridge deflection
44 x2     = Y(:,2); % equal to first time derivative of qn
45 x3     = Y(:,3); % equal to uw, mass deflection

```

```

46 x4          = Y(:,4); % equal to first time derivate of uw
47
48 % Obtain full solution for the displacement of the bridge at midspan
49 r          = L/2;    % midspan [m]
50 M_shape     = sin(pi*r/L); % mode shape, will result in 1 for midspan
51 H_bridge_x  = x1.*M_shape; % bridge vertical position [m]
52 H_vehicle_x = x3; % vehicle vertical position [m]
53
54 % Obtain velocities and accelerations by differentiation
55 dt         = T(2);
56
57 V_bridge_mid = diff(H_bridge_x)./T(2); % bridge velocity [m/s]
58 A_bridge_mid = diff(V_bridge_mid)./T(2); % bridge acceleration [m/
    s2]
59
60 V_vehicle    = diff(H_vehicle_x)./T(2); % vehicle velocity [m/s]
61 A_vehicle    = diff(V_vehicle)./T(2); % vehicle acceleration [m/s2]
62
63 % 3. Plot output
64 plot(T,H_bridge_x, '-r', 'LineWidth', 1)
65 xlabel('Time [s]')
66 ylabel('Midpoint Displacement [m]')
67
68 ax = gca; % current axes
69 ax.XAxisLocation = 'origin';
70 ax.TickLength = [0.001 0.001];
71 ax.YTickLabel = {-0.003, -0.0025, -0.002, -0.0015, -0.001, -0.0005, 0, 0.0005};
72 ax.YLim = [-0.003 0.0005];
73
74 % 4. Write results to file
75 %bridge deflection
76 fileID     = fopen('0.txt', 'w');
77 fprintf(fileID, '%9s %20.16f\n', 'timestep:', dt);
78 fprintf(fileID, '%25s \n', 'yAxisLabel:deflection [m]');
79 fprintf(fileID, '%23s \n', 'title:bridge deflection');
80 fprintf(fileID, '%13s \n', 'matlab ub_mid');
81 fprintf(fileID, '%20.16f\n', H_bridge_x);
82 fclose(fileID);
83
84 %sprung mass displacement
85 fileID     = fopen('1.txt', 'w');
86 fprintf(fileID, '%9s %20.16f\n', 'timestep:', dt);
87 fprintf(fileID, '%27s \n', 'yAxisLabel:vertical DOF [m]');
88 fprintf(fileID, '%30s \n', 'title:sprung mass vertical DOF');
89 fprintf(fileID, '%10s \n', 'matlab uv1');
90 fprintf(fileID, '%20.16f\n', H_vehicle_x);
91 fclose(fileID);
92
93 %sprung mass velocity
94 fileID     = fopen('2.txt', 'w');
95 fprintf(fileID, '%9s %20.16f\n', 'timestep:', dt);
96 fprintf(fileID, '%25s \n', 'yAxisLabel:velocity [m/s]');
97 fprintf(fileID, '%26s \n', 'title:sprung mass velocity');

```

```

98 fprintf(fileID, '%10s \n', 'matlab vv1');
99 fprintf(fileID, '%20.16f\n', V_vehicle);
100 fclose(fileID);
101
102 %sprung mass acceleration
103 fileID = fopen('3.txt', 'w');
104 fprintf(fileID, '%9s %20.16f\n', 'timestep:', dt);
105 fprintf(fileID, '%30s \n', 'yAxisLabel:acceleration [m/s2]');
106 fprintf(fileID, '%30s \n', 'title:sprung mass acceleration');
107 fprintf(fileID, '%10s \n', 'matlab av1');
108 fprintf(fileID, '%20.16f\n', A_vehicle);
109 fclose(fileID);

```

### E.1.2 ODE solver script

```

1 % Title:      Ordinary differential equation solver
2 % Date:      February 12, 2016
3 % Last modified:  March 31, 2016
4 % Description:  defines all functions for master script
5
6 function fvalue = odesolver(t1,x,n,m_vehicle,v,m_bridge,L,g,Omega_bridge,
    Omega_vehicle)
7 % Set of ordinary differential equations
8 %   f1 = x2
9 %   f2 = -A1*x1+A2*x3-A3
10 %   f3 = x4
11 %   f4 = B1*x1-B2*x3
12
13 L1 = v*t1; % current position of vehicle [m]
14 H1 = heaviside(L-L1)-1+heaviside(L1); % heaviside functions Theta(L1)
15
16 % Define constants
17 A1 = (2*Omega_vehicle^2*m_vehicle)/(m_bridge*L)*H1*((sin(n*pi*L1/L))^2)+Omega_bridge^2;
18 A2 = (2*Omega_vehicle^2*m_vehicle)/(m_bridge*L)*H1*sin(n*pi*L1/L);
19 A3 = (2*m_vehicle*g)/(m_bridge*L)*H1*sin(n*pi*L1/L);
20 B1 = Omega_vehicle^2*sin(n*pi*L1/L);
21 B2 = Omega_vehicle^2;
22
23 %
24 % system of first order ordinary differential equations
25 fvalue = zeros(4,1);
26 fvalue(1) = x(2);
27 fvalue(2) = -(A1)*x(1)+(A2)*x(3)-(A3);
28 fvalue(3) = x(4);
29 fvalue(4) = (B1)*x(1)-(B2)*x(3);
30 end

```

### E.1.3 Verification

The derived analytical-numerical method implemented in Matlab can be compared to literature. This comparison is made using the following parameters:

- spring stiffness  $k_v = 1\,595\,000\text{ N/m}$ ;
- sprung mass  $m_v = 5750\text{ kg}$ ;
- velocity of mass  $v = 27.78\text{ m/s}$ ;
- Young's Modulus beam  $E_b = 2.87 \times 10^9\text{ N/m}^2$ ;
- Moment of inertia beam  $I_b = 2.90\text{ m}^4$ ;
- Mass beam  $m_b = 2303\text{ kg/m}$ ;
- Length beam  $L = 25\text{ m}$ ;

and can be seen in Figure E.1.

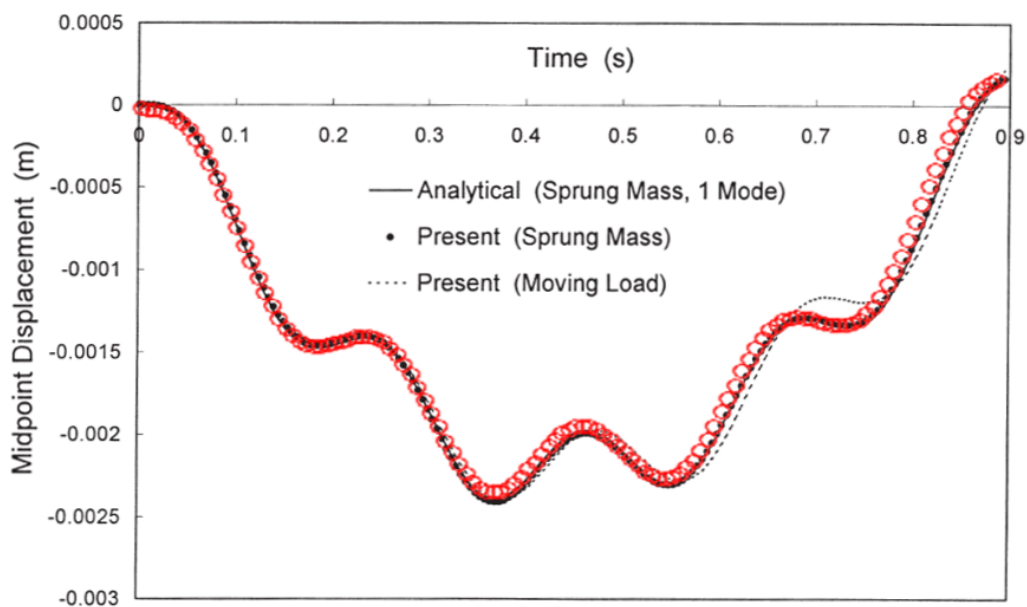


**Figure E.1:** Comparison between results from literature [34, fig. 6] (black) and Matlab results (red).

It can be concluded the analytical-numerical solution of the equations of motion solved in Matlab compare very well with results from literature. Therefore the Matlab solution can be used to verify results from Ansys modelling.

## E.2 Multiple 1 DOF moving sprung masses in Matlab

The system of partial differential equations for two one degree of freedom moving sprung masses solved in section D.4, must be rewritten to a system of first order ordinary differential equations, so it can be solved in Matlab. Applying a change of variables by defining  $x_1$  through  $x_6$  as

$$\begin{aligned}x_1 &= q_n, \\x_2 &= \dot{q}_n, \\x_3 &= u_{v,1}, \\x_4 &= \dot{u}_{v,1}, \\x_5 &= u_{v,2}, \\x_6 &= \dot{u}_{v,2},\end{aligned}\tag{E.3}$$

and defining their derivatives as

$$\begin{aligned}\dot{x}_1 &= x_2, \\ \dot{x}_2 &= -(A_1 + A_4 + A_7)q_n + A_3u_{v,1} + A_6u_{v,2} - A_2 - A_5, \\ \dot{x}_3 &= x_4, \\ \dot{x}_4 &= B_2q_n - B_1u_{v,1}, \\ \dot{x}_5 &= x_6, \\ \dot{x}_6 &= C_2q_n - C_1u_{v,2}.\end{aligned}\tag{E.4}$$

This can be solved in Matlab, using the following scripts. The constants  $B_2$  and  $C_2$  differ from the derived equations, in the way they include the appropriate heaviside function  $\theta(x_1 - x_{0,r})$ .

### E.2.1 Multiple 1 DOF moving sprung masses script

```
1 % Title:           Multiple SDOF moving sprung masses
2 % Date:           February 12, 2016
3 % Last modified:  April 1, 2016
4 % Description:    Analytical-numerical solver of multiple moving sprung
                    masses on simply supported beam
5
6 clear all;
7 clc;
8
9 % 1. Defining variables
10 n      = 1; % number of modes
11 L      = 25; % length bridge [m]
12 v      = 27.78; % velocity vehicle [m/s]
13 g      = 9.81; % gravitational acceleration [m/s^2]
14 m_vehicle = 5750; % mass [kg]
15 k_vehicle = 1.595e6; % spring stiffnes [N/m]
16 L_bogie1 = 0; % start position bogie 1
```

```

17 L_bogie2    = 8; % start position bogie 2
18 E_b         = 8.67e10; % Youngs modulus bridge [N/m^2]
19 m_bridge    = 2303; % mass bridge [kg/m]
20 h_b         = 2.77; % height beam [m]
21 w_b         = 1.63; % width beam [m]
22 I_b         = (1/12)*w_b*h_b^3; % Moment of inertia beam [m^4]
23 EI          = E_b*I_b; % stiffness bridge [Nm^2]
24 t0          = 0; % start time [s]
25 tf          = (2*(L+L_bogie2)/v); % end time [s]
26 nsteps      = 850; % amount of time steps
27 tspan       = linspace(t0,tf,nsteps); % timespan for solution [s]
28 Omega_bridge = (n^2*pi^2)/L^2*sqrt(EI/m_bridge); % frequency bridge (
    euler-bernoulli beam) [rad/s]
29 Omega_bogie1 = sqrt(k_vehicle/m_vehicle); % frequency bogie1 [rad/s]
30 Omega_bogie2 = sqrt(k_vehicle/m_vehicle); % frequency bogie2 [rad/s]
31
32 % Initial conditions
33 y_0         = [0; 0; 0; 0; 0; 0]; % initial conditions for the equation f1,
    f2, f3, f4, f5 and f6 of the solver
34
35 % 2. Solve system of ODE using ode45 runga kutta solver, pass on
    variables
36 [T,Y]       = ode45(@(t1,x) odesolver_mult(t1,x,n,L_bogie1,L_bogie2,
    m_vehicle,v,m_bridge,L,g,Omega_bridge,Omega_bogie1,Omega_bogie2),tspan
    ,y_0);
37
38 % Explanation:
39 % T = output, array of time points with related solutions
40 % Y = output, array of solutions for every time point
41 % t1 = input, current time point parameter
42 % x = input, current location parameter
43 % the rest is input
44
45 % Extract parts of solution from rows of vector
46 x1          = Y(:,1); % equal to qn, time related part of bridge deflection
47 x2          = Y(:,2); % equal to first time derivative of qn
48 x3          = Y(:,3); % equal to uv1, first bogie deflection
49 x4          = Y(:,4); % equal to first time derivate of uw1
50 x5          = Y(:,5); % equal to uv2, second bogie deflection
51 x6          = Y(:,6); % equal to first time derivate of uw2
52
53 % Obtain full solution for the displacement of the bridge at midspan
54 r           = L/2; % midspan [m]
55 M_shape     = sin(pi*r/L); % mode shape, will result in 1 for midspan
56 H_bridge_x  = x1.*M_shape; % bridge vertical position [m]
57 H_bogie1_x  = x3; % bogie 1 vertical position [m]
58 H_bogie2_x  = x5; % bogie 2 vertical position [m]
59
60 % Obtain velocities and accelerations by differentiation
61 dt          = T(2);
62
63 V_bridge_mid = diff(H_bridge_x)./T(2); % bridge velocity [m/s]

```

```

64 A_bridge_mid    = diff(V_bridge_mid)./T(2);    % bridge acceleration [m/
      s2]
65
66 V_bogie1       = diff(H_bogie1_x)./T(2);      % bogie1 velocity [m/s]
67 A_bogie1       = diff(V_bogie1)./T(2);      % bogie1 acceleration [m/s2]
68
69 V_bogie2       = diff(H_bogie2_x)./T(2);      % bogie2 velocity [m/s]
70 A_bogie2       = diff(V_bogie2)./T(2);      % bogie2 acceleration [m/s2]
71
72 % 3. Plot output
73 plot(T,H_bridge_x, '-k', 'LineWidth', 2)
74 xlabel('Time [s]')
75 ylabel('Midpoint Displacement [m]')
76
77 % 4. Write results to file
78 %bridge deflection
79 fileID         = fopen('0.txt','w');
80 fprintf(fileID, '%9s %20.16f\n', 'timestep:', dt);
81 fprintf(fileID, '%25s \n', 'yAxisLabel:deflection [m]');
82 fprintf(fileID, '%23s \n', 'title:bridge deflection');
83 fprintf(fileID, '%13s \n', 'matlab ub_mid');
84 fprintf(fileID, '%20.16f\n', H_bridge_x);
85 fclose(fileID);
86
87 %sprung mass displacement
88 fileID         = fopen('1.txt','w');
89 fprintf(fileID, '%9s %20.16f\n', 'timestep:', dt);
90 fprintf(fileID, '%27s \n', 'yAxisLabel:vertical DOF [m]');
91 fprintf(fileID, '%30s \n', 'title:sprung mass vertical DOF');
92 fprintf(fileID, '%22s \n', 'matlab uv1, matlab uv2');
93 fprintf(fileID, '%20.16f, %20.16f\n', [H_bogie1_x,H_bogie2_x]');
94 fclose(fileID);
95
96 %sprung mass velocity
97 fileID         = fopen('2.txt','w');
98 fprintf(fileID, '%9s %20.16f\n', 'timestep:', dt);
99 fprintf(fileID, '%25s \n', 'yAxisLabel:velocity [m/s]');
100 fprintf(fileID, '%26s \n', 'title:sprung mass velocity');
101 fprintf(fileID, '%22s \n', 'matlab vv1, matlab vv2');
102 fprintf(fileID, '%20.16f, %20.16f\n', [V_bogie1,V_bogie2]');
103 fclose(fileID);
104
105 %sprung mass acceleration
106 fileID         = fopen('3.txt','w');
107 fprintf(fileID, '%9s %20.16f\n', 'timestep:', dt);
108 fprintf(fileID, '%30s \n', 'yAxisLabel:acceleration [m/s2]');
109 fprintf(fileID, '%30s \n', 'title:sprung mass acceleration');
110 fprintf(fileID, '%22s \n', 'matlab av1, matlab av2');
111 fprintf(fileID, '%20.16f, %20.16f\n', [A_bogie1,A_bogie2]');
112 fclose(fileID);

```

## E.2.2 Multiple ODE solver script

```

1 % Title: Ordinary differential equation solver for 2 bogies
2 % Date: February 12, 2016
3 % Description: defines all functions for master script
4 % Last modified: March 7, 2016
5
6 function fvalue = odesolver_mult(t1,x,n,L_bogie1,L_bogie2,m_vehicle,v,
   m_bridge,L,g,Omega_bridge,Omega_bogie1,Omega_bogie2)
7 % Set of ordinary differential equations
8 % f1 = x2
9 % f2 = -(A1+A4+A7)*x1+A3*x3+A6*x5-A2-A5
10 % f3 = x4
11 % f4 = B2*x1-B1*x3
12 % f5 = x6
13 % f6 = C2*x1-C1*x5
14
15 L1 = v*t1-L_bogie1; % current position of bogie 1 [m]
16 L2 = v*t1-L_bogie2; % current position of bogie 2 [m]
17
18 H1 = heaviside(L-L1)-1+heaviside(L1); % heaviside functions Theta(L1)
19 H2 = heaviside(L-L2)-1+heaviside(L2); % heaviside functions Theta(L2)
20
21 % Define constants
22 A1 = Omega_bridge^2;
23 A2 = (2*m_vehicle*g)/(m_bridge*L)*H1*sin(n*pi*L1/L);
24 A3 = (2*Omega_bogie1^2*m_vehicle)/(m_bridge*L)*H1*sin(n*pi*L1/L);
25 A4 = (2*Omega_bogie1^2*m_vehicle)/(m_bridge*L)*H1*((sin(n*pi*L2/L))^2)
   ;
26 A5 = (2*m_vehicle*g)/(m_bridge*L)*H2*(sin(n*pi*L2/L));
27 A6 = (2*Omega_bogie2^2*m_vehicle)/(m_bridge*L)*H2*(sin(n*pi*L2/L));
28 A7 = (2*Omega_bogie2^2*m_vehicle)/(m_bridge*L)*H2*((sin(n*pi*L2/L))^2)
   ;
29 B1 = Omega_bogie1^2;
30 B2 = Omega_bogie1^2*H1*sin(n*pi*L1/L);
31 C1 = Omega_bogie2^2;
32 C2 = Omega_bogie2^2*H2*sin(n*pi*L2/L);
33
34 %
35 % system of first order ordinary differential equations
36 fvalue = zeros(6,1);
37 fvalue(1) = x(2);
38 fvalue(2) = -(A1+A4+A7)*x(1)+(A3)*x(3)+A6*x(5)-A2-A5;
39 fvalue(3) = x(4);
40 fvalue(4) = (B2)*x(1)-(B1)*x(3);
41 fvalue(5) = x(6);
42 fvalue(6) = (C2)*x(1)-(C1)*x(5);
43 end

```

### E.2.3 Verification

The multiple 1 DOF Matlab solution is not compared to literature in the way this was done in subsection E.1.3. However, it can be compared to the results of the Ansys model, which can be viewed in section K.2.



## Finite Element Modelling

To calculate the expected displacements, velocities and accelerations when a train passes a tied-arch bridge, a model was created. This appendix describes how the modelling was performed using the program Ansys. The models were created using the Mechanical APDL (Ansys Parametric Design Language) and all the code is included, so it can be reproduced by the reader. This appendix is referenced from section 2.7.

### F.1 Modelling procedure

An Ansys analysis consists of three stages in general:

1. Pre-processing; defining the model
2. Analysis; let loads act and compute displacements, strains and stresses
3. Post-processing; view the results and derivatives of the results

Within Ansys there are different ways of modelling. One could use the classic Ansys interface, where models can be made and run using menus and buttons to select options. The classic environment can be used with APDL as well, where commands are issued using text input instead of mouse clicks. Although one needs to learn the exact syntax of the language, the input code can be easily parametrized, debugged, documented and routines such as do-loops can be used to automate certain actions.

A third way of using Ansys is by using the Workbench environment, an easy to use interface, but with the disadvantage that the program makes a lot of choices for the user, and when something unexpected occurs it is harder to determine where the fault is.

In this thesis it was chosen to use Ansys Mechanical APDL, version 16.1.0, which meant manually typing code and debugging it in the classic Ansys environment.

## F.2 Elements

The finite element model is built up using elements, which generally consist of connected nodes. To model lumped masses such as the wheels, the bogie frame or the coach of the train mass elements can be used. Other objects can be modelled in a similar fashion, by choosing Ansys elements which act like the object does in real life and supplying relevant parameters.

The elements mentioned in this report will be briefly discussed in the following sections.

### F.2.1 MASS21 - mass elements

The MASS21 element is a point element, which can have up to six degrees of freedom, three translations and three rotations. In the more simple vehicle models the option KEYOPT(3) is set to 4, making it a 2D mass without rotary inertia. This means the degrees of freedom are limited to translations in x- or y-direction. This is not the case for the full coach vehicle model, which has a rotational degree of freedom and the mass moment of inertia must be included. The quantity of the mass can be defined with a real constant. [60]

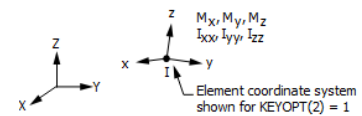


Figure F.1: MASS21 Geometry [60, fig. 21.1]

### F.2.2 BEAM3 - beam elements

The BEAM3 element is a two-node beam element which can have up to three degrees of freedom at each node. The beam uses Euler-Bernoulli beam theory, but by defining a non-zero shear deflection constant SHEARZ, it can make use of Timoshenko beam theory.

“The element is defined by two nodes, the cross-sectional area, the area moment of inertia, the height, and the material properties.” [61]

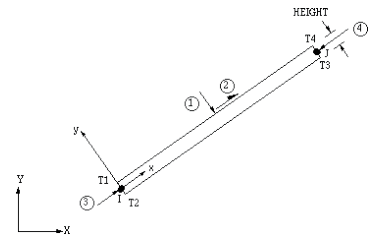


Figure F.2: BEAM3 Geometry [61]

### F.2.3 BEAM188 - beam elements

The BEAM188 element is a two-node beam element which can have up to six degrees of freedom at each node. It uses Timoshenko beam theory which includes first order shear deformation effects, in contrast to Euler-Bernoulli beam theory. By default it is based on linear shape functions, which means all element solution quantities are constant along the length. However, this can be made more sophisticated by using quadratic or cubic shape functions.

The beam element is a one-dimensional line element in space, cross sectional properties are provided separately. For the three-dimensional bridge model the SECTYPE command is used with the properties *beam* and “hrec”, “hats” or “I” for a box-, hat- or I-shaped cross section respectively. The SECDATA command is

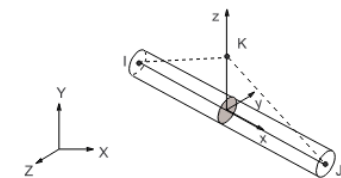


Figure F.3: BEAM188 Geometry [60]

used to provide the widths, heights and thicknesses of the cross sections, from which the areas and moments of inertia are calculated automatically.

If this beam type is used in a two-dimensional environment, certain degrees of freedom must be restrained, to prevent rigid body movement.[60]

### F.2.4 LINK8 - bar elements

The LINK8 element is a two-node bar element which can have up to three translational degrees of freedom at each node. It differs from beam elements in the fact no bending is considered, only uniaxial tension or compression can take place. The element is defined by the cross-sectional area, an optional initial strain and material properties such as Young's Modulus and density. [62]

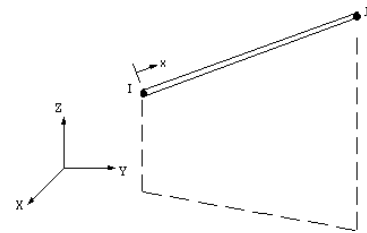


**Figure F.4:** LINK8 Geometry [62]

### F.2.5 COMBIN14 - spring-dashpot elements

The COMBIN14 element can be used as a longitudinal spring-damper and is a uniaxial tension-compression element with up to three degrees of freedom at each node. It can also be used as a torsional spring-damper. The element is defined by two nodes, a spring constant  $k$  [force/length] and two damping coefficients  $c$  [force · time/length], one normal one and another one to enable usage of non-linear damping. [60]

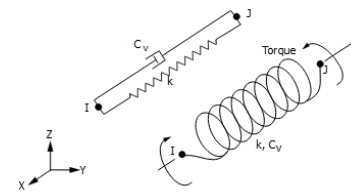


**Figure F.5:** COMBIN14 Geometry [60, fig 14.1]

### F.2.6 CONTA175 - contact elements

The CONTA175 element is a one node element used to represent contact and sliding with target elements. The contact element forms a pair with the target element, contact is achieved when the element surface penetrates the target segment element. Contact forces are developed in a direction normal to the target surface. These contact forces are a product of contact stiffness and contact gap size, which essentially means there exists a stiff spring between contact and target elements.

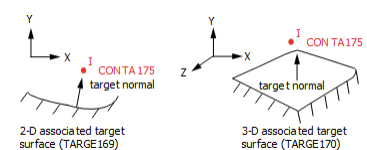


**Figure F.6:** CONTA175 Geometry [60, fig 175.1]

By setting KEYOPT(2) to 1, the penalty method is used as contact algorithm. This means a contact spring is used, as described earlier. There are a large number of additional KEYOPTs which can be used to influence the way of analysis. [60]

### F.2.7 TARGE169 - target elements

The TARGE169 element is used to represent a target surface over the beam for the associated contact elements. The contact is defined using pair-based contact, where the contact and target elements share a real constant set identification number.

The boundary conditions for rigid target nodes are automatically constrained by the program, to fix the target elements on the surface of the beam elements. [60]

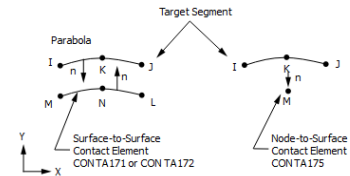


Figure F.7: TARGE169 Geometry [60, fig 169.1]

### F.2.8 CONTAC48 - contact elements

The CONTAC48 element was able to represent contact between a node and a surface in 2D. In the current version of Ansys the element is deprecated, it is advised to use CONTA175 and TARGE169 instead. Although the element can still be used in an Ansys analysis, the corresponding command GCGEN does not work as it used to work any more.

Similarly to the CONTA175 and TARGE169 element pair, it works as a spring with a penalty contact stiffness. [63]

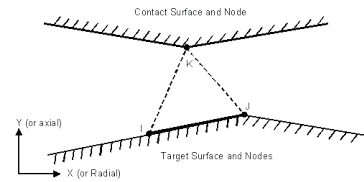


Figure F.8: CONTAC48 Geometry [63]

## F.3 Analysis type

It is possible to use different analysis types when modelling. The analysis types used are described in this section.

### F.3.1 Static analysis

A static structural analysis determines the displacements, stresses, strains, and forces in structures or components caused by loads that do not induce significant inertia and damping effects. Steady loading and response conditions are assumed; that is, the loads and the structure's response are assumed to vary slowly with respect to time. Although this type of analysis is not sufficient for the purpose of this report, it can be used to verify simple situations. [60]

### F.3.2 Modal analysis

A modal analysis determines the vibration characteristics (natural frequencies and mode shapes) of a structure. [60] It is useful to determine the natural frequencies of complex structures, for which this is not feasible to by hand.

### F.3.3 Transient analysis

A transient analysis can be used to model vibrations and accelerations over time, therefore also called a time-history analysis, it is the analysis suited to model dynamic interaction. There are two sub-methods possible, explicit dynamic analysis or implicit dynamic analysis.

### Explicit

With an explicit analysis the result in each step depends only on the quantities obtained in the preceding step. An example would be the central difference time integration method, which is a Newmark- $\beta$  with  $\beta = 0$  and  $\gamma = 0.5$ . The time steps must be chosen smaller than the Courant time step (time it takes a sound wave to travel across an element). [64] This time is usually very small (micro seconds), which leads to a lot of solution steps needed to model events which take several seconds or minutes. Therefore an explicit transient analysis is more suited for events which take a short time, like to model explosions causing large deformations.

### Implicit

With an implicit analysis the expression for a certain step includes one or more values pertaining to the same step. Several iterations are needed at each step. Often the Newmark- $\beta$  time integration method is used. This method is stable with the trapezoidal rule, in which the parameters  $\beta = 0.25$  and  $\gamma = 0.5$ . The method of solution can be *full*, which uses a Newton-Raphson method, or *reduced*, which is limited to linear structures with constant matrices and constant time step size. Unlike the explicit analysis, the implicit analysis has no limit on the size of the time step. This has the benefit the time step can be chosen several orders of magnitude larger than explicit time steps, which makes it possible to obtain a solution faster.

## F.4 Time integration methods

To perform an implicit transient analysis, as described in section F.3.3, various time integration methods can be used. The following methods are available:

- Direct integration method;
- Mode-superposition method;
- Fourier transformation method.

These methods are further elaborated on in the following subsections.

### F.4.1 Direct integration method

With direct integration methods multi-DOF differential equations can be solved numerically. There are different methods available, like the Newmark- $\beta$  method, Wilson-theta method or Runge-Kutta method. In Ansys two time integration schemes can be used. By default the Newmark- $\beta$  method is used, which was proposed by Newmark in 1959 and is a single-step method. In such a step-by-step analysis a prediction is made what the solution would be one small time increment away, at  $t + \Delta t$ . [2, App. B]

The second method which can be used in Ansys is the Hilber-Hughes-Taylor Alpha method (HHT). This method is a modification of the Newmark- $\beta$  method, with an additional parameter  $\gamma$ . This parameter can be used to specify “numerical damping” of unwanted high frequencies.

### F.4.2 Mode-superposition method

With the mode-superposition method, first a modal analysis is performed to compute the natural frequencies and modes shapes. Afterwards a time integration of  $n$  significant eigenmodes is done. [40, page 34, 144]

### F.4.3 Fourier transformation method

With the Fourier transformation method, the partial differential equation is transformed to the frequency domain, where it consists of ordinary differential equations which can be solved using a time advancement scheme. To extract the solution at a certain time  $t$ , it can be transformed back to the time domain using an inverse Fourier transformation.

## F.5 Numerical differentiation

Although velocities and accelerations can be obtained from Ansys using direct get functions, they can also be obtained by numerically differentiate the displacements. This can be done with different techniques. [65, ch. 3]

The forward difference method is defined as

$$\frac{f(x+h) - f(x)}{h}, \quad (\text{F.1})$$

where  $h$  is the step size and should be larger than zero. The error is of order  $O(h)$ .

The backwards difference method is defined as

$$\frac{f(x) - f(x-h)}{h}, \quad (\text{F.2})$$

where  $h$  is the step size and should be larger than zero. The error is of order  $O(h)$ .

The central difference method is defined as

$$\frac{f(x+h) - f(x-h)}{2h}, \quad (\text{F.3})$$

where  $h$  is the step size and should be larger than zero. The error is of order  $O(h^2)$ .

From these three techniques the method used in the Ansys models is the backwards difference method, since at a given time step only the current and the previous displacements are known.

## Contact force model

One way to solve the interaction between vehicles and bridges, is to represent the vehicle using a moving contact force and move it over the bridge. [2, ch. 8] In this appendix the proposed method and its applicability for the assessment of passenger comfort in this report is analysed. This appendix is referenced from subsection 3.1.1.

### G.1 Ansys APDL code

In the paper *Vibration analysis of a multi-span continuous bridge subject to complex traffic loading and vehicle dynamic interaction* the contact force method is presented. [66] One of the authors, Mister Kang, kindly provided the Ansys APDL code mentioned in their paper.

```
1 finish$/clear$/prep7
2 l=16$ne=100$nn=ne+1$v=160/3.6
3 dl=l/ne$dt=dl/v
4
5 *dim,uv,,nn
6 *dim,vv,,nn
7 *dim,ub,,nn
8 *dim,vb,,nn
9 *dim,ab,,nn
10
11 et,1,mass21,,4$r,11,46900$r,12,16900
12 et,2,combin14,,2$r,21,4.87e6,3.14e5
13 et,3,beam3$mp,ex,3,2.05e10$mp,nuxy,3,0.2$mp,dens,3,9360$r,3,1,1,1
14
15 type,1$real,11$n,202,10,1.5$e,202
16 real,12$n,201,10,1$e,201
17
18 type,2$real,21$en,202,202,201
19
20 *do,i,1,nn
```

```

21 n,i,(i-1)*dl
22 *enddo
23 type,3$real,3$mat,3
24 *do,i,1,ne
25 e,i,i+1
26 *enddo
27
28 d,1,ux,,,,,uy$d,nn,uy$d,201,all
29 finish
30 /solu
31 antype,4
32 time,dt/1000
33 timint,off
34 solve
35 uv(1)=uy(202)
36 vv(1)=0
37 ub(1)=0
38 vb(1)=0
39 ab(1)=0
40
41 timint,on
42 time,dt
43 f,2,fy,-(16900*9.8+46900*9.8)
44 solve
45
46 *do,ii,2,nn-1
47 uv(ii)=uy(202)
48 vv(ii)=(uv(ii)-uv(ii-1))/dt
49 ub(ii)=uy(ii+1)
50 vb(ii)=(ub(ii)-ub(ii-1))/dt
51 ab(ii)=(vb(ii)-vb(ii-1))/dt
52 time,ii*dt
53 fdele,all,all
54 f,ii+1,fy,-(4.87e6*(ub(ii)-uv(ii))+3.14e5*(vb(ii)-vv(ii))
      +16900*9.8+16900*ab(ii)+46900*9.8)
55 d,201,uy,ub(ii)
56 solve
57 *enddo
58
59
60 /post26
61 nc=node(l/2,0,0)
62 nsol,2,nc,u,y
63 plvar,2

```

## G.2 Interpretation

An interpretation of the code from section G.1 will be given in the following sections.

### G.2.1 Elements

The vehicle is modelled as a sprung mass which consists of a small mass, a spring-damper and a large mass. They are placed together somewhere in the coordinate system, but are not physically attached to the beam. For the masses, the MASS21 element is used, for the spring-damper the COMBIN14 element is used. The beam is modelled by beam elements of the type BEAM3. The beam is simply supported. A more detailed description of these elements is provided in section F.2.



Figure G.1: Pre-processing of contact force model

### G.2.2 One DOF moving sprung mass

The sprung mass is not literally moved over the beam, instead a contact force from the sprung mass is moved over the beam. In the first load step this force is the weight of the sprung masses multiplied by the gravitational acceleration.

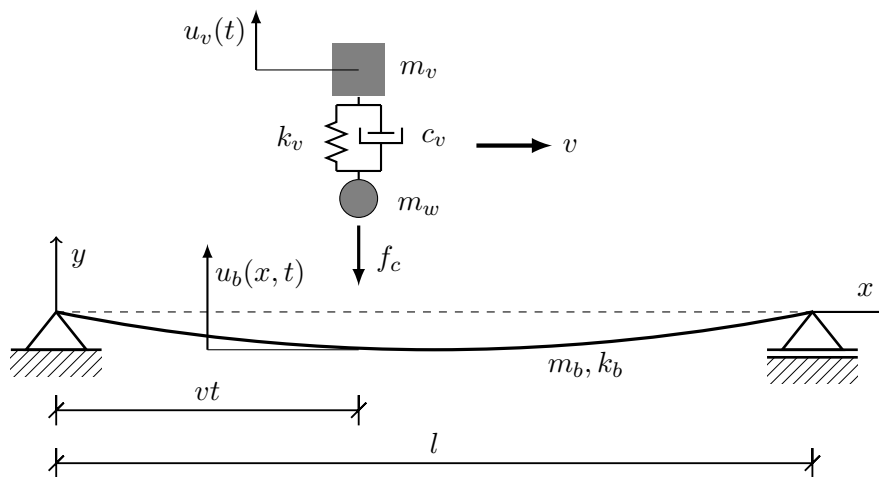


Figure G.2: Contact force model

- $l$  = length of beam [m]
- $m_b$  = beam mass per unit length [kg/m]

- $k_b$  = beam stiffness [N/m]
- $v$  = speed of sprung mass [m/s]
- $t$  = time [s]
- $g$  = gravitational acceleration [m/s<sup>2</sup>]
- $u_b(x, t)$  = deflection of beam [m]
- $u_v(t)$  = deflection of vehicle mass [m]
- $m_w$  = mass of wheel/bogie [kg]
- $m_v$  = mass of vehicle [kg]
- $k_v$  = spring stiffness vehicle [N/m]
- $c_v$  = damping value vehicle [Ns/m]
- $f_c$  = contact force [N]

In the subsequent load steps a loop is used to move the contact force  $f_c$  over the beam. To store data between load steps, five vectors are used. These vectors contain the displacement, velocity and acceleration of the bridge and the vehicle. During every cycle of the loop, the following is done.

1. The five vector arrays are filled with a new entry. The displacement of the vehicle is defined as the vertical displacement of the large mass and the displacement of the bridge as the vertical displacement of one node to the right of the current position in the loop.
2. The time is defined as the current loop index times  $dt$ . Therefore it is incremented each loop.
3. All (old) forces are deleted.
4. A new force is applied to the next beam node. The quantity of this force is:  

$$f_c = -k_v \cdot (u_b - u_v) + c_v \cdot (\dot{u}_b - \dot{u}_v) + m_w \cdot g + m_w \cdot \ddot{u}_b + m_v \cdot g$$
which is in line with the expressions presented in section D.3.
5. The vertical position of the wheel mass is not an independent variable but is set equal to  $u_b$  every time step. This means the bottom mass of the sprung mass is constrained to displace the same amount as the bridge at the current beam node. This “no jump” condition prevents the vehicle and the bridge to loose contact.
6. increment loop iterator with one, which means to move to the next node.

So although the beam and the sprung mass are not visually connected in the model, they do interact with each other. The beam is influenced by the sprung mass due to the contact force. The sprung mass is influenced by the beam due to the imposed displacement.

For this model some assumptions and modelling choices are made, it is good to realise what they are.



**Figure G.3:**  $N_{th}$  load step on moving contact force model

- No-jump condition: train wheel exactly follows bridge deflection;
- The mass times gravitational acceleration of the beam is neglected. This force influences the initial deflection shape of the bridge. It is not very complicated to add this to the model, by providing a distributed load equal to the bridge mass times gravitational acceleration. Another way is to position the bridge nodes not in a horizontal line, but in the actual shape it would deflect due to self weight, taking into account possible pre camber.

### G.2.3 Results

The results of this model can be seen in Figure G.4.

In Figure G.4a it can be observed the bridge, which is undamped, continues to vibrate in its first natural frequency after the bogie has left the bridge. This frequency can be computed as

$$\omega_{bridge} = \frac{n^2 \pi^2}{L^2} \sqrt{\frac{EI}{m}} = \frac{1^2 \pi^2}{25^2} \sqrt{\frac{8.29 \cdot 10^9}{2303}} = 29.95 \text{ rad/s}, \quad (\text{G.1})$$

which is translated to Hertz

$$n_{bridge} = \frac{\omega_{bridge}}{2\pi} = \frac{29.95}{2\pi} = 4.77 \text{ Hz}. \quad (\text{G.2})$$

A Fourier transform of Figure G.4a shows the vibration visible has a frequency of 4.43 Hz, which is close to the calculated 4.77 Hz.

The vertical displacement of the bogie in Figure G.4b has a vibration with a frequency of 2.77 Hz. The natural frequency of the bogie (which is a 1 DOF sprung mass) can be calculated as

$$\omega_{bogie} = \sqrt{\frac{k_{bogie}}{m_{bogie}}} \frac{1}{2\pi} = \sqrt{\frac{1595000}{5750}} \frac{1}{2\pi} = 2.65 \text{ Hz}. \quad (\text{G.3})$$

To further verify this model, it is compared with analytical results. This can be found in section K.1.

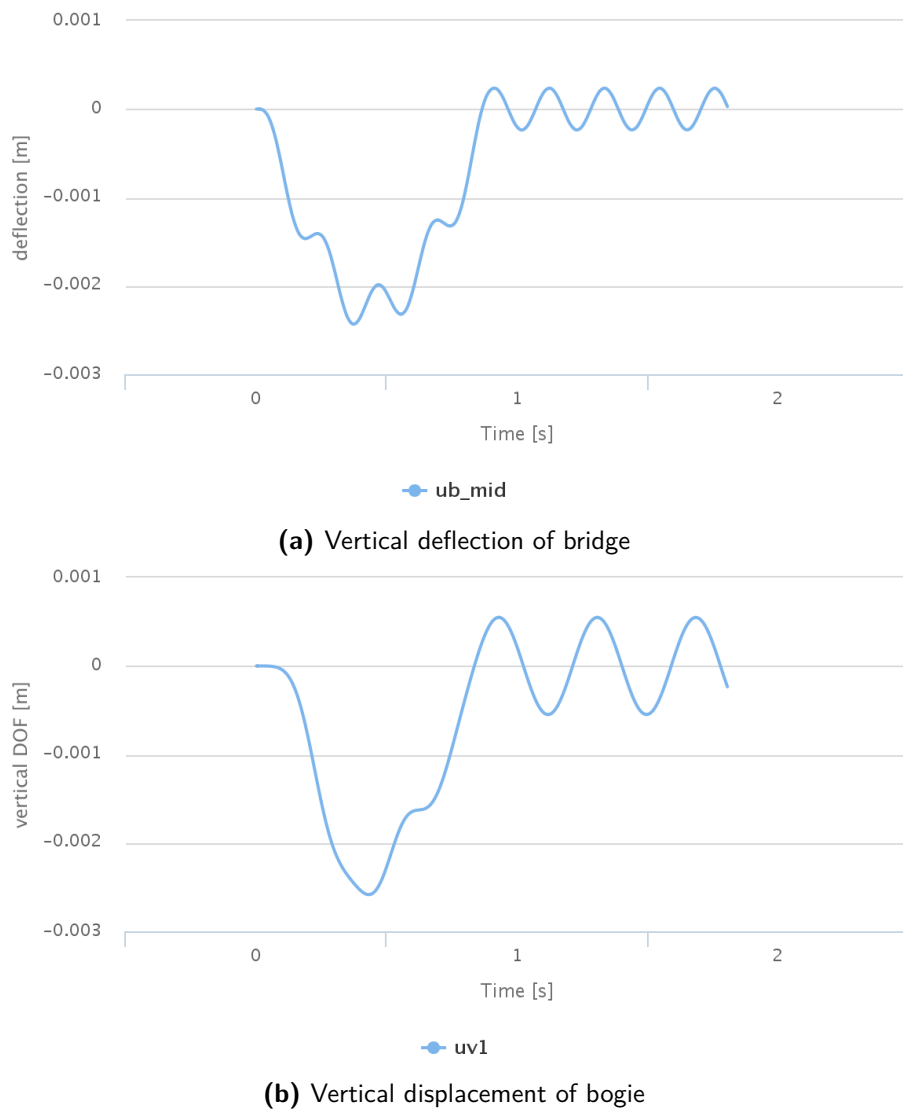


**Figure G.4:** Beam deflection and sprung mass displacement plots. A 5750 kg sprung mass moves over the 25 meters long beam with a velocity of 100 km/h. See also [online](#).

---

# Appendix H

---

## Bowe model

In his PhD thesis titled *Dynamic interaction of trains and railway bridges using wheel rail contact method* Cathal Bowe describes his approach to model a mass travelling over a simply supported beam in Ansys. [67] This model is an inspiration, but unfortunately it cannot be reproduced in the current Ansys version, since deprecated elements are used. This appendix is referenced from subsection 3.1.2.

### H.1 Ansys APDL code

```
1 /title ,2D beam - 09/07/2001
2
3 /solu
4 antype ,4
5 trnopt ,full
6 lumpm ,0
7 nlgem ,1
8 nropt ,auto , ,
9 eqslv , ,1e-8,0,
10
11 finish
12 /solu
13 time ,.000001
14 autots ,1
15 deltim ,.0000005,.0000005,.0000005,1
16 kbc ,1
17 tsres ,erase
18 outres ,all ,all
19 acel ,0,0,0,
20
21 *ask ,qnebc ,"number of beam elements",16
22 nebc=qnebc
23 length=20
```

```

24 lenbn=length/nebc
25
26 /prep7
27 et,1,beam3
28 r,1,1,3.81,,1,,,,
29 uimp,1,ex,,29.43e6,
30 uimp,1,dens,,34.088,
31 uimp,1,nuxy,,.2,
32
33 *do,i,1,nebc+1
34 n,i,lenbn*(i-1),0,0
35 *enddo
36
37 *do,i,1,nebc
38 e,i,i+1
39 *enddo
40
41 d,node(0,0,0),,,,,,ux,uy,,,,,
42 d,node(length,0,0),,,,,,uy,,,,,
43
44 eplot
45 timint,0
46 eplot
47
48 *ask,speed,speed of train,27.778 !what is the speed of the train?
49 time=length/speed
50 *get,hnode,node,,num,max,,,, !highest node no. so far
51 nnode=hnode+1 !initial node number
52
53 *set,wx1,0
54 *set,wy1,0
55 *set,load,-56.4
56 tstep1=.002
57
58 /prep7
59 et,20,mass21 !wheelset
60 keyopt,20,3,4
61 r,20,0, !wheelset = 0kg
62
63 et,21,contac48 !contact
64 keyopt,21,7,1
65 r,21,1.595e3,,.001,,,, !contact stiffness
66
67 n,100,wx1,wy1
68 type,20
69 mat,1
70 real,20
71 esys,0
72 secnum,
73 tshap,pilo
74 e,100
75
76 nsel,none

```

```

77 flst ,5 ,qnebc+1,1,orde ,2
78 fitem ,5 ,1
79 fitem ,5 ,-(qnebc+1)
80 nsel ,s , , ,p51x
81 cm ,t1 ,node
82
83 nsel ,none
84 flst ,5 ,1,1,orde ,1
85 fitem ,5 ,100
86 nsel ,s , , ,p51x
87 cm ,c1 ,node
88 allsel ,all
89
90 type , 21
91 mat , 1
92 real , 21
93 esys , 0
94 secnum ,
95 tshap ,line
96 gcgen ,c1,t1, , ,top,
97
98 *dim,m,table,2,1, ,time !10 m/s
99 m(1,0,1) = 0.0001
100 m(1,1,1) = 0
101 m(2,0,1) = time
102 m(2,1,1) = time*speed
103
104 flst ,2,1,1,orde ,1
105 fitem ,2,100
106 /go
107 d,p51x, , ,%m% , , ,ux, , , , ,
108
109 flst ,2,1,1,orde ,1
110 fitem ,2,100
111 /go
112 f,p51x,fy,load
113
114 allsel ,all
115 numcmp ,all
116
117 finish
118 /solu
119
120 /status ,solu
121 solve
122
123 timint ,1
124 tintp ,0.005, , ,0.5,0.5,5
125 time ,length/speed
126 autots ,1
127 deltim ,tstep1,tstep1,tstep1,1
128 kbc ,1
129 tsres ,erase

```

```

130 outres ,all ,all ,
131
132 /status ,solu
133 solve
134 finish

```

## H.2 Interpretation

An interpretation of the code from section H.1 will be given in the following sections.

### H.2.1 Elements

The mass is modelled with a MASS21 element and the beam with a BEAM3 element. The contact between the mass and the beam is modelled with a CONTAC48 element. A more detailed description of these elements is provided in section F.2.

### H.2.2 Moving constraints

Instead of imposing a velocity, another method is used to move the mass over the beam. The following code shows this:

```

1 time=length/speed
2
3 *dim,m,table,2,1, ,time
4 m(1,0,1) = 0.0001
5 m(1,1,1) = 0
6 m(2,0,1) = time
7 m(2,1,1) = time*speed
8
9 d ,p51x , , %m% , , , ux , , , ,

```

So a  $2 \times 2$  matrix is made, for a length of 20 meters, a speed of  $27.78 \text{ m s}^{-1}$  and a time of 0.72 seconds the following applies:

$$\begin{matrix} & \begin{matrix} time & location \end{matrix} \\ \begin{matrix} start \\ end \end{matrix} & \begin{pmatrix} 0.0001 & 0 \\ 0.72 & 20 \end{pmatrix} \end{matrix} \quad (\text{H.1})$$

The mass element is selected (p51x means a graphical pick selection) and the displacement in x-direction DOF is constrained by applying the start and end time and location combinations defined in the  $2 \times 2$  matrix, called a table.

## H.3 Conclusion

The fact that Mr. Bowe succeeded to perform this Ansys analysis using contact elements in 2009 is certainly promising when considering the feasibility of this method. However, since the

---

CONTAC48 element type is deprecated in the Ansys version used by the author (version 16.1), it cannot be reproduced. It will merely serve as an inspiration for a direct contact model using modern element types.



---

# Appendix I

---

## Direct contact model

Based on the Contact force model from Appendix G and the Bowe model from Appendix H, a direct contact model is presented in this appendix. It is attempted to model the contact between a train and a bridge as the contact between a moving mass and a simply supported beam. This appendix is referenced from subsection 3.1.2.

### I.1 Elements

The elements used in the direct contact model can be seen in Figure I.1. Based on the contact force model, the train is modelled with a MASS21 element. Since the CONTACT48 element from the Bowe model does not work in the current Ansys version any more, a couple of CONTACT175 and TARGET169 elements is used for contact. Instead of the previously used older two-dimensional BEAM3 element, the newer three-dimensional BEAM188 element is used. For this reason it is important to correctly constrain the necessary degrees of freedom to prevent movement or rotation in the z-direction.

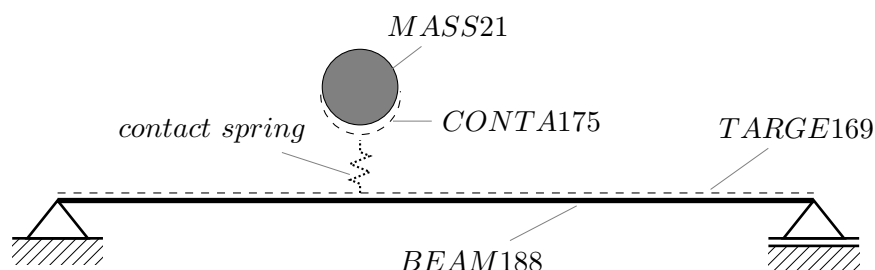


**Figure I.1:** Direct contact model

A more detailed description of these elements is provided in section F.2.

## I.2 Stationary contact

The biggest challenge is to achieve contact between the mass element and the beam elements. To do this the element types for the mass, contact element, target element and beam element are defined:

```

1 et ,1 ,mass21
2 keyopt ,1 ,3 ,4      ! rotary inertia options
3 r ,1 ,m1            ! mass
4
5 et ,2 ,conta175     ! 2-d node-to-surface contact element
6 keyopt ,2 ,2 ,4     ! penalty function
7 keyopt ,2 ,12 ,2    ! no separation , sliding permitted
8 r ,2 , , -1e12      ! FKN, negative means absolute value
9 rmod ,2 ,6 , -0.6   ! pin ball region
10
11 et ,3 ,targe169    ! 2-d target segment
12
13 et ,4 ,beam188
14 sectype ,4 ,beam ,rect      ! rectangular beam
15 secdata ,w_b ,h_b          ! dimensional properties
16 mp ,ex ,4 ,E_b            ! elastic modulus
17 mp ,nuxy ,4 ,mu_b         ! poissons ratio
18 mp ,dens ,4 ,rho_b        ! mass density

```

The mass is placed in the middle of the beam, with the contact element at the same location:

```

1 ! define mass element with contact element at same element
2 n ,201 , ( l /2) ,0      ! mass in middle of beam
3 type ,1
4 real ,1
5 e ,201                  ! mass element
6 type ,2
7 real ,2
8 e ,201                  ! contact element

```

The beam is directly meshed using nodes connected by elements:

```

1 !place nodes along the bridge length
2 *do ,i ,1 ,nn
3 n ,i ,(i-1)*dl
4 *enddo
5
6 !select beam properties
7 type ,4
8 real ,4
9 mat ,4
10 secnum ,4
11
12 !beam elements
13 *do ,i ,1 ,ne          !Do-loop index i from 1 to 100
14 e ,i ,i+1             !I (first node) = i , J (second node) = i+1
15 *enddo

```

Afterwards, the target elements are put on the beam elements, using the **esurf** command:

```

1 !select beam nodes
2 esel ,s ,type , ,4
3 nsle
4
5 !put target elements , connected to contact elements on surface of beam
6 type ,3
7 real ,2
8 esurf
9 allsel ,all

```

The last step is to define the constraints, so the beam can deflect and rotate in y-direction, but other degrees of freedom are constrained:

```

1 !define degrees of freedom
2 d,1,ux, , , ,uy,uz,rotx,roty !left end of beam
3 d,mn,uy, , , ,uz,rotx,roty !right end of beam

```

Using this method contact between the mass element and the beam elements is successfully achieved, and verified for a static and dynamic stationary situation.

### I.3 Moving contact

After the stationary verification in the previous section, the mass is verified when moving over the simply supported beam. The line of code which puts the mass in the middle of the beam

```

1 n,201,(l/2),0

```

is replaced with a line of code which puts the mass at the left side of the beam.

```

1 n,201,0,0

```

Furthermore, the horizontal degree of freedom of the mass is restrained by

```

1 d,201,velx,v

```

which gives it a velocity of  $v$  in positive x-direction.

This analysis gives results, but unfortunately they are not in good agreement with the analytical-numerical solution from section E.1 using the same input parameters. As can be observed at the comparison in Figure I.2, the method in Ansys produces too large deflections.

The reason for this is not exactly known by the author, but the following factors certainly play a role.

- The beam is not damped and the gravity load is applied suddenly. Hence the drop directly at the beginning of the graph (see Figure I.2). This will give an infinitely long vibration of the beam, due to self weight and inertial response. One possible solution could be to slowly increment the gravity acceleration from zero to  $9.81 \text{ m/s}^2$ , before letting the mass move over the beam.

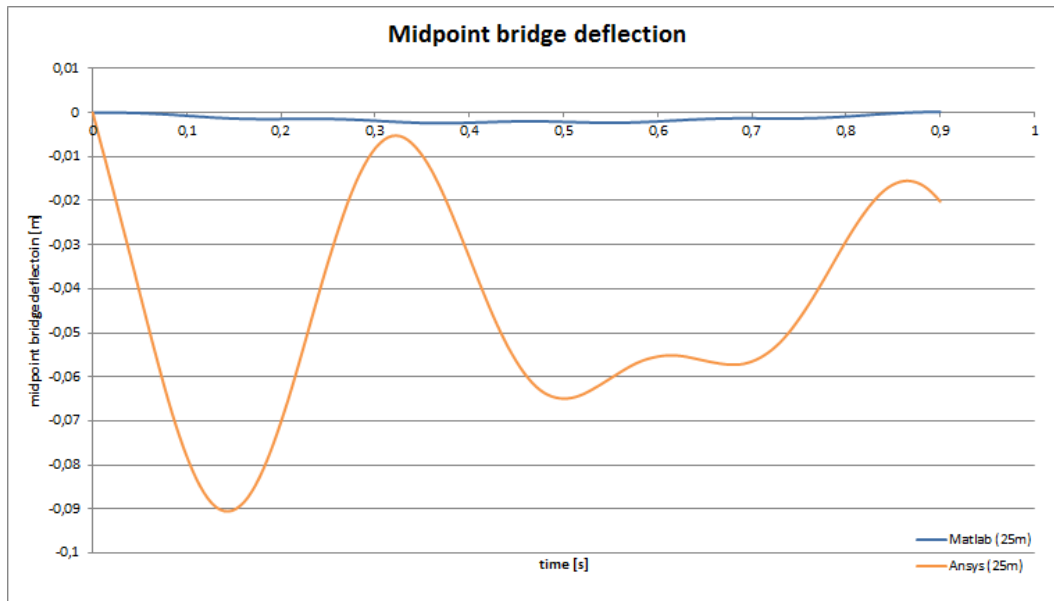


**Figure I.2:** Midpoint bridge deflection, Ansys compared to Matlab. Bridge is a 25 meters long simply supported beam. Single 1 DOF sprung mass moves over it with a velocity of 100 km/h.

- The stiffness of the contact spring has an influence on both the beam and mass deflection. Increasing the stiffness above a certain threshold causes errors. A possible solution is manipulating the contact element by modifying one of the many KEYOPTs to have correct stiffness and contact behaviour.

## I.4 Conclusion

Although it is technically possible to model the vehicle – bridge interaction in Ansys using a moving mass over a beam, it is quite complex, error prone and computationally expensive. It is therefore chosen to abandon this approach and use the contact force model instead.

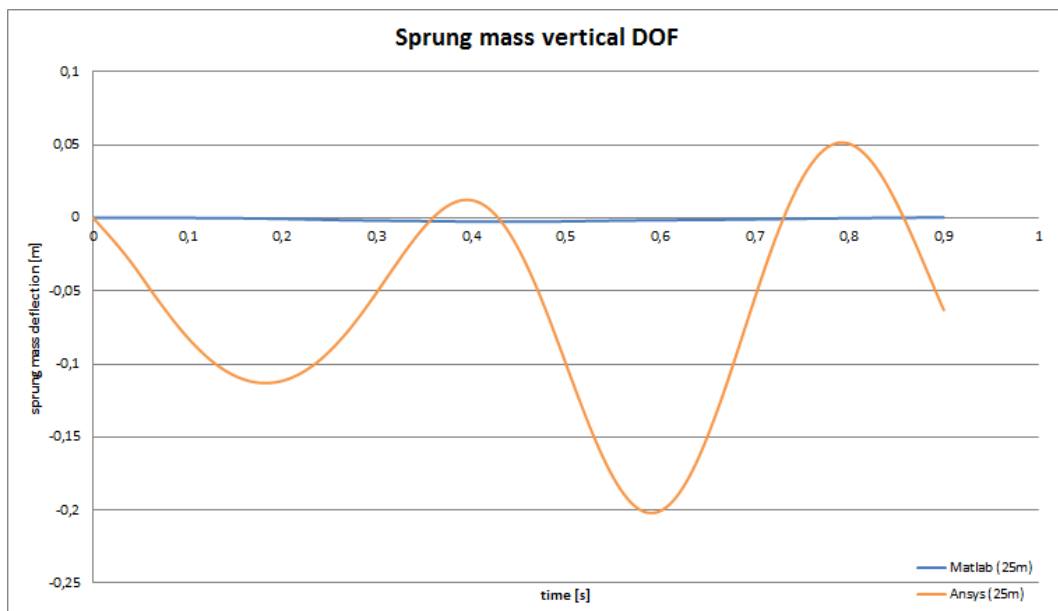


**Figure I.3:** Sprung mass vertical DOF, Ansys compared to Matlab. Bridge is a 25 meters long simply supported beam. Single 1 DOF sprung mass moves over it with a velocity of 100 km/h.



## Multiple 1 DOF sprung masses

The single 1 DOF sprung mass from Appendix G can be extended to multiple contact forces moving over the bridge. In this appendix an implementation of multiple 1 DOF sprung masses in Ansys is given in section J.1 and is explained in section J.2. The results and verification can be seen in subsection E.2.3. This appendix is referenced from subsection 3.2.2.

### J.1 Ansys APDL code

```
1 !Name:      beam_multiple_bogies
2 !Date:      February 22, 2016
3 !Last modified: March 7, 2016
4 !Description: Ansys contact force model with multiple bogies (up to 12)
5
6 !*****
7 finish
8 /clear
9 /prep7
10
11 !*****
12 !define some input variables
13 !general
14 l      = 75          !length bridge [m]
15 v      = 27.78       !velocity [m/s]
16 g      = 9.81        !gravitational acceleration [m/s2]]
17 ne     = 750         !number of elements
18 nn     = ne + 1      !number of nodes
19 dl     = l / ne      !delta length of small element
20 dt     = dl / v      !delta time of one time step
21
22 !vehicles
23 m1     = 5750        !vehicle mass [kg]
24 m2     = 1e-8        !wheel mass [kg]
```

```

25 k1    = 1595000      !spring stiffness [N/m]
26 c1    = 0           !damping value [Ns/m]
27 nv    = 6           !number of travelling sprung masses
28 l1    = 0           !position of bogie 1 [m]
29 l2    = -24         !position of bogie 2 [m]
30 l3    = -27         !position of bogie 3 [m]
31 l4    = -51         !position of bogie 4 [m]
32 l5    = -54         !position of bogie 5 [m]
33 l6    = -78         !position of bogie 6 [m]
34 l7    = -81         !position of bogie 7 [m]
35 l8    = -105        !position of bogie 8 [m]
36 l9    = -108        !position of bogie 9 [m]
37 l10   = -132        !position of bogie 10 [m]
38 l11   = -135        !position of bogie 11 [m]
39 l12   = -159        !position of bogie 12 [m]
40 l1_n  = 2           !node number of bogie 1
41 l2_n  = nint(l2/dl) !node number of bogie 2
42 l3_n  = nint(l3/dl) !node number of bogie 3
43 l4_n  = nint(l4/dl) !node number of bogie 4
44 l5_n  = nint(l5/dl) !node number of bogie 5
45 l6_n  = nint(l6/dl) !node number of bogie 6
46 l7_n  = nint(l7/dl) !node number of bogie 7
47 l8_n  = nint(l8/dl) !node number of bogie 8
48 l9_n  = nint(l9/dl) !node number of bogie 9
49 l10_n = nint(l10/dl) !node number of bogie 10
50 l11_n = nint(l11/dl) !node number of bogie 11
51 l12_n = nint(l12/dl) !node number of bogie 12
52
53 !bridge
54 E_b    = 8.67e10     !Youngs modulus [N/m^2]
55 mu     = 0.2         !poissons ratio [-]
56 A_b    = 4.52        !Area beam [m^2]
57 m_b    = (2303/A_b)  !mass density 2303/4.52 [kg/m^3]
58 h_b    = 2.77        !height beam [m]
59 w_b    = (A_b/h_b)   !width beam [m]
60 Izz    = 2.887       !Moment of inertia beam [m^4]
61
62 nn_t   = nn+abs(l%nv%n)+1 !array dimension counter
63
64 !*****
65 !define the dimension of some output variables
66 !bridge
67 *dim,ub_mid,,nn_t      !displacement bridge midspan
68
69 !masses
70 *do,i,1,nv
71   *dim,uv%i%,,nn_t     !displacement bogie
72   *dim,vv%i%,,nn_t     !velocity bogie
73   *dim,av%i%,,nn_t     !acceleration bogie
74   *dim,ub%i%,,nn_t     !displacement bridge
75   *dim,vb%i%,,nn_t     !velocity bridge
76   *dim,ab%i%,,nn_t     !acceleration bridge
77 *enddo

```

```

78
79 !*****
80 !define element types
81 !define bogies
82 et,1,mass21,,4
83
84 !bogie
85 r,11,m1          !bogie upper mass
86 r,12,m2          !bogie lower mass
87
88 !define spring-damper
89 et,2,combin14,,2
90
91 !vehicle 1
92 r,21,k1,c1       !spring and damper values
93
94 !define beam
95 et,3,beam3
96 mp,ex,3,E_b
97 mp,nuxy,3,mu
98 mp,dens,3,m_b
99 r,3,A_b,Izz,h_b
100
101 !*****
102 !mesh nodes and elements for bogies and bridge
103 !bogies
104 *do,i,1,nv
105   !place bogie masses
106   type,1
107   real,11
108   n,(1000+2*i),(5+i),1.5    !upper mass
109   e,(1000+2*i)
110   real,12
111   n,(1000+i+(i-1)),(5+i),1  !lower mass
112   e,(1000+i+(i-1))
113
114   !place vehicle spring-dampers
115   type,2
116   real,21
117   en,(1000+2*i),(1000+2*i),(1000+i+(i-1))
118
119   !constrain lower mass, all DOF
120   d,(1000+i+(i-1)),all
121 *enddo
122
123 !place nodes for bridge
124 *do,i,1,nn
125   n,i,(i-1)*dl
126 *enddo
127
128 !place bridge elements
129 type,3
130 real,3

```

```

131 mat,3
132 secnum,3
133 *do,i,1,ne
134     e,i,i+1
135 *enddo
136
137 !bridge simply supported DOF
138 d,1,ux,,,,uy
139 d,nn,uy
140
141 !*****
142 !start transient analysis mode
143 finish
144 /solu
145 antype,trans
146
147 !first perform a static load step
148 time,dt/1000
149 timint,off      !no transient effects
150 solve
151
152 !*****
153 !initial conditions
154 !bridge
155 ub_mid(1)=uy(node(l/2,0,0))
156
157 !bogies
158 *do,i,1,nv
159     uv%i%(1)=uy(1000+2*i)
160     vv%i%(1)=0
161     av%i%(1)=0
162     ub%i%(1)=0
163     vb%i%(1)=0
164     ab%i%(1)=0
165 *enddo
166
167 !now perform a transient analysis (default = full), first only apply a
    load at node 2
168 timint,on      !include transient effects
169 time,dt
170 f,2,fy,-(m1*g)
171 solve
172
173 !*****
174 !loop over bridge, move vehicle step by step and compute solution for
    every step
175 *do,ii,2,nn_t
176     !write data to arrays
177     !bridge
178     ub_mid(ii)=uy(node(l/2,0,0))
179
180     !bogies
181     *do,i,1,nv

```

```

182     uv%i%(ii)=uy(1000+2*i)
183     vv%i%(ii)=(uv%i%(ii)-uv%i%(ii-1))/dt
184     av%i%(ii)=(vv%i%(ii)-vv%i%(ii-1))/dt
185     ub%i%(ii)=uy(l%i%_n+1)
186     vb%i%(ii)=(ub%i%(ii)-ub%i%(ii-1))/dt
187     ab%i%(ii)=(vb%i%(ii)-vb%i%(ii-1))/dt
188 *enddo
189
190 time , ii*dt
191 fdele , all , all
192
193 !move vehicles one node
194 *do , i , 1 , nv
195     l%i%_n = l%i%_n+1
196 *enddo
197
198 !apply contact force on beam, if bogie is already/still on beam
199 *do , i , 1 , nv
200     *if , l%i%_n , GT , 0 , AND , l%i%_n , LE , nn-1 , THEN
201         f , l%i%_n , fy , (-m1*g-m1*av%i%(ii)+k1*(uv%i%(ii)-ub%i%(ii)))
202     *endif
203 *enddo
204
205 !give vehicles reaction displacement
206 *do , i , 1 , nv
207     d , (1000+i+(i-1)) , uy , ub%i%(ii)
208 *enddo
209
210 solve
211 *enddo
212
213 !*****
214 !write results to output file
215 *do , i , 1 , nv
216 *c fopen , results_v%i%_l%i%_one%.out
217 *vwrite , uv%i%(1) , vv%i%(1) , av%i%(1) , ub%i%(1) , vb%i%(1) , ab%i%(1) , ub_mid(1)
218 (F20.16 , F20.16 , F20.16 , F20.16 , F20.16 , F20.16 , F20.16)
219 *c fclose
220 *enddo

```

## J.2 Code explanation

As seen in section J.1, a train with six coaches is modelled, by assuming twelve bogies each carrying half of the coach mass. Of course, less bogies can be modelled by lowering the parameter “nv”, if required. The x-location of these bogies is defined, which is used to compute a node number depending on the mesh size. This node number is negative and fictitious, there exist no nodes before the bridge, but by incrementing the node number of the bogies by one each loop, the bogies are simulated to move until they reach node 1, which exists on the bridge. To prevent bogies which are not on the bridge yet or already past the bridge to act on the bridge, their position is checked with an if-statement.



## Simple model verifications

To know if the to simple models make sense, they must be verified by comparing to results which are known to be correct. In section K.1 and section K.2 these models are compared to the analytical-numerical results from Matlab. This appendix is referenced from section 3.2.

### K.1 Contact force model

In this section the contact force model from Appendix G is compared with the Matlab solution of a single degree of freedom moving sprung mass from section E.1. To let Ansys produce accurate results, a convergence study is done first.

#### K.1.1 Ansys APDL code

To compare with the Matlab solution, the same parameters as from literature are used, see subsection E.1.3.

```
1 !Name:      beam_convergence_study
2 !Date:      February 22, 2016
3 !Last modified: March 7, 2016
4 !Description: Contact force model – convergence study
5
6 finish
7 /clear
8 /prep7
9
10 !define some input variables
11 l = 25          !length bridge [m]
12 g = 9.81       !gravitational acceleration [m/s2]]
13 m1 = 5750      !vehicle mass [kg]
14 m2 = 1e-8      !wheel mass [kg]
15 k1 = 1595000   !spring stiffness [N/m]
```

```

16 c1 = 0           !damping value [Ns/m]
17 E_b = 2.87e9    !Youngs modulus [N/m^2]
18 mu = 0.2       !poissons ratio [-]
19 A_b = 4.52      !Area beam [m^2]
20 m_b = (2303/A_b) !mass density 2303/4.52 [kg/m^3]
21 h_b = 2.77     !height beam [m]
22 w_b = (A_b/h_b) !width beam [m]
23 Izz = 2.887    !Moment of inertia beam [m^4]
24 ne = 100       !number of elements
25 nn = ne + 1    !number of nodes
26 v = 27.78      !velocity [m/s]
27 dl = l / ne    !delta length of small element
28 dt = dl / v    !delta time of one time step
29
30 !define the dimension of some output variables
31 *dim,uv,,nn     !displacement vehicle
32 *dim,vv,,nn     !velocity vehicle
33 *dim,av,,nn     !acceleration vehicle
34 *dim,ub,,nn     !displacement bridge
35 *dim,vb,,nn     !velocity bridge
36 *dim,ab,,nn     !acceleration bridge
37 *dim,ub_mid,,nn !displacement bridge midspan
38
39 !define two masses
40 et,1,mass21,,4
41 r,11,m1         !vehicle mass
42 r,12,m2         !wheel mass
43
44 !define spring-damper
45 et,2,combin14,,2
46 r,21,k1,c1     !spring and damper values
47
48 !define beam
49 et,3,beam3
50 mp,ex,3,E_b
51 mp,nuxy,3,mu
52 mp,dens,3,m_b
53 r,3,A_b,Izz,h_b
54
55 !define two mass elements, each consisting of one node
56 type,1
57 real,11
58 n,1002,10,1.5  !X = 10, Y = 1.5
59 e,1002
60 real,12
61 n,1001,10,1    !X = 10, Y = 1
62 e,1001
63
64 !define spring-damper element, consisting of two nodes, connecting both
    masses
65 type,2
66 real,21
67 en,1002,1002,1001

```

```

68
69 !define nodes along the bridge length
70 *do , i , 1 , nn
71 n , i , ( i - 1 ) * dl
72 !d , i , uz
73 *enddo
74
75 !define a number of beam elements , all consisting of 2 nodes previously
    defined
76 type , 3
77 real , 3
78 mat , 3
79 secnum , 3
80 *do , i , 1 , ne
81 e , i , i + 1
82 *enddo
83
84 !define degrees of freedom
85 d , 1 , ux , , , , uy
86 d , nn , uy
87 d , 1001 , all
88
89 !start transient analysis mode
90 finish
91 /solu
92 antype , trans
93
94 !first perform a static analysis load step , needed to define nonzero
    initial displacement (free vibration under initial state)
95 time , dt / 1000
96 timint , off !no transient effects
97 solve
98 uv ( 1 ) = uy ( 1002 )
99 vv ( 1 ) = 0
100 av ( 1 ) = 0
101 ub ( 1 ) = 0
102 vb ( 1 ) = 0
103 ab ( 1 ) = 0
104 ub_mid ( 1 ) = uy ( node ( l / 2 , 0 , 0 ) )
105
106 !now perform a transient analysis (default = full) , first only apply a
    load at node 2
107 timint , on !include transient effects
108 time , dt
109 f , 2 , fy , - ( m1 * g )
110 solve
111
112 !loop over bridge , move vehicle step by step and compute solution for
    every step
113 *do , ii , 2 , nn - 1
114 uv ( ii ) = uy ( 1002 )
115 vv ( ii ) = ( uv ( ii ) - uv ( ii - 1 ) ) / dt
116 av ( ii ) = ( vv ( ii ) - vv ( ii - 1 ) ) / dt

```

```

117 ub(ii)=uy(ii+1)
118 vb(ii)=(ub(ii)-ub(ii-1))/dt
119 ab(ii)=(vb(ii)-vb(ii-1))/dt
120 ub_mid(ii)=uy(node(l/2,0,0))
121 time,ii*dt
122 fdele,all,all
123 f,ii+1,fy,(-m1*g-m1*av(ii)+k1*(uv(ii)-ub(ii)))
124 d,1001,uy,ub(ii)
125 solve
126 *enddo
127
128 !define results output name
129 *set,res_name,'results_%ne%.out'
130
131 !write arrays to output file
132 *cfcopen,res_name !open file for writing
133 *vwrite,uv(1),vv(1),av(1),ub(1),vb(1),ab(1),ub_mid(1) !write arrays to
file
134 (F20.16,F20.16,F20.16,F20.16,F20.16,F20.16,F20.16) !Fortran format
style
135 *cfclose

```

### K.1.2 Convergence study

To study the convergence, the parameter  $ne$  is increased with increments of 10, which results in a decreasing time step (in the limit of delta time going to zero, the solution becomes very accurate). The bridge displacement at midspan is taken as a measure and is compared to the Matlab solution. The normalized value of this can be seen in Figure K.1. At around 250 elements (ten times the bridge length) the good convergence is reached, with a difference of 2.5% from the Matlab result.

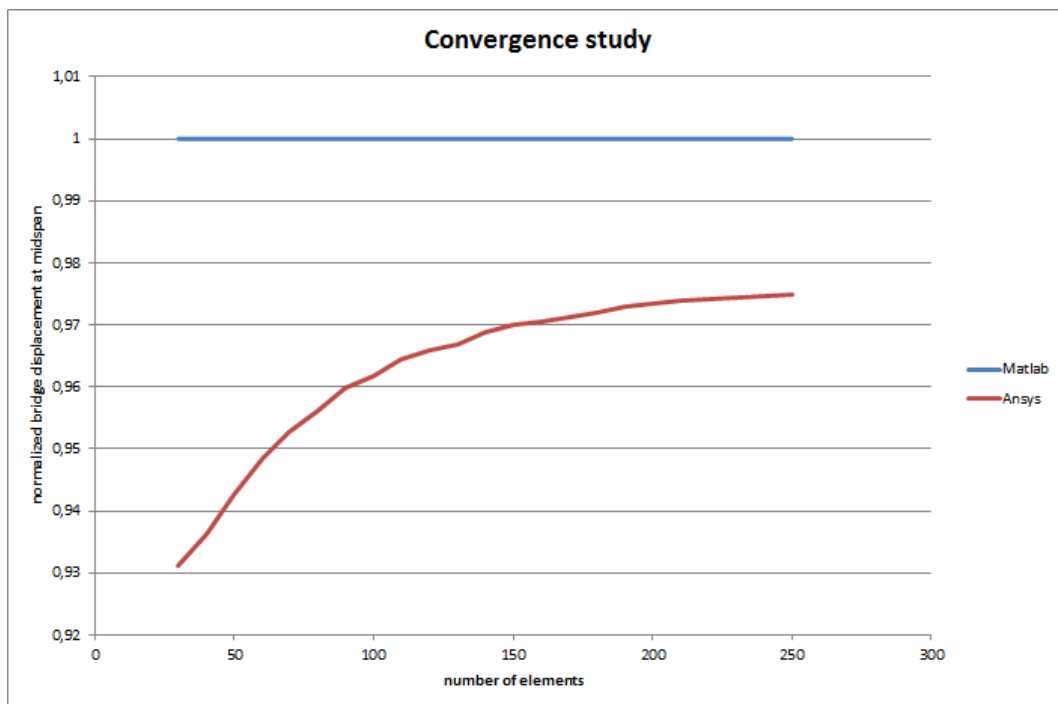


**Figure K.1:** Convergence study: normalized midpoint bridge deflection with increasing mesh density, Ansys compared to Matlab

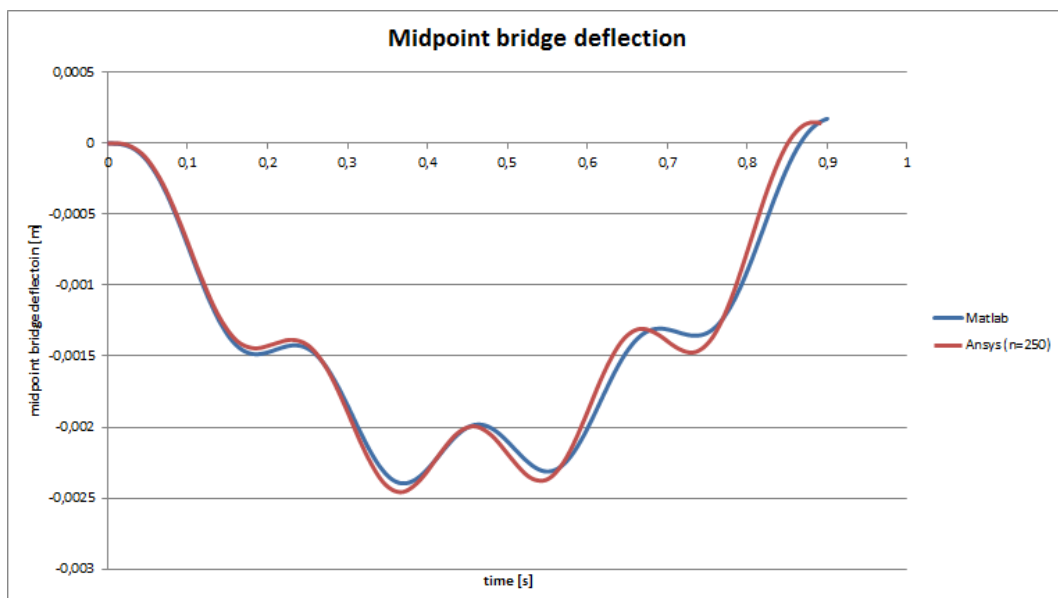


**Figure K.2:** Convergence study: midpoint bridge deflection over time, Ansys compared to Matlab

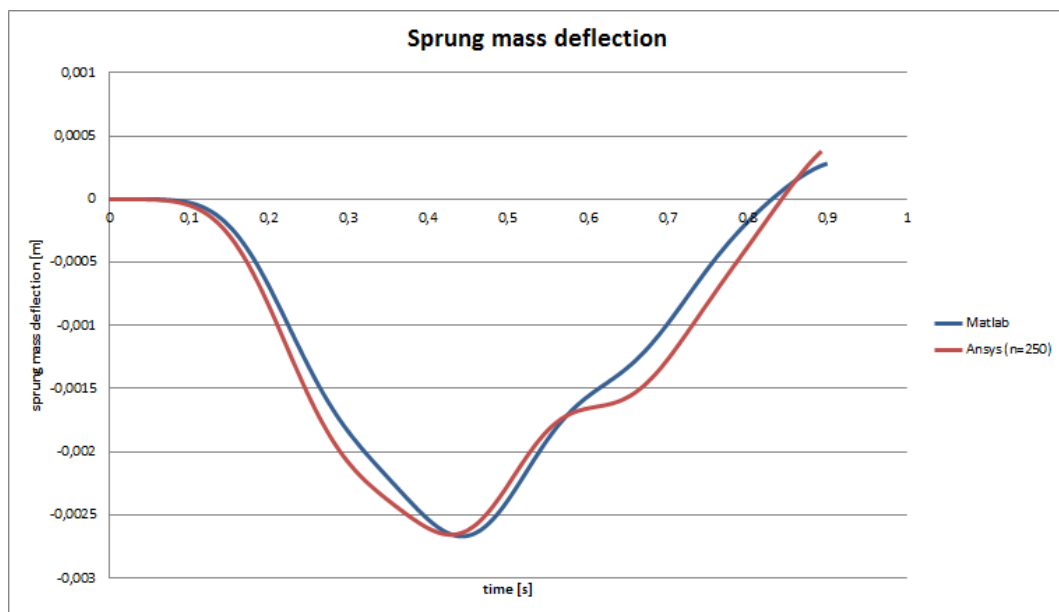


**Figure K.3:** Convergence study: sprung mass deflection over time, Ansys compared to Matlab

## K.2 Multiple 1 DOF sprung masses

In this section the multiple 1 DOF sprung masses model from Appendix J is compared with the Matlab solution of multiple single degree of freedom moving sprung masses from section E.2. This comparison is made using the following parameters, largely the same as for the case of a single 1 DOF sprung mass:

- spring stiffness  $k_v = 1\,595\,000\text{ N/m}$ ;
- sprung mass  $m_v = 5750\text{ kg}$ ;
- velocity of mass  $v = 27.78\text{ m/s}$ ;
- Young's Modulus beam  $E_b = 2.87 \times 10^9\text{ N/m}^2$ ;
- Moment of inertia beam  $I_b = 2.90\text{ m}^4$ ;
- Mass beam  $m_b = 2303\text{ kg/m}$ ;
- Length beam  $L = 75\text{ m}$ ;
- number of sprung masses  $nv = 2$ ;

and can be seen in Figure K.4, Figure K.5 and Figure K.6.

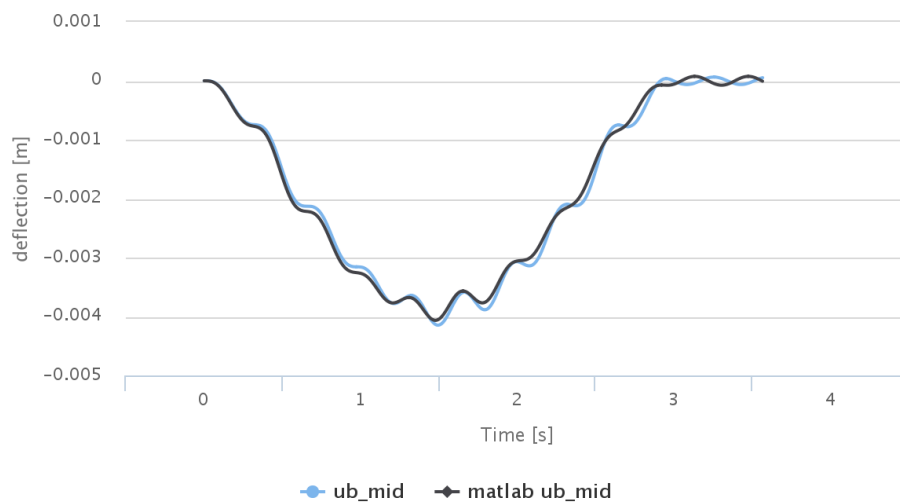


**Figure K.4:** Midpoint bridge deflection, Ansys compared to Matlab. See also [online](#).

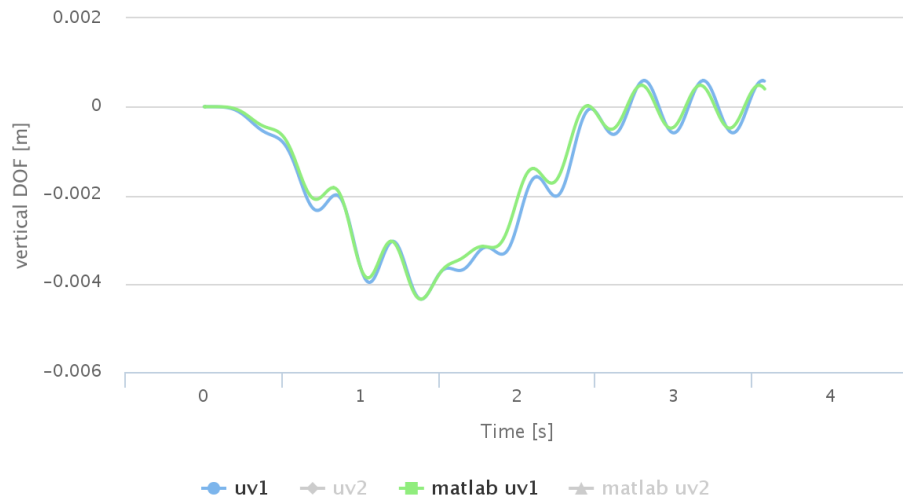


**Figure K.5:** Bogie 1 vertical displacement, Ansys compared to Matlab. See also [online](#).

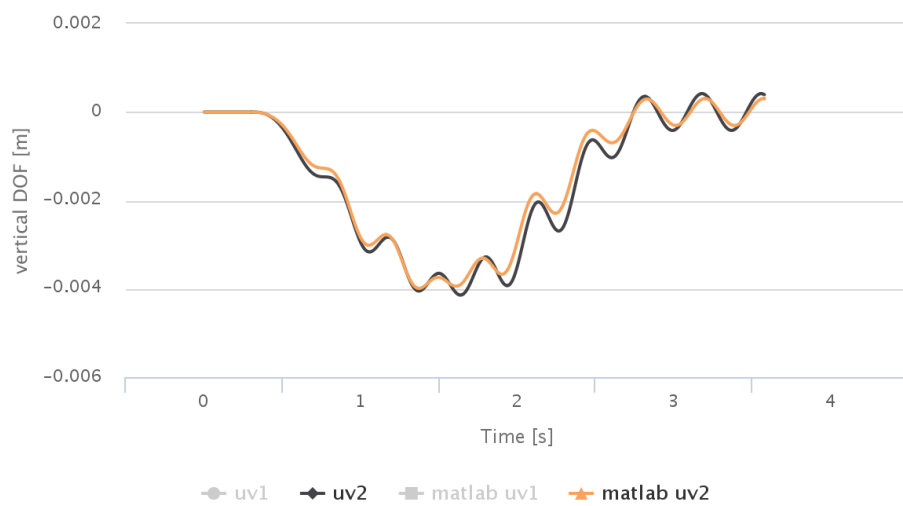


**Figure K.6:** Bogie 2 vertical displacement, Ansys compared to Matlab. See also [online](#).

It can be concluded the analytical-numerical solution of the equations of motion solved in Matlab compares the Ansys model results. Although this verification is done for only two moving sprung masses, there is confidence the accuracy remains comparable when extending the train model to more than two sprung masses.



---

# Appendix L

---

## Modelling results

This appendix contains some results of Ansys modelling. First something is said about the used integration method in section L.1 and section L.2. In section L.3 the behaviour of the two bridge models is described. In section L.4 the three vehicle models are presented and their results explained. A complete model comparison is performed in section L.5. This appendix is referenced from section 3.3 and section 3.4.

### L.1 Newmark- $\beta$ versus HHT

Initially the Newmark- $\beta$  method was used in the Ansys analyses, it is the default integration method. However, in certain cases high frequency noise was observed. Therefore it was decided to use the Hilber-Hughes-Taylor (HHT) method instead, which features numerical damping. This significantly reduced the high frequency noise in the acceleration plots. In Figure L.1 an acceleration plot of two 1 DOF bogies travelling over the 2D tied-arch bridge is shown. Choosing the correct  $\gamma$  value is a trade-of between as much damping of high frequency noise and as minimum damping of low frequency signal, which should not be altered artificially. A value of  $\gamma = 0.01$  is chosen and used throughout the analyses, with which any erroneous participation of the higher modes can be damped out and the lower modes are scarcely affected. [60, par. 15.2.2.1]

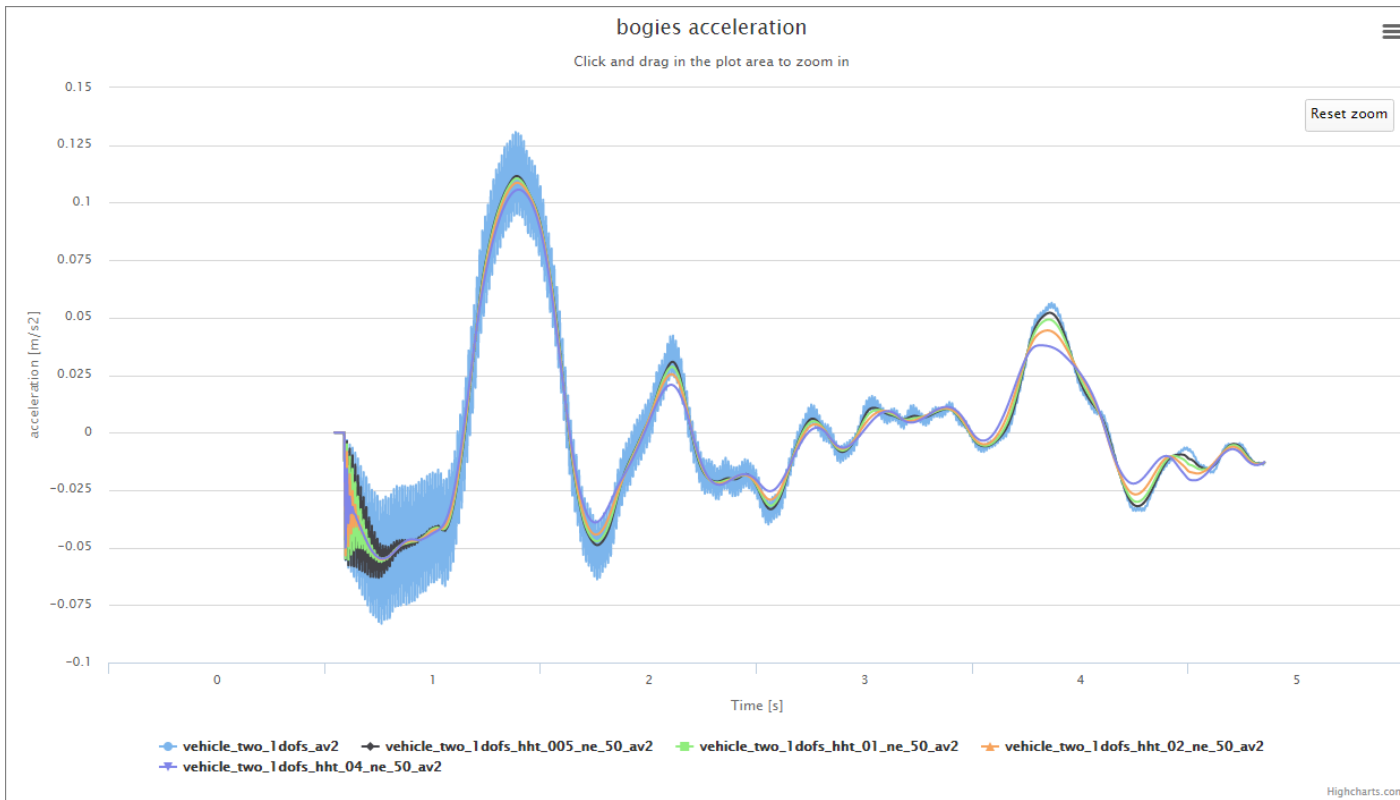


**Figure L.1:** The blue line is the Newmark method. The black line is HHT with  $\gamma = 0.005$ , the green  $\gamma = 0.01$ , the orange  $\gamma = 0.02$  and the purple  $\gamma = 0.04$ . See also [online](#).

## L.2 Backwards difference versus direct get

There are different methods to obtain node displacements, velocities and accelerations. With the so-called “direct get” method a function is used to obtain nodal displacements, velocities or accelerations directly from the associated vectors every time step. Unfortunately using this method causes high frequency vibrations to appear in abrupt changes of acceleration. Therefore it was chosen to use numerical differentiation instead, as mentioned in section F.5. The displacements are obtained directly from their vector every time step, but the velocities and accelerations are obtained by backwards differentiation of the displacements. This results in smoother transitions at discontinuities which take place when the train enters or leaves the bridge. This method of filtering erroneous high-frequency components is also mentioned in literature. [68, p. 502]

## L.3 Bridge models

Apart from the simply supported beams in the simple models, two bridge models are considered, a two dimensional tied-arch bridge and a three dimensional tied-arch bridge. The results of analyses with these bridge models will be treated in this section.

### L.3.1 2D tied-arch bridge

The creation of the 2D tied-arch bridge model is fully described in Appendix M. This section will focus on some results obtained for this model.

From the midspan and one-quarter-span bridge deflections in Figure L.2 it can be observed the vehicle model has a small influence on the bridge response, which is in accordance with literature [69]. Furthermore it can be seen the deflection at one-quarter-span is considerably larger than the deflection at midspan. This result is also to be expected for tied-arch bridges with vertical hangers.

When performing a Fourier transform as seen in Figure L.3 one finds both in the bridge midpoint and the bridge at one-quarter peaks at certain frequencies. For both graphs the highest frequency

is caused by global deflection of the bridge, 0.10 Hz and 0.20 Hz respectively. This is easy to understand, looking at the graphs a sinusoid with one period in 10 seconds or two periods in 10 seconds can be seen.

The second and third peaks are at approximately 1.37 Hz and 1.90 Hz and correspond with the first and second natural frequencies of the bridge model of 1.38 Hz and 1.91 Hz, as can be seen in subsection M.3.3. The peaks in this area are related to those, since after a pulse load a structure starts to vibrate in its natural frequencies and will continue to do so indefinitely, if it is undamped.

There are higher frequency peaks, such as at 3.16 Hz, related to the third natural frequency of 3.12 Hz, but their amplitude is considerably smaller than the first two peaks.

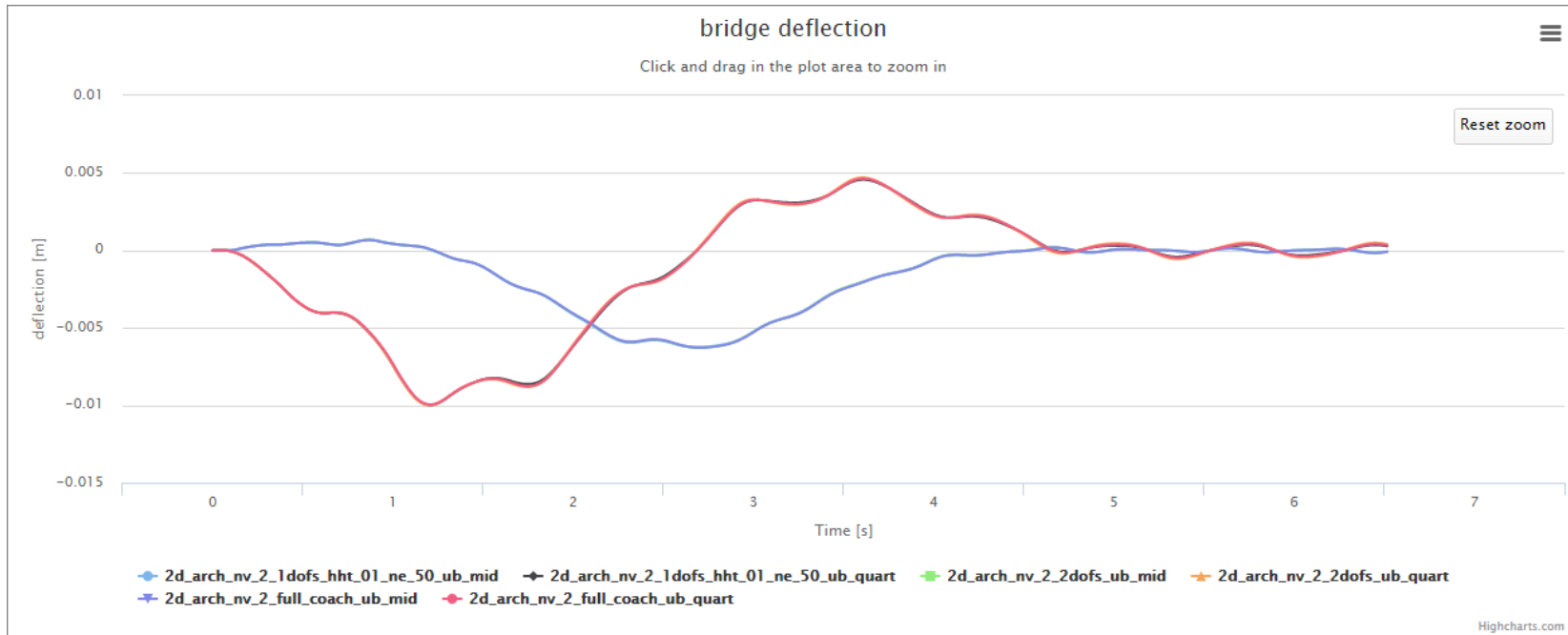


**Figure L.2:** Comparison between 1 DOF bogie schematization, 2 DOF bogie schematization and full coach schematization. The train model goes with a velocity of 125 km/h over the 2D bridge model. Blue, green and purple lines are the bridge deflection at midspan. Black, orange and pink lines are the bridge deflection at one-quarter-span. See also [online](#).

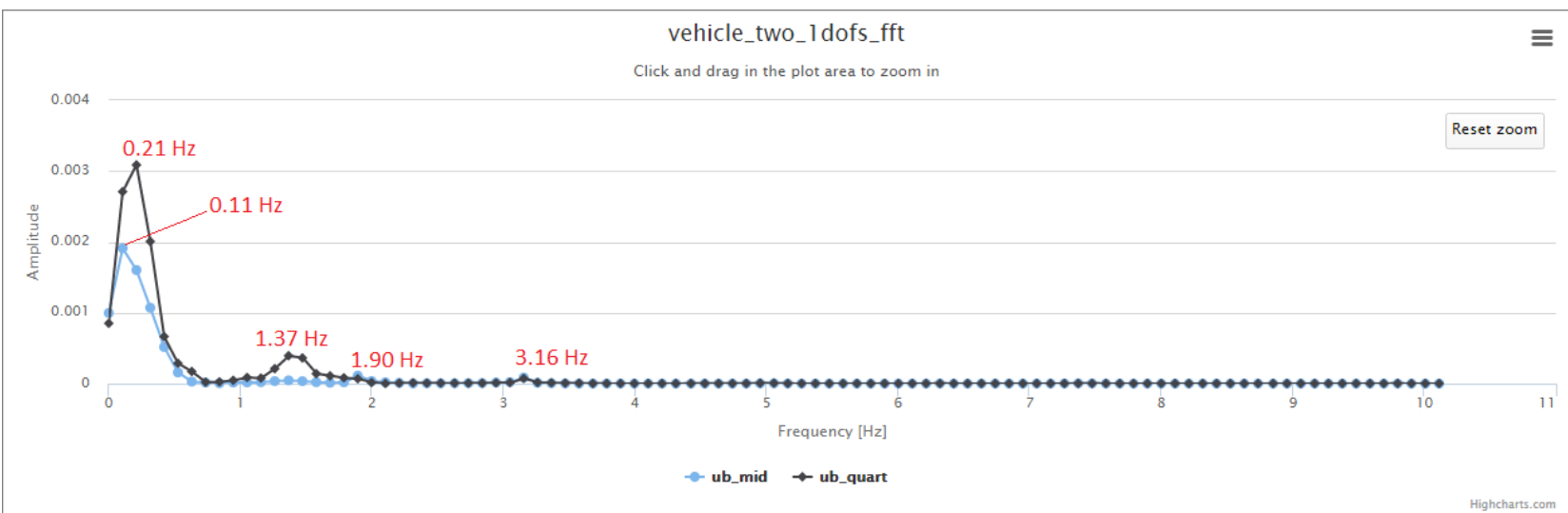


**Figure L.3:** Fast fourier transform of bridge deflection graphs from Figure L.2. See also [online](#).

### L.3.2 3D tied-arch bridge

The creation of the 3D tied-arch bridge model is fully described in Appendix N. This section will focus on some results obtained for this model.

The global static behaviour of the 3D bridge model corresponds very well with the 2D bridge model, as shown in section N.3. Its midspan and one-quarter-span bridge deflections are as in the case of the 2D bridge model.

When performing a Fourier transform as seen in Figure L.5 one finds for both the midspan and the one-quarter span deflection in Figure L.4 peaks at certain frequencies. For both graphs the highest frequency is caused by global deflection of the bridge, 0.11 Hz and 0.21 Hz respectively. This is easy to understand, looking at the graphs a sinusoid with one period in 10 seconds or two periods in 10 seconds can be seen.

The second and third peaks are at approximately 1.05 Hz and 1.79 Hz and correspond with the first and second natural frequencies of the bridge model of 1.11 Hz and 1.84 Hz, as can be seen in subsection N.3.3. The peaks in this area are related to those, since after a pulse load this structure starts to vibrate in its natural frequencies and will continue to do so indefinitely, if it is undamped.

There are higher frequency peaks, like at 2.63 Hz, related to the third natural frequency of 2.64 Hz, but their amplitude is considerably smaller than the first two peaks.

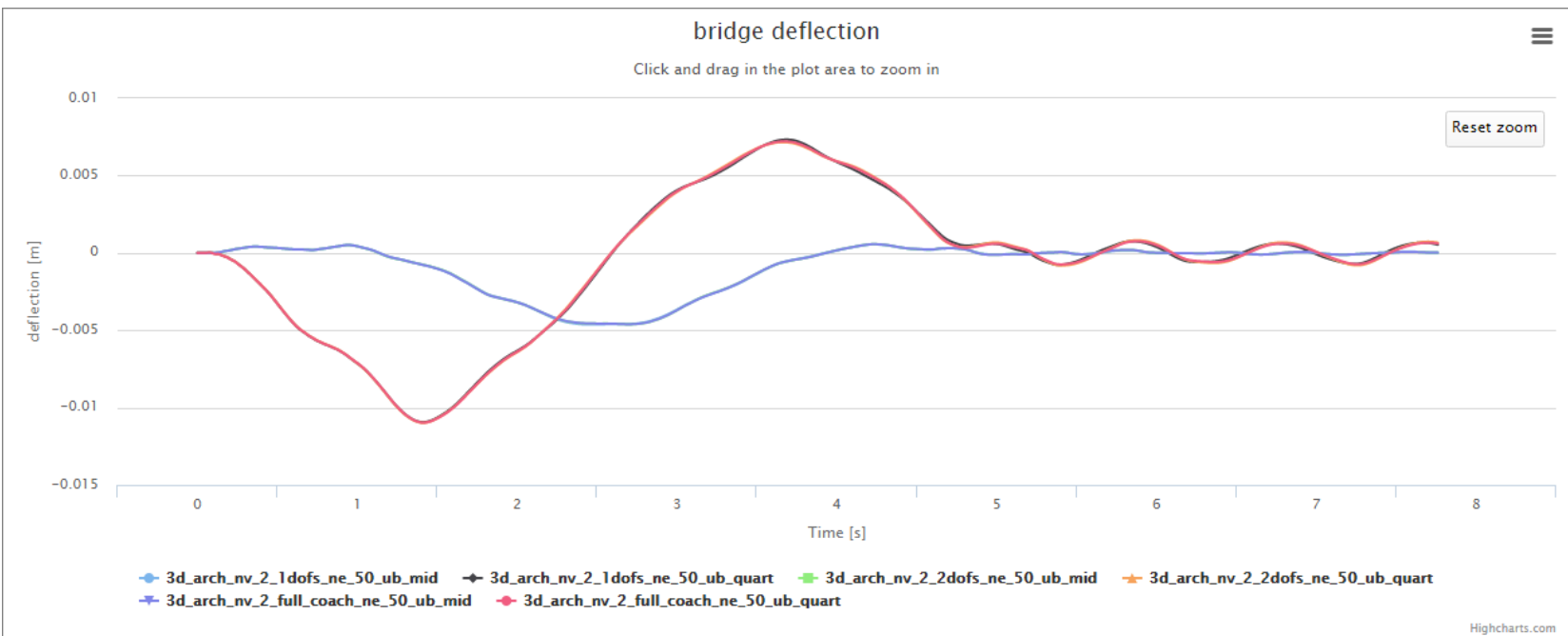


**Figure L.4:** Comparison between 1 DOF bogie schematization, 2 DOF bogie schematization and full coach schematization. The train model goes with a velocity of 125 km/h over the 3D bridge model. Blue, green and purple lines are the bridge deflection at midspan. Black, orange and pink lines are the bridge deflection at one-quarter-span. See also [online](#).

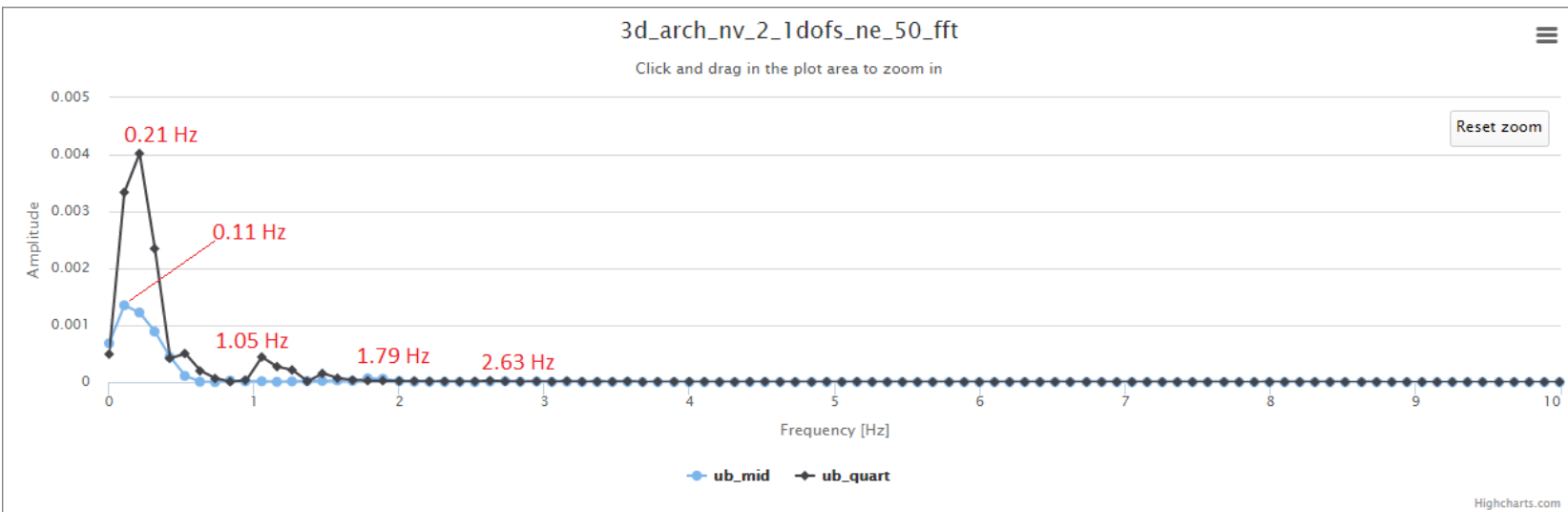


**Figure L.5:** Fast fourier transform of bridge deflection graphs from Figure L.4. See also [online](#).

### L.3.3 Comparison of bridge models

In section N.3 the global static behaviour of the 2D and 3D bridge models are compared and prove to be comparable. In Figure L.6 a comparison of the midspan deflection of the bridge is shown. The 2D bridge deflects approximately 12 millimetres, while the 3D bridge deflects 8 millimetres on one side and 16 millimetres at the other side, which is 12 millimetres on average as well.

In Figure L.7 a comparison of the deflection of the bridge at one-quarter of the span is shown. The 2D bridge deflects at one-quarter-span approximately 17 millimetres, while the 3D bridge deflects 19 millimetres on one side and 25 millimetres at the other side, both more than the 2D bridge. So in this case the 2D bridge model and the 3D bridge model do not correspond so well as with the midspan deflection.

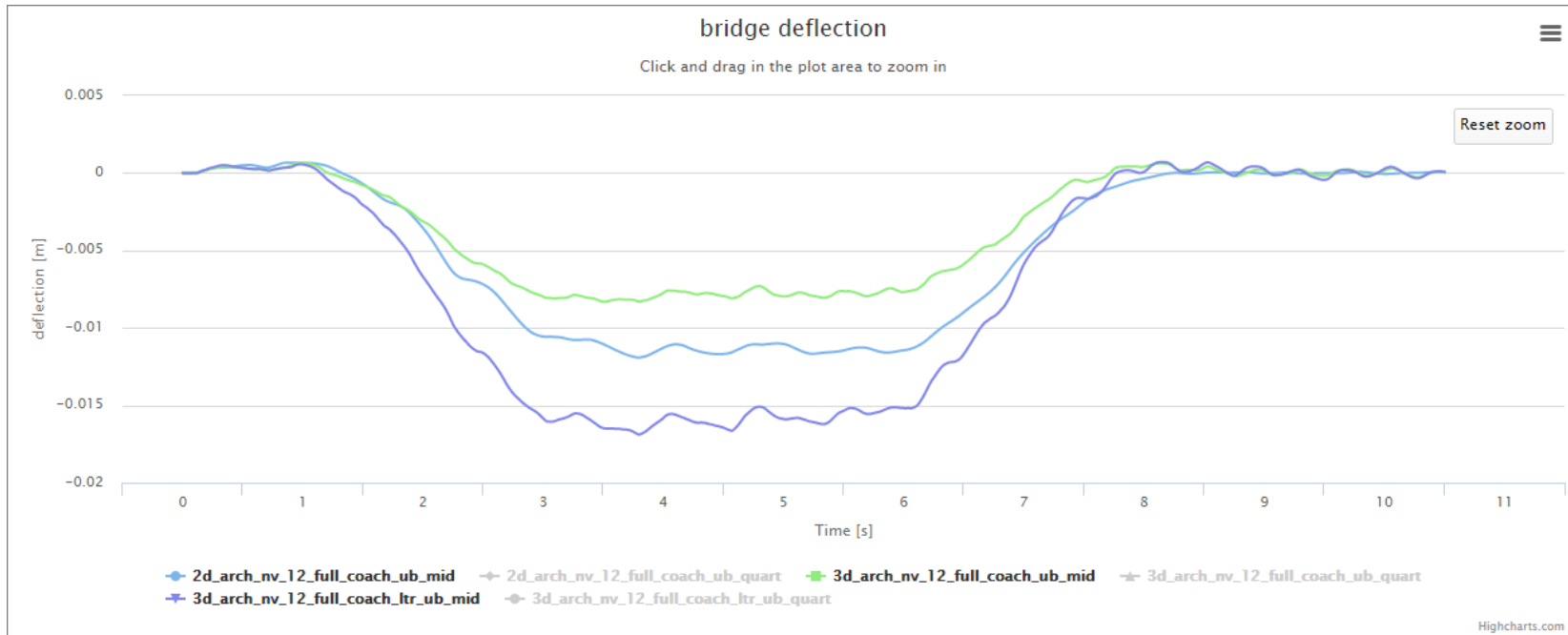


**Figure L.6:** Comparison between 2D and 3D bridge model deflections. The train model goes with a velocity of 125 km/h over the bridge models. The blue line is the deflection at midspan of the 2D bridge model, the green and purple lines are the deflection at midspan of the 3D bridge model, at the left and right side of the bridge. See also [online](#).

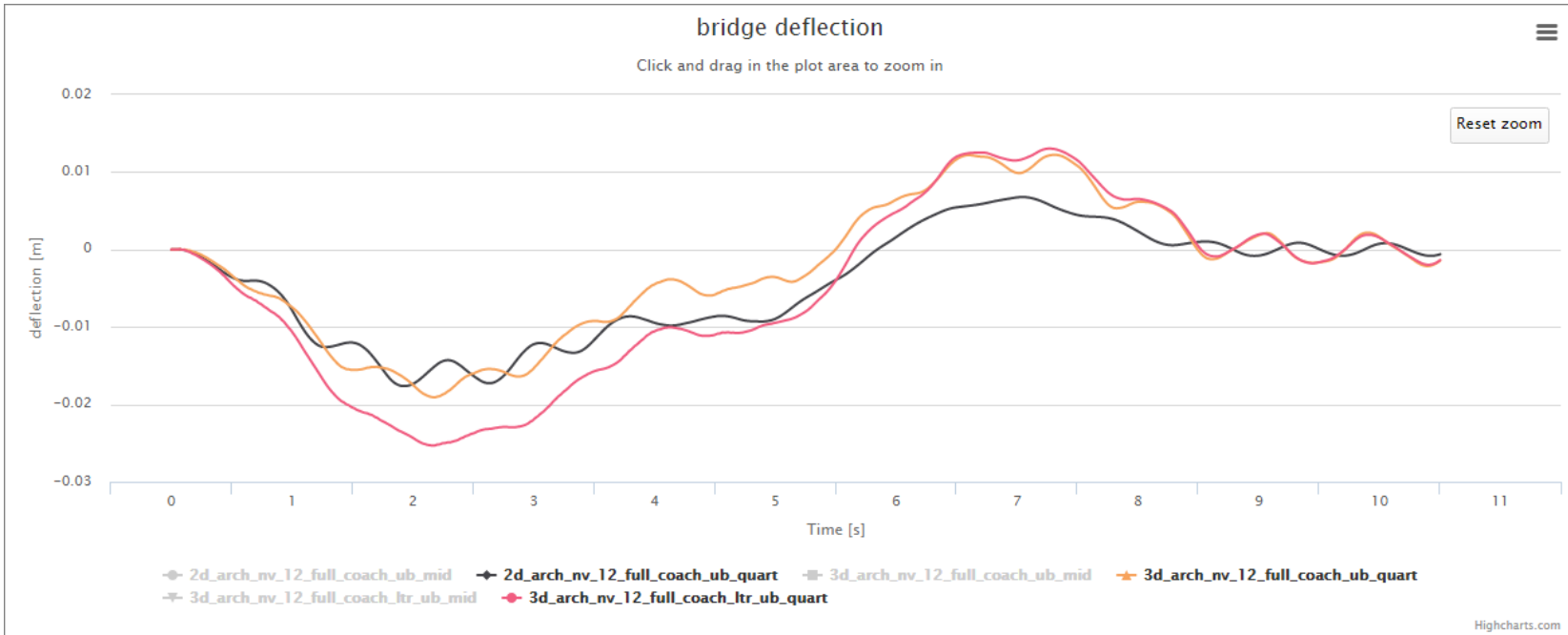


**Figure L.7:** Comparison between 2D and 3D bridge model deflections. The train goes with a velocity of 125 km/h over the bridge models. The black line is the deflection at one-quarter of the 2D bridge model, the orange and pink lines are the deflection at one-quarter of the 3D bridge model, at the left and right side of the bridge. See also [online](#).

## L.4 Vehicle models

In section C.3 three vehicle models are introduced, a 1 DOF schematization, a 2 DOF schematization and a full coach schematization of a train. These three vehicle models are treated in this section.

### L.4.1 1 DOF schematization

The most simple vehicle model is a schematization of masses and spring-dampers in Ansys, as seen in Figure L.8.

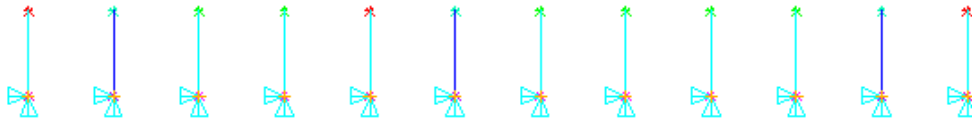


**Figure L.8:** 1 DOF vehicle model in Ansys. Here a train consisting of 12 bogie is shown.

The following code has been used.<sup>1</sup> This apdl file can be used together with the 2d arch bridge code<sup>2</sup> or the 3d arch bridge code, which request sections from this code using labels.

```

1  !Name:      vehicle_sdof_bogies
2  !Date:      April 18, 2016
3  !Last modified: May 10, 2016
4  !Description: vehicle model of SDOF bogies
5
6  :vars      !label
7  !*****
8  !define some input variables
9  !general
10 gamma_d    = 0.1          !Gamma, numerical damping in HHT
11 !coaches
12 m_1m       = 0.5*51500    !motor coach mass [kg]
13 m_1t       = 0.5*43500    !trailer coach mass [kg]
14 !motor bogie
15 m_2m       = 8620         !motor frame mass [kg]
16 m_3m       = 2*1200       !two motor wheelsets mass [kg]
17 k_pm       = 5000000      !primary stiffness motor bogie [N/m]
18 c_pm       = 103804       !primary damping motor bogie [Ns/m]
19 k_sm       = 920000       !secondary stiffness motor bogie [N/m]
20 c_sm       = 81670        !secondary damping motor bogie [Ns/m]

```

<sup>1</sup>[https://github.com/benjaminkomen/benjaminkomen.github.io/blob/master/ansys/6\\_complexer\\_bogies/vehicle\\_sdof\\_bogies.inp](https://github.com/benjaminkomen/benjaminkomen.github.io/blob/master/ansys/6_complexer_bogies/vehicle_sdof_bogies.inp)

<sup>2</sup>[https://github.com/benjaminkomen/benjaminkomen.github.io/blob/master/ansys/6\\_complexer\\_bogies/2d\\_arch\\_sdof\\_bogies.inp](https://github.com/benjaminkomen/benjaminkomen.github.io/blob/master/ansys/6_complexer_bogies/2d_arch_sdof_bogies.inp)

```

21 !trailer bogie
22 m_2t = 4970 !trailer frame mass [kg]
23 m_3t = 2*1700 !two trailer wheelsets mass [kg]
24 k_pt = 3400000 !primary stiffnes trailer bogie [N/m]
25 c_pt = 64996 !primary damping trailer bogie [Ns/m]
26 k_st = 920000 !secondary stiffnes trailer bogie [N/m]
27 c_st = 75829 !secondary damping trailer bogie [Ns/m]
28
29 nv = 12 !number of bogies
30
31 *dim,bog_x,,12 !bogies initial x-coordinate positions array
    assuming 6 part VIRM
32 bog_x(1) = 0
33 bog_x(2) = -20
34 bog_x(3) = bog_x(2) - 3.55 - 3.05
35 bog_x(4) = bog_x(3) - 20
36 bog_x(5) = bog_x(4) - 3.05 - 3.55
37 bog_x(6) = bog_x(5) - 20
38 bog_x(7) = bog_x(6) - 3.55 - 3.05
39 bog_x(8) = bog_x(7) - 20
40 bog_x(9) = bog_x(8) - 3.05 - 3.55
41 bog_x(10) = bog_x(9) - 20
42 bog_x(11) = bog_x(10) - 3.55 - 3.05
43 bog_x(12) = bog_x(11) - 20
44
45 *dim,bog_n,,nv !bogies initial node positions array
46 bog_n(1) = 2 !node number of bogie 1
47
48 *do,i,2,nv
49 bog_n(%i%) = nint(bog_x(%i%)/dl)
50 *enddo
51
52 /eof !switch back to master file
53 :etypes !label
54 !*****
55 !define element types
56 !define bogies
57 et,4,mass21,,4
58 !motor coach + motor bogie
59 r,11,m_1m !motor coach mass + motor frame mass
60 r,13,(m_3m+m_2m) !motor bogie wheelsets
61 !motor coach + trailer bogie
62 r,14,m_1m !motor coach mass + trailer frame mass
63 r,16,(m_3t+m_2t) !trailer bogie wheelsets
64 !trailer coach + trailer bogie
65 r,17,m_1t !trailer coach mass + trailer frame mass
66 r,19,(m_3t+m_2t) !trailer bogie wheelsets
67
68 !define spring-damper
69 et,5,combin14,,2
70 r,21,k_sm,c_sm !motor bogie secondary suspension
71 r,23,k_st,c_st !trailer bogie secondary suspension
72

```

```

73 /eof
74 : meshing                !label
75 !*****
76 !meshing
77 !bogies
78 *do ,i,1,nv
79   !bogies 1, 5 and 12 use r 14, 16, 23
80   *if ,i,eq,1,or,i,eq,5,then
81     !place masses
82     type,4
83     real,14
84     n,(10000*i+3),i,31    !upper mass
85     e,(10000*i+3)
86     real,16
87     n,(10000*i+1),i,30    !lower mass
88     e,(10000*i+1)
89     !place spring-dampers
90     type,5
91     real,23
92     en,(10000*i+3),(10000*i+3),(10000*i+1)
93   *elseif ,i,eq,12,then
94     !place masses
95     type,4
96     real,14
97     n,(10000*i+3),i,31    !upper mass
98     e,(10000*i+3)
99     real,16
100    n,(10000*i+1),i,30    !lower mass
101    e,(10000*i+1)
102    !place spring-dampers
103    type,5
104    real,23
105    en,(10000*i+3),(10000*i+3),(10000*i+1)
106  !bogies 2, 6 and 11 use r 11, 13, 21
107  *elseif ,i,eq,2,or,i,eq,6,then
108    !place masses
109    type,4
110    real,11
111    n,(10000*i+3),i,31    !upper mass
112    e,(10000*i+3)
113    real,13
114    n,(10000*i+1),i,30    !lower mass
115    e,(10000*i+1)
116    !place spring-dampers
117    type,5
118    real,21
119    en,(10000*i+3),(10000*i+3),(10000*i+1)
120  *elseif ,i,eq,11,then
121    !place masses
122    type,4
123    real,11
124    n,(10000*i+3),i,31    !upper mass
125    e,(10000*i+3)

```

```

126     real ,13
127     n,(10000*i+1),i,30    !lower mass
128     e,(10000*i+1)
129     !place spring-dampers
130     type,5
131     real ,21
132     en,(10000*i+3),(10000*i+3),(10000*i+1)
133     !the other bogies use r 17, 19, 23
134     *else
135         !place masses
136         type,4
137         real ,17
138         n,(10000*i+3),i,31    !upper mass
139         e,(10000*i+3)
140         real ,19
141         n,(10000*i+1),i,30    !lower mass
142         e,(10000*i+1)
143         !place spring-dampers
144         type,5
145         real ,23
146         en,(10000*i+3),(10000*i+3),(10000*i+1)
147     *endif
148     !constrain lower mass, all DOF
149     d,(10000*i+1),all
150 *enddo
151
152 /eof
153 :initcon          !label
154 !*****
155 !initial conditions
156 !bogies
157 *do,i,1,nv
158     uv(1,i)=uy(10000*i+3)
159     vv(1,i)=0
160     av(1,i)=0
161     ub(1,i)=0
162     vb(1,i)=0
163     ab(1,i)=0
164 *enddo
165
166 !determine node numbers on vehicle path_br, backwards compatible with 2d
    bridge
167 *dim,path_br,,nng
168 cur_x = 0
169 *do,i,1,nng
170     path_br(i) = node(cur_x,0,7.15)
171     cur_x = cur_x + dl
172 *enddo
173
174 *dim,mask,,elmiqr(0,14)
175
176 !now perform a transient analysis (default = full), first only apply a
    load at node 2

```

```

177 timint ,on                !include transient effects
178 trnopt , , , , , hht      !use HHT instead of Newmark
179 tintp , gamma_d          !damp out numerical noise
180 time , dt
181 f , path_br(2) , fy , -((m_1m+m_2t+m_3t)*g)
182 outres , all , all
183 solve
184
185 /eof
186 :mainrun                  !label
187 !*****
188 !loop over bridge
189 *do , ii , 2 , nn_t
190     !write data to arrays
191     t(ii)=(ii-1)*dt
192     !bridge
193     ub_mid(ii)=uy(node(l/2,0,0))
194     ub_25(ii)=uy(node(l/4,0,0))
195
196     !bogies
197     *do , i , 1 , nv
198         uv(ii,i)=uy(10000*i+3)
199         vv(ii,i)=(uv(ii,i)-uv(ii-1,i))/dt
200         av(ii,i)=(vv(ii,i)-vv(ii-1,i))/dt
201
202         !bridge deflection under bogie is bridge node deflection , if bogie is
                still on beam , else zero (post approach bridge no deflection)
203         *if , bog_n(i) , GE , path_br(1) , AND , bog_n(i) , LE , path_br(nng-1) , THEN
204             ub(ii,i)=uy(bog_n(i))
205             vb(ii,i)=vy(bog_n(i))
206             ab(ii,i)=ay(bog_n(i))
207         *else
208             ub(ii,i)=0
209             vb(ii,i)=0
210             ab(ii,i)=0
211         *endif
212     *enddo
213
214     time , ii*dt
215     fdele , all , all
216
217     !move vehicles one node
218     *do , i , 1 , nv
219         *if , bog_n(i) , LT , 0 , OR , bog_n(i) , GE , path_br(nng-1) , THEN
220             !if bogies are before/past bridge , increment with 1
221             bog_n(i) = bog_n(i)+1
222         *elseif , bog_n(i) , eq , 0 , THEN
223             !if bogies reach the bridge , give them node number of start bridge ,
                not necessarily 1
224             bog_n(i) = path_br(1)
225         *else
226             !if bogies are on the bridge , give them next node number in vehicle
                path_br

```

```

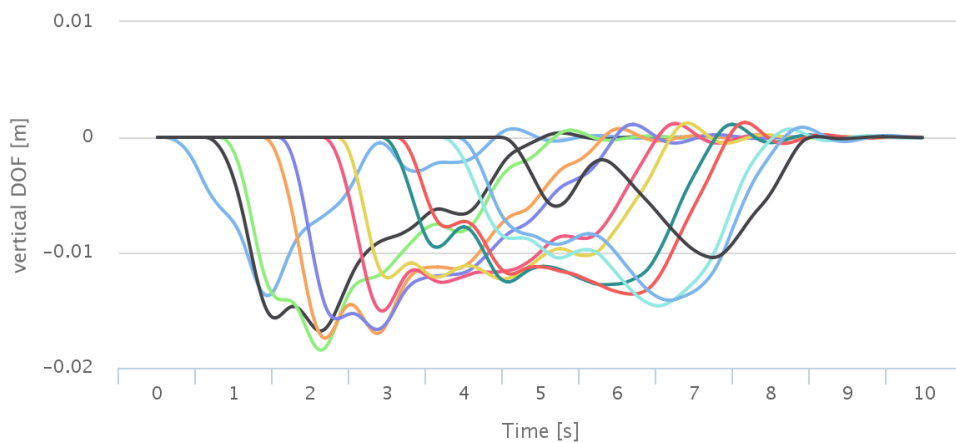
227     scal = bog_n(i)
228     *voper,mask(1),path_br(1),eq,scal !find location of bog_n(i) in
        vector path_br()
229     *vscfun,location,lmax,mask(1)
230     bog_n(i) = path_br(location+1)
231     *endif
232 *enddo
233
234 !apply contact force on beam, if bogie is already/still on beam
235 *do,i,1,nv
236     *if,bog_n(i),GE,path_br(1),AND,bog_n(i),LE,path_br(nng-1),THEN
237         !applied contact force depends on motor/trailer bogie and motor/
            trailer coach; there are 3 combinations
238         *if,i,eq,1,or,i,eq,5,then
239             f,bog_n(i),fy,(-(m_1m+m_2t+m_3t)*g-m_3t*ab(ii,i)+k_pt*(uv(ii,i)-
                ub(ii,i))+c_pt*(vv(ii,i)-vb(ii,i)))
240         *elseif,i,eq,12,then
241             f,bog_n(i),fy,(-(m_1m+m_2t+m_3t)*g-m_3t*ab(ii,i)+k_pt*(uv(ii,i)-
                ub(ii,i))+c_pt*(vv(ii,i)-vb(ii,i)))
242         *elseif,i,eq,2,or,i,eq,6,then
243             f,bog_n(i),fy,(-(m_1m+m_2m+m_3m)*g-m_3m*ab(ii,i)+k_pm*(uv(ii,i)-
                ub(ii,i))+c_pm*(vv(ii,i)-vb(ii,i)))
244         *elseif,i,eq,11,then
245             f,bog_n(i),fy,(-(m_1m+m_2m+m_3m)*g-m_3m*ab(ii,i)+k_pm*(uv(ii,i)-
                ub(ii,i))+c_pm*(vv(ii,i)-vb(ii,i)))
246         *else
247             f,bog_n(i),fy,(-(m_1t+m_2t+m_3t)*g-m_3t*ab(ii,i)+k_pt*(uv(ii,i)-
                ub(ii,i))+c_pt*(vv(ii,i)-vb(ii,i)))
248         *endif
249     *endif
250 *enddo
251
252 !give vehicles reaction displacement
253 *do,i,1,nv
254     d,(10000*i+1),uy,ub(ii,i)
255 *enddo
256 outres,all,all
257 solve
258 *enddo
259
260 /eof

```

The first labelled section “vars” contains some variable definitions, mainly the train properties such as masses, spring stiffnesses and so forth. The second section called “etypes” defines element types for the masses and spring-dashpots using the previously defined values. The meshing is done in the third section named “meshing”, where the nodes and elements are given a location. There are three combinations of coach mass, bogie mass and trailer or motor suspension depending on the location in the train. For the distribution of trailer and motor coaches or bogies, see Figure C.4.

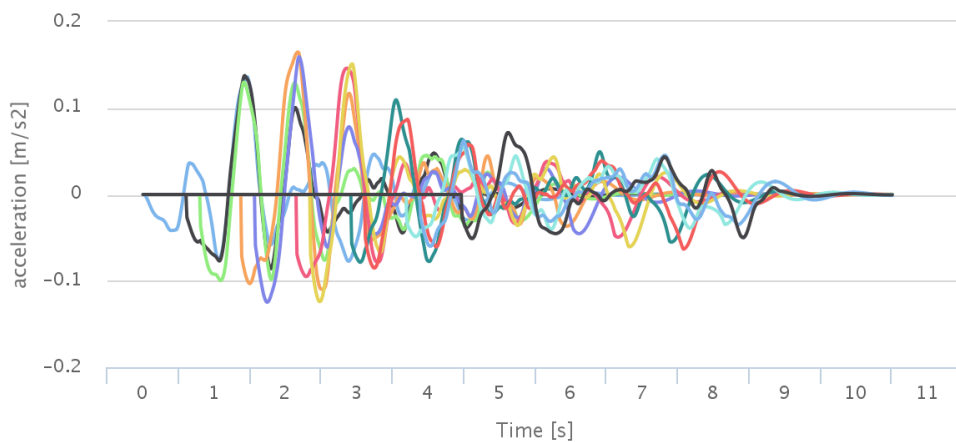
The modelling starts in the fourth section, “initcon” where initial conditions and a first load step are defined. Afterwards the real modelling is done in section “mainrun”, where the bogies are moved over the bridge and the displacements, velocities and accelerations are calculated. In

Figure L.9 a plot of the displacements and the accelerations of this vehicle model with two bogies can be seen. It can be observed the vehicle above the third bogie has the highest displacement and the vehicle above the fourth bogie the highest acceleration. When the bogies enter the bridge a high frequency vibrations in the acceleration plot will appear, if these are obtained from Ansys using the “direct get” method. Therefore the “backwards differentiation” method is used, see section L.2.



uv1 uv2 uv3 uv4 uv5 uv6 uv7 uv8 uv9  
uv10 uv11 uv12

(a) Vehicle above bogies displacement



av1 av2 av3 av4 av5 av6 av7 av8 av9  
av10 av11 av12

(b) Vehicle above bogies acceleration

**Figure L.9:** Vehicle displacement and acceleration of vehicle above twelve bogies. The bogies go with a velocity of 125 km/h over the 2D bridge model. See also [online](#).

## L.4.2 2 DOF schematization

A little more complex vehicle model is a schematization of masses and spring-dampers in Ansys with two degrees of freedom, as seen in Figure L.10.

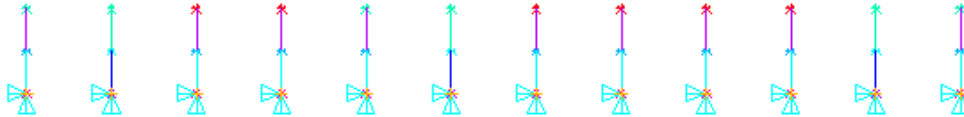


**Figure L.10:** 2 DOF vehicle model in Ansys. Here a train consisting of 12 bogie is shown.

The following code has been used.<sup>3</sup> This apdl file can be used together with the 2d arch bridge code<sup>4</sup> or the 3d arch bridge code, which request sections from this code using labels.

```

1  !Name:      vehicle_2dof_bogies
2  !Date:      April 18, 2016
3  !Last modified: May 10, 2016
4  !Description: vehicle model of 2DOF bogies
5
6  :vars      !label
7  !*****
8  !define some input variables
9  !general
10 gamma_d    = 0.1      !Gamma, numerical damping in HHT
11 !coaches
12 m_1m       = 0.5*51500 !motor coach mass [kg]
13 m_1t       = 0.5*43500 !trailer coach mass [kg]
14 !motor bogie
15 m_2m       = 8620      !motor frame mass [kg]
16 m_3m       = 2*1200    !two motor wheelsets mass [kg]
17 k_pm       = 5000000    !primary stiffness motor bogie [N/m]
18 c_pm       = 103804    !primary damping motor bogie [Ns/m]
19 k_sm       = 920000    !secondary stiffness motor bogie [N/m]
20 c_sm       = 81670     !secondary damping motor bogie [Ns/m]
21 !trailer bogie
22 m_2t       = 4970      !trailer frame mass [kg]
23 m_3t       = 2*1700    !two trailer wheelsets mass [kg]
24 k_pt       = 3400000    !primary stiffness trailer bogie [N/m]
25 c_pt       = 64996     !primary damping trailer bogie [Ns/m]
26 k_st       = 920000    !secondary stiffness trailer bogie [N/m]
27 c_st       = 75829     !secondary damping trailer bogie [Ns/m]
28
29 nv         = 12        !number of bogies
30

```

<sup>3</sup>[https://github.com/benjaminkomen/benjaminkomen.github.io/blob/master/ansys/6\\_complexer\\_bogies/vehicle\\_2dof\\_bogies.inp](https://github.com/benjaminkomen/benjaminkomen.github.io/blob/master/ansys/6_complexer_bogies/vehicle_2dof_bogies.inp)

<sup>4</sup>[https://github.com/benjaminkomen/benjaminkomen.github.io/blob/master/ansys/6\\_complexer\\_bogies/2d\\_arch\\_2dof\\_bogies.inp](https://github.com/benjaminkomen/benjaminkomen.github.io/blob/master/ansys/6_complexer_bogies/2d_arch_2dof_bogies.inp)

```

31 *dim,bog_x,,12          !bogies initial x-coordinate positions array
    assuming 6 part VIRM
32 bog_x(1) = 0
33 bog_x(2) = -20
34 bog_x(3) = bog_x(2) -3.55 -3.05
35 bog_x(4) = bog_x(3) -20
36 bog_x(5) = bog_x(4) -3.05 -3.55
37 bog_x(6) = bog_x(5) -20
38 bog_x(7) = bog_x(6) -3.55 -3.05
39 bog_x(8) = bog_x(7) -20
40 bog_x(9) = bog_x(8) -3.05 -3.55
41 bog_x(10) = bog_x(9) -20
42 bog_x(11) = bog_x(10) -3.55 -3.05
43 bog_x(12) = bog_x(11) -20
44
45 *dim,bog_n,,nv          !bogies initial node positions array
46 bog_n(1) = 2            !node number of bogie 1
47
48 *do,i,2,nv
49   bog_n(%i%) = nint(bog_x(%i%)/dl)
50 *enddo
51
52 /eof                    !switch back to master file
53 :etypes                  !label
54 !*****
55 !define element types
56 !define bogies
57 et,4,mass21,,4
58 r,11,m_1m               !motor coach mass
59 r,12,m_2m               !motor bogie frame
60 r,13,m_3m               !motor bogie wheelsets
61 r,14,m_1t               !trailer coach mass
62 r,15,m_2t               !trailer bogie frame
63 r,16,m_3t               !trailer bogie wheelsets
64
65 !define spring-damper
66 et,5,combin14,,2
67 r,21,k_pm,c_pm         !motor bogie primary suspension
68 r,22,k_sm,c_sm         !motor bogie secondary suspension
69 r,23,k_pt,c_pt         !trailer bogie primary suspension
70 r,24,k_st,c_st         !trailer bogie secondary suspension
71
72 /eof
73 :meshing                 !label
74 !*****
75 !meshing
76 !bogies
77 *do,i,1,nv
78   type,4
79   !bogies 1,2,5,6,11 and 12 at motor coaches, the rest trailer coaches
80   *if,i,eq,1,or,i,eq,2,then
81     !place motor bogies
82     real,11

```

```

83     n,(10000*i+3),i,31      !upper mass
84     e,(10000*i+3)
85 *elseif ,i,eq,5,or,i,eq,6,then
86     !place motor bogies
87     real ,11
88     n,(10000*i+3),i,31      !upper mass
89     e,(10000*i+3)
90 *elseif ,i,eq,11,or,i,eq,12,then
91     !place motor bogies
92     real ,11
93     n,(10000*i+3),i,31      !upper mass
94     e,(10000*i+3)
95 *else
96     !place trailer bogies
97     real ,14
98     n,(10000*i+3),i,31      !upper mass
99     e,(10000*i+3)
100 *endif
101 !bogies 2,6 and 11 are motor bogies , the rest are trailer bogies
102 *if ,i,eq,2,or,i,eq,6,then
103     !place motor bogies
104     type ,4
105     real ,12
106     n,(10000*i+2),i,30.5    !middle mass
107     e,(10000*i+2)
108     real ,13
109     n,(10000*i+1),i,30      !lower mass
110     e,(10000*i+1)
111     !place spring-dampers
112     type ,5
113     real ,21
114     en,(10000*i+2),(10000*i+2),(10000*i+1) !primary suspension
115     real ,22
116     en,(10000*i+3),(10000*i+3),(10000*i+2) !secondary suspension
117 *elseif ,i,eq,11,then
118     !place motor bogies
119     type ,4
120     real ,12
121     n,(10000*i+2),i,30.5    !middle mass
122     e,(10000*i+2)
123     real ,13
124     n,(10000*i+1),i,30      !lower mass
125     e,(10000*i+1)
126     !place spring-dampers
127     type ,5
128     real ,21
129     en,(10000*i+2),(10000*i+2),(10000*i+1) !primary suspension
130     real ,22
131     en,(10000*i+3),(10000*i+3),(10000*i+2) !secondary suspension
132 *else
133     !place trailer bogies
134     type ,4
135     real ,15

```

```

136     n,(10000*i+2),i,30.5    !middle mass
137     e,(10000*i+2)
138     real,16
139     n,(10000*i+1),i,30    !lower mass
140     e,(10000*i+1)
141     !place spring-dampers
142     type,5
143     real,23
144     en,(10000*i+2),(10000*i+2),(10000*i+1) !primary suspension
145     real,24
146     en,(10000*i+3),(10000*i+3),(10000*i+2) !secondary suspension
147     *endif
148     !constrain lower mass, all DOF
149     d,(10000*i+1),all
150 *enddo
151
152 /eof
153 :initcon          !label
154 !*****
155 !initial conditions
156 !bogies
157 *do,i,1,nv
158     uv(1,i)=uy(10000*i+3)
159     vv(1,i)=0
160     av(1,i)=0
161     ub(1,i)=0
162     vb(1,i)=0
163     ab(1,i)=0
164 *enddo
165
166 !determine node numbers on vehicle path_br, backwards compatible with 2d
167     bridge
168 *dim,path_br,,nng
169 cur_x = 0
170 *do,i,1,nng
171     path_br(i) = node(cur_x,0,7.15)
172     cur_x = cur_x + dl
173 *enddo
174 *dim,mask,,elmiqr(0,14)
175
176 !now perform a transient analysis (default = full), first only apply a
177     load at node 2
178 timint,on          !include transient effects
179 trnopt,,,,,hht    !use HHT instead of Newmark
180 tintp,gamma_d     !damp out numerical noise
181 time,dt
182 f,path_br(2),fy,-((m_1m+m_2t+m_3t)*g)
183 outres,all,all
184 solve
185
186 /eof
187 :mainrun          !label

```

```

187 !*****
188 !loop over bridge
189 *do,ii,2,nn_t
190   !write data to arrays
191   t(ii)=(ii-1)*dt
192   !bridge
193   ub_mid(ii)=uy(node(l/2,0,0))
194   ub_25(ii)=uy(node(l/4,0,0))
195
196   !bogies
197   *do,i,1,nv
198     uv(ii,i)=uy(10000*i+3)
199     vv(ii,i)=(uv(ii,i)-uv(ii-1,i))/dt
200     av(ii,i)=(vv(ii,i)-vv(ii-1,i))/dt
201
202     !bridge deflection under bogie is bridge node deflection, if bogie is
203     !still on beam, else zero (post approach bridge no deflection)
204     *if,bog_n(i),GE,path_br(1),AND,bog_n(i),LE,path_br(nng-1),THEN
205       ub(ii,i)=uy(bog_n(i))
206       vb(ii,i)=vy(bog_n(i))
207       ab(ii,i)=ay(bog_n(i))
208     *else
209       ub(ii,i)=0
210       vb(ii,i)=0
211       ab(ii,i)=0
212     *endif
213   *enddo
214
215   time,ii*dt
216   fdele,all,all
217
218   !move vehicles one node
219   *do,i,1,nv
220     *if,bog_n(i),LT,0,OR,bog_n(i),GE,path_br(nng-1),THEN
221       !if bogies are before/past bridge, increment with 1
222       bog_n(i) = bog_n(i)+1
223     *elseif,bog_n(i),eq,0,THEN
224       !if bogies reach the bridge, give them node number of start bridge,
225       !not necessarily 1
226       bog_n(i) = path_br(1)
227     *else
228       !if bogies are on the bridge, give them next node number in vehicle
229       !path_br
230       scal = bog_n(i)
231       *voper,mask(1),path_br(1),eq,scal !find location of bog_n(i) in
232       !vector path_br()
233       *vscfun,location,lmax,mask(1)
234       bog_n(i) = path_br(location+1)
235     *endif
236   *enddo
237
238   !apply contact force on beam, if bogie is already/still on beam
239   *do,i,1,nv

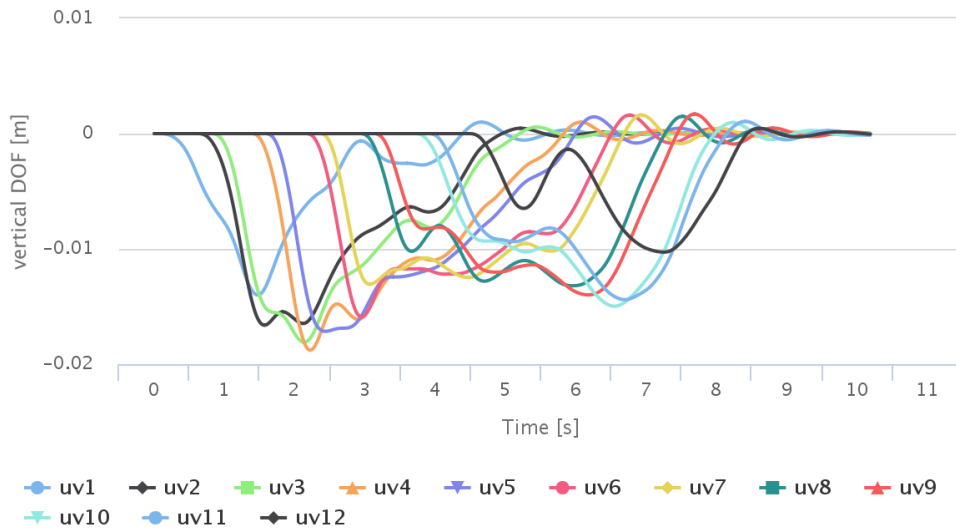
```

```

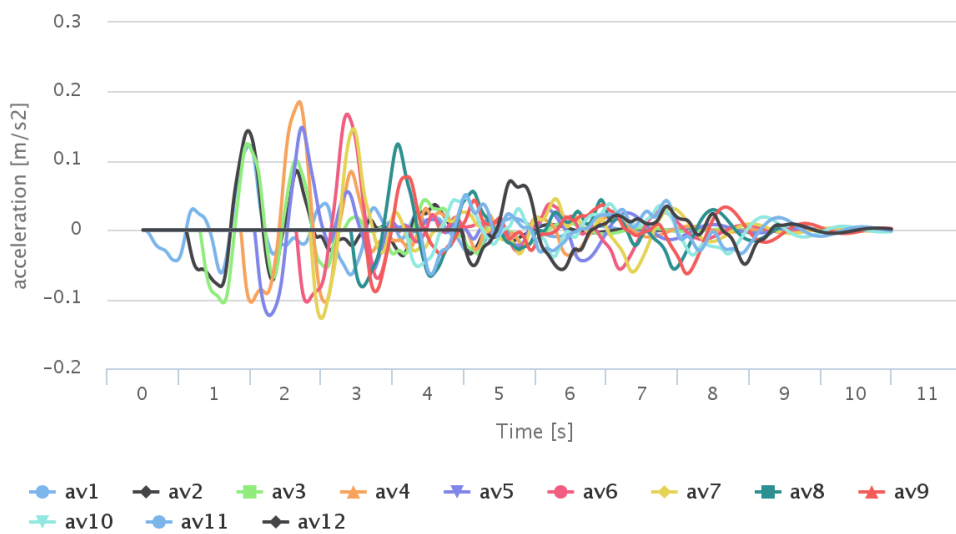
236 *if , bog_n(i) , GE , path_br(1) , AND , bog_n(i) , LE , path_br(nng-1) , THEN
237   !applied contact force depends on motor/trailer bogie and motor/
      trailer coach; there are 3 combinations
238 *if , i , eq , 1 , or , i , eq , 5 , then
239   f , bog_n(i) , fy , ( -(m_1m+m_2t+m_3t)*g-m_3t*ab(ii,i)+k_pt*(uv(ii,i)-
      ub(ii,i))+c_pt*(vv(ii,i)-vb(ii,i)))
240 *elseif , i , eq , 12 , then
241   f , bog_n(i) , fy , ( -(m_1m+m_2t+m_3t)*g-m_3t*ab(ii,i)+k_pt*(uv(ii,i)-
      ub(ii,i))+c_pt*(vv(ii,i)-vb(ii,i)))
242 *elseif , i , eq , 2 , or , i , eq , 6 , then
243   f , bog_n(i) , fy , ( -(m_1m+m_2m+m_3m)*g-m_3m*ab(ii,i)+k_pm*(uv(ii,i)-
      ub(ii,i))+c_pm*(vv(ii,i)-vb(ii,i)))
244 *elseif , i , eq , 11 , then
245   f , bog_n(i) , fy , ( -(m_1m+m_2m+m_3m)*g-m_3m*ab(ii,i)+k_pm*(uv(ii,i)-
      ub(ii,i))+c_pm*(vv(ii,i)-vb(ii,i)))
246 *else
247   f , bog_n(i) , fy , ( -(m_1t+m_2t+m_3t)*g-m_3t*ab(ii,i)+k_pt*(uv(ii,i)-
      ub(ii,i))+c_pt*(vv(ii,i)-vb(ii,i)))
248 *endif
249 *endif
250 *enddo
251
252 !give vehicles reaction displacement
253 *do , i , 1 , nv
254   d , (10000*i+1) , uy , ub(ii,i)
255 *enddo
256 outres , all , all
257 solve
258 *enddo
259
260 /eof

```

This code is not very different compared to the code for the 1 DOF schematization. The same input parameters are used, but extra element types are defined to also cover the separate frame mass and include primary suspension. The meshing is also expanded with the addition of the frame masses and primary suspensions. The modelling phase is largely the same. In Figure L.11 a plot of the displacements and the accelerations of this vehicle model with two bogies can be seen. The vehicle above the fourth bogie has the highest displacement and highest acceleration.



(a) Vehicle above bogies displacement



(b) Vehicle above bogies acceleration

**Figure L.11:** Vehicle displacement and acceleration of vehicle above twelve bogies. The bogies go with a velocity of 125 km/h over the 2D bridge model. See also [online](#).

### L.4.3 Full coach schematization

The most complex vehicle model made is a schematization where the bogies are connected with a massless very stiff beam, as seen in Figure L.12.



**Figure L.12:** Full coach vehicle model in Ansys. Here a train consisting of 6 coaches is shown.

The following code has been used.<sup>5</sup> This apdl file can be used together with the 2d arch bridge code <sup>6</sup> or the 3d arch bridge code, which request sections from this code using labels.

```

1  !Name:      vehicle_full_coach
2  !Date:      April 18, 2016
3  !Last modified: May 9, 2016
4  !Description: vehicle model of full coach
5
6  :vars      !label
7  !*****
8  !define some input variables
9  !general
10 gamma_d    = 0.1          !Gamma, numerical damping in HHT
11 m_d        = 1e-8        !dummy mass [kg]
12 !coaches
13 m_1m       = 51500        !motor coach mass [kg]
14 m_1t       = 43500        !trailer coach mass [kg]
15 I_m        = 3091341      !motor coach mass moment of inertia [kg m2]
16 I_t        = 2611133      !trailer coach mass moment of inertia [kg m2]
17 A_co       = 1           !Cross sectional area coach [m2]
18 I_co       = 10000        !Moment of inertia coach [m4]
19 H_co       = 1           !Height coach [m]
20 E_co       = 2.1e11       !Youngs modulus coach [N/m2]
21 mu_co      = 0.2         !Poissons ratio coach
22 rho_co     = 1e-8        !density coach [kg/m3]
23 !motor bogie
24 m_2m       = 8620        !motor frame mass [kg]
25 m_3m       = 2*1200      !two motor wheelsets mass [kg]
26 k_pm       = 5000000     !primary stiffness motor bogie [N/m]
27 c_pm       = 103804      !primary damping motor bogie [Ns/m]
28 k_sm       = 920000      !secondary stiffness motor bogie [N/m]
29 c_sm       = 81670       !secondary damping motor bogie [Ns/m]
30 !trailer bogie
31 m_2t       = 4970        !trailer frame mass [kg]
32 m_3t       = 2*1700      !two trailer wheelsets mass [kg]
33 k_pt       = 3400000     !primary stiffnes trailer bogie [N/m]
34 c_pt       = 64996       !primary damping trailer bogie [Ns/m]
35 k_st       = 920000      !secondary stiffnes trailer bogie [N/m]

```

<sup>5</sup>[https://github.com/benjaminkomen/benjaminkomen.github.io/blob/master/ansys/6\\_complexer\\_bogies/vehicle\\_full\\_coach.inp](https://github.com/benjaminkomen/benjaminkomen.github.io/blob/master/ansys/6_complexer_bogies/vehicle_full_coach.inp)

<sup>6</sup>[https://github.com/benjaminkomen/benjaminkomen.github.io/blob/master/ansys/6\\_complexer\\_bogies/2d\\_arch\\_full\\_coach.inp](https://github.com/benjaminkomen/benjaminkomen.github.io/blob/master/ansys/6_complexer_bogies/2d_arch_full_coach.inp)

```

36 c_st    = 75829          !secondary damping trailer bogie [Ns/m]
37
38 nv     = 12            !number of bogies
39 nco    = nv/2         !number of coaches
40
41 *dim,bog_x,,12        !bogies initial x-coordinate positions array
    assuming 6 part VIRM
42 bog_x(1) = 0
43 bog_x(2) = -20
44 bog_x(3) = bog_x(2) - 3.55 - 3.05
45 bog_x(4) = bog_x(3) - 20
46 bog_x(5) = bog_x(4) - 3.05 - 3.55
47 bog_x(6) = bog_x(5) - 20
48 bog_x(7) = bog_x(6) - 3.55 - 3.05
49 bog_x(8) = bog_x(7) - 20
50 bog_x(9) = bog_x(8) - 3.05 - 3.55
51 bog_x(10) = bog_x(9) - 20
52 bog_x(11) = bog_x(10) - 3.55 - 3.05
53 bog_x(12) = bog_x(11) - 20
54
55 *dim,bog_n,,nv        !bogies initial node positions array
56 bog_n(1) = 2          !node number of bogie 1
57
58 *do,i,2,nv
59   bog_n(%i%) = nint(bog_x(%i%)/dl)
60 *enddo
61
62 /eof                  !switch back to master file
63 :etypes               !label
64 !*****
65 !define material types
66 !coach
67 mp,ex,13,E_co
68 mp,nuxy,13,mu_co
69 mp,dens,13,rho_co
70 mp,alpx,13,alph_st
71
72 !*****
73 !define element types
74 !define bogies
75 et,4,mass21,,4
76 r,12,m_2m          !motor bogie frame
77 r,13,m_3m          !motor bogie wheelsets
78 r,15,m_2t          !trailer bogie frame
79 r,16,m_3t          !trailer bogie wheelsets
80 r,17,m_d           !dummy mass
81
82 !define spring-damper
83 et,5,combin14,,2
84 r,21,k_pm,c_pm     !motor bogie primary suspension
85 r,22,k_sm,c_sm     !motor bogie secondary suspension
86 r,23,k_pt,c_pt     !trailer bogie primary suspension
87 r,24,k_st,c_st     !trailer bogie secondary suspension

```

```

88
89 !mass coach
90 et,12,mass21,,3
91 r,11,m_1m,I_m !motor coach mass
92 r,14,m_1t,I_t !trailer coach mass
93
94 !coach beam
95 et,13,beam3
96 r,31,A_co,I_co,H_co
97
98 /eof
99 :meshing !label
100 !*****
101 !meshing
102 *do,i,1,nc0
103 !coach 1 and 3
104 *if,i,eq,1,or,i,eq,3,then
105 !place masses
106 type,4
107 real,16
108 n,(10000*(2*i-1)+1),abs(bog_x(2*i-1)),30 !wheels mass left
109 e,(10000*(2*i-1)+1)
110 real,13
111 n,(10000*(2*i)+1),abs(bog_x(2*i)),30 !wheels mass right
112 e,(10000*(2*i)+1)
113 real,15
114 n,(10000*(2*i-1)+2),abs(bog_x(2*i-1)),30.5 !frame mass left
115 e,(10000*(2*i-1)+2)
116 real,12
117 n,(10000*(2*i)+2),abs(bog_x(2*i)),30.5 !frame mass right
118 e,(10000*(2*i)+2)
119 real,17
120 n,(10000*(2*i-1)+3),abs(bog_x(2*i-1)),31 !dummy mass left
121 e,(10000*(2*i-1)+3)
122 n,(10000*(2*i)+3),abs(bog_x(2*i)),31 !dummy mass right
123 e,(10000*(2*i)+3)
124 type,12
125 real,11
126 xpos = ((abs(bog_x(2*i))+abs(bog_x(2*i-1)))/2)
127 n,(10000*(2*i-1)+4),xpos,31 !coach mass
128 e,(10000*(2*i-1)+4)
129 !place spring-dampers
130 type,5
131 real,23
132 en,(10000*(2*i-1)+2),(10000*(2*i-1)+2),(10000*(2*i-1)+1) !left
!primary suspension
133 real,21
134 en,(10000*(2*i)+2),(10000*(2*i)+2),(10000*(2*i)+1) !right
!primary suspension
135 real,24
136 en,(10000*(2*i-1)+3),(10000*(2*i-1)+3),(10000*(2*i-1)+2) !left
!secondary suspension
137 real,22

```

```

138     en,(10000*(2*i)+3),(10000*(2*i)+3),(10000*(2*i)+2)      !right
        secondary suspension
139 !coach 6
140 *elseif,i,eq,6,then
141     !place masses
142     type,4
143     real,13
144     n,(10000*(2*i-1)+1),abs(bog_x(2*i-1)),30 !wheels mass left
145     e,(10000*(2*i-1)+1)
146     real,16
147     n,(10000*(2*i)+1),abs(bog_x(2*i)),30 !wheels mass right
148     e,(10000*(2*i)+1)
149     real,12
150     n,(10000*(2*i-1)+2),abs(bog_x(2*i-1)),30.5 !frame mass left
151     e,(10000*(2*i-1)+2)
152     real,15
153     n,(10000*(2*i)+2),abs(bog_x(2*i)),30.5 !frame mass right
154     e,(10000*(2*i)+2)
155     real,17
156     n,(10000*(2*i-1)+3),abs(bog_x(2*i-1)),31 !dummy mass left
157     e,(10000*(2*i-1)+3)
158     n,(10000*(2*i)+3),abs(bog_x(2*i)),31 !dummy mass right
159     e,(10000*(2*i)+3)
160     type,12
161     real,11
162     xpos = ((abs(bog_x(2*i))+abs(bog_x(2*i-1)))/2)
163     n,(10000*(2*i-1)+4),xpos,31 !coach mass
164     e,(10000*(2*i-1)+4)
165     !place spring-dampers
166     type,5
167     real,21
168     en,(10000*(2*i-1)+2),(10000*(2*i-1)+2),(10000*(2*i-1)+1) !left
        primary suspension
169     real,23
170     en,(10000*(2*i)+2),(10000*(2*i)+2),(10000*(2*i)+1)      !right
        primary suspension
171     real,22
172     en,(10000*(2*i-1)+3),(10000*(2*i-1)+3),(10000*(2*i-1)+2) !left
        secondary suspension
173     real,24
174     en,(10000*(2*i)+3),(10000*(2*i)+3),(10000*(2*i)+2)      !right
        secondary suspension
175 !the rest: coach 2,4,5
176 *else
177     !place masses
178     type,4
179     real,16
180     n,(10000*(2*i-1)+1),abs(bog_x(2*i-1)),30 !wheels mass left
181     e,(10000*(2*i-1)+1)
182     n,(10000*(2*i)+1),abs(bog_x(2*i)),30 !wheels mass right
183     e,(10000*(2*i)+1)
184     real,15
185     n,(10000*(2*i-1)+2),abs(bog_x(2*i-1)),30.5 !frame mass left

```

```

186     e,(10000*(2*i-1)+2)
187     n,(10000*(2*i)+2),abs(bog_x(2*i)),30.5 !frame mass right
188     e,(10000*(2*i)+2)
189     real,17
190     n,(10000*(2*i-1)+3),abs(bog_x(2*i-1)),31 !dummy mass left
191     e,(10000*(2*i-1)+3)
192     n,(10000*(2*i)+3),abs(bog_x(2*i)),31 !dummy mass right
193     e,(10000*(2*i)+3)
194     type,12
195     real,14
196     xpos = ((abs(bog_x(2*i))+abs(bog_x(2*i-1)))/2)
197     n,(10000*(2*i-1)+4),xpos,31 !coach mass
198     e,(10000*(2*i-1)+4)
199     !place spring-dampers
200     type,5
201     real,23
202     en,(10000*(2*i-1)+2),(10000*(2*i-1)+2),(10000*(2*i-1)+1) !left
        primary suspension
203     en,(10000*(2*i)+2),(10000*(2*i)+2),(10000*(2*i)+1) !right
        primary suspension
204     real,24
205     en,(10000*(2*i-1)+3),(10000*(2*i-1)+3),(10000*(2*i-1)+2) !left
        secondary suspension
206     en,(10000*(2*i)+3),(10000*(2*i)+3),(10000*(2*i)+2) !right
        secondary suspension
207 *endif
208 !place coach beam
209 type,13
210 real,31
211 mat,13
212 e,(10000*(2*i-1)+3),(10000*(2*i-1)+4) !left beam part
213 e,(10000*(2*i-1)+4),(10000*(2*i)+3) !right beam part
214 !constrain coach beam
215 ld,(10000*(2*i-1)+3),ux !left beam end
216 ld,(10000*(2*i)+3),ux !right beam end
217 !constrain lower mass, all DOF
218 d,(10000*(2*i-1)+1),all !left wheels mass
219 d,(10000*(2*i)+1),all !right wheels mass
220 *enddo
221
222 /eof
223 :initcon !label
224 !*****
225 !initial conditions
226 !bogies
227 *do,i,1,nc0
228 !left bogie
229 uv(1,(2*i-1))=uy(10000*(2*i-1)+3)
230 vv(1,(2*i-1))=0
231 av(1,(2*i-1))=0
232 ub(1,(2*i-1))=0
233 vb(1,(2*i-1))=0
234 ab(1,(2*i-1))=0

```

```

235     !right bogie
236     uv(1,(2*i))=uy(10000*(2*i)+3)
237     vv(1,(2*i))=0
238     av(1,(2*i))=0
239     ub(1,(2*i))=0
240     vb(1,(2*i))=0
241     ab(1,(2*i))=0
242 *enddo
243
244 !determine node numbers on vehicle path_br, backwards compatible with 2d
      bridge
245 *dim,path_br,,nng
246 cur_x = 0
247 *do,i,1,nng
248     path_br(i) = node(cur_x,0,7.15)
249     cur_x = cur_x + dl
250 *enddo
251
252 *dim,mask,,elmiqr(0,14)
253
254 !now perform a transient analysis (default = full), first only apply a
      load at node 2
255 timint,on                !include transient effects
256 trnopt,,,,,hht          !use HHT instead of Newmark
257 tintp,gamma_d           !damp out numerical noise
258 time,dt
259 f,path_br(2),fy,-((m_1m+m_2t+m_3t)*g)
260 outres,all,all
261 solve
262
263 /eof
264 :mainrun                !label
265 !*****
266 !loop over bridge
267 *do,ii,2,nn_t
268     !write data to arrays
269     t(ii)=(ii-1)*dt
270     !bridge
271     ub_mid(ii)=uy(node(l/2,0,0))
272     ub_25(ii)=uy(node(l/4,0,0))
273
274     !bogies
275     *do,i,1,nc0
276         !left bogie
277         uv(ii,(2*i-1))=uy(10000*(2*i-1)+3)
278         vv(ii,(2*i-1))=(uv(ii,(2*i-1))-uv(ii-1,(2*i-1)))/dt
279         av(ii,(2*i-1))=(vv(ii,(2*i-1))-vv(ii-1,(2*i-1)))/dt
280         !right bogie
281         uv(ii,(2*i))=uy(10000*(2*i)+3)
282         vv(ii,(2*i))=(uv(ii,(2*i))-uv(ii-1,(2*i)))/dt
283         av(ii,(2*i))=(vv(ii,(2*i))-vv(ii-1,(2*i)))/dt
284     *enddo
285

```

```

286 *do , i , 1 , nv
287   !bridge deflection under bogie is bridge node deflection , if bogie is
      still on beam , else zero (post approach bridge no deflection)
288 *if , bog_n(i) , GE , path_br(1) , AND , bog_n(i) , LE , path_br(nng-1) , THEN
289   ub(ii , i) = uy(bog_n(i)+1)
290   vb(ii , i) = vy(bog_n(i)+1)
291   ab(ii , i) = ay(bog_n(i)+1)
292 *else
293   ub(ii , i) = 0
294   vb(ii , i) = 0
295   ab(ii , i) = 0
296 *endif
297 *enddo
298
299 time , ii*dt
300 fdele , all , all
301
302 !move vehicles one node
303 *do , i , 1 , nv
304   *if , bog_n(i) , LT , 0 , OR , bog_n(i) , GE , path_br(nng-1) , THEN
305     !if bogies are before/past bridge , increment with 1
306     bog_n(i) = bog_n(i)+1
307   *elseif , bog_n(i) , eq , 0 , THEN
308     !if bogies reach the bridge , give them node number of start bridge ,
      not necessarily 1
309     bog_n(i) = path_br(1)
310   *else
311     !if bogies are on the bridge , give them next node number in vehicle
      path_br
312     scal = bog_n(i)
313     *voper , mask(1) , path_br(1) , eq , scal   !find location of bog_n(i) in
      vector path_br()
314     *vscfun , location , lmax , mask(1)
315     bog_n(i) = path_br(location+1)
316   *endif
317 *enddo
318
319 !apply contact force on beam , if bogie is already/still on beam
320 *do , i , 1 , nv
321   *if , bog_n(i) , GE , path_br(1) , AND , bog_n(i) , LE , path_br(nng-1) , THEN
322     !applied contact force depends on motor/trailer bogie and motor/
      trailer coach ; there are 3 combinations
323     *if , i , eq , 1 , or , i , eq , 5 , then
324       f , bog_n(i) , fy , ( -(0.5*m_1m+m_2t+m_3t)*g-m_3t*ab(ii , i)+k_pt*(uv(ii ,
        i)-ub(ii , i))+c_pt*(vv(ii , i)-vb(ii , i)))
325     *elseif , i , eq , 12 , then
326       f , bog_n(i) , fy , ( -(0.5*m_1m+m_2t+m_3t)*g-m_3t*ab(ii , i)+k_pt*(uv(ii ,
        i)-ub(ii , i))+c_pt*(vv(ii , i)-vb(ii , i)))
327     *elseif , i , eq , 2 , or , i , eq , 6 , then
328       f , bog_n(i) , fy , ( -(0.5*m_1m+m_2m+m_3m)*g-m_3m*ab(ii , i)+k_pm*(uv(ii ,
        i)-ub(ii , i))+c_pm*(vv(ii , i)-vb(ii , i)))
329     *elseif , i , eq , 11 , then

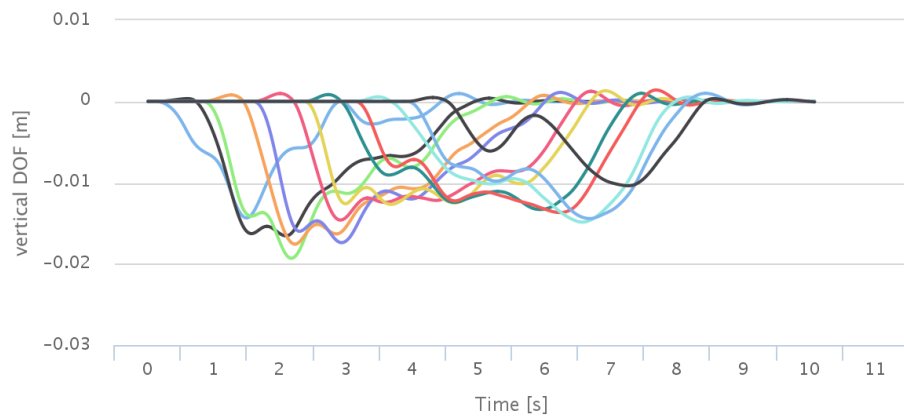
```

```

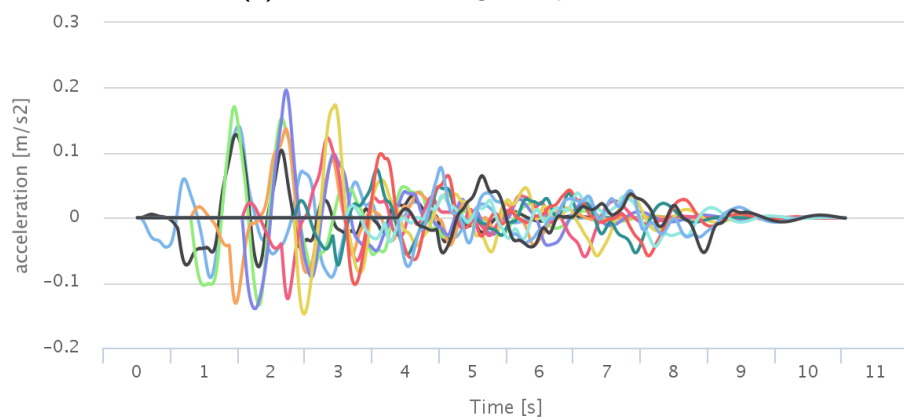
330         f , bog_n(i) , fy , ( -(0.5*m_1m+m_2m+m_3m)*g-m_3m*ab(ii,i)+k_pm*(uv(ii,
           i)-ub(ii,i))+c_pm*(vv(ii,i)-vb(ii,i)))
331     *else
332         f , bog_n(i) , fy , ( -(0.5*m_1t+m_2t+m_3t)*g-m_3t*ab(ii,i)+k_pt*(uv(ii,
           i)-ub(ii,i))+c_pt*(vv(ii,i)-vb(ii,i)))
333     *endif
334 *endif
335 *enddo
336
337 !give vehicles reaction displacement
338 *do , i , 1 , nv
339     d , (10000*i+1) , uy , ub(ii,i)
340 *enddo
341 outres , all , all
342 solve
343 *enddo
344
345 /eof

```

Previously the mass elements had key option 3 set to 4, making it a 2D mass without rotary inertia. But for the coach mass the mass moment of inertia should be used, since it is a degree of freedom. Therefore the key option 3 is set to 3, giving it an extra degree of freedom of rotation around its z-axis. The mass moment of inertia is defined as a real constant in addition to the mass. In Figure L.13 a plot of the displacements and the accelerations of this vehicle model with a full coach can be seen. It can be observed the vehicle above the third bogie has the highest displacement and the vehicle above the fifth bogie the highest acceleration. The front and rear of the coaches are connected which cause them to influence each other, called the pitching or interlocking effect. [2, p. 262]



(a) Vehicle above bogies displacement



(b) Vehicle above bogies acceleration

**Figure L.13:** Vehicle displacement and acceleration of six coaches consisting of twelve bogies. The full coaches go with a velocity of 125 km/h over the 2D bridge model. See also [online](#).



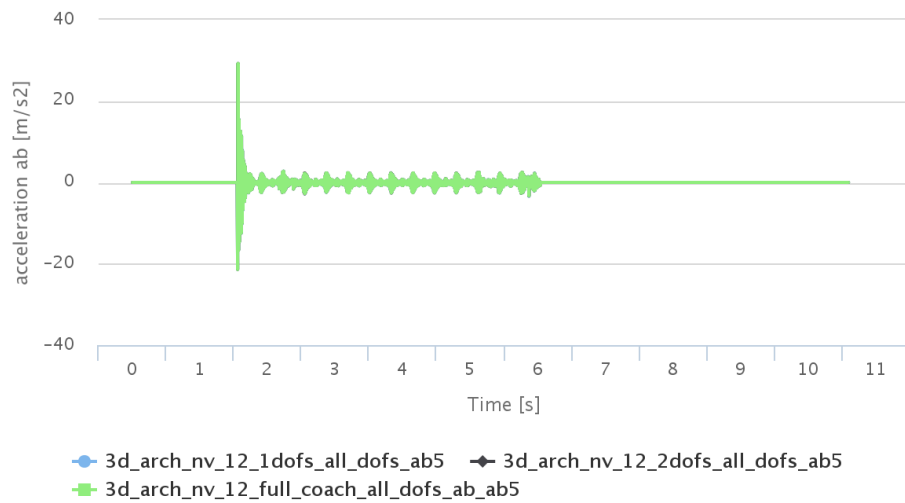


**Figure L.15:** Comparison of 1 DOF bogie schematization, 2 DOF bogie schematization and full coach schematization travelling with a velocity of 125 km/h over the 3D bridge model. The acceleration of the wheel mass at the position of the fifth bogie is shown. See also [online](#).

The frequency response of Figure L.15 is shown in Figure L.16. It can be observed the frequencies are rather high, but this is mainly due to the fact the bridge is not damped and this acceleration is directly related to the bridge.

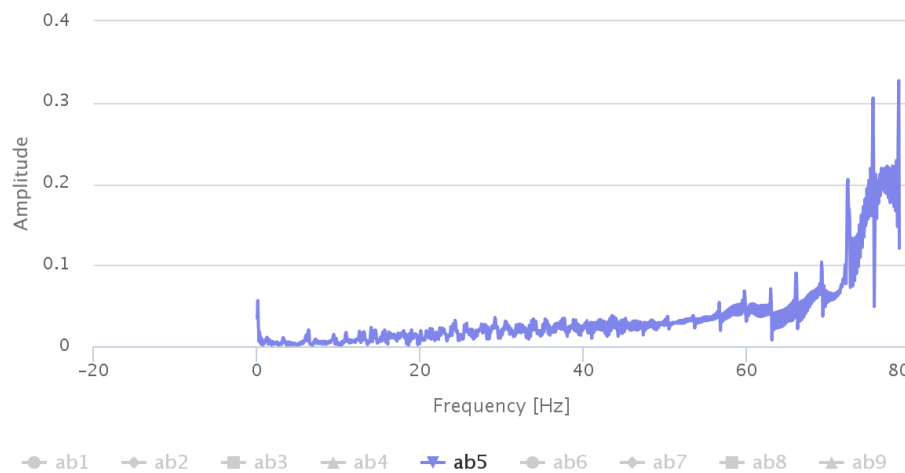


**Figure L.16:** Frequency response of Figure L.15. The frequencies of the acceleration of the wheel mass at the position of the fifth bogie is shown. See also [online](#).

In Figure L.17 the frame acceleration (af) is plotted, at position B in the vehicle models. The 1 DOF bogie schematization is not plotted, because it does not contain a separate frame mass. The lines are quite similar, although there are differences up to 16%.

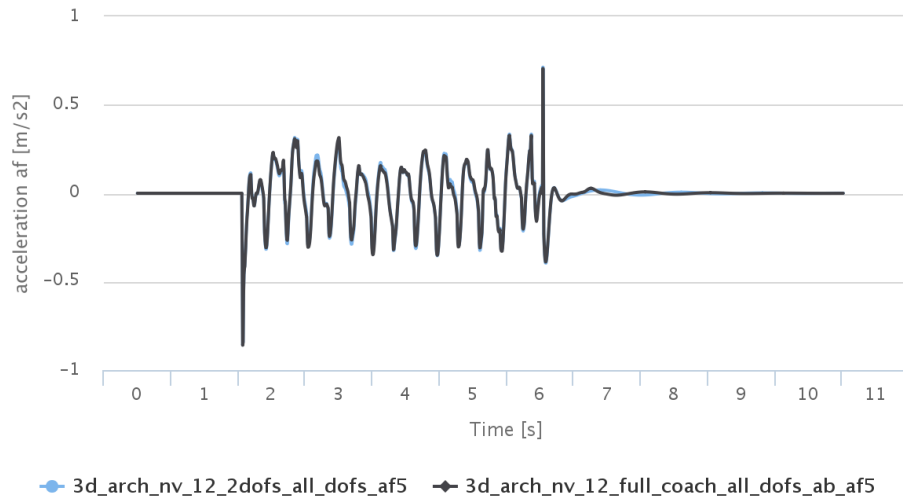


**Figure L.17:** Comparison of 2 DOF bogie schematization and full coach schematization travelling with a velocity of 125 km/h over the 3D bridge model. The acceleration of the frame mass at the position of the fifth bogie is shown. See also [online](#).

The frequency response of Figure L.17 is shown in Figure L.18. The highest response can be observed at 3.15 Hz, which is — together with the higher frequencies — related to the cross-beam effect, see subsection L.5.2. Furthermore there are peaks around 1.12 Hz, most likely related to the bogies' natural frequencies.

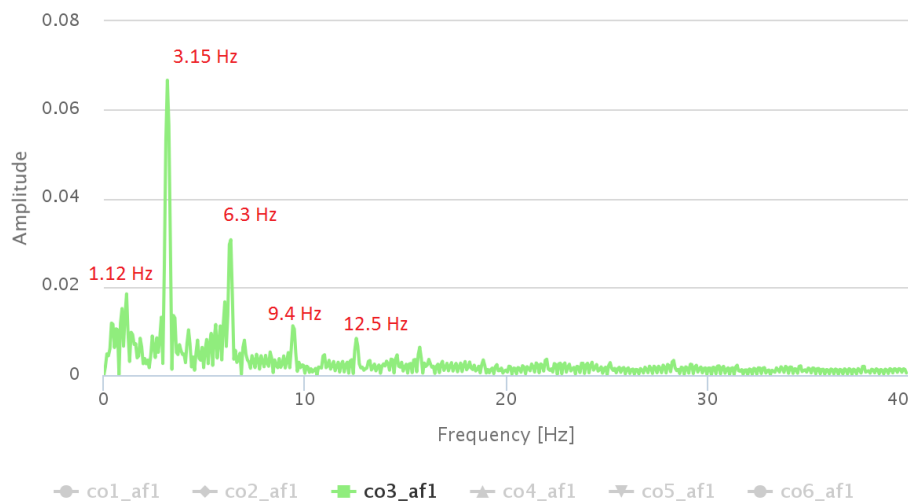


**Figure L.18:** Frequency response of Figure L.17. The frequencies of the acceleration of the frame mass at the position of the fifth bogie is shown. See also [online](#).

For the full coach schematization there are two extra plots of the vertical DOF and rotational DOF at the coach mass centre, which the other vehicle schematizations do not have. In Figure L.19 the acceleration plot of the coach mass, at the centre of the vehicle, is shown.

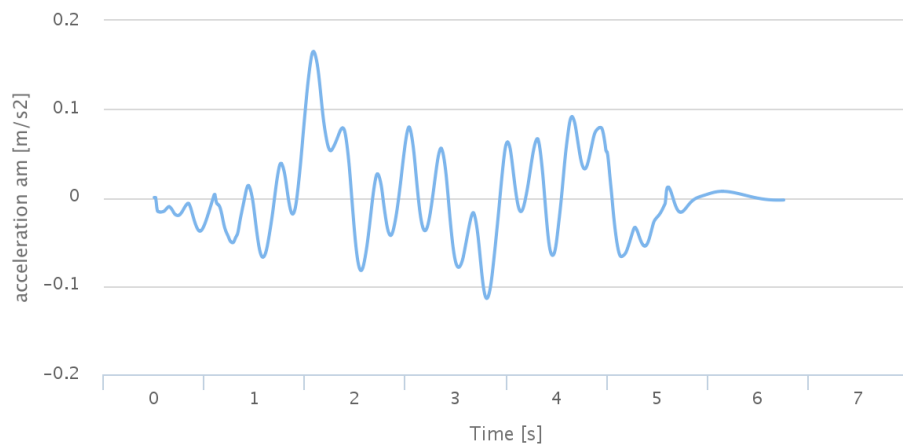


**Figure L.19:** Full coach model, coach mass vertical acceleration of first coach. See also [online](#).

In Figure L.20 the frequency response of the acceleration plot in Figure L.19 is shown. Again a high response related to the cross-beam effect is observed at 3.15 Hz and higher. There is a peak at around 1.1 Hz, related to the natural frequency of the suspension system. In addition there are peaks at 0.45 Hz and 1.5 Hz which cannot be directly related to a natural frequency of the vehicle or the bridge.

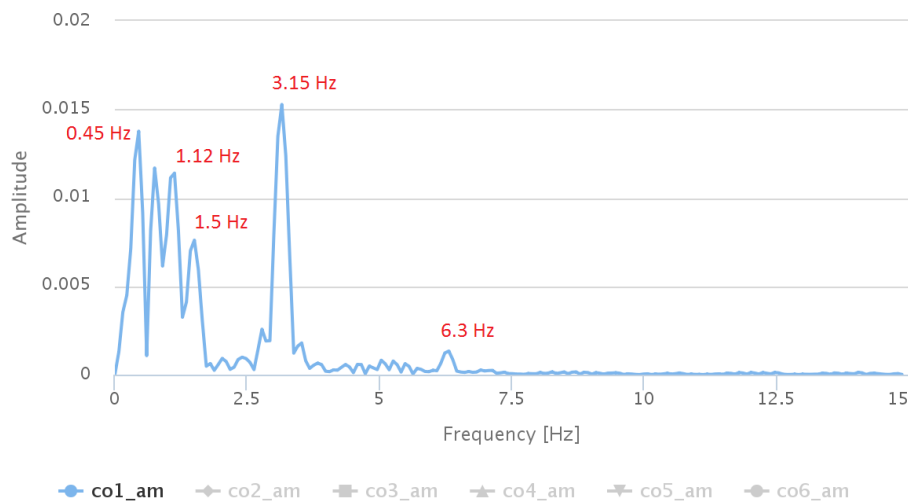


**Figure L.20:** Frequency response of Figure L.19. The frequencies of the acceleration of the vehicle mass at the position of the first coach is shown. See also [online](#).

In Figure L.21 the acceleration plot of the coach mass rotation, at the centre of the vehicle, is shown.

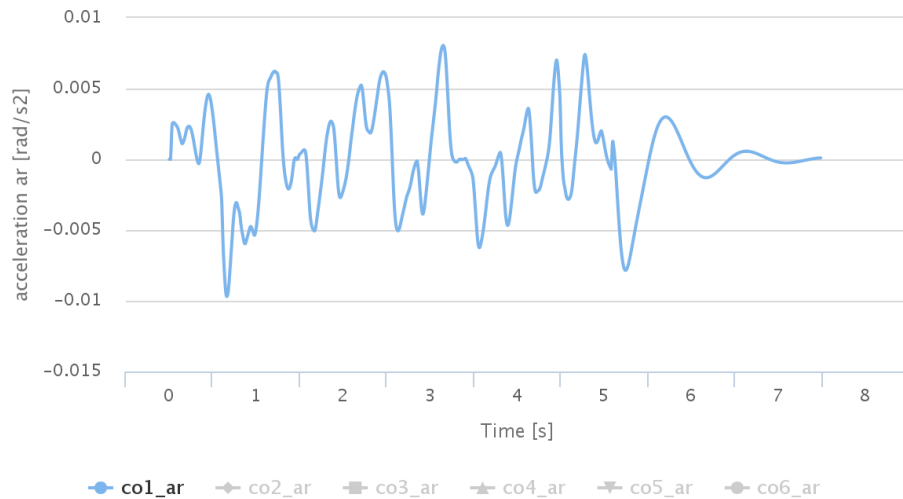


**Figure L.21:** Full coach model, coach mass rotational acceleration of first coach. See also [online](#).

In Figure L.22 the frequency response of the acceleration plot in Figure L.21 is shown. Again a high response related to the cross-beam effect is observed at 3.15 Hz and higher. There is a peak at around 1.1 Hz, related to the natural frequency of the suspension system. In addition there is a peak at 1.6 Hz which cannot be directly related to a natural frequency of the vehicle or the bridge.

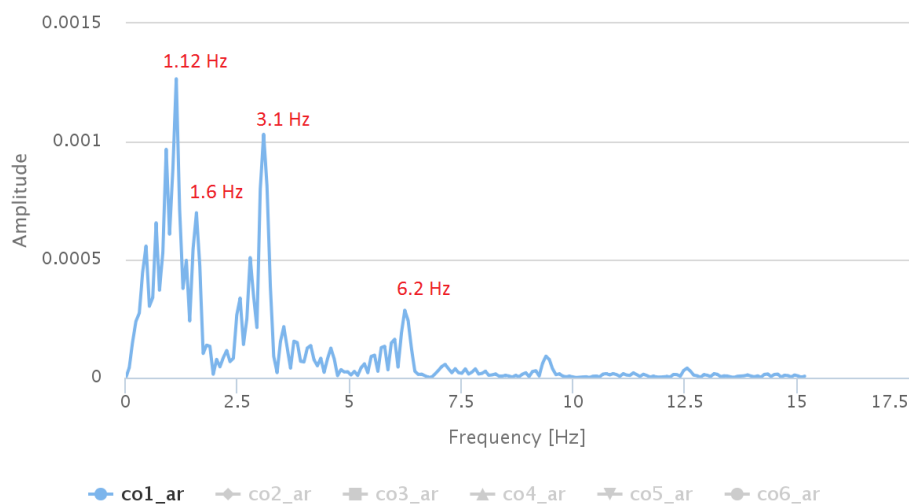


**Figure L.22:** Frequency response of Figure L.21. The frequencies of the rotational acceleration of the vehicle mass at the position of the first coach is shown. See also [online](#).

## L.5.2 Cross-beam effect

In all vehicle acceleration plots with a velocity of 125 km/h, a peak at 3.15 Hz can be observed, as well as peaks at 6.2 Hz, 9.4 Hz etc. of descending amplitude, related to the higher modes of this vibration. These peaks can be explained as being related to the cross-beam effect [5, par. 2.5.1], a difference in stiffness of the bridge at the location of the transverse beams and hangers. As noted in subsection D.8.1, the frequency related to a wavelength (the transverse beam/ hanger spacing of 11.03 m) and a certain velocity (train velocity) can be calculated as

$$f = \frac{v}{\lambda} = \frac{\frac{125}{3.6}}{11.03} = 3.15 \text{ Hz} \quad (\text{L.1})$$

for a velocity of 125 km/h and for a velocity of 200 km/h this would be

$$f = \frac{v}{\lambda} = \frac{\frac{200}{3.6}}{11.03} = 5.04 \text{ Hz}. \quad (\text{L.2})$$

When comparing two frequency plots of acceleration plot with these two velocities, peaks of these specific frequencies can be observed.

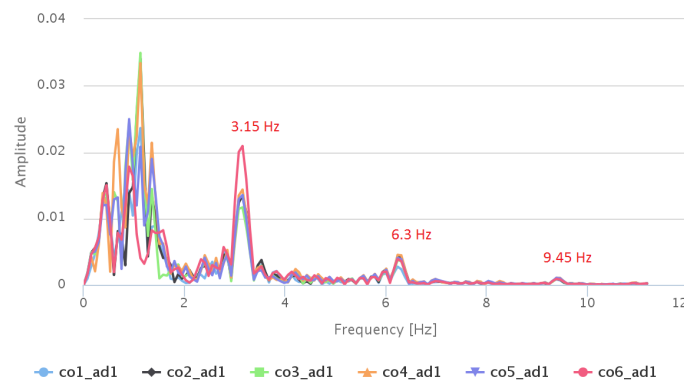


**Figure L.23:** Frequency plot of full coach model moving over a 3D bridge model with a velocity of 125 km/h. See also [online](#).

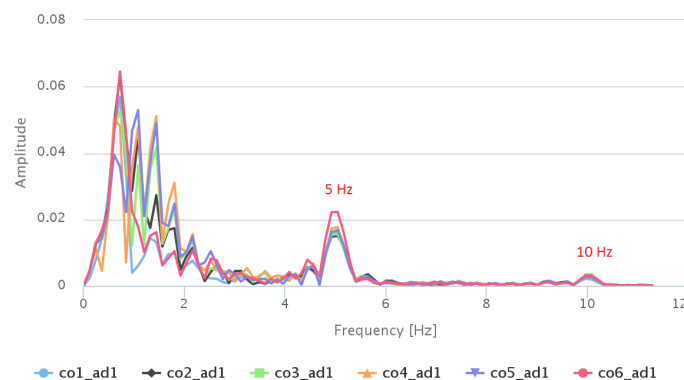


**Figure L.24:** Frequency plot of full coach model moving over a 3D bridge model with a velocity of 200 km/h. See also [online](#).



---

# Appendix M

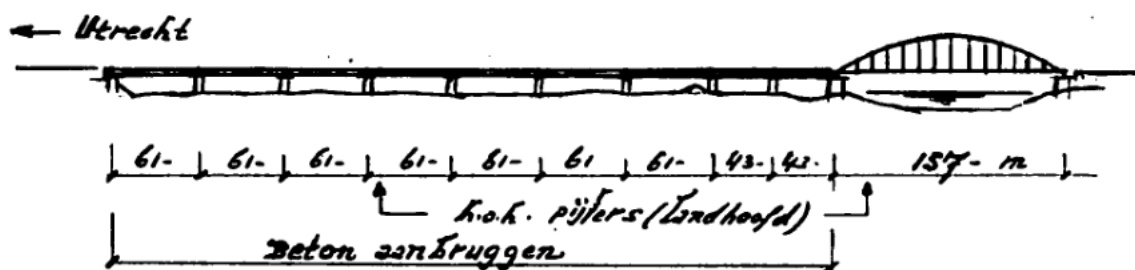
---

## 2D tied-arch bridge model

This appendix describes the 2D tied-arch bridge model created in Ansys. To compare with an existing bridge the Ansys model is based on the *Kuilenburgse spoorbrug*. In section M.1 the structural components of the *Kuilenburgse spoorbrug* are discussed. Based on this bridge an Ansys 2D model is presented in section M.2. Afterwards the model is verified in section M.3. This appendix is referenced from section 3.3.



(a) View on Kuilenburgse spoorbrug (2016)



(b) Sketch of Kuilenburgse spoorbrug [70]

Figure M.1: Kuilenburgse spoorbrug

## M.1 Railway bridge near Culemborg

The *Kuilenburgse spoorbrug* is a railway bridge over the river *Lek* near *Culemborg*, in the Netherlands. It was constructed in 1981 and consists of several concrete approach bridges and a steel tied-arch bridge crossing the river, see Figure M.1. The focus of this report will be solely on the tied-arch bridge and not the approach bridges. [71, p. 29 - 38]

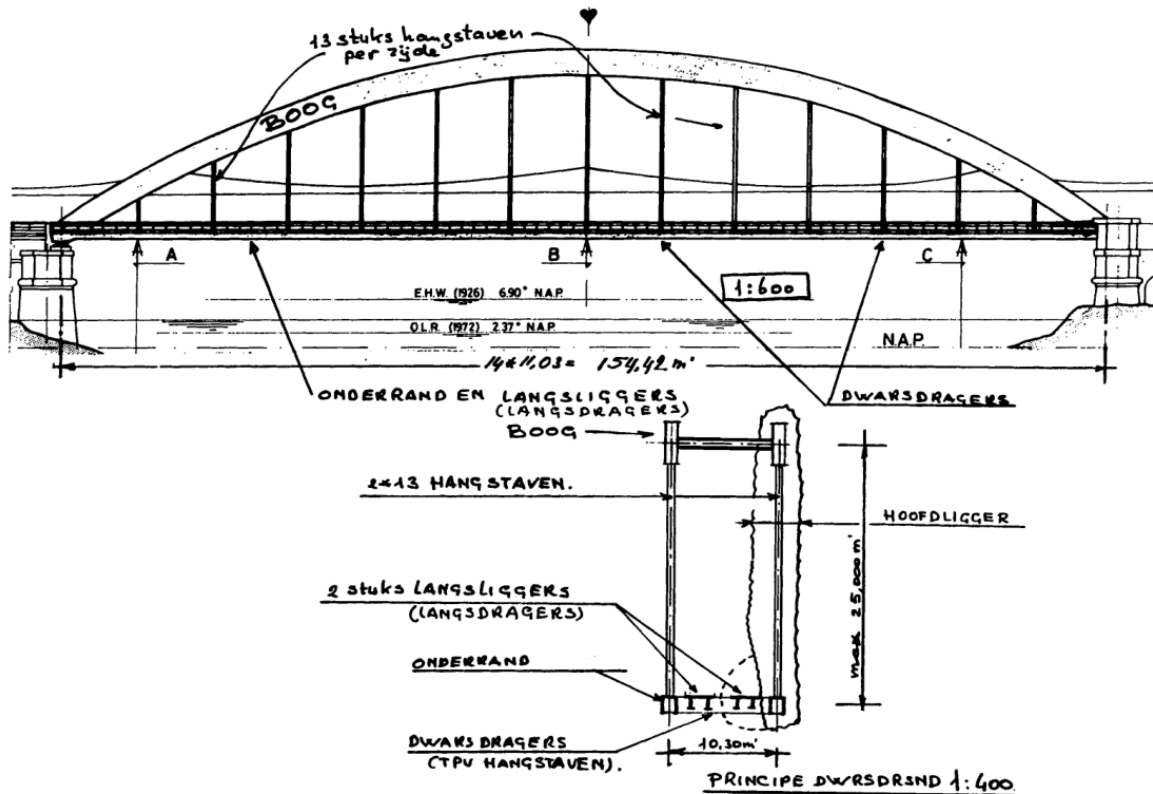
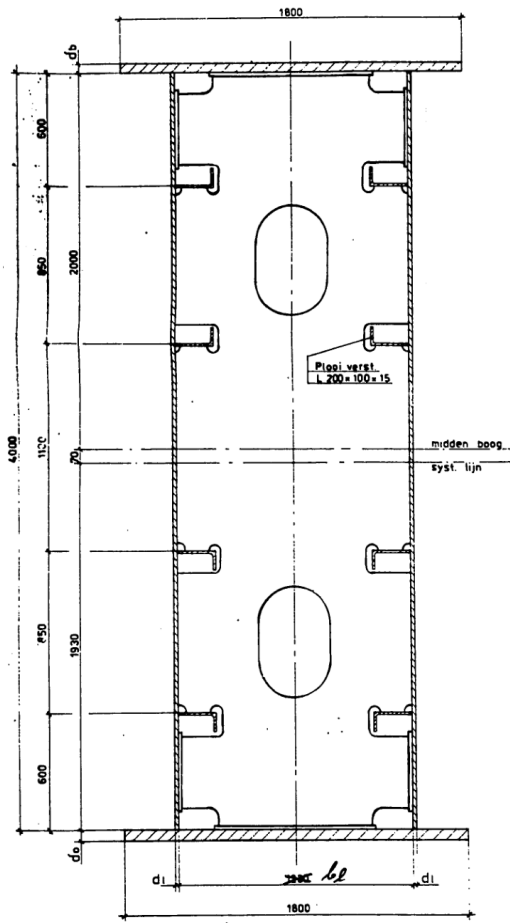


Figure M.2: Kuilenburgse spoorbrug in longitudinal and transverse direction [72, fig. 1]

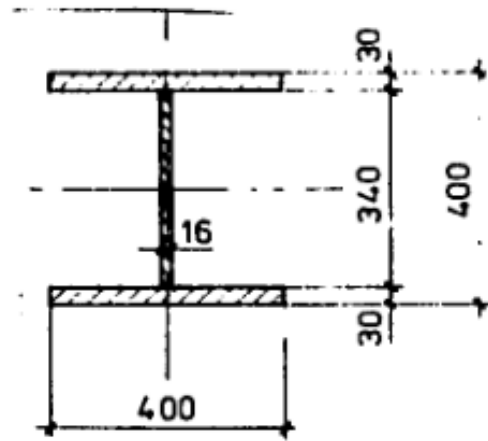
In longitudinal direction the bridge consists of a parabolic shaped arch, with its highest point of 25 meters at midspan, the main girder with a length of 154.42 meters and 13 hangers, at intervals of 11.03 meters from each other. In transverse direction the bridge consist of two main girders with a center-to-center distance of 10.30 meters, two longitudinal girders with a center-to-center distance of 4 meters and transverse girders with a center-to-center distance of 11.03 meters, at every hanger, see Figure M.2.

### M.1.1 Construction elements

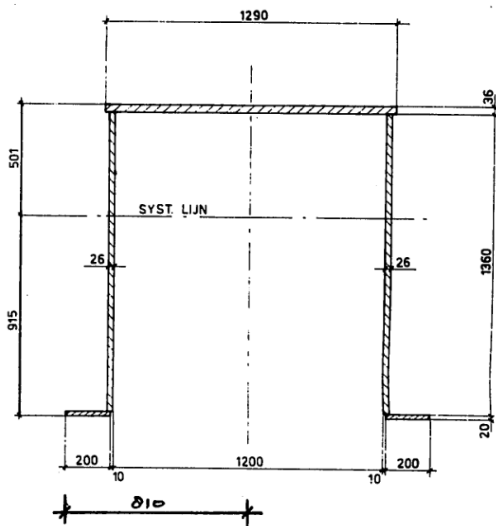
The relevant construction elements are the arch, hangers, main girder and longitudinal girder, for their cross sections see Figure M.3.



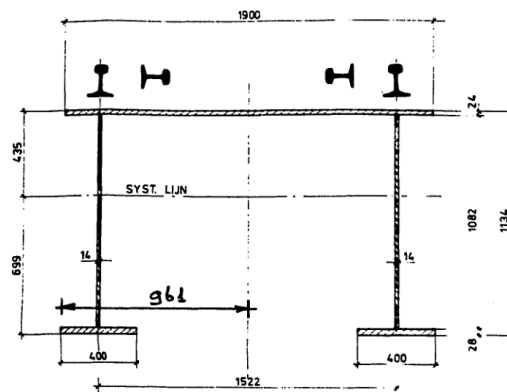
(a) Cross section arch [73]



(b) Cross section hanger [73]



(c) Cross section main girder [73]



(d) Cross section longitudinal girder [73]

Figure M.3: Cross-sections of: arch (a), hanger (b), main girder (c) and longitudinal girder (d).

## M.1.2 Self-weight

The self-weight of the various elements of the Kuilenburgse spoorbrug is presented in Table M.1. For structural calculations a total value of 2 446 800 kg is used, without the inspection vehicle and the bearing plates.

**Table M.1:** Self-weight distribution of Kuilenburgse spoorbrug.<sup>a</sup>

Category	Element	Mass	Unit
arch	Arches, including stiffeners and hanger connections	1 066 500	kg
hanger	Hangers, without connections	89 500	kg
arch	Arch bracing	114 000	kg
girder	End portals	24 500	kg
girder	Bottom edges with hanger connections	373 200	kg
girder	Bottom wind bracing	35 200	kg
girder	Transverse girders	124 700	kg
girder	Longitudinal girders	294 000	kg
girder	Stiff end parts	42 900	kg
girder	Guidance beams	34 700	kg
girder	Support structure grating floor	102 500	kg
girder	Railings on bottom edges	7 400	kg
arch	Support structure, gratings and railings on arches	25 800	kg
girder	Inspection vehicle runway girder	13 100	kg
girder	Rails UIC54 and connections	41 200	kg
girder	Grating floor, including timber structure	35 000	kg
arch	Corrosion protection coating and paint	10 200	kg
girder	Maintenance facilities	10 100	kg
-	Bearing plates at supports	25 200	kg
arch	Deviations due to paint, material thickness etc.	2 300	kg
-	Inspection vehicle	3 000	kg
-	Total	2 475 000	kg

<sup>a</sup> Based on [29, p. A-9, A-10], categories added by author.

## M.2 Ansys model

This section describes the two-dimensional model of the Kuilenburgse spoorbrug, made in Ansys. First the code is presented in subsection M.2.1. In the subsequent sections the various parts of this code are explained.

### M.2.1 Ansys APDL code

The following code has been used.

```

1 !Name:      2d_arch_bridge
2 !Date:      March 1, 2016

```

```

3  !Last modified: May 17, 2016
4  !Description: Ansys model of 2d arch bridge
5
6  !*****
7  finish
8  /clear
9  /prep7
10
11 !define some input variables
12 !general
13 l      = 154.42      !length bridge [m]
14 l_sp   = 11.03      !hanger spacing [m]
15 nh     = 13         !number of hangers
16 v      = 100/3.6    !velocity [m/s]
17 g      = 9.81       !gravitational acceleration [m/s2]
18 ne     = 50         !number of elements between hangers
19 nn     = ne + 1     !number of nodes between hangers
20 ng     = ((nh+1)*ne)+1 !number of nodes on girder
21 dl     = l / ne     !delta length of small element
22 dl2    = l_sp / ne  !delta length keypoints girder
23 dt     = dl / v     !delta time of one time step
24
25 !steel
26 E_st   = 2.1e11     !Youngs modulus [N/m2]
27 rho_st = 7850       !Density steel [kg/m3]
28 alph_st = 12e-6     !Thermal coefficient [1/K]
29 mu_st  = 0.3        !Poissons ratio
30
31 !equivalent arch
32 A_arch = 0.598      !Cross sectional area [m2]
33 I_arch = 1.599      !Moment of inertia arch [m4]
34 H_arch = 4.00       !Height arch [m]
35 mod_arch = 1.577    !mass modification factor
36
37 !equivalent girder
38 A_girder = 0.447    !Cross sectional area [m2]
39 I_girder = 0.107    !Moment of inertia arch [m4]
40 H_girder = 1.42     !Height arch [m]
41 mod_gir  = 2.101    !mass modification factor
42
43 !equivalent hanger
44 A_hanger = 0.059    !Cross sectional area [m2]
45 I_hanger = 1.75e-3  !Moment of inertia arch [m4]
46 H_hanger = 0.40     !Height arch [m]
47
48 nn_t    = nn+1      !array dimension counter
49
50 !*****
51 !define material types
52 !steel arch
53 mp, ex,1,E_st
54 mp,nuxy,1,mu_st
55 mp,dens,1,mod_arch*rho_st

```

```

56 mp,alpx,1,alph_st
57
58 !steel girder
59 mp,ex,2,E_st
60 mp,nuxy,2,mu_st
61 mp,dens,2,mod_gir*rho_st
62 mp,alpx,2,alph_st
63
64 !steel hanger
65 mp,ex,3,E_st
66 mp,nuxy,3,mu_st
67 mp,dens,3,rho_st
68 mp,alpx,3,alph_st
69
70 !*****
71 !define element types
72 !arch
73 et,1,beam3
74 r,1,A_arch,I_arch,H_arch
75
76 !girder
77 et,2,beam3
78 r,2,A_girder,I_girder,H_girder
79
80 !hanger as beam
81 et,3,beam3
82 r,3,A_hanger,I_hanger,H_hanger
83
84 !*****
85 !place keypoints and lines and attach properties
86 !girder
87 *do,i,1,ng
88   k,i,(i-1)*dl2,0,0
89   *if,i,ne,1,then
90     l,i-1,i
91   *endif
92 *enddo
93
94 latt,2,2,2           !associate selected lines with material 2,
                      real constant set 2 and element type 2
95 lsel,none
96
97 *get,key_end,kp,,num,max           !get highest keypoint of girder
98
99 !arch and hangers
100 *do,i,1,nh
101   cur_x = i*l_sp           !current x position of hanger
102   cur_y = 0.647585*cur_x-0.00419366*cur_x**2 !current y position of
                      hanger
103   k,,cur_x,cur_y,0           !arch keypoint
104
105 *get,maxkey,kp,,num,max           !current maximum keypoint number
106 lsel,none

```

```

107 *if , i , eq , 1 , then
108     l , 1 , maxkey                !first arch segment from keypoint 1 to
        maxkey
109     latt , 1 , 1 , 1             !associate selected lines with material 1 ,
        real constant set 1 and element type 1
110 *elseif , i , eq , nh , then
111     l , maxkey - 1 , maxkey
112     l , maxkey , key_end         !last arch segment from keypoint to
        key_end
113     latt , 1 , 1 , 1
114 *else
115     l , maxkey - 1 , maxkey       !other arch segments , from previous
        keypoint to current
116     latt , 1 , 1 , 1
117 *endif
118 lsel , none
119 key_gir = kp( cur_x , 0 , 0 )    !keypoint number , bottom of current
        hanger
120 l , key_gir , maxkey            !hanger line
121 latt , 3 , 3 , 3                !associate selected lines with material 1 ,
        real constant set 3 and element type 3
122 *enddo
123
124 lsel , all
125
126 !*****
127 !meshing
128 !girder
129 lsel , s , type , , 2           !select all lines of element type 2
130 lsize , all , , 1              !number of element divisions per line
131 lmesh , all                    !generate nodes and line elements along all selected
        lines
132
133 !arch
134 lsel , s , type , , 1           !select all lines of element type 1
135 lsize , all , 3                !number of element divisions per line
136 lmesh , all                    !generate nodes and line elements along all selected
        lines
137
138 !hangers
139 lsel , s , type , , 3           !select all lines of element type 3
140 lsize , all , 3                !number of element divisions per line
141 lmesh , all                    !generate nodes and line elements along all selected
        lines
142
143 !*****
144 !DOFs
145 !bridge simply supported DOF
146 nsel , s , loc , x , 0         !x = 0
147 nsel , r , loc , y , 0         !y = 0
148 d , all , ux , , , , uy
149 nsel , s , loc , x , l         !x = l
150 nsel , r , loc , y , 0         !y = 0

```

```

151 d,all,uy
152 allsel
153
154 !*****
155 !end of preprocessor, begin static analysis
156 finish

```

## M.2.2 Geometry

To construct the arch bridge in Ansys the following procedure is used. First keypoints are defined at specific coordinates. Afterwards lines are drawn between those keypoints and material and element properties are attached to those lines. Lastly the lines are meshed, which results in the creation of nodes and elements.

Since the bogies should be able to move over the bridge, the geometry of the girder is defined first. This way it can be made sure the nodes will be numbered from 1 to  $n$ . When defining the keypoints, it is made sure they are equally spaced so the bogies move correctly over them. In addition, it is made sure keypoints will be defined every 11.03 meters, so they can be used to connect the girder with the hangers.

To define the keypoints of the arch, the location of them must be known first. The mathematical function which describes the shape of the parabola is obtained, using a Wolfram Alpha query.<sup>1</sup> This results in the parabola function

$$y = 0.647585x - 0.00419366x^2, \quad (\text{M.1})$$

which can be used to find  $y$ -coordinates at the  $x$ -coordinates of the hangers.

After all the keypoints and lines of the girder, arch and hangers are defined and meshed to nodes and elements, the supports are defined. This results in the bridge model, as seen in Figure M.4.

## M.2.3 Element data

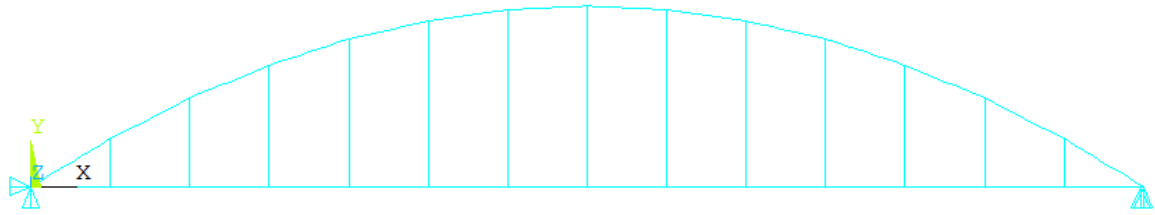
For this two-dimensional model, the bridge will be modelled in three parts. A girder, an arch and hangers, all with BEAM3 elements. This element type is more extensively described in section F.2. For the relevant cross sections as previously mentioned in Figure M.3, the relevant data is extracted and summarized in Table M.2. In the real Kuilenburgse spoorbrug some parameters such as thickness vary over the length of the bridge. For simplicity an average and constant value is used in this model.

The real three-dimensional transverse cross section of the bridge is translated to equivalent cross sections, to be used in the two-dimensional model. This process is illustrated in Figure M.5. The main girders and longitudinal girders are combined in an equivalent girder, because they both contribute to the tension tie of the tied-arch bridge. [29, p. 149]

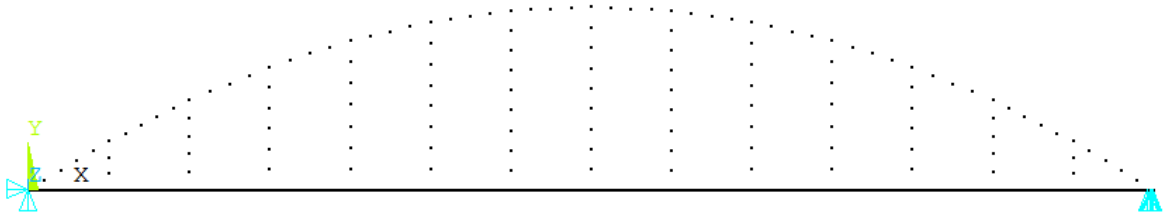
This process results in the data, as seen in Table M.3. This table also includes the masses, obtained by aggregating over the masses by the categories in Table M.1.

The material properties for steel as noted in Table M.4 are used.

<sup>1</sup>[http://www.wolframalpha.com/input/?i=parabola+passing+through+\(0,0\),\(77.21,25\),\(154.42,0\)](http://www.wolframalpha.com/input/?i=parabola+passing+through+(0,0),(77.21,25),(154.42,0))



(a) Elements of 2D arch bridge model in Ansys



(b) Nodes of 2D arch bridge model in Ansys

**Figure M.4:** Geometry of arch bridge model in Ansys

To obtain the correct mass distribution the density of steel is multiplied by a factor for the arch and the girder. The distributed load due to self-weight can be computed in two different ways:

$$\begin{aligned} q_1 &= mod_{el} \cdot \rho \cdot g \cdot A, \\ q_2 &= \frac{m \cdot g}{l}. \end{aligned} \quad (M.2)$$

The first way is by multiplying the density, gravitational acceleration and area with an unknown modification factor  $mod_{el}$  of an element type. The second way is by multiplying the total element mass with the gravitational acceleration and dividing by the element length. Since both ways should produce the same result, they can be set equal to each other to derive

$$mod_{el} = \frac{m}{\rho \cdot l \cdot A}. \quad (M.3)$$

With the total masses, areas and lengths of the equivalent arch and equivalent girder known, the modification factors can be found to manipulate the density input into Ansys. In this manner the mass distribution of the bridge in Ansys would be comparable to that of the real bridge, which has an influence on the dynamic behaviour due to the mass times acceleration.

The length of the arch is computed by rectification of the parabola function

$$l_{arch} = \int_0^{l_{bridge}} \sqrt{1 + \left[ \frac{d}{dx} (0.647585x - 0.00419366x^2) \right]^2} dx = 164.62 \text{ m}. \quad (M.4)$$

With this information the modification factors for the mass density of the arch and girder can be found as

$$\begin{aligned} mod_{arch} &= \frac{m_{arch}}{\rho_{steel} \cdot l_{arch} \cdot A_{arch}} = \frac{1218800}{7850 \cdot 164.62 \cdot 0.598} = 1.577, \\ mod_{gir} &= \frac{m_{girder}}{\rho_{steel} \cdot l_{girder} \cdot A_{girder}} = \frac{1138500}{7850 \cdot 154.42 \cdot 0.447} = 2.101. \end{aligned} \quad (M.5)$$

**Table M.2:** Cross sectional data <sup>a</sup>

Element	Parameter	Value	Unit
Arch	Height	4.00	m
Arch	Cross sectional area	0.299	m <sup>2</sup>
Arch	Moment of inertia	0.799	m <sup>4</sup>
Hanger	Height	0.40	m
Hanger	Cross sectional area	0.0294	m <sup>2</sup>
Hanger	Moment of inertia	$8.756 \times 10^{-4}$	m <sup>4</sup>
Main girder	Height	1.42	m
Main girder	Cross sectional area	0.125	m <sup>2</sup>
Main girder	Moment of inertia	$3.156 \times 10^{-2}$	m <sup>4</sup>
Longitudinal girder	Height	1.13	m
Longitudinal girder	Cross sectional area	0.0983	m <sup>2</sup>
Longitudinal girder	Moment of inertia	$2.214 \times 10^{-2}$	m <sup>4</sup>

<sup>a</sup> Source [73]

With these mass modifications taken into account, the total mass of the 2D arch bridge model is 2 464 267 kg, which is 0.71 % less than the total mass of the Kuilenburgse spoorbrug of 2 446 800 kg.

## M.3 Verification

To verify this model, two checks are performed. First, the midspan deflection in a fully loaded situation is compared to a hand calculation. Second, the deflection at one quarter of the bridge length in an anti-symmetric loading situation is compared to a hand calculation.

### M.3.1 Full loading

The first verification is of a fully loaded tied-arch bridge with vertical hangers, as can be seen in Figure M.6. The verification will be of the deflection at midspan.

#### Hand calculation

For the purpose of the hand calculation the arch bridge is simplified to a frame, as seen in Figure M.6. [74, p. 239]

The following input parameters are assumed:

- $l_{bridge} = 154.42$  m
- $q = 90\,000$  N/m

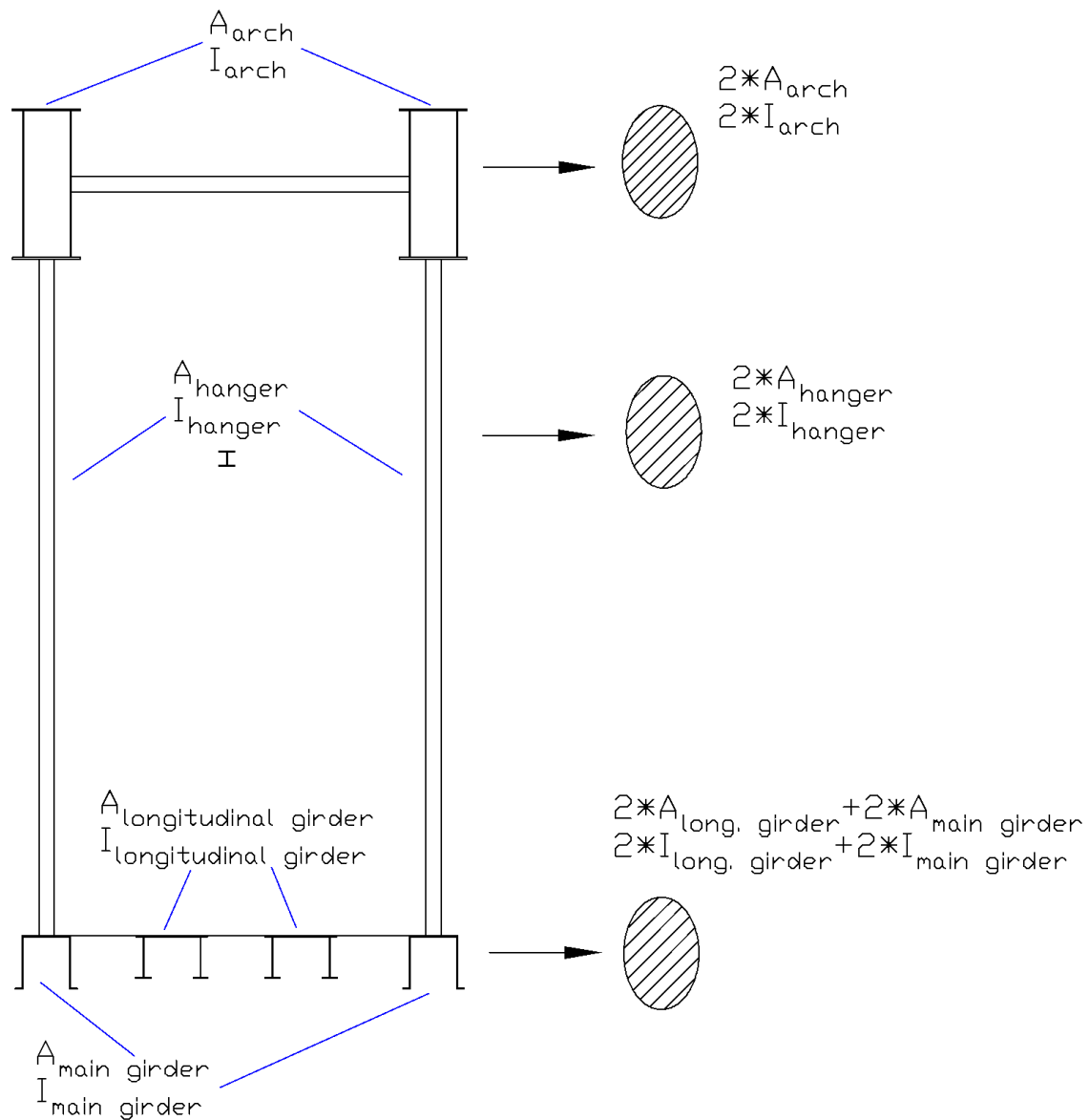


**Figure M.5:** Real cross section (left), equivalent cross sections (right)

The lengths are calculated as

$$\begin{aligned}
 l_1 &= \sqrt{l_2^2 + l_3^2} = \sqrt{77.21^2 + 25^2} = 81.1565 \text{ m}, \\
 l_2 &= \frac{l_{\text{bridge}}}{2} = \frac{154.42}{2} = 77.21 \text{ m}, \\
 l_3 &= 25 \text{ m}, \\
 l_4 &= l_2 = 77.21 \text{ m}, \\
 l_5 &= l_1 = 81.16 \text{ m}.
 \end{aligned}
 \tag{M.6}$$

**Table M.3:** Equivalent cross sectional data <sup>a</sup>

Element	Parameter	Value	Unit
Equivalent arch	Height	4.00	m
Equivalent arch	Cross sectional area	0.598	m <sup>2</sup>
Equivalent arch	Moment of inertia	1.599	m <sup>4</sup>
Equivalent arch	Mass	1 218 800	kg
Equivalent hanger	Height	0.40	m
Equivalent hanger	Cross sectional area	0.059	m <sup>2</sup>
Equivalent hanger	Moment of inertia	$1.75 \times 10^{-3}$	m <sup>4</sup>
Equivalent hanger	Mass	89 500	kg
Equivalent girder	Height	1.42	m
Equivalent girder	Cross sectional area	0.447	m <sup>2</sup>
Equivalent girder	Moment of inertia	0.107	m <sup>4</sup>
Equivalent girder	Mass	1 138 500	kg

<sup>a</sup> Derived from Table M.2 and Table M.1.

**Table M.4:** Material properties steel.

Parameter	Symbol	Value	Unit
Young's Modulus	$E$	$2.1 \times 10^{11}$	N/m <sup>2</sup>
Thermal coefficient	$\alpha$	$12 \times 10^{-6}$	m/(m · K)
Poisson's ratio	$\nu$	0.3	-
Density	$\rho$	7850	kg/m <sup>3</sup>

The load in the middle of the arch and the reaction forces at the supports are

$$\begin{aligned}
 F &= \frac{1}{2} \cdot q \cdot l_{bridge} = \frac{1}{2} \cdot 90000 \cdot 154.42 = 6\,948\,900 \text{ N}, \\
 R_A &= \frac{1}{2} F = \frac{1}{2} \cdot 6\,948\,900 = 3\,474\,450 \text{ N}, \\
 R_B &= \frac{1}{2} F = \frac{1}{2} \cdot 6\,948\,900 = 3\,474\,450 \text{ N}.
 \end{aligned}
 \tag{M.7}$$

The normal forces in the frame segments can be calculated as

$$\begin{aligned}
 N_1 &= \frac{l_1}{l_3} \cdot R_A = \frac{81.16}{25} \cdot 3\,474\,450 = 11\,278\,973.71 \text{ N}, \\
 N_2 &= \frac{l_2}{l_1} \cdot N_1 = \frac{77.21}{81.16} \cdot 11\,278\,973.71 = 10\,730\,491.38 \text{ N}, \\
 N_3 &= F = 6\,948\,900 \text{ N}, \\
 N_4 &= N_2 = 10\,730\,491.38 \text{ N}, \\
 N_5 &= N_1 = 11\,278\,973.71 \text{ N}.
 \end{aligned}
 \tag{M.8}$$

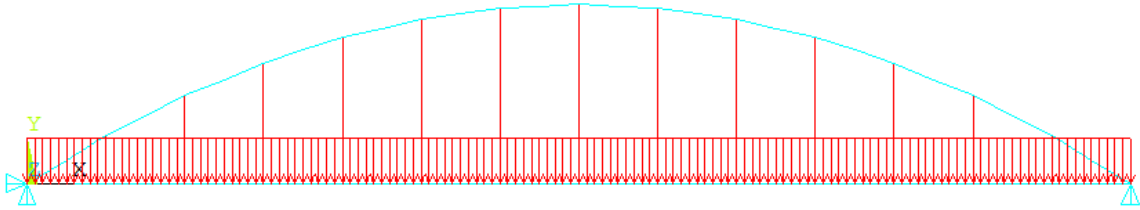


**Figure M.6:** Tied-arch bridge, fully loaded

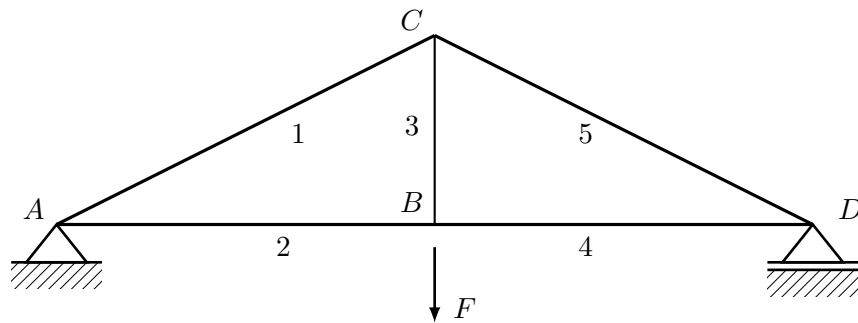


**Figure M.7:** Arch bridge seen as a frame

The stresses due to these normal forces in the frame segments can be calculated as

$$\begin{aligned}
 \sigma_1 &= \frac{N_1}{A_{arch}} = \frac{11278973.71}{0.598} = 18\,861\,160.1 \text{ N/m}^2, \\
 \sigma_2 &= \frac{N_2}{A_{girder}} = \frac{10730491.38}{0.447} = 24\,005\,573.6 \text{ N/m}^2, \\
 \sigma_3 &= \frac{N_3}{A_{hanger}} = \frac{6948900}{0.059} = 117\,777\,966.1 \text{ N/m}^2, \\
 \sigma_4 &= \frac{N_4}{A_{girder}} = \frac{10730491.38}{0.447} = 24\,005\,573.6 \text{ N/m}^2, \\
 \sigma_5 &= \frac{N_5}{A_{arch}} = \frac{11278973.71}{0.598} = 18\,861\,160.1 \text{ N/m}^2.
 \end{aligned} \tag{M.9}$$

The elongations of frame segment one and two can be determined as

$$\begin{aligned}
 \Delta l_1 &= \frac{\sigma_1}{E_{steel}} \cdot l_1 = \frac{18861160.1}{2.1 \cdot 10^{11}} \cdot 81.1565 = 7.29 \times 10^{-3} \text{ m}, \\
 \Delta l_2 &= \frac{\sigma_2}{E_{steel}} \cdot l_2 = \frac{24005573.6}{2.1 \cdot 10^{11}} \cdot 77.21 = 8.83 \times 10^{-3} \text{ m}.
 \end{aligned} \tag{M.10}$$

The deflection at midspan can now be determined as

$$\begin{aligned}
 \delta_{mid-span} &= l_3 - \sqrt{(l_1 - \Delta l_1)^2 - (l_2 + \Delta l_2)^2} = \\
 &= 25 - \sqrt{(81.1565 - 7.29 \cdot 10^{-3})^2 - (77.21 + 8.83 \cdot 10^{-3})^2} = 0.050\,973 \text{ m}.
 \end{aligned} \tag{M.11}$$

## Ansysis calculation

The Ansys calculation is performed using the code mentioned in subsection M.2.1. The following code is added at the end to apply a distributed loading over half the bridge length:

```

1 !full loading over girder
2 esel ,s ,type , ,2
3 sbeam ,all , ,pres ,90000 ,90000 !distributed load on girder
4 allsel

```

This results in a maximum deflection at approximately one quarter of the bridge length of 0.0611 meters, as seen in Figure M.8.

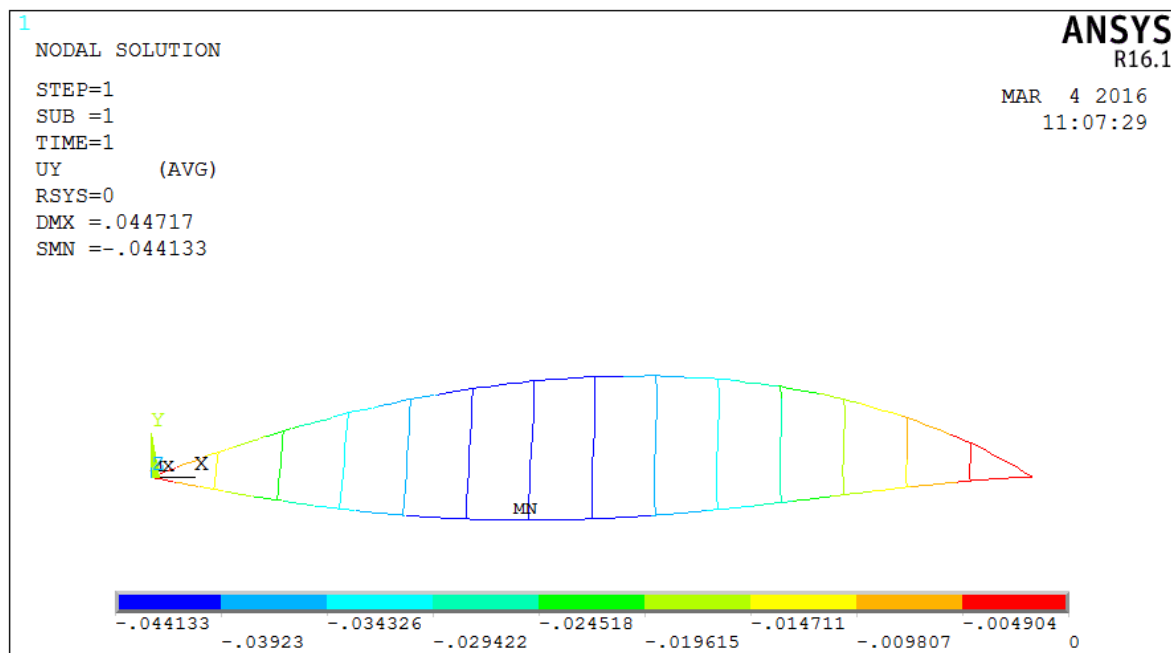


Figure M.8: Deflection of fully loaded tied-arch bridge

## Conclusion

By comparing the results of the hand calculation in section M.3.1 and the Ansys calculation in section M.3.1, a difference in maximum deflection at half the span is found. The hand calculation produced a result of 0.050 973 meters and the Ansys calculation a result of 0.044 133 meters. The difference is 13.42%. This means the results are in the same order of magnitude and are reasonably close enough.

### M.3.2 Anti-symmetric loading

The second verification is one of a tied-arch bridge with vertical hangers, which is anti-symmetrically loaded by a distributed load directed downwards in the left half and upwards in the right half of the girder, as can be seen in Figure M.9. The verification will be of the deflection at one quarter of the span. [74, p. 239]

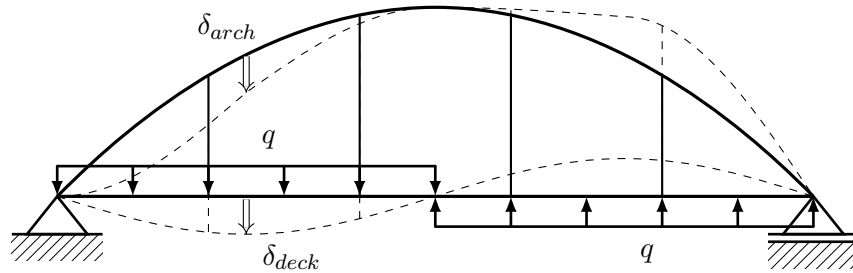


Figure M.9: Half loaded arch bridge

### Hand calculation

For the hand calculation the following input parameters are used:

- $l = l_{half} = \frac{l_{bridge}}{2} = \frac{154.42}{2} = 71.21 \text{ m}$
- $q = 90\,000 \text{ N/m}$

There are two deflection formulas, which are often-used formulas for a simply supported beam with a distributed load

$$\begin{aligned}\delta_{arch} &= \frac{5}{384} \frac{pl^4}{EI_{arch}}, \\ \delta_{deck} &= \frac{5}{384} \frac{(q-p)l^4}{EI_{deck}}.\end{aligned}\quad (\text{M.12})$$

Assuming the hangers provide a rigid connection between the deck and the arch and elongate relatively little,

$$\delta_{arch} \approx \delta_{deck} \quad \Rightarrow \quad \frac{5}{384} \frac{pl^4}{EI_{arch}} = \frac{5}{384} \frac{(q-p)l^4}{EI_{deck}} \quad \Rightarrow \quad p = \frac{q}{1 + \frac{EI_{deck}}{EI_{arch}}}. \quad (\text{M.13})$$

The parameter  $p$  is the amount of load, taken by the arch. This amount depends on the stiffness ratio between arch and deck, stiffer structural parts attract more load. The arch load can be calculated as

$$p = \frac{q}{1 + \frac{EI_{deck}}{EI_{arch}}} = \frac{90000}{1 + \frac{2.1 \cdot 10^{11} \cdot 0.107}{2.1 \cdot 10^{11} \cdot 1.599}} = 84\,355.22 \text{ N/m}. \quad (\text{M.14})$$

This means the arch takes a very large part (84355/90000) of the load, compared to the deck. The deflection can be computed as

$$\delta_{deck} = \frac{5}{384} \frac{(q-p)l^4}{EI_{deck}} = \frac{5}{384} \frac{(90000 - 84355.22)71.21^4}{2.1 \cdot 10^{11} \cdot 0.107} = 0.116\,246 \text{ m}. \quad (\text{M.15})$$

## Ansysis calculation

The Ansys calculation is performed using the code mentioned in subsection M.2.1. The following code is added at the end to apply a distributed anti-symmetric loading. The left half is loaded downwards and the right half is loaded upwards:

```

1  !anti symmetric loading over girder
2  esel ,s ,type , ,2
3  esel ,r ,cent ,x ,0 ,( l /2)  !only select left half
4  sbeam ,all , ,pres ,90000 ,90000
5  allsel
6
7  esel ,s ,type , ,2
8  esel ,r ,cent ,x ,( l /2) ,l  !only select right half
9  sbeam ,all , ,pres , -90000 , -90000
10 allsel

```

This results in a maximum deflection at approximately one quarter of the bridge length of 0.086 meters, as seen in Figure M.10.

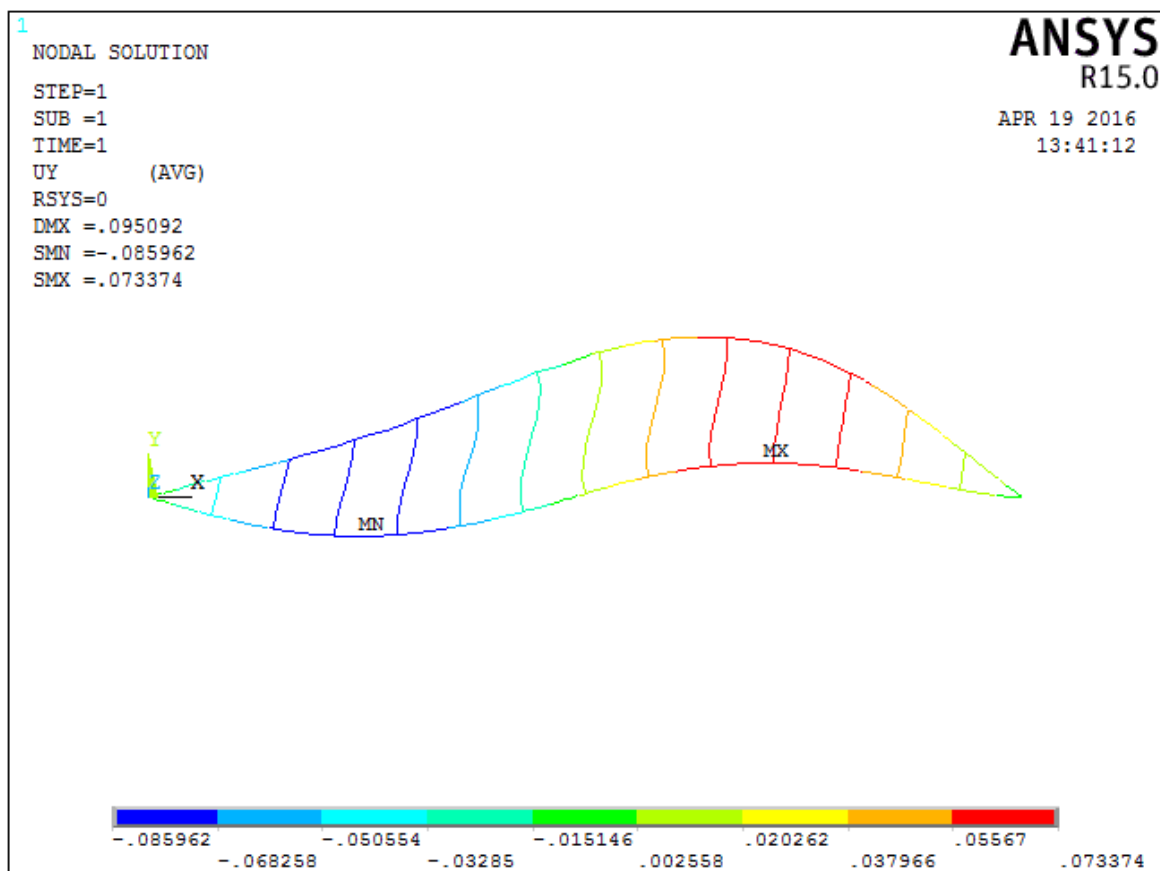


Figure M.10: Deflection of anti-symmetrically loaded tied-arch bridge

## Conclusion

By comparing the results of the hand calculation in section M.3.2 and the Ansys calculation in section M.3.2, a difference in maximum deflection at one quarter of the span is found. The hand calculation produced a result of 0.116246 meters and the Ansys calculation a result of 0.085962 meters. The difference is 26.05 %, which is large, but both results are still in the same order of magnitude.

### M.3.3 Mode shapes

Another thing which can be done is computing the natural frequencies of the arch bridge. This can be done using the following code, which calculates the first 100 natural frequencies and mode shapes:

```

1  !begin modal analysis
2  finish
3  /solu
4  antype,modal
5  modopt,subsp,100,,,
6  eqslv,front
7  mxpand,100,,,
8  solve
9
10 finish
11 /post1
12 set,list

```

The first three mode shapes and their corresponding frequencies can be seen in Figure M.11.

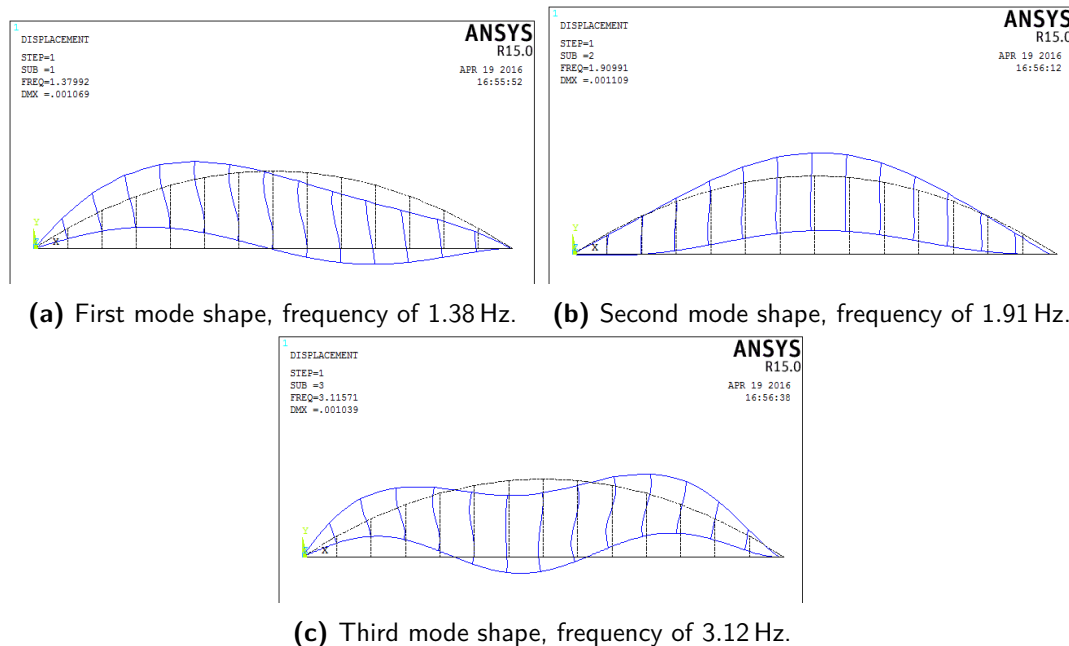


**Figure M.11:** First three mode shapes and natural frequencies of 2D tied-arch bridge model.



# 3D tied-arch bridge model

This appendix describes the 3D tied-arch bridge model created in Ansys, which is an expansion of the 2D model from Appendix M. In section N.1 some input data from the existing Kuilenburgse spoorbrug will be presented. The derived Ansys model will be presented in section N.2 and a verification is presented in section N.3. This appendix is referenced from section 3.3.

## N.1 Railway bridge near Culemborg

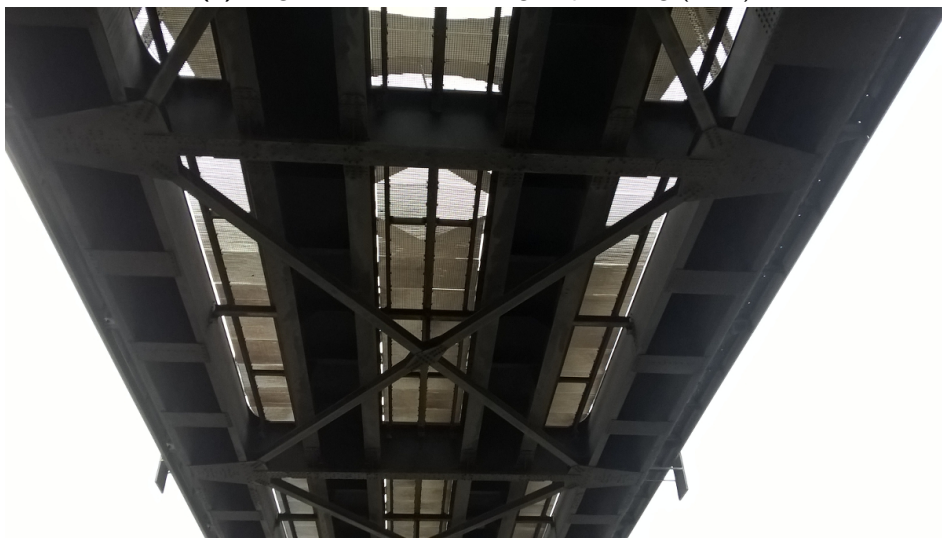
An introduction to the Kuilenburgse spoorbrug is already given in section M.1. However, in the three-dimensional situation some additional things are relevant to discuss. In Figure N.1 the Kuilenburgse spoorbrug is illustrated by two photos.

### N.1.1 Construction elements

The additional relevant construction elements are the transverse girders, end portals, arch bracings and bottom bracings for their cross sections see Figure N.2. The arch, hangers, main and longitudinal girders are still relevant, but already presented in subsection M.1.1.

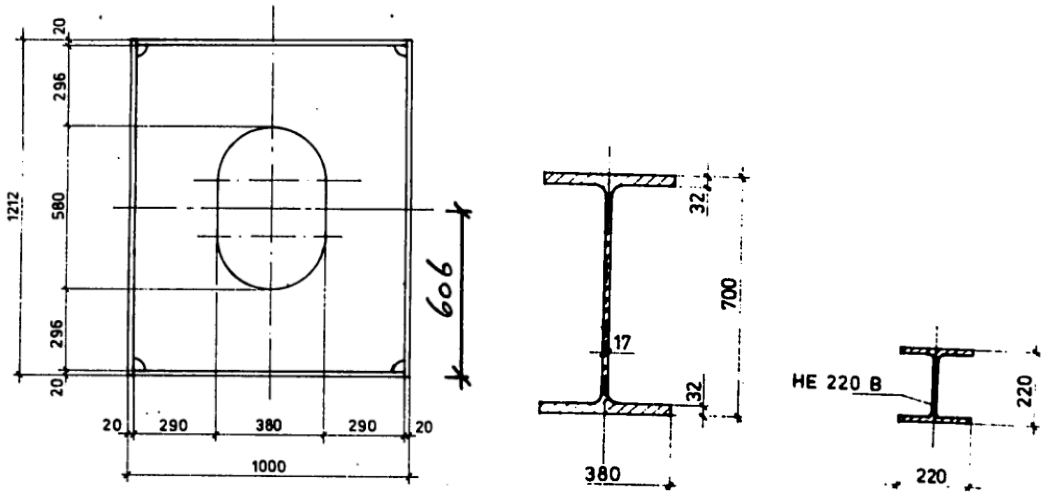


(a) Angle view on Kuilenburgse spoorbrug (2016)



(b) Bottom view on Kuilenburgse spoorbrug (2016)

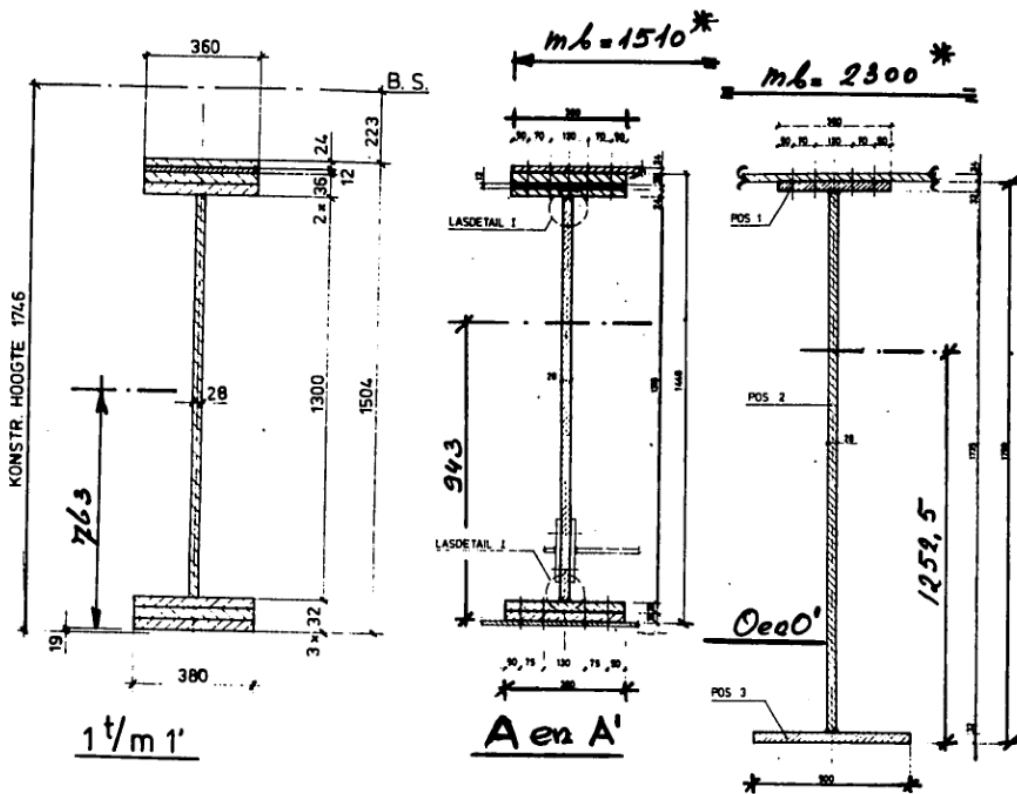
**Figure N.1:** Photos of the Kuilenburgse spoorbrug



(a) Cross section end portal [73]

(b) Cross section arch [73]

(c) Cross section bottom bracing [73]



(d) Cross section transverse girders [73]

Figure N.2: Cross-sections of various bridge elements.

## N.2 Ansys model

The three-dimensional model of the Kuilenburgse spoorbrug can be constructed in Ansys using the code presented in subsection N.2.1. In the subsequent sections the various parts of this code are explained.

### N.2.1 Ansys APDL code

The following code has been used.

```

1  !Name:      3d_arch_bridge
2  !Date:      March 14, 2016
3  !Last modified: May 17, 2016
4  !Description: Ansys model of 3D arch bridge
5
6  !*****
7  finish
8  /clear
9  /prep7
10
11 !define some input variables
12 !general
13 l      = 154.42      !length bridge [m]
14 l_sp   = 11.03      !hanger spacing [m]
15 l_tr   = 10.3       !transverse length [m]
16 l_l1   = 3.15       !distance to first long girder [m]
17 l_l2   = 7.15       !distance to second long girder [m]
18 nh     = 13         !number of hangers
19 v      = 125/3.6     !velocity [m/s]
20 g      = 9.81        !gravitational acceleration [m/s2]
21 ne     = 25         !number of elements between hangers
22 nn     = ne + 1     !number of nodes between hangers
23 neg    = ((nh+1)*ne) !number of elements on long girder
24 nng    = neg+1      !number of nodes on long girder
25 dl     = l / neg    !delta length of small element [m]
26 dl2    = l_sp / ne  !delta length keypoints long girder [m]
27 dt     = dl / v     !delta time of one time step [t]
28
29 !steel
30 E_st   = 2.1e11      !Youngs modulus [N/m2]
31 rho_st = 7850        !Density steel [kg/m3]
32 alph_st = 12e-6     !Thermal coefficient [1/K]
33 mu_st  = 0.3        !Poissons ratio
34
35 !arch
36 H_arch = 4.00       !Height arch [m]
37 W_arch = 1.80       !Width arch [m]
38 tw_arch = 18/1000   !Web thickness [m]
39 tf_arch = 44/1000   !Flange thickness [m]
40 mod_arch = 1.43     !mass modification factor
41
42 !main girder

```

```

43 H_mgir    = 1.42      !Height main girder [m]
44 W1_mgir    = 0.200    !Width brim main girder [m]
45 W3_mgir    = 1.290    !Width top of the hat main girder [m]
46 tb_mgir    = 20/1000  !Brim thickness main girder [m]
47 th_mgir    = 36/1000  !Top flange thickness main girder [m]
48 tw_mgir    = 26/1000  !Web thickness main girder [m]
49 mod_mgir   = 1.58     !mass modification factor
50
51 !hanger
52 H_hang     = 0.40     !Height hanger [m]
53 W_hang     = 0.40     !Width hanger [m]
54 tw_hang    = 16/1000  !Web thickness hanger [m]
55 tf_hang    = 30/1000  !Flange thickness hanger [m]
56 mod_hang   = 0.83     !mass modification factor
57
58 !longitudinal girder
59 H_lgir     = 1.134    !Height long girder [m]
60 W1_lgir     = 0.400    !Width brim long girder [m]
61 W3_lgir     = 1.900    !Width top of the hat long girder [m]
62 tb_lgir     = 28/1000  !Brim thickness long girder [m]
63 th_lgir     = 24/1000  !Top flange thickness long girder [m]
64 tw_lgir     = 14/1000  !Web thickness long girder [m]
65 mod_lgir    = 1.98     !mass modification factor
66
67 !transverse girder 0
68 H_gir0     = 1.773    !Height trans girder 0 [m]
69 W1_gir0     = 0.900    !Width bottom trans girder 0 [m]
70 W2_gir0     = 1.046    !Width top trans girder 0 [m]
71 tw_gir0     = 20/1000  !Web thickness trans girder 0 [m]
72 tf1_gir0    = 32/1000  !Flange bottom thickness trans girder 0 [m]
73 tf2_gir0    = 66/1000  !Flange top thickness trans girder 0 [m]
74
75 !transverse girder A
76 H_girA     = 1.448    !Height trans girder A [m]
77 W1_girA     = 0.460    !Width bottom trans girder A [m]
78 W2_girA     = 0.694    !Width top trans girder A [m]
79 tw_girA     = 20/1000  !Web thickness trans girder A [m]
80 tf1_girA    = 64/1000  !Flange bottom thickness trans girder A [m]
81 tf2_girA    = 96/1000  !Flange top thickness trans girder A [m]
82
83 !transverse girder
84 H_tgir     = 1.504    !Height trans girder [m]
85 W1_tgir     = 0.380    !Width bottom trans girder [m]
86 W2_tgir     = 0.360    !Width top trans girder [m]
87 tw_tgir     = 28/1000  !Web thickness trans girder [m]
88 tf1_tgir    = 96/1000  !Flange bottom thickness trans girder [m]
89 tf2_tgir    = 0.108    !Flange top thickness trans girder [m]
90 mod_tgir    = 0.79     !mass modification factor
91
92 !end portal
93 H_por      = 1.212    !Height portal [m]
94 W_por      = 1.000    !Width portal [m]
95 tw_por     = 20/1000  !Web thickness portal [m]

```

```

96 tf_por      = 20/1000      !Flange thickness portal [m]
97 mod_por     = 1.74        !mass modification factor
98
99 !arch bracing
100 H_brac     = 0.700        !Height bracing [m]
101 W_brac     = 0.380        !Width bracing [m]
102 tw_brac    = 17/1000     !Web thickness bracing [m]
103 tf_brac    = 32/1000     !Flange thickness bracing [m]
104 mod_brac   = 1.22        !mass modification factor
105
106 !bottom bracing
107 A_bot      = 9.1e-3       !Area bottom bracing [m2]
108 mod_bot    = 1.17        !mass modification factor
109
110 nn_t       = nn+1        !array dimension counter
111
112 !*****
113 !define material types
114 !steel arch
115 mp, ex,1,E_st
116 mp,nuxy,1,mu_st
117 mp,dens,1,rho_st*mod_arch
118 mp,alpx,1,alph_st
119
120 !steel main girder
121 mp, ex,2,E_st
122 mp,nuxy,2,mu_st
123 mp,dens,2,rho_st*mod_mgir
124 mp,alpx,2,alph_st
125
126 !steel hanger
127 mp, ex,3,E_st
128 mp,nuxy,3,mu_st
129 mp,dens,3,rho_st*mod_hang
130 mp,alpx,3,alph_st
131
132 !steel longitudinal girder
133 mp, ex,6,E_st
134 mp,nuxy,6,mu_st
135 mp,dens,6,rho_st*mod_lgir
136 mp,alpx,6,alph_st
137
138 !steel transverse girder 0
139 mp, ex,7,E_st
140 mp,nuxy,7,mu_st
141 mp,dens,7,rho_st*mod_tgir
142 mp,alpx,7,alph_st
143
144 !steel transverse girder A
145 mp, ex,8,E_st
146 mp,nuxy,8,mu_st
147 mp,dens,8,rho_st*mod_tgir
148 mp,alpx,8,alph_st

```

```

149
150 !steel transverse girder
151 mp, ex,9,E_st
152 mp,nuxy,9,mu_st
153 mp,dens,9,rho_st*mod_tgir
154 mp,alpx,9,alph_st
155
156 !steel end portal
157 mp, ex,10,E_st
158 mp,nuxy,10,mu_st
159 mp,dens,10,rho_st*mod_por
160 mp,alpx,10,alph_st
161
162 !steel arch bracing
163 mp, ex,11,E_st
164 mp,nuxy,11,mu_st
165 mp,dens,11,rho_st*mod_brac
166 mp,alpx,11,alph_st
167
168 !steel bottom bracing
169 mp, ex,14,E_st
170 mp,nuxy,14,mu_st
171 mp,dens,14,rho_st*mod_bot
172 mp,alpx,14,alph_st
173
174 !*****
175 !define element types and cross sections
176 !arch
177 et,1,beam188
178 sectype,1,beam,hrec ! hollow rectangle
179 secdata,W_arch,H_arch,tw_arch,tw_arch,tf_arch,tf_arch
180
181 !main girder
182 et,2,beam188
183 sectype,2,beam,hats ! hat-shaped profile
184 secdata,W1_mgir,W1_mgir,W3_mgir,H_mgir,tb_mgir,tb_mgir,th_mgir,tw_mgir,
    tw_mgir
185
186 !hanger
187 et,3,beam188
188 sectype,3,beam,I ! I-profile
189 secdata,W_hang,W_hang,H_hang,tf_hang,tf_hang,tw_hang
190
191 !longitudinal girder
192 et,6,beam188
193 sectype,6,beam,hats ! hat-shaped profile
194 secdata,W1_lgir,W1_lgir,W3_lgir,H_lgir,tb_lgir,tb_lgir,th_lgir,tw_lgir,
    tw_lgir
195
196 !transverse girder 0
197 et,7,beam188
198 sectype,7,beam,I ! I-profile
199 secdata,W1_gir0,W2_gir0,H_gir0,tf1_gir0,tf2_gir0,tw_gir0

```

```

200
201 !transverse girder A
202 et,8,beam188
203 sectype,8,beam,I ! I-profile
204 secdata,W1_girA,W2_girA,H_girA,tf1_girA,tf2_girA,tw_girA
205
206 !transverse girder
207 et,9,beam188
208 sectype,9,beam,I ! I-profile
209 secdata,W1_tgir,W2_tgir,H_tgir,tf1_tgir,tf2_tgir,tw_tgir
210
211 !end portal
212 et,10,beam188
213 sectype,10,beam,hrec ! hollow rectangle
214 secdata,W_por,H_por,tw_por,tw_por,tf_por,tf_por
215
216 !arch bracings
217 et,11,beam188
218 sectype,11,beam,I ! I-profile
219 secdata,W_brac,W_brac,H_brac,tf_brac,tf_brac,tw_brac
220
221 !bottom bracings
222 et,14,link8
223 r,41,A_bot
224
225 !*****
226 !place keypoints and lines and attach properties
227 !west main girder
228 *get,cur_max,kp,,num,max !current maximum keypoint number
229 cur_x = 0
230 lsel,none
231 *do,i,1,nh+1
232 *if,cur_max,eq,0,then
233 k,1,0,0,0
234 cur_max = 1
235 *elseif,i,eq,1,then
236 k,cur_max,0,0,0
237 cur_max = cur_max + 1
238 *elseif,cur_x,le,l_sp,then
239 !mesh first segment finer to have keypoints for trans girder A
240 *do,ii,1,ne
241 cur_max = cur_max + 1
242 k,cur_max,ii*d12,0,0
243 l,cur_max-1,cur_max
244 *enddo
245 *elseif,cur_x,ge,13*l_sp,then
246 cur_max = cur_max + 1
247 k,cur_max,(i-1)*l_sp,0,0
248 l,cur_max-1,cur_max
249 !mesh last segment finer to have keypoints for trans girder A
250 *do,ii,1,ne
251 cur_max = cur_max + 1
252 k,cur_max,cur_x+ii*d12,0,0

```

```

253     l , cur_max-1, cur_max
254 *enddo
255 *else
256     cur_max = cur_max + 1
257     k , cur_max , (i-1)*l_sp, 0, 0
258     l , cur_max-1, cur_max
259 *endif
260 cur_x = cur_x + l_sp
261 *enddo
262
263 kb2w = cur_max + 1           !define orientation keypoint number
264 k , kb2w , 0 , 100 , 0      !create orientation keypoint
265
266 latt , 2 , , 2 , , kb2w , , 2           !associate selected lines with material
267     2 , element type 2 and sectype 2
268
269 !least main girder
270 *get , cur_max , kp , , num , max       !current maximum keypoint number
271 cur_x = 0
272 *do , i , 1 , nh+1
273     *if , cur_max , eq , 0 , then
274         k , 1 , 0 , 0 , l_tr
275         cur_max = 1
276     *elseif , i , eq , 1 , then
277         cur_max = cur_max + 1
278         k , cur_max , 0 , 0 , l_tr
279     *elseif , cur_x , le , l_sp , then
280         !mesh first segment finer to have keypoints for trans girder A
281         *do , ii , 1 , ne
282             cur_max = cur_max + 1
283             k , cur_max , ii*d12 , 0 , l_tr
284             l , cur_max-1 , cur_max
285         *enddo
286     *elseif , cur_x , ge , 13*l_sp , then
287         cur_max = cur_max + 1
288         k , cur_max , (i-1)*l_sp , 0 , l_tr
289         l , cur_max-1 , cur_max
290         !mesh last segment finer to have keypoints for trans girder A
291         *do , ii , 1 , ne
292             cur_max = cur_max + 1
293             k , cur_max , cur_x+ii*d12 , 0 , l_tr
294             l , cur_max-1 , cur_max
295         *enddo
296     *else
297         cur_max = cur_max + 1
298         k , cur_max , (i-1)*l_sp , 0 , l_tr
299         l , cur_max-1 , cur_max
300     *endif
301     cur_x = cur_x + l_sp
302 *enddo
303
304 kb2e = cur_max + 1           !define orientation keypoint number

```

```

305 k, kb2e, 0, 100, 1, tr           !create orientation keypoint
306
307 latt, 2, , 2, , kb2e, , 2       !associate selected lines with material
    2, element type 2 and sectype 2
308 lsel, none
309
310 !west longitudinal girder
311 *get, cur_max, kp, , num, max     !current maximum keypoint number
312 *do, i, 1, nng
313     *if, cur_max, eq, 0, then
314         k, 1, (i-1)*dl2, 0, 1_11
315         cur_max = 2
316     *elseif, i, eq, 1, then
317         cur_max = cur_max + 1
318         k, cur_max, (i-1)*dl2, 0, 1_11
319     *else
320         cur_max = cur_max + 1
321         k, cur_max, (i-1)*dl2, 0, 1_11
322         l, cur_max-1, cur_max
323     *endif
324 *enddo
325
326 kb6w = cur_max + 1               !define orientation keypoint number
327 k, kb6w, 0, 100, 1, 11         !create orientation keypoint
328
329 latt, 6, , 6, , kb6w, , 6
330 lsel, none
331
332 !east longitudinal girder
333 *get, cur_max, kp, , num, max     !current maximum keypoint number
334 *do, i, 1, nng
335     *if, cur_max, eq, 0, then
336         k, 1, (i-1)*dl2, 0, 1_12
337         cur_max = 2
338     *elseif, i, eq, 1, then
339         cur_max = cur_max + 1
340         k, cur_max, (i-1)*dl2, 0, 1_12
341     *else
342         cur_max = cur_max + 1
343         k, cur_max, (i-1)*dl2, 0, 1_12
344         l, cur_max-1, cur_max
345     *endif
346 *enddo
347
348 kb6e = cur_max + 1               !define orientation keypoint number
349 k, kb6e, 0, 100, 1, 12         !create orientation keypoint
350
351 latt, 6, , 6, , kb6e, , 6
352 lsel, none
353
354 !end transverse girders 0
355 !left end bridge
356 key_01 = kp(0, 0, 0)

```

```

357 key_02 = kp(0,0,1_11)
358 key_03 = kp(0,0,1_12)
359 key_04 = kp(0,0,1_tr)
360
361 l ,key_01 ,key_02
362 l ,key_02 ,key_03
363 l ,key_03 ,key_04
364
365 latt ,7 , ,7 , ,kb2e , ,7
366 lsel ,none
367
368 !right end bridge
369 key_05 = kp(1,0,0)
370 key_06 = kp(1,0,1_11)
371 key_07 = kp(1,0,1_12)
372 key_08 = kp(1,0,1_tr)
373
374 l ,key_05 ,key_06
375 l ,key_06 ,key_07
376 l ,key_07 ,key_08
377
378 *get ,cur_max ,kp , ,num ,max           !current maximum keypoint number
379 kb7 = cur_max + 1                       !define orientation keypoint number
380 k ,kb7 ,1 ,100 ,0                       !create orientation keypoint
381
382 latt ,7 , ,7 , ,kb7 , ,7
383 lsel ,none
384
385 !end transverse girders A
386 !left end bridge
387 key_A1 = kp(4.469,0,0)
388 key_A2 = kp(4.469,0,1_11)
389 key_A3 = kp(4.469,0,1_12)
390 key_A4 = kp(4.469,0,1_tr)
391
392 kbetw ,key_A2 ,key_A3
393 key_Am1 = kp(4.469,0,(1_tr/2))
394
395 l ,key_A1 ,key_A2
396 l ,key_A2 ,key_Am1
397 l ,key_Am1 ,key_A3
398 l ,key_A3 ,key_A4
399
400 *get ,cur_max ,kp , ,num ,max           !current maximum keypoint number
401 kb81 = cur_max + 1                       !define orientation keypoint number
402 k ,kb81 ,4.469 ,100 ,0
403
404 latt ,8 , ,8 , ,kb81 , ,8
405 lsel ,none
406
407 !right end bridge
408 key_A5 = kp(1-4.469,0,0)
409 key_A6 = kp(1-4.469,0,1_11)

```

```

410 key_A7 = kp( l-4.469,0,l_12)
411 key_A8 = kp( l-4.469,0,l_tr)
412
413 kbetw ,key_A6 ,key_A7
414 key_Am2 = kp( l-4.469,0,(l_tr/2))
415
416 l ,key_A5 ,key_A6
417 l ,key_A6 ,key_Am2
418 l ,key_Am2 ,key_A7
419 l ,key_A7 ,key_A8
420
421 *get ,cur_max ,kp , , num ,max           !current maximum keypoint number
422 kb8r = cur_max + 1                       !define orientation keypoint number
423 k ,kb8r , ( l-4.469) ,100,0
424
425 latt ,8 , ,8 , ,kb8r , ,8
426 lsel ,none
427
428 !bottom bracings at beginning and end of bridge
429 !bottom bracings
430 !define some existing keypoints
431 key_b1 = kp(l_sp,0,0)
432 key_b4 = kp(l_sp,0,l_tr)
433 key_b5 = kp( l-l_sp,0,0)
434 key_b8 = kp( l-l_sp,0,l_tr)
435
436 !make lines between keypoints
437 l ,key_01 ,key_Am1
438 l ,key_Am1 ,key_b4
439 l ,key_04 ,key_Am1
440 l ,key_Am1 ,key_b1
441
442 l ,key_05 ,key_Am2
443 l ,key_Am2 ,key_b8
444 l ,key_08 ,key_Am2
445 l ,key_Am2 ,key_b5
446
447 latt ,14,41,14                           !mat 14, real const 41, elem type 14
448 lsel ,none
449
450 !transverse girders and bottom bracings
451 *do ,i ,1 ,nh+1
452     cur_x = i*l_sp
453     key_t1 = kp( cur_x ,0 ,0)
454     key_t2 = kp( cur_x ,0 ,l_11)
455     key_t3 = kp( cur_x ,0 ,l_12)
456     key_t4 = kp( cur_x ,0 ,l_tr)
457     !only execute the transverse girders part for 0<i<14
458     *if ,i ,le ,nh ,then
459         !transverse girders
460         l ,key_t1 ,key_t2
461         l ,key_t2 ,key_t3
462         l ,key_t3 ,key_t4

```

```

463
464     *get , cur_max , kp , , num , max           !current maximum keypoint number
465     kb9%i% = cur_max + 1                       !define orientation keypoint number
466     k , kb9%i% , cur_x , 100 , 0
467
468     latt , 9 , , 9 , , kb9%i% , , 9
469     lsel , none
470 *endif
471
472 !normal bracings in the middle part
473 *if , i , gt , 1 , and , i , le , nh , then
474     !bottom bracings
475     key_t1i = kp((cur_x-1_sp) , 0 , 0)
476     key_t4i = kp((cur_x-1_sp) , 0 , 1_tr)
477     l , key_t1i , key_t4
478     l , key_t1 , key_t4i
479
480     latt , 14 , 41 , 14                       !mat 14, real const 41, elem type 14
481     lsel , none
482 *endif
483 *enddo
484
485 !arch and hangers
486 *do , i , 1 , 2*nh+1
487     cur_x = i*0.5*1_sp                       !current x position of hanger
488     cur_y = 0.647585*cur_x-0.00419366*cur_x**2 !current y position of
         hanger
489     *get , maxkey , kp , , num , max           !current maximum keypoint number
490
491     !arch segments
492     k , maxkey+1 , cur_x , cur_y , 0           !arch west keypoint
493     k , maxkey+2 , cur_x , cur_y , 1_tr       !arch east keypoint
494     lsel , none
495     *if , i , eq , 1 , then
496         l , key_01 , maxkey+1                 !first arch seg west
497         latt , 1 , , 1 , , kb2w , , 1
498         lsel , none
499         l , key_04 , maxkey+2                 !first arch seg east
500         latt , 1 , , 1 , , kb2e , , 1
501         lsel , none
502     *elseif , i , eq , 2*nh+1 , then
503         l , maxkey-1 , maxkey+1               !arch seg west
504         l , maxkey+1 , key_05                 !last arch seg west
505         latt , 1 , , 1 , , kb7 , , 1
506         lsel , none
507         l , maxkey , maxkey+2                 !arch seg east
508         l , maxkey+2 , key_08                 !last arch seg east
509         latt , 1 , , 1 , , kb2e , , 1
510         lsel , none
511     *else
512         l , maxkey-1 , maxkey+1               !arch seg west
513         latt , 1 , , 1 , , kb2w , , 1
514         lsel , none

```

```

515     l,maxkey,maxkey+2           !arch seg east
516     latt,1,,1,,kb2e,,1
517     lsel,none
518 *endif
519     lsel,none
520
521 !hangers on even keypoints
522 mod_i = mod(i,2)               !modulus of i
523 *if,mod_i,eq,0,then
524     key_gir1 = kp(cur_x,0,0)    !keypoint number, bottom of current
525     hanger
526     key_gir2 = kp(cur_x,0,1_tr)
527     l,key_gir1,maxkey+1        !hanger line
528     !latt,3,,3,,,,3           !associate selected lines with material
529     3, real constant set 3 and element type 3
530     l,key_gir2,maxkey+2
531     latt,3,,3,,,,3
532 *endif
533 *enddo
534 lsel,none
535
536 !end portals
537 cur_x = 1.5*l_sp               !x position end portal 1
538 cur_y = 0.647585*cur_x-0.00419366*cur_x**2 !y position end portal 1
539
540 key_p1 = kp(cur_x,cur_y,0)
541 key_p2 = kp(cur_x,cur_y,1_tr)
542 l,key_p1,key_p2
543
544 *get,cur_max,kp,,num,max      !current maximum keypoint number
545 kb10l = cur_max + 1          !define orientation keypoint number
546 k,kb10l,cur_x,100,0
547
548 latt,10,,10,,kb10l,,10
549 lsel,none
550
551 key_p3 = kp(l-cur_x,cur_y,0)
552 key_p4 = kp(l-cur_x,cur_y,1_tr)
553 l,key_p3,key_p4
554
555 *get,cur_max,kp,,num,max      !current maximum keypoint number
556 kb10r = cur_max + 1          !define orientation keypoint number
557 k,kb10r,(l-cur_x),100,0
558
559 latt,10,,10,,kb10r,,10
560 lsel,none
561
562 !arch bracings
563 *do,i,1,nh-2
564     cur_x = 1.5*l_sp+i*l_sp
565     cur_y = 0.647585*cur_x-0.00419366*cur_x**2
566
567     prev_x = cur_x-l_sp

```

```

566 prev_y = 0.647585*prev_x - 0.00419366*prev_x**2
567
568 cur_key1 = kp(cur_x, cur_y, 0)
569 cur_key2 = kp(cur_x, cur_y, 1_tr)
570 prev_key1 = kp(prev_x, prev_y, 0)
571 prev_key2 = kp(prev_x, prev_y, 1_tr)
572
573 l, prev_key1, cur_key2          !bracing west - east
574
575 *get, cur_max, kp, , num, max          !current maximum keypoint number
576 kb11%i%w = cur_max + 1                !define orientation keypoint number
577 k, kb11%i%w, prev_x, 100, 0
578
579 latt, 11, , 11, , kb11%i%w, , 11
580 lsel, none
581
582 l, prev_key2, cur_key1          !bracing east - west
583
584 *get, cur_max, kp, , num, max          !current maximum keypoint number
585 kb11%i%e = cur_max + 1                !define orientation keypoint number
586 k, kb11%i%e, prev_x, 100, 1_tr
587
588 latt, 11, , 11, , kb11%i%e, , 11
589 lsel, none
590 *enddo
591
592 lsel, all
593
594 !*****
595 !meshing
596 !longitudinal girders separate to have fine mesh for train dt
597 lsel, s, type, , 6                !select all lines of element type 6
598 lsel, a, type, , 14                !also bottom bracings are link8 and should be meshed
599                                     as one
599 lesize, all, , , 1                !number of element divisions per line
600 lmesh, all                          !generate nodes and line elements along all selected
601                                     lines
602
603 !the rest
604 lsel, inve
605 lesize, all, 3                      !number of element divisions per line
606 lmesh, all                          !generate nodes and line elements along all selected
607                                     lines
608
609 !*****
610 !DOFs
611 !set tolerance to lower value to exactly select nodes
612 seltol, 1.0e-6
613
614 !one support completely constrained
615 nsel, s, loc, x, 0                !x = 0
616 nsel, r, loc, y, 0                !y = 0
617 nsel, r, loc, z, 0                !z = 0

```

```

616 d,all,ux,,,,,uy,uz
617
618 !second support one way constrained
619 nsel,s,loc,x,0      !x = 0
620 nsel,r,loc,y,0      !y = 0
621 nsel,r,loc,z,1_tr   !z = 10.3
622 d,all,uy
623
624 !third support one way constrained
625 nsel,s,loc,x,l      !x = 154.42
626 nsel,r,loc,y,0      !y = 0
627 nsel,r,loc,z,1_tr   !z = 10.3
628 d,all,uy
629
630 !fourth support one way constrained
631 nsel,s,loc,x,l      !x = 154.42
632 nsel,r,loc,y,0      !y = 0
633 nsel,r,loc,z,0      !z = 0
634 d,all,uy,,,,,uz
635
636 allsel
637
638 !*****
639 !end of preprocessor, begin static analysis
640 finish

```

## N.2.2 Geometry

To construct the arch bridge in Ansys, roughly the same procedure as with the two-dimensional model can be followed. The longitudinal girders use closely spaced keypoints, because the train will move over them and the time step must be small enough to get accurate results. The rest of the beam elements are meshed at intervals of 3 meters. After all the keypoints and lines of the girder, arch and hangers are defined and meshed to nodes and elements, the supports are defined. This results in the bridge model, as seen in Figure N.4. There are four supports at the corners of the bridge, with simply supported DOFs and sliding allowed in certain directions, as seen in Figure N.3.

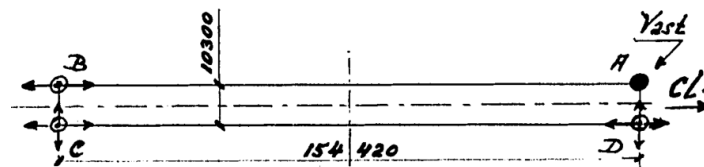
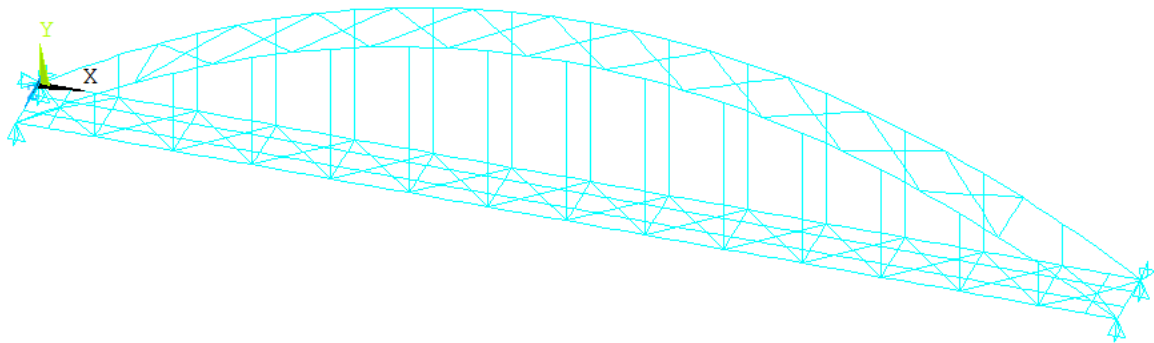


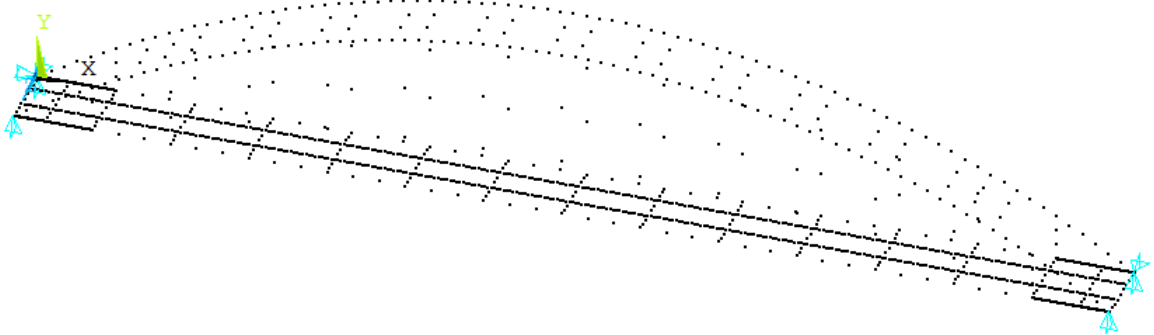
Figure N.3: Supports degrees of freedom [29, page A-7]

## N.2.3 Element data

For this three-dimensional model, the bridge is mainly modelled with BEAM188 elements. These elements are more extensively described in section F.2. While the BEAM3 elements used in the



(a) Elements of 3D arch bridge model in Ansys



(b) Nodes of 3D arch bridge model in Ansys

**Figure N.4:** Geometry of 3D arch bridge model in Ansys

two-dimensional bridge model could be described with their height, area and moment of inertia, the BEAM188 elements need more specific cross sectional data. This also enables to visualise the cross sections (see Figure N.5), which is useful to see if their orientation is correct. The orientation of beams can be changed by using orientation keypoints. The needed cross sectional data can be seen in Table N.1 and Table N.2. In the real Kuilenburgse spoorbrug some parameters such as thickness vary over the length of the bridge. For simplicity an average and constant value is used in this model. The bottom bracings are modelled with LINK8 elements, because their bending stiffness is negligible in comparison with the other elements, their main function is providing stability in lateral direction.

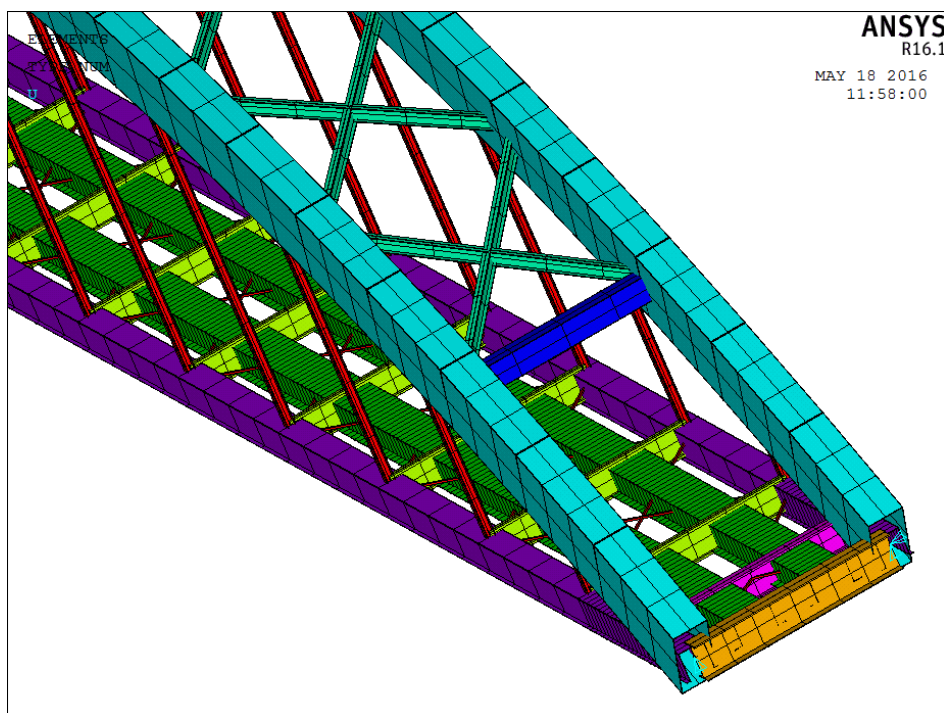


**Figure N.5:** 3D bridge model with all cross sections used

**Table N.1:** Cross sectional data 2 <sup>a</sup>

Parameter	Value	Unit
<b>Arch</b>		
Height	4.000	m
Width	1.800	m
Web thickness	0.018	m
Flange thickness	0.044	m
<b>Main girder</b>		
Height	1.420	m
Brim width	0.200	m
Top width	1.290	m
Brim thickness	0.020	m
Top flange thickness	0.036	m
Web thickness	0.026	m
<b>Hanger</b>		
Height	0.400	m
Width	0.400	m
Web thickness	0.016	m
Flange thickness	0.030	m
<b>Longitudinal girder</b>		
Height	1.134	m
Brim width	0.400	m
Top width	1.900	m
Brim thickness	0.028	m
Top flange thickness	0.024	m
Web thickness	0.014	m
<b>Arch bracing</b>		
Height	0.700	m
Width	0.380	m
Web thickness	0.017	m
Flange thickness	0.032	m

<sup>a</sup> Source [73]**Table N.2:** Cross sectional data 3 <sup>a</sup>

Parameter	Value	Unit
<b>Transverse girder 0</b>		
Height	1.773	m
Bottom width	0.900	m
Top width	1.046	m
Web thickness	0.020	m
Bottom flange thickness	0.032	m
Top flange thickness	0.066	m
<b>Transverse girder A</b>		
Height	1.448	m
Bottom width	0.460	m
Top width	0.694	m
Web thickness	0.020	m
Bottom flange thickness	0.064	m
Top flange thickness	0.096	m
<b>Transverse girder</b>		
Height	1.504	m
Bottom width	0.380	m
Top width	0.360	m
Web thickness	0.028	m
Bottom flange thickness	0.096	m
Top flange thickness	0.108	m
<b>End portal</b>		
Height	1.212	m
Width	1.000	m
Web thickness	0.020	m
Flange thickness	0.020	m
<b>Bottom bracing</b>		
Area	$9.1 \times 10^{-3}$	m <sup>2</sup>

<sup>a</sup> Source [73]

Some values for the transverse girder 0 and A are estimated, because they were blurry in the source figure. This results in slightly wrong moments of inertia.

### N.2.4 Mass modification

The material properties for steel as noted in Table M.4 are used. Because the Ansys model does not contain all elements exactly as the real Kuilenburgse spoorbrug does, the density of the elements has been modified to let the total mass of the bridge and the mass distribution be as close to the real situation as possible. Both the mass and the stiffness influence the dynamic behaviour and must correspond to the real situation, to model it accurately.

First the masses were retrieved from unmodified model using the following commands:

```
1 /uis,msgpop,3
2 irlf,-1
3 psolve,elform
4 psolve,elprep
5 irlist
```

Afterwards these masses were compared to the Kuilenburgse spoorbrug mass, an aggregation by element type as seen in Table N.3. Dividing these two values results in the mass modification factors, which were multiplied with the density of the elements in Ansys.

**Table N.3:** Mass modification of Ansys 3D bridge model

Element type	Mass Kuil. brug [kg]	Mass Ansys model [kg]	Modification factor
Arch	1 104 800	773 317	1.43
Main girder	481 400	303 941	1.58
Hanger	89 500	107 298	0.83
Longitudinal girder	472 700	238 308	1.98
Transverse girder <sup>a</sup>	124 700	158 411	0.79
End portal	24 500	14 049	1.74
Arch bracing	114 000	93 616	1.22
Bottom bracing	35 200	30 207	1.17
<b>Total</b>	<b>2 446 800</b>	<b>1 719 147</b>	-

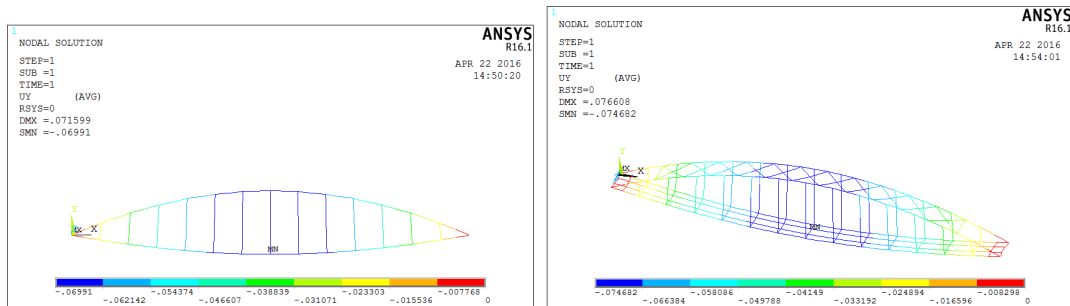
<sup>a</sup> The transverse girder, transverse girder 0 and transverse girder A used in the Ansys model are summed. See Table M.1 for the masses of the Kuilenburgse spoorbrug.

### N.3 Verification

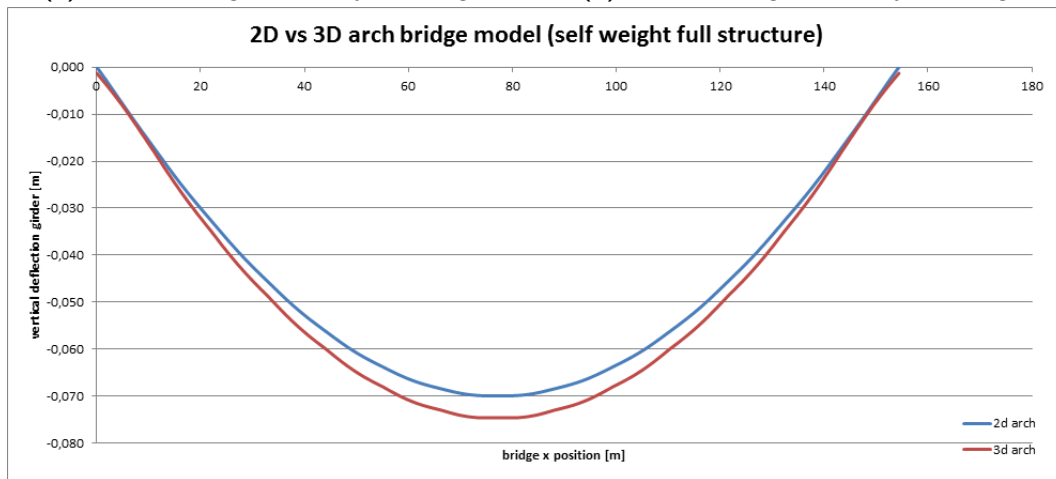
To verify this model, it is compared to the 2D bridge model, described in Appendix M. This comparison is done based on vertical deflection due to self-weight and due to anti-symmetric loading, as well as a comparison of natural frequencies and mode shapes.

#### N.3.1 Self-weight

In Figure N.6 the deflection of the bridge models due to self-weight can be seen. Both have had mass modifications to let them have the same mass as the Kuilenburgse spoorbrug. Furthermore, the two-dimensional model has profiles with equivalent stiffness, to make it equivalently stiff compared to a three-dimensional situation. The resulting deflection is plotted in Figure N.6c. It can be observed the 3D bridge model deflects a little more, but the difference is reasonably small.



(a) 2D arch bridge loaded by self-weight (b) 3D arch bridge loaded by self-weight

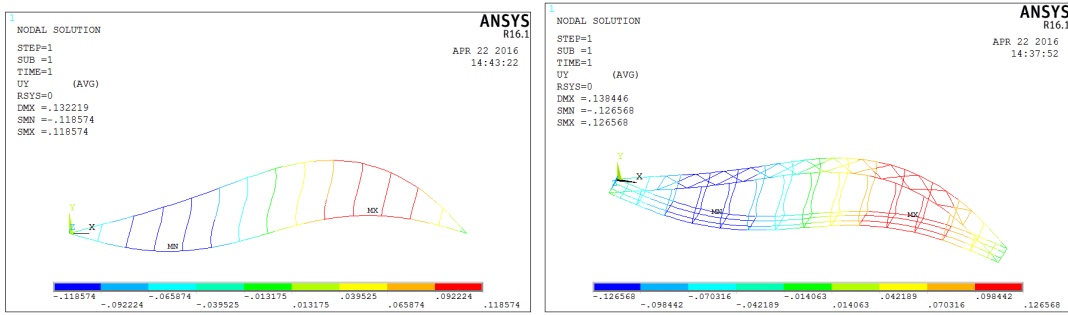


(c) 2D and 3D arch bridge deflection

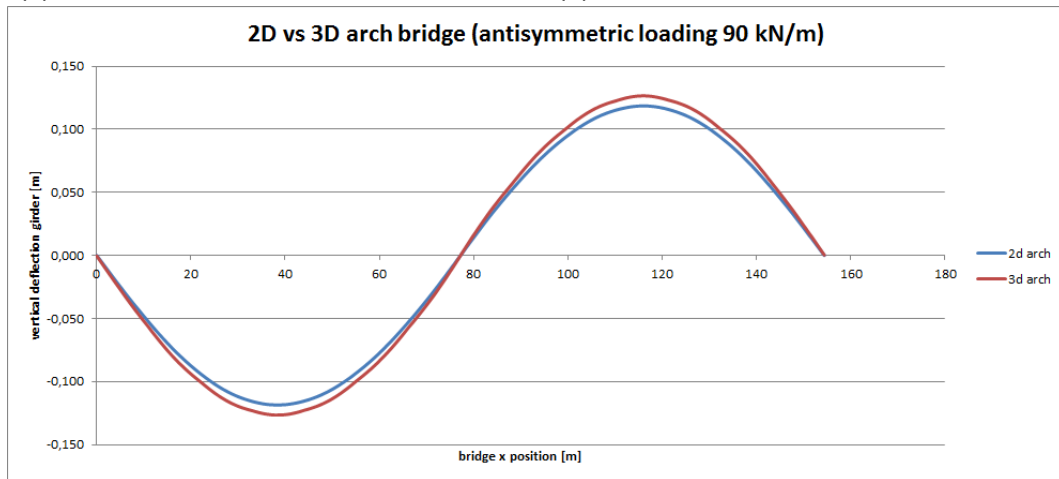
Figure N.6: 2D and 3D arch bridge models loaded by self-weight

#### N.3.2 Anti-symmetric loading

In Figure N.7 the deflection of the bridge models due to anti-symmetric loading can be seen. The resulting deflection is plotted in Figure N.7c. It can be observed the 3D bridge model deflects a little more, but the difference is reasonably small.



(a) 2D arch bridge anti-symmetrically loaded (b) 3D arch bridge anti-symmetrically loaded



(c) 2D and 3D arch bridge deflection

Figure N.7: 2D and 3D arch bridge models anti-symmetrically loaded

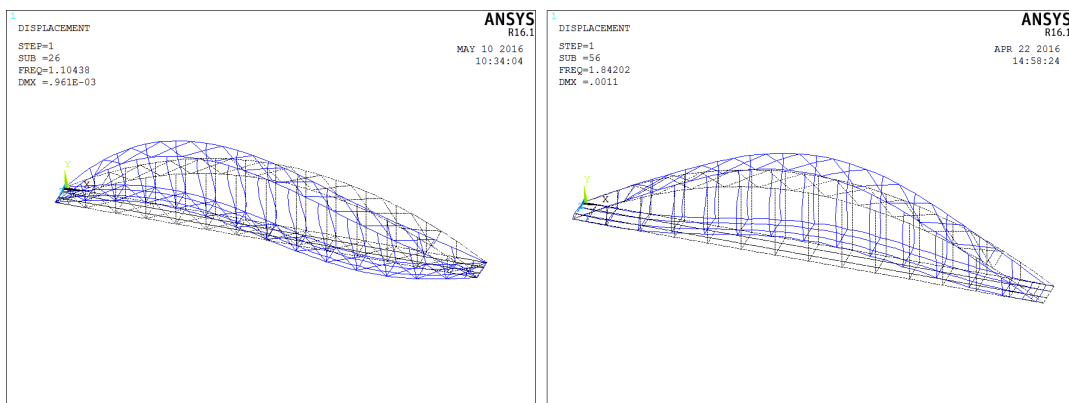
### N.3.3 Mode shapes

In subsection M.3.3 the first three mode shapes and corresponding natural frequencies of the 2D bridge model are presented. In Figure N.8 the first three mode shapes for the 3D bridge model can be seen.

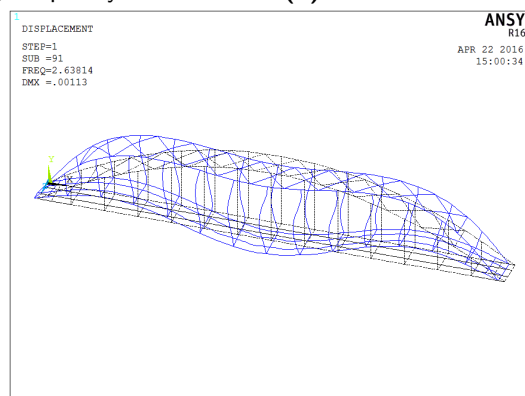
It can be noted there is a difference in frequency. The comparison can be seen in Table N.4.

Table N.4: Natural frequency comparison between 2D and 3D bridge models.

Mode shape	2D bridge [Hz]	3D bridge [Hz]	difference
1	1.38	1.10	19.6 %
2	1.91	1.84	3.7 %
3	3.12	2.64	15.4 %



(a) First mode shape, frequency of 1.10 Hz. (b) Second mode shape, frequency of 1.84 Hz.



(c) Third mode shape, frequency of 2.64 Hz.

**Figure N.8:** First three mode shapes and natural frequencies of 3D tied-arch bridge model.



## Acceleration measurements

In this appendix the conducted acceleration measurements in trains passing a tied-arch bridge are explained. In section O.1 the choice of bridge is explained. Afterwards the used measurement equipment is detailed in section O.2. Then the trial measurements are reported in section O.3. With among others the experience from these measurements an experimental setup is developed and explained in section O.4. Finally the real measurements are described in section O.5. This appendix is referenced from chapter 4.

### O.1 Bridge choice

To choose a bridge, the list of bridges in Table O.1 was used. Not every bridge on this list was suitable for the experiment, only bridges which could abide to the following selection criteria were considered, in accordance with section 1.4:

- The bridge is made of steel;
- The bridge is a tied-arch bridge;
- The bridge is simply supported and does not have continuous stiffening parts;
- The bridge has vertical hangers;
- The bridge is used for passenger transport.

The bridges fulfilling the aforementioned criteria are:

- Kuilenburgse spoorbrug;
- Spoorbrug Oosterbeek;
- Vlakebrug;

- Spoorbrug Twentekanaal.

Initially the Spoorbrug Twentekanaal was chosen from this list, because construction drawings were readily available. However, after performing the trial measurements on this bridge, it was decided to choose another bridge, and the Kuilenburgse spoorbrug was chosen for the real measurements.

**Table O.1:** List of some of the longest span railway bridges in the Netherlands.<sup>a</sup>

Name	Span [m]	Location	Year
Spoorbrug Muiderberg	255	Muiderberg	2016
Werkspoorbrug	237	Utrecht	2002
Spoorbrug Nijmegen	235	Nijmegen	1984
Muiderspoorbrug	188	Diemen	1972
Schalkwijkse spoorbrug	188	Schalkwijk	1976
Demka-spoorbrug	173	Utrecht	1970
Vleutensespoorbrug	169	Utrecht	1969
Calandbrug	155	Rotterdam	1969
Kuilenburge spoorbrug	154	Culemborg	1983
Hanzeboog	150	Zwolle	2011
Dintelhavenspoorbrug	140	Rotterdam	1999
Kreekrakspoorbrug	140	Middenhof	1971
Spoorbrug Oosterbeek	132	Arnhem	1952
Vlakebrug	130	Hansweert	1992
Dr. W. Hupkesbrug	125	Zaltbommel	1947
Spoorbrug Nootdorpboog	125	Nootdorp	2005
Brug bij Westervoort	117	Westervoort	1979
Baanhoekbrug	110	Sliedrecht	1983
Spoorbrug Dukenburg	110	Nijmegen	1977
Hedelse spoorbrug	107	Hedel	1946
Brug Hollandsch Diep	105	Dordrecht	2005
Moerdijkspoorbrug	104	Moerdijk	1955
Suurhoffbrug	100	Rotterdam	1972
IJsselspoorbrug	99	Deventer	1982
Spoorbrug Twentekanaal	92	Zutphen	2005
IJsselspoorbrug	89	Zutphen	1985
Walfridusbrug	89	Groningen	2003
Spoorbrug Dordrecht	88	Dordrecht	1994

<sup>a</sup> Adapted from data received from ProRail (R. van der Zwan, personal communication, Sept 22, 2015).

## O.2 Measurement equipment

To measure the accelerations a train passenger experiences due to a train passing a tied-arch bridge, certain equipment is necessary. Essentially an accelerometer and a device to store the

measured data is necessary. In ISO 10056 dedicated equipment such as transducers, amplifier, filter and recorder are mentioned. However, the necessity for this equipment can be omitted by using modern smartphones which contain accurate accelerometers. According to research where several smartphones are compared to professional equipment, modern smartphone accelerometers have an inaccuracy of only 1% to 5%. [31] Since such a small inaccuracy seems reasonable, it was chosen to use a Samsung Galaxy Tab 2, which contains a BMA254 acceleration sensor manufactured by Bosch. Reference is made to the data sheet of a similar sensor, the BMA255. [75]

To process the data measured by the acceleration sensor, a smartphone application “VXaccelerator” was used. [32] The application is a modified version of an existing accelerometer application, with some useful modifications which are convenient to perform measurements. With the used hardware it is able to measure accelerations in vertical direction with a sampling frequency of 63 Hertz. To measure the train velocity a GPS enabled smartphone is used (Microsoft Lumia 640).

### O.3 Trial measurements

To test if the planned method of measuring accelerations works as intended, two measurements at the *Spoorbrug Twentekanaal* were performed, which is one of the bridge considered suitable in section O.1. However, after closer inspection of the bridge, it became clear the hangers were not completely vertical but a little bit inclined, which made the bridge stiffer than a bridge with exactly vertical hangers. Therefore it did not meet the bridge selection criteria after all.

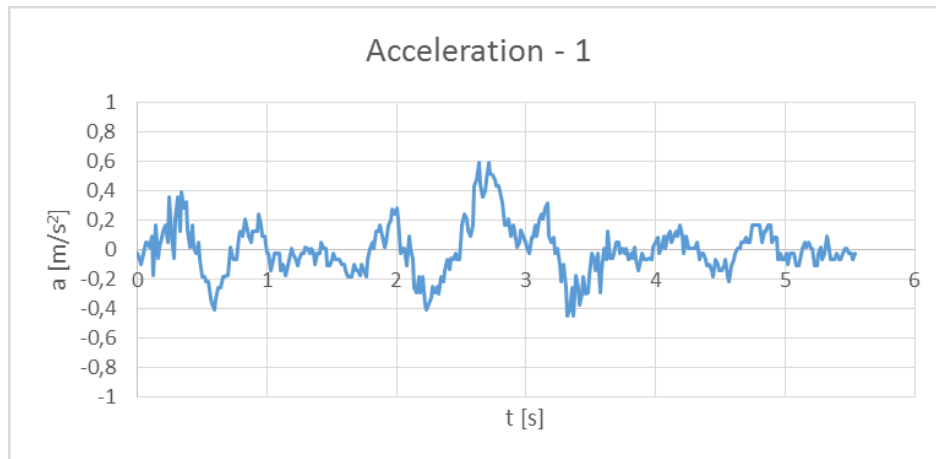


**Figure O.1:** Spoorbrug Twentekanaal hanger inclination

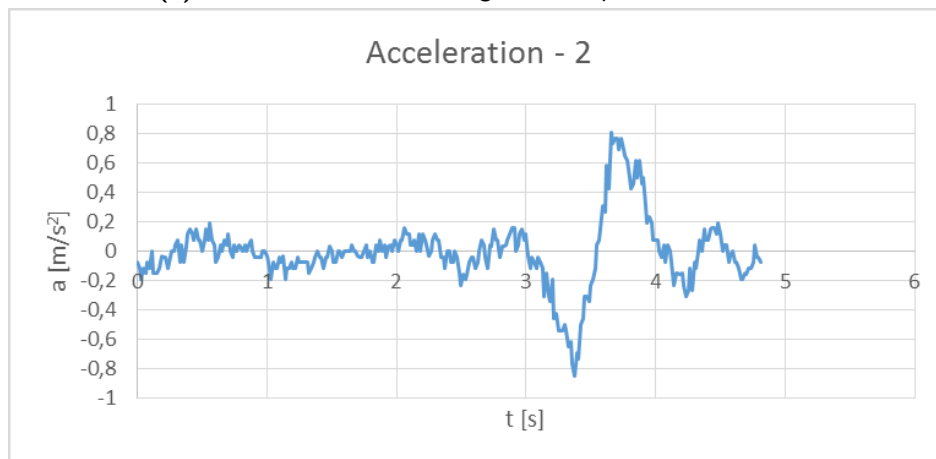
To measure on the Spoorbrug Twentekanaal a train ride from Zutphen to Deventer was made. The tablet was used to measure the vertical acceleration and the smartphone to measure the velocity. The train type and number were recorded, as can be seen in Table O.2. The velocity when passing the bridge was 65 km/h, which amounts to a duration of 5.54 seconds. The tablet was positioned on the vestibule floor, exactly above a bogie. To exclude gravitational acceleration, the device was calibrated at the location of the measurement.

After arriving in Deventer, a returning train was boarded, to perform a second measurement. This

time the velocity was slightly higher, with a magnitude of 75 km/h. The accelerations versus time plots can be seen in Figure O.2.



(a) Measurement 1, travelling from Zutphen to Deventer.



(b) Measurement 2, travelling from Deventer to Zutphen.

**Figure O.2:** Acceleration time histories of measurements performed in trains travelling over the Spoorbrug Twentekanaal.

**Table O.2:** Trial measurements information

<b>Measurement</b>	<b>1</b>	<b>2</b>
<b>Date</b>	Dec 28, 2015	Dec 28, 2015
<b>Start time</b>	13:07	13:55
<b>Duration [s]</b>	5.54	4.80
<b>Start location</b>	Zutphen	Deventer
<b>End location</b>	Deventer	Zutphen
<b>Train type</b>	NID	NID
<b>Train number</b>	7612	7635
<b>Velocity [km/h]</b>	65	75
<b>Location</b>	vestibule floor	vestibule floor
<b>Calibration [m/s<sup>2</sup>]<sup>a</sup></b>	9.73	9.77

<sup>a</sup> The gravity acceleration which is subtracted from the measured data.

## O.4 Experimental setup

With the information from standards (see Appendix P) and the experience from the trial measurements as described in the previous section, an experimental setup was developed. This experimental setup would be used to perform real measurements as accurate as possible.

### O.4.1 Data to record

Every measurement should include the following metadata:

- Date;
- Start and end time ride;
- Start and end location ride;
- Local weather conditions (wet/dry rails);
- Train type and number;
- Coach type and number;
- Bogie type (motor or trailer);
- Amount of coaches in EMU;
- Loading conditions (empty/full with passengers);
- Start and end time measurement;
- Start and end sample number;
- Train velocity;
- Calibration of app;
- File name of data.

This metadata gives the necessary context to the measured data file, which makes a correct interpretation possible. Furthermore, several parameters are kept constant, to prevent them from influencing the experiment. The location of measurement in the train is kept constant to the vestibule floor of the last coach, the type of train is always VIRM. The metadata is written on data input sheets, see Figure O.3.

### O.4.2 Activities

The activities necessary to perform during a round trip are:

- Calibrate the tablet on the departure station;
- When the train arrives, count the number of coaches and write this down;
- Get in and walk to the back of the train, write down how full the train is;
- In the last coach, write down the train number and coach number, stay at vestibule floor;
- Position tablet on floor, a little before the bridge, start measuring;
- At the same time, measure velocity;
- Write down sample number at the exact beginning and end of the bridge;
- End measuring and go to sit;
- (First time only) calculate time between bridge and station;
- Get out at the destination station;
- Walk to the departure platform;
- Count the number of coaches and write this down on a new data input sheet;
- Get in, walk to the back of the train, write down how full the train is;
- In the last coach, write down the train number and coach number and go sit;
- When train nears the bridge, go to vestibule floor and position table on the floor;
- A little before the bridge, start measuring;
- Also measure the train velocity;
- Write down sample number at the exact beginning and end of the bridge;
- End measurements and go sit;
- Get out at the initial departure station and repeat procedure.

Ride number

## Data input sheet

---

### General

Date

Start time ride

End time ride

Start location ride

End location ride

### Train

Train type

Train number

Loading train

Coach number

Coaches amount

Weather

### Measurements

Start time

End time

Velocity

File name

Sample start

Sample end

Calibration

### Notes

**Figure O.3:** Data input sheet used to record metadata from measurements.

## O.5 Real measurements

With the developed experimental setup, real measurements were conducted on the *Kuilenburgse spoorbrug* on March 24, 2016. For this purpose 8 trips between Station Utrecht Centraal and Station 's-Hertogenbosch were made by intercity VIRM trains. These trains cover the distance of 48 kilometers in 27 minutes. At a distance of approximately 16 kilometers from Station Utrecht Centraal the Kuilenburgse spoorbrug is located, where the measurements are performed. As explained in section O.4, the measurements were done using a tablet with an acceleration sensor and application to process the data, which was positioned on the vestibule floor of the last coach of the train, see Figure O.4.



**Figure O.4:** Photo of experimental setup, location of measuring device on vestibule floor of train.

### O.5.1 Results

In Table O.3 the full metadata information which was gathered during the measurements can be seen. The velocity differed slightly, but was often close to 125 km/h. The length and loading of the train varied quite a lot, there were obvious quiet and rush hours.

In Figure O.5 the acceleration measurements can be seen. The recording was started some time before the bridge and ended some time after the bridge. It was attempted to capture the start and end moment of the bridge, which is marked blue in the graphs. Because it was difficult to determine these moments accurately an error of  $\pm 1$  or 2 seconds can be expected.

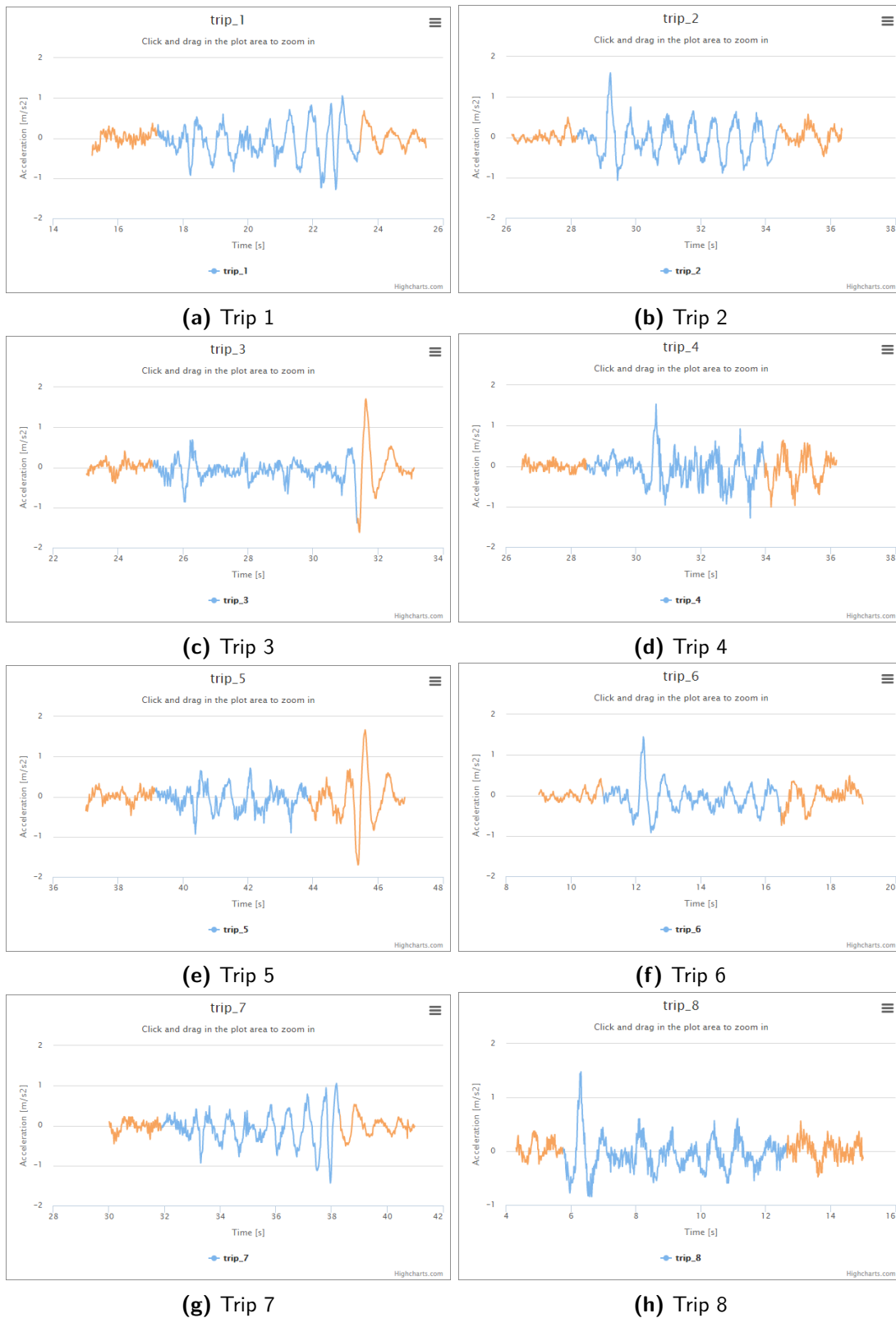


**Figure O.5:** Acceleration plots of real measurements. These plots can also be viewed [online](#), as well as the raw data [here](#). The blue parts of the graphs denote the part of the acceleration measurements on the bridge, as estimated.

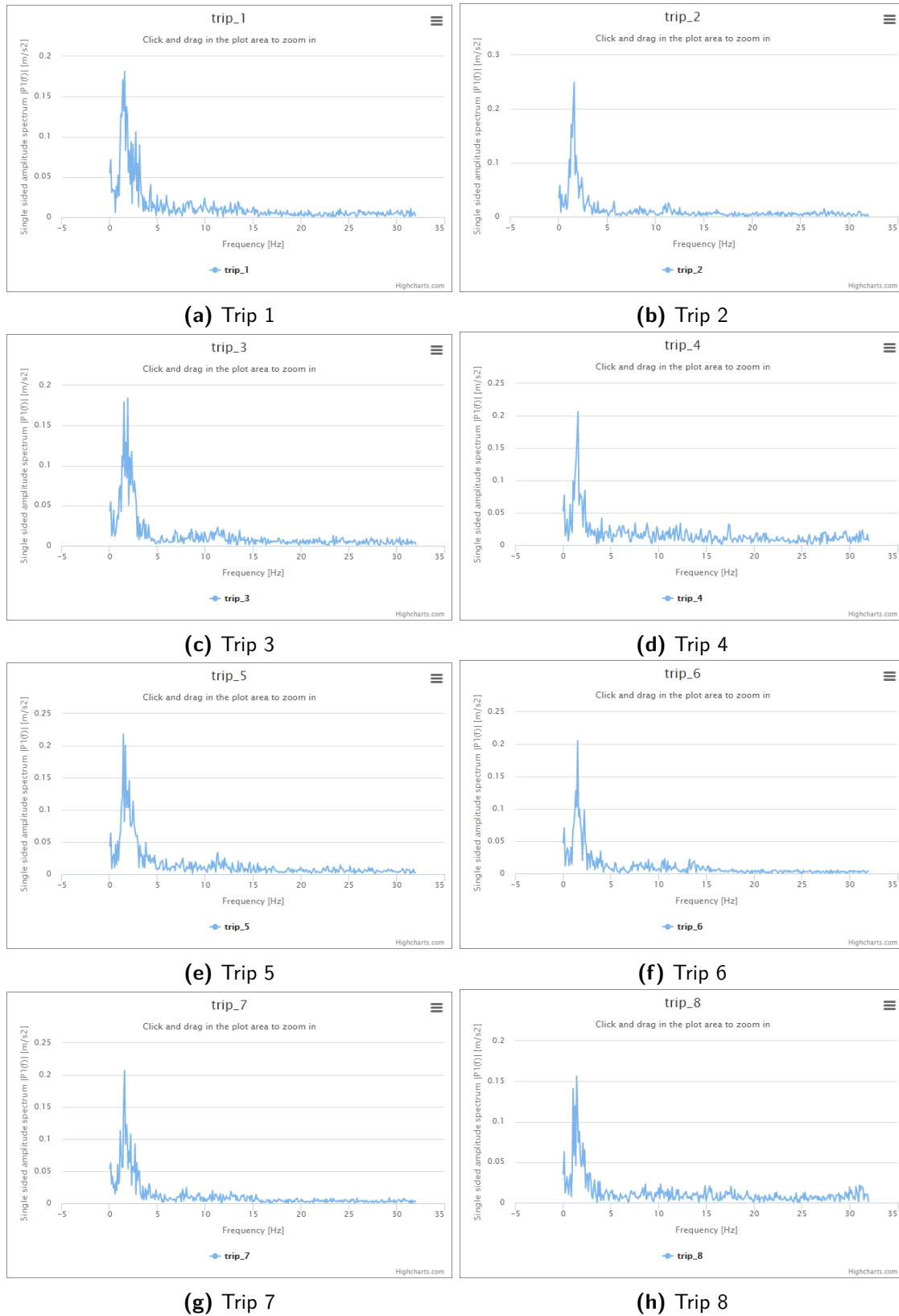


**Figure O.6:** Fourier plots of real measurements. These plots can also be viewed [online](#), as well as the raw data [here](#). On average all 8 plots show one dominant peak around 1.5 Hertz.

**Table O.3:** Time schedule

#	Start time	End time	Start location	End location	Train num.	Loading	# coaches	Vel. [km/h]	S. start <sup>a</sup>	S. end <sup>a</sup>
<b>1</b>	9:11	9:35	Utrecht CS	's-Hertogenbosch	9516	1/2 full	6+6	130	1100	1500
<b>2</b>	9:53	10:21	's-Hertogenbosch	Utrecht CS	9575	1/4 full	4+4	125	1800	2200
<b>3</b>	10:38	11:05	Utrecht CS	's-Hertogenbosch	8648	full	6	110	1600	2000
<b>4</b>	11:23	11:51	's-Hertogenbosch	Utrecht CS	8655	3/4 full	6	125	1800	2150
<b>5</b>	12:07	12:35	Utrecht CS	's-Hertogenbosch	8657	1/4 full	4+6	120	2500	2800
<b>6</b>	12:53	13:21	's-Hertogenbosch	Utrecht CS	9560	full	4	125	700	1050
<b>7</b>	13:37	14:05	Utrecht CS	's-Hertogenbosch	8702	full	6	125	2000	2400
<b>8</b>	14:23	14:51	's-Hertogenbosch	Utrecht CS	8648	1/2 full	6	125	400	800

The sample start and sample end numbers are a rough estimation.

In all 8 measurements the date was March 24, 2016, the weather was dry, the calibration was  $9.75 \text{ m/s}^2$  and the train type was VIRM.

In Figure O.6 the fourier transformation of the acceleration measurements can be seen. This was done with a Matlab script, as seen in subsection O.5.2. The script reads the data from a text file and puts it into an array using a third-party function `txt2mat`.<sup>1</sup> Because the time steps are not exactly equally spaced, which is needed for the fast fourier transform to work, the data is interpolated to get regular time steps. Afterwards the fourier transform is performed, using Matlab's built-in fast fourier transform function. Afterwards some mathematical operations are performed and finally the data is written to a text file.

### O.5.2 FFT Matlab script

```

1  %Name:          FFT on acceleration measurements
2  %Author:       Benjamin Komen
3  %Date:         March 26, 2016
4  %Last modified: March 28, 2016
5  %Description:  Read text file and applies fft and writes result
6
7  clear all;
8  clc;
9
10 % read data into array using third-party script
11 file_name = 'full';
12 file_ext  = '.txt';
13 file_path = '../experiment-data/trip_4_alt/';
14 input_path = strcat(file_path, file_name, file_ext);
15 data_array = txt2mat(input_path);
16
17 time_vec = data_array(:,1);           % time points [s]
18 acc_vec  = data_array(:,2);           % acceleration data points [m/s2]
19 Fs       = 64;                       % Sampling frequency [Hz = 1/s]
20 dt       = 1/Fs;                     % Sampling period [s]
21
22 time_eq  = min(time_vec):dt:max(time_vec); % vector of equally spaced
        time steps
23 vq      = interp1(time_vec, acc_vec, time_eq, 'spline'); % interpolate it to
        get regular time steps
24 L       = length(vq);                % length of vector [-]
25
26 acc_fft  = fft(acc_vec);              % compute fft [m/s2]
27
28 P2       = abs(acc_fft/L);             % two-sided spectrum [m/s2]
29 P1       = P2(1:L/2+1);               % one-sided spectrum [m/s2]
30 P1(2:end-1) = 2*P1(2:end-1);         % ?
31
32 f        = Fs*(0:(L/2))/L;           % frequency vector [Hz]
33 T        = table([f.'], [P1]);        % define output matrix
34
35 % write results to file
36 output_path = strcat(file_path, 'fft/', file_name, file_ext); %output
        file name
37 writetable(T, output_path);          % write to file

```

<sup>1</sup><http://www.mathworks.com/matlabcentral/fileexchange/18430-txt2mat/content/txt2mat.m>.



---

# Appendix P

---

## Comfort standards

There are several standards which deal with measuring vibrations in trains. Unfortunately there is no specific standard which deals with ride comfort in trains on bridges. However, there are several more standards dealing with mechanical vibration or ride comfort on railway track, which can be used. This appendix gives an overview of these comfort standards. This appendix is referenced from section 2.2 and chapter 4.

### P.1 ISO 2631-1

The standard ISO 2631-1 is named “Mechanical vibration and shock - Evaluation of human exposure to whole-body vibration - Part 1: General requirements” [10] and is amended in 2010, by standard ISO 2631-1:1997/Amd.1:2010. This standard does not have passenger comfort in railway vehicles as its specific topic. It covers how to measure vibrations, how to evaluate the measurements and the application on health, comfort and motion sickness. The relevant information is summarized in the following sections.

#### P.1.1 Measurements

To quantify the vibration magnitude, accelerations should be measured. The coordinate system used for the measurements, should be as in Figure P.1.

Measurements should be done at the interface between the human body and the source of its vibration, for example seat surface, seat back of feet. The duration of the measurement shall be sufficient to ensure reasonable statistical precision.

The weighted RMS acceleration shall be determined for each axis of translational vibration (x-, y- and z-axes) at the surface which supports the person. If the weighted value determined in any axis is less than 25 % of the maximum value determined at the same point but in another axis it can be excluded.

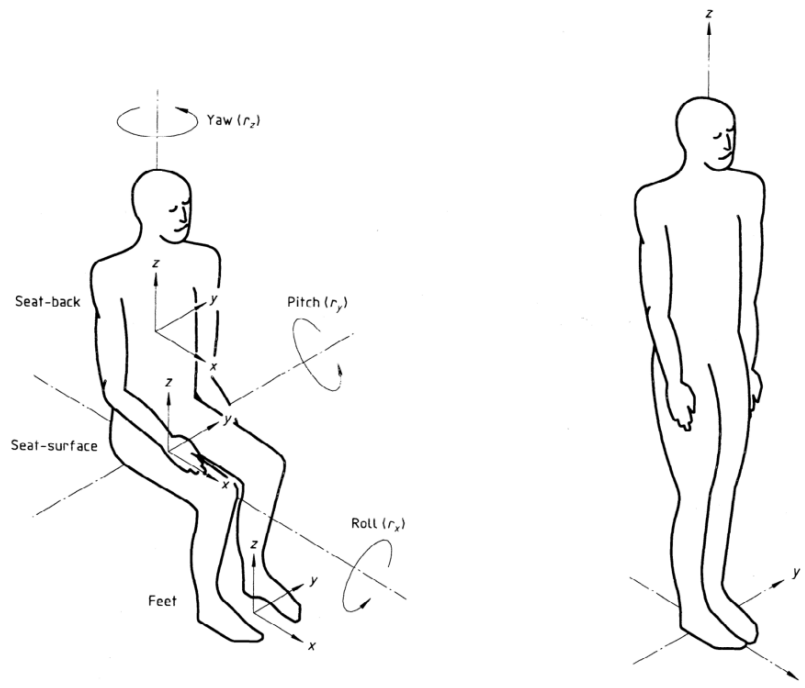


**Figure P.1:** Basicentric axes of the human body [10, fig. 1]

### P.1.2 Interpretation

Normally the basic evaluation method using the weighted root-mean-square acceleration can be used, unless the crest factor (ratio between peak values and RMS value) is higher than 9. A frequency band limitation should be applied to cut off frequencies below 0.4 Hz and above 100 Hz, but the range relevant for comfort is from 0.5 Hz to 80 Hz.

For railway vehicles the frequency-weighting curve  $W_b$  should be used, instead of curve  $W_k$ . Curve  $W_b$  deviates slightly from curve  $W_k$ , primarily below 4 Hz and is considered the appropriate curve for the z-direction.

A limit for comfort is not defined, but values for approximate indications of comfort perception are provided, see Table P.1.

**Table P.1:** Approximate indications of likely reactions to various magnitudes of overall vibration total values in public transport.

<b>Magnitude [<math>\text{m/s}^2</math>]</b>	<b>Perception</b>
< 0.315	not uncomfortable
0.315 - 0.63	a little uncomfortable
0.5 - 1	fairly uncomfortable
0.8 - 1.6	uncomfortable
1.25 - 2.5	very uncomfortable
> 2	extremely uncomfortable

Source: [10, C.2.3]

## P.2 ISO 2631-4

The standard ISO 2631-4 is named “ISO 2631-4:2001 Mechanical vibration and shock – Evaluation of human exposure to whole-body vibration – Part 4: Guidelines for the evaluation of the effects of vibration and rotational motion on passenger and crew comfort in fixed-guideway transport systems”. The standard has the evaluation of ride comfort as its topic. The relevant information is summarized in the following sections.

### P.2.1 Measurements

Seats and berths are not permanent parts of the vehicle and are likely to be replaced a number of times during the life of the vehicle. Taking measurements at these interfaces may not be as useful as taking measurements on the vehicle structure, therefore it may be more appropriate to take measurements at rigid portions of the vehicle structure, such as the floor.

There are several factors which can influence the outcome of the tests, therefore these should be reported:

- Condition of test vehicle's suspensions;
- Conditions of the track section used;
- Load conditions, whether the cars are empty or fully laden;
- The position of the car in the train;
- The direction of travel;
- Measurement location in the vehicle.

It is not always correct to treat the vehicle as a rigid body. Therefore measurements should be carried out at both ends of the vehicle and middle. For double-decker vehicles, measurements should be made on the lower deck at both ends of the vehicle, and at the middle, and on the upper deck at the middle of the vehicle. Because vehicle designs vary so widely, the measuring locations should be recorded and reported in detail.

### P.2.2 Interpretation

The frequency range of motions expected to impact ride comfort significantly in the vertical direction, is 0.5 Hz to 20 Hz. As mentioned in ISO 2631-1, the frequency-weighting curve  $W_b$  should be used, instead of curve  $W_k$ . It deviates slightly, as can be seen in Figure P.2. Annex A of ISO 2631-4 provides specifications of frequency weighting  $W_b$ , including parameters of the transfer function, the transfer functions and a table containing the frequency weighting in one-third-octave bands.

As an alternative to the RMS-based method of evaluation of ride comfort mentioned in ISO 2631-1, there is a statistical method available. This method is described in ISO 10056, it uses the 95 percentile of the weighted RMS values, measured at intervals of 5 seconds over a period of 5 minutes.

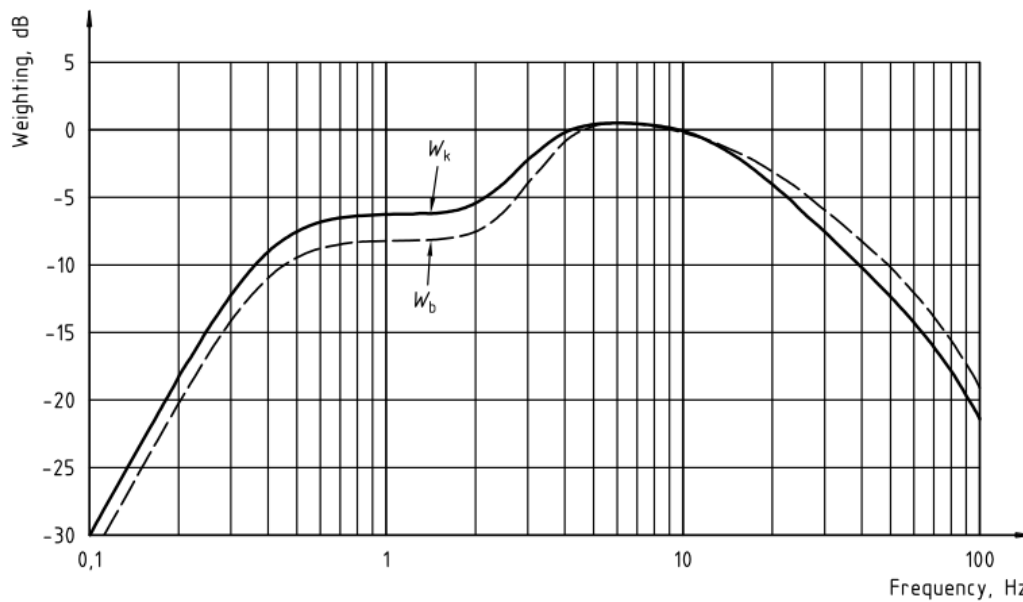


Figure P.2: Frequency weighting curves for  $W_b$  and  $W_k$  [15, fig. 1]

## P.3 EN 12299

The standard EN 12299 is named “EN 12299:2009 Railway applications – Ride comfort for passengers – Measurement and evaluation”. It replaces a pre-standard from 1999, called ENV 12299:1999. The relevant information is summarized in the following sections.

### P.3.1 Comfort evaluation methods

To quantify the ride comfort a Standard Method for Mean Comfort evaluation is defined, which takes into account the vibration exposure measured on the floor. In addition there are several other methods:

- the Continuous Comfort method, for short time effects;
- the Complete Method for Mean Comfort evaluation, for seated and standing;
- the Comfort on Discrete Events, for things like sudden jerks;
- the Comfort on Curve Transitions, for curved railway track.

Not all of these methods are suited for this research, such as the comfort on curve transitions which generally do.

### P.3.2 Measurements

In the vertical direction the frequency range of motions expected is up to 40 Hz due to track characteristics, suspensions characteristics, wheel defects or vehicle body modes.

The minimum time required is four test zones of 5 minutes, during which the test speed should be kept constant for Mean Comfort evaluation. The vehicle characteristics such as mass, centre of gravity, inertia, stiffness and damping are of influence to the comfort. The measurements shall be carried out at the centre of the body and at both ends of the passenger compartment. See Figure P.3. In the case of standing position studies on urban transit stock, an accelerometer shall also be placed on the vestibule floor.

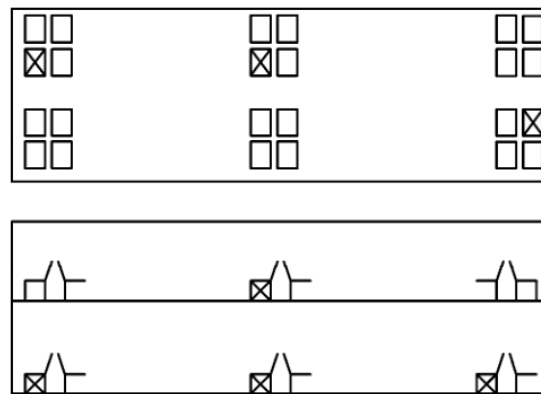


**Figure P.3:** Location of measuring points Double-Deck vehicle [33, fig. 2]

A measuring system consists of the following measuring equipment: transducers (accelerometers, gyroscopes), amplifiers and processing filters and recording equipment. The precision of the equipment shall be defined and the calibration shall be verified at regular periods. The equipment has several requirements, such as a sensitivity of less than  $0.05 \text{ m/s}^2$ . It is important to fix the transducer to the floor, so that it can perform the same motion as the structure it is fixed to.

The test report should include the following things: [33, Annex D]

- Aim of the test;
- The test performer and company;
- Reference to test specification, documentation of measuring system and applied standards;
- Date and time;
- Location;
- Local weather conditions (wet/dry rails);
- Vehicle characteristics and identification;
- Vehicle loading conditions;
- Vehicle structural details;
- Vehicle wheel profiles;
- Vehicle bogie type and suspension details;

- Operational number of the vehicle;
- Type of track;
- Track irregularities or track quality;
- Vehicle speed;
- Measuring points;
- Measurement transducers;
- Equipment calibration;
- Processing applied and software used.

### P.3.3 Interpretation

After measuring accelerations, the signals should be frequency weighted. Afterwards, the RMS-values over 5 seconds time periods should be calculated in the following way, which results in Continuous Comfort.

$$a_{Zj}^{W_i}(t) = \left[ \frac{1}{T} \int_{t-T}^t (\ddot{z}_{w_i}^*(\tau))^2 d\tau \right]^{0.5} \quad (\text{P.1})$$

For the Complete Method a calculation of the 95-th percentile over a period of 5 minutes should be done as well. For each measuring point the Mean Comfort index should be calculated. The partial Comfort Index for vertical direction can be calculated with:

$$N_{MVz} = 6 \cdot a_{ZP95}^{W_b} \quad (\text{P.2})$$

The comfort index  $N_{MV}$ , based on measurements in three directions, has a perception scale, like ISO 2631-1 has (see Table P.1), which can be seen in Table P.2.

**Table P.2:** Scale for the  $N_{MV}$  comfort index

Comfort index	Perception
$N_{MV} < 1.5$	very comfortable
$1.5 \leq N_{MV} < 2.5$	comfortable
$2.5 \leq N_{MV} < 3.5$	medium
$3.5 \leq N_{MV} < 4.5$	uncomfortable
$N_{MV} \geq 4.5$	very uncomfortable

Source: [33, table 8]

A preliminary scale for comfort indexes in y- or z-direction is also given, see Table P.3. The continuous comfort in z-direction is defined as  $C_{Cz}(t) = a_{ZP}^{W_b}(t)$ .

According to [33, C.1], the weighting curve for  $W_b$  is not the same as in ISO 2631-4. Annex C details the filter functions of the weighting curves.

**Table P.3:** Scale for the  $C_{Cz}(t)$  comfort index

Comfort index [ $\text{m/s}^2$ ]	Perception
$C_{Cz}(t) < 0.20$	very comfortable
$0.20 \leq C_{Cz}(t) < 0.30$	comfortable
$0.30 \leq C_{Cz}(t) < 0.40$	medium
$0.40 \leq C_{Cz}(t)$	less uncomfortable

Source: [33, table 9]

The upper limit of the frequency range in the vertical direction may be reduced to 40 Hz if this has been justified by a prior test, by means of a two-pole low-pass filter with Butterworth characteristics having an asymptotic gradient of  $-12$  dB per octave. [33, C.2.6]

## P.4 Further reading

For more information and the background of these standards, the reader is referred to UIC leaflet 513 and research report ERRI D190, among others.

---

# Bibliography

- [1] "NEN-EN 1991-2:2003 - Eurocode 1 - Actions on structures - Part 2: Traffic loads on bridges," 2003.
- [2] Y. Yang, J. Yau, and Y. Wuy, *Vehicle-bridge interaction dynamics: with applications to high-speed railways*. World Scientific Publishing Co., 2004.
- [3] J. M. Biggs, *Introduction to Structural Dynamics*. McGraw-Hill Companies, 1964.
- [4] "NEN-EN 1990:2002/a1:2006 - Eurocode: Basis of Structural Design - Annex 2: Application for bridges," 2002.
- [5] L. Fryba, *Dynamics of Railway Bridges*. Thomas Telford Ltd, 1996.
- [6] A. Palmstrom, *Designers Guide to Eurocode 1: Actions on Bridges (Eurocode Designers' Guide)*. Thomas Telford Publishing, 2010.
- [7] "ENV 1991-3:1995 - Eurocode 1 - Basis of design and actions on structures - Part 3: Traffic loads on bridges," 1995.
- [8] "ERRI D 190/DT 307 - Permissible deflection of steel and composite bridges for velocities  $v > 160$  km/h - The effects of 1 and 2 hz transient vertical vibration on discomfort," 1994.
- [9] C. W. de Silva, *Vibration: Fundamentals and Practice, Second Edition*. CRC Press, 2006.
- [10] "ISO 2631-1:1997 Mechanical vibration and shock – Evaluation of human exposure to whole-body vibration – Part 1: General requirements," 1997.
- [11] S. Sabin, A. Hamad, R. Chitwood, and M. Qureshi, "Understanding discrepancies in vibration amplitude readings between different instruments," *ORBIT*, vol. 26, no. 1, pp. 41–57, 2006.
- [12] R. Calçada, R. Delgado, A. C. e Matos, J. M. Goicolea, and F. Gabaldon, *Track-Bridge Interaction on High-Speed Railways: Selected and revised papers from the Workshop on Track-Bridge Interaction on High-Speed Railways, Porto, Portugal, 15-16 October, 2007*. CRC Press, 2008.

- [13] W. Bruggers, "Comfort related design of railway bridges," Master's thesis, Delft University of Technology, 2002.
- [14] M. J. Griffin, *Handbook of Human Vibration*. Academic Press, 1990.
- [15] "ISO 2631-4:2001 Mechanical vibration and shock – Evaluation of human exposure to whole-body vibration – Part 4: Guidelines for the evaluation of the effects of vibration and rotational motion on passenger and crew comfort in fixed-guideway transport systems," 2001.
- [16] Kounosu, "Victoria Falls Bridge." [https://commons.wikimedia.org/wiki/File:Victoria\\_Falls\\_Bridge\\_from\\_North\(Zambia-side\).jpg](https://commons.wikimedia.org/wiki/File:Victoria_Falls_Bridge_from_North(Zambia-side).jpg). Accessed October 30, 2015.
- [17] J. Henderson, "Bayonne Bridge." [https://commons.wikimedia.org/wiki/File:Bayonne\\_Bridge\\_Collins\\_Pk\\_jeh-2.JPG](https://commons.wikimedia.org/wiki/File:Bayonne_Bridge_Collins_Pk_jeh-2.JPG). Accessed October 30, 2015.
- [18] "Neville Island Bridge." <http://saiengr.com/sites/default/files/project/nbis-and-fracture-critical-fcm-bridge-inventory/inspection/paste1392347933.png>. Accessed October 30, 2015.
- [19] "Tied-arch bridge loading." [http://www.steelconstruction.info/images/1/1a/R7\\_Fig3.PNG](http://www.steelconstruction.info/images/1/1a/R7_Fig3.PNG). Accessed February 15, 2016.
- [20] W.-F. Chen, *Handbook of Structural Engineering*. CRC Press, 1997.
- [21] C. Esveld, *Modern Railway Track*. Zaltbommel: MRT-Productions, 2001.
- [22] C. Liebscher, "DD-IRM als intercity." [https://commons.wikimedia.org/wiki/File:Bahnhof\\_Den\\_Helder\\_04\\_DD-IRM.JPG](https://commons.wikimedia.org/wiki/File:Bahnhof_Den_Helder_04_DD-IRM.JPG). Accessed November 9, 2015.
- [23] "STORK RMO 9000 bogies." <https://www.flickr.com/photos/alcoalbe/15567834292/in/album-72157648434098530/>. Accessed November 17, 2015.
- [24] A. K. Chopra, *Dynamics of Structures: Theory and Applications to Earthquake Engineering (2nd Edition)*. Prentice Hall, 2000.
- [25] C. Johansson, *Simplified dynamic analysis of railway bridges under high-speed trains*. Licentiate thesis, KTH Royal Institute of Technology, 2013.
- [26] Y.-B. Yang, C. Lin, and J. Yau, "Extracting bridge frequencies from the dynamic response of a passing vehicle," *Journal of Sound and Vibration*, vol. 272, pp. 471–493, may 2004.
- [27] L. Fryba, *Vibration of Solids and Structures Under Moving Loads*. Thomas Telford Ltd, 1972.
- [28] C. Johansson, C. Pacoste, and R. Karoumi, "Closed-form solution for the mode superposition analysis of the vibration in multi-span beam bridges caused by concentrated moving loads," *Computers & Structures*, vol. 119, pp. 85–94, apr 2013.
- [29] S. Bruinsma and A. van der Linoen, "Overbrugging van de Lek bij Culemborg - deel 2," Report 420/117/K15.937/546, Nederlandse Spoorwegen, 1980.
- [30] S.-H. Ju and H.-T. Lin, "Numerical investigation of a steel arch bridge and interaction with high-speed trains," *Engineering Structures*, vol. 25, pp. 241–250, jan 2003.

- [31] M. Feng, Y. Fukuda, M. Mizuta, and E. Ozer, "Citizen sensors for SHM: Use of accelerometer data from smartphones," *Sensors*, vol. 15, pp. 2980–2998, jan 2015.
- [32] "VXaccelerator Android application." <https://github.com/benjaminkomen/VXaccelerator>. Accessed April 11, 2016.
- [33] "EN 12299:2009 - Railway applications - Ride comfort for passengers - Measurement and evaluation," 2009.
- [34] Y.-B. Yang and Y.-S. Wu, "A versatile element for analyzing vehicle–bridge interaction response," *Engineering Structures*, vol. 23, pp. 452–469, may 2001.
- [35] I. Bucknall, "New Eurocode Requirements for the Design of High Speed Railway Bridges," *IABSE Symposium Report*, vol. 87, pp. 17–24, jan 2003.
- [36] "NEN-EN 1990+A1+A1/C2/NB - National Annex to NEN-EN 1990+A1+A1/C2: Eurocode: Basis of Structural Design," 2011.
- [37] "NEN 1008:1963 - Directions for the design of steel bridges (VOSB 1963)," 1963.
- [38] "NEN 6706:2007 - Technische grondslagen voor bouwconstructies - TGB 1990 - Verkeersbelastingen op bruggen," 2005.
- [39] "UIC." <http://www.uic.org/1922-UIC-a-long-life-organisation>. Accessed November 10, 2015.
- [40] R. Calçada, R. Delgado, A. C. e Matos, J. M. Goicolea, and F. Gabaldon, *Bridges for High-Speed Railways: Revised Papers from the Workshop, Porto, Portugal, 3 - 4 June 2004*. CRC Press, 2008.
- [41] U. K. Ghosh, *Design and Construction of Steel Bridges*. CRC Press, 2006.
- [42] W.-F. Chen and L. Duan, *Bridge Engineering Handbook*. CRC Press, 1999.
- [43] M. Chlosta, "Secundaire spanningen in dwarsverbandstaven van stalen boogbruggen," B.S. Thesis, Delft University of Technology, 2008.
- [44] "Per Tveit Homepage." <http://home.uia.no/pert/index.php/Home>. Accessed November 4, 2015.
- [45] D. Dzihan, "Longitudinal reinforcement in tied arch bridges," Master's thesis, Delft University of Technology, feb 2015.
- [46] M. Hirt and J.-P. Lebet, *Steel Bridges: Conceptual and Structural Design of Steel and Steel-Concrete Composite Bridges*. EPFL Press, 2013.
- [47] "NEN-EN 15528:2015 - Railway applications - Line categories for managing the interface between load limits of vehicles and infrastructure," 2015.
- [48] "Treinmaterieel." <http://wiki.ovinnederland.nl/w/index.php?title=Categorie:Treinmaterieel&oldid=49226>. Accessed November 4, 2015.
- [49] "Nederlands treinstel." [https://nl.wikipedia.org/w/index.php?title=Categorie:Nederlands\\_treinstel&oldid=40242481](https://nl.wikipedia.org/w/index.php?title=Categorie:Nederlands_treinstel&oldid=40242481). Accessed November 4, 2015.

- [50] S. Iwnicki, *Handbook of Railway Vehicle Dynamics*. CRC Press, 2006.
- [51] "Forum beneluxspoor.net – irm bouwtekeningen." <http://forum.beneluxspoor.net/?topic=20851.0>. Accessed March 17, 2016.
- [52] "Trainfever forum." <http://www.train-fever.com/forums/user/jonathan078nl/replies/page/4/>. Accessed March 17, 2016.
- [53] "Coach composition of VIRM trains." <http://arthurstreinenpagina.nl/Treinstellen/Elektrische%20treinstellen/Dubbeldeks%20Interregio%20Materieel/VIRM-VI,%20EL6/samenstellingen.html>. Accessed April 7, 2016.
- [54] E. Ting, J. Genin, and J. Ginsberg, "A general algorithm for moving mass problems," *Journal of Sound and Vibration*, vol. 33, pp. 49–58, mar 1974.
- [55] Y. Yang and C. Lin, "Vehicle–bridge interaction dynamics and potential applications," *Journal of Sound and Vibration*, vol. 284, pp. 205–226, jun 2005.
- [56] D. van der Poel, "Lateral railway bridge vibrations – modelling of lateral dynamic railway bridge behaviour," Master's thesis, Delft University of Technology, 2015.
- [57] "Beam mode shapes." [http://www.steelconstruction.info/File:G\\_Fig8a.PNG](http://www.steelconstruction.info/File:G_Fig8a.PNG). Accessed February 2, 2016.
- [58] Q.-L. Zhang, A. Vrouwenvelder, and J. Wardenier, "Numerical simulation of train–bridge interactive dynamics," *Computers & Structures*, vol. 79, pp. 1059–1075, apr 2001.
- [59] K. Liu, G. D. Roeck, and G. Lombaert, "The effect of dynamic train–bridge interaction on the bridge response during a train passage," *Journal of Sound and Vibration*, vol. 325, pp. 240–251, aug 2009.
- [60] SAS IP, Inc, *ANSYS Inc. Documentation for Release 16.1*.
- [61] "BEAM3 2-D Elastic Beam." [http://www.ansys.stuba.sk/html/elem\\_55/chapter4/ES4-3.htm](http://www.ansys.stuba.sk/html/elem_55/chapter4/ES4-3.htm). Accessed January 28, 2016.
- [62] "LINK8 3-D Spar." [http://www.ansys.stuba.sk/html/elem\\_55/chapter4/ES4-8.htm](http://www.ansys.stuba.sk/html/elem_55/chapter4/ES4-8.htm). Accessed February 26, 2016.
- [63] "CONTAC48 Element Description." [http://ansys.net/old\\_undocumented/Hlp\\_E\\_CONTAC48.html](http://ansys.net/old_undocumented/Hlp_E_CONTAC48.html). Accessed January 27, 2016.
- [64] "LS-DYNA Support: What are the differences between implicit and explicit?" <http://www.dynasupport.com/faq/general/what-are-the-differences-between-implicit-and-explicit>. Accessed April 12, 2016.
- [65] C. Vuik, P. van Beek, F. Vermolen, and J. van Kan, *Numerieke Methoden voor Differentiaalvergelijkingen*. VSSD, 2006.
- [66] L. Wang, X. Kang, and P. Jiang, "Vibration analysis of a multi-span continuous bridge subject to complex traffic loading and vehicle dynamic interaction," *KSCE Journal of Civil Engineering*, vol. 0, pp. 1–10, mar 2015.

- 
- [67] C. Bowe, *Dynamic interaction of trains and railway bridges using wheel rail contact method*. PhD thesis, National University of Ireland, 2009.
- [68] T. J. R. Hughes, *The Finite Element Method: Linear Static and Dynamic Finite Element Analysis*. Prentice Hall, 1987.
- [69] J.-D. Yau, Y.-B. Yang, and S.-R. Kuo, "Impact response of high speed rail bridges and riding comfort of rail cars," *Engineering Structures*, vol. 21, pp. 836–844, sep 1999.
- [70] S. Bruinsma and A. van der Linoen, "Overbrugging van de Lek bij Culemborg - deel 1," Report 420/117/K15.937/546, Nederlandse Spoorwegen, 1980.
- [71] H. van Maarschalkerwaard, S. Bruinsma, and J. Erkelens, "Vervanging van de spoorbrug over de lek bij culemborg," *Bouwen met Staal*, no. 60, pp. 29–38, 1982.
- [72] A. Schillemans, A. Hemel, and J. Pieterse, "Spoorbrug over de Lek bij Culemborg - controleberekening," Report E2285-01-001, DHV, 1991.
- [73] S. Bruinsma and A. van der Linoen, "Overbrugging van de Lek bij Culemborg - Bijlage 1," Report 420/117/K15.937/546, Nederlandse Spoorwegen, 1980.
- [74] A. Romeijn, "Lecture notes CT5125 Steel bridges – part 2," 2006.
- [75] "Data sheet - BMA 255 - digital, triaxial acceleration sensor." [https://ae-bst.resource.bosch.com/media/\\_tech/media/datasheets/BST-BMA255-DS004-05\\_published.pdf](https://ae-bst.resource.bosch.com/media/_tech/media/datasheets/BST-BMA255-DS004-05_published.pdf). Accessed January 19, 2016.

